Approaches to understanding the role of the cerebellum in sensorimotor control and learning: the big picture of the little brain

Dissertation

der Mathematisch-
Naturwissenschaftlichen Fakultät

und
der Medizinischen Fakultät

der Eberhard-Karls-Universität Tübingen

vorgelegt von

Akshay Markanday

aus Chandigarh, Indien

2020

Tag der mündlichen Prüfung: 09.06.2021

Dekan der Math.-Nat. Fakultät:	Prof. Dr. Thilo Stehle
Dekan der Medizinischen Fakultät:	Prof. Dr. Bernd Pichler
1. Berichterstatter:	Prof. Dr. Hans-Peter Thier
2. Berichterstatter:	Prof. Dr. Fahad Sultan
Prüfungskommission:	Prof. Dr. Hans-Peter Thier
	Prof. Dr. Fahad Sultan
	Prof. Dr. Ziad M. Hafed
	Prof. Dr. Hansjörg Scherberger

Erklärung / Declaration:

Ich erkläre, dass ich die zur Promotion eingereichte Arbeit mit dem Titel:

"**Approaches to understanding the role of the cerebellum in sensorimotor control and learning: the big picture of the little brain**"

selbständig verfasst, nur die angegebenen Quellen und Hilfsmittel benutzt und wörtlich oder inhaltlich übernommene Stellen als solche gekennzeichnet habe. Ich versichere an Eidesstatt, dass diese Angaben wahr sind und dass ich nichts verschwiegen habe. Mir ist bekannt, dass die falsche Abgabe einer Versicherung an Eides statt mit Freiheitsstrafe bis zu drei Jahren oder mit Geldstrafe bestraft wird.

I hereby declare that I have produced the work entitled:

*"**Approaches to understanding the role of the cerebellum in sensorimotor control and learning: the big picture of the little brain**",*

submitted for the award of a doctorate, on my own (without external help), have used only the sources and aids indicated and have marked passages included from other works, whether verbatim or in content, as such. I swear upon oath that these statements are true and that I have not concealed anything. I am aware that making a false declaration under oath is punishable by a term of imprisonment of up to three years or by a fine.

Tübingen, den ....

Datum / Date Unterschrift /Signature

Life is divided into three terms - that which was, which is, and which will be.
Let us learn from the past to profit by the present, and from the present,
to live better in the future.

William Wordsworth

Table of Contents

1. ABSTRACT

It is well-established that the damage or removal of the cerebellar cortex not only leads to severe deficits in fine control and coordination of movements but also impairs the ability to correct the motor behavior, thus pointing towards the role of the cerebellum in sensorimotor control and learning. However, the understanding of how this is achieved by the cerebellum remains unclear. This dissertation offers different approaches that try to elucidate the cerebellar mechanisms underlying motor control and learning, while also tackling an important methodological barrier associated with these questions. The first approach (Appendix 1) thoroughly investigates different kinematic variables of fast and precise index finger movements in cerebellar patients and healthy controls. Here I demonstrate that the increased end-point variability—"motor noise"—observed in cerebellar patients is a direct consequence of the loss of a cerebellum-based velocity-duration trade-off mechanism that consistently adjusts movement duration by utilizing the information on the expected velocity of the upcoming movement. Understanding the neural underpinnings of these cerebellar mechanisms requires direct access to the core element of the canonical cerebellar microcircuitry—the Purkinje cell. One of the most intriguing and debated features of the Purkinje cell discharge, the only output of the cerebellar cortex, is the complex spikes. However, owing to their complex wave morphology accompanied by extremely low firing rates, detecting these events is an immense challenge. The second approach (Appendix 2) in this dissertation deals with the long-standing problem of complex spike detection, by offering a fast and reliable, fully automated deep-learning based algorithm that not only detects these events with impeccable accuracy but also provides useful information on their duration. The direct benefits of this approach form the basis of the third approach (Appendix 3), which specifically deals with the role of complex spikes recorded in

a repetitive saccade paradigm. Different findings, based on highly specific paradigms, have led to divergent views on the role of these events. In this approach, I demonstrate that in addition to conveying error-related information, as well as information on the metrics of both primary and corrective saccades, complex spike activity also seems to predict the upcoming events. Furthermore, complex spikes convey this information in a time-specific manner, with changes in complex spike firing probability paralleled by changes in their duration. Hence, complex spikes are fully capable of conveying a vast spectrum of behaviorally relevant information in a multiplexed manner, all together in one task. These findings are compatible with both classical and non-classical roles of complex spikes, thereby proposing a broader framework for their roles. Lastly, I present an overall picture of the role of the cerebellum in the form of a review (Appendix 4) that focuses on the oculomotor system as a model for motor control and learning. In conclusion, the thesis discusses the implications of the results obtained for future work on our view of the cerebellum.

2. INTRODUCTION

In an endless quest for knowledge, where novel ideas keep setting new milestones, the only possible way to track progress is to look back at the terminus a quo, which, if not completely forgotten, gradually fades away with time. Quite similar is the case of cerebellum research, where most studies not only begin but are also strongly anchored to the fundamental idea that the cerebellum is necessary for motor control and learning, without completely realizing the amount of time and effort invested in achieving that milestone.

2.1 Historical background

One of the earliest descriptions of the cerebellum, according to Galen, can be traced back to the works of Aristotle who described this structure as the "little brain", *paregkephalis*, in comparison to the larger brain *egkefalos*—the cerebrum (Marshall and Magoun, 2013). Although his views dominated the field of medicine for more than a millennium, it was only during the Renaissance that Andreas Vesalius (1543) challenged Galen's doctrine about the human cerebellum that was largely based on anatomical studies on animals. It took another two centuries until Vincenzo Malacarne (1776) published the first-ever work entirely dedicated to the cerebellum and provided the most accurate anatomical description of the cerebellar cortex and its nuclei available at that time. However, the first foundations of the functional role of the cerebellum were laid only during the mid-19th century. Jean Pierre Flourens (1824), based on careful evaluation of the effects of cerebellar lesions in chicken, postulated that movement coordination, as opposed to movement initiation was a property of the cerebellum. On the other hand, Luigi Luciani (1891), resorting to improved surgical lesions in dogs and monkeys, was able to arrive at a more fine-grained characterization of the consequences of lesions. He distinguished three basic deficits in muscle control that resulted from the loss of cerebellum—*asthenia* (physical weakness or loss of strength), *atonia* (lack of normal muscle tone), and *astasia* (inability to walk, stand or even sit without assistance). Finally, based on the loss of movement accuracy observed in lesioned animals, he also characterized the fourth deficit by adding *dysmetria* to the list.

These experimental findings deeply influenced the clinical interpretation of cerebellar lesions and disease that led to the seminal works of the two great neurologists, Joseph Babinski, and Sir Gordon Holmes. By describing the patients'

deficits in generating rapid movement sequences (*dysdiadochokinesis*) resulting from the lack of coordination of antagonistic muscles, Babinski (1902) confirmed that Flourens' observations on the consequences of experimental lesions of the chicken cerebellum also applied to lesions of the human cerebellum due to disease. On the other hand, Holmes (1917) provided an in-depth description of a variety of functional deficits based on his extensive and careful investigations of patients with comparatively small cerebellar lesions due to gunshot injuries during the first world war. The diversity of functional deficits led him to challenge the theory of the unitary function of the cerebellum (Holmes, 1917). Holmes confirmed and extended Luciani's conclusions (Glickstein et al. 2009) and provided a detailed description of well-characterized cerebellar symptoms that are still guiding the clinical assessment of patients suffering from a cerebellar disease.

The understanding of the functional role of the cerebellum, originally solely based on lesion experiments and clinical observations, was paralleled by advancements of histological techniques in the mid-19th century, that, for the first time, provided insights into the internal structure of the cerebellar cortex. Evangelista Purkinje (1837) was the first to identify a distinct type of neuron in the cerebellar cortex, later dubbed as the Purkinje cell, making up the middle layer of the three-layered cerebellar cortex. And it was the discovery of the Golgi staining method introduced by Camilio Golgi (1883) that soon led to the pioneering work of both art and science by Santiago Ramón y Cajal (1894) in which he described the two major afferents to the cerebellar cortex—the mossy fibers, and the climbing fibers. It took another half a century until the possibility of electrophysiological recordings allowed Sir John Eccles (Eccles, 1967) to expand Cajal's findings and to draw a first picture of the functional architecture of the cerebellar cortex. His work paved the path for the development of the

influential concept of error-based motor learning, accommodated by the cerebellar cortex, collectively known as the Marr-Albus-Ito hypothesis (Marr, 1969; Albus, 1971; Ito, 1972). This soon became the epicenter of several contemporary ideas discussing the role of the cerebellum.

2.2 Cerebellar architecture and the canonical microcircuitry

The cerebellar cortex is a highly folded structure that constitutes around 80% of all neurons found in the entire human brain (Azevedo et al., 2009; Herculano-Houzel, 2009). In any species that has been studied, unfolding the cerebellar cortex reveals that the surface area of this structure is actually quite large. This rule also holds for humans whose cerebellum is particularly large in absolute terms (Sultan and Braitenberg, 1993; Sereno et al., 2020). Considering that humans are equipped with an exquisite set of fine sensorimotor skills, a large cerebellum may suggest a role in learning and performing a complex repertoire of movements. However, the largest of all vertebrate cerebella in relative terms is exhibited by elephants (Maseko et al., 2012). At first glance, one might take this fact as an argument against the motor skill view. After all, elephants lack fingers, hands and also their locomotor repertoire does not sport a particular level of sophistication. Yet, they dispose of a trunk moved in almost infinitely different ways, supporting a remarkable degree of precision and sophistication (Endo et al., 2001), accompanied by trunk-eye coordination to reach, grasp and manipulate objects in the environment (Pettigrew et al., 2010). In other words, trunk control is reminiscent of reaching and grasping behavior in humans. This might be taken as an argument supporting the assumption that a well-developed cerebellar cortex is needed to cope up with the excessive computational demands incurred by the complexity of the effector and the motor skills it accommodates.

Much effort has been invested in unraveling the architecture of the cerebellar cortex (*Figure 1a*) and its underlying canonical microcircuitry (*Figure 1b*) as the knowledge of its principles is a key to understanding the nature of computations underlying complex motor behaviors. With three distinct layers, the crystal-like structure of the cerebellar cortex comprises of the outermost molecular layer (*Figure 1a*) in which the parallel fibers (see brown lines in *Figure 1a* and 1*b*), originating from the granule cells in the innermost granular layer, bifurcate and run laterally in two opposite directions orthogonal to the vast and planar dendritic arbor of individual Purkinje cells (PC), lined up sagittally in the PC layer. While each parallel fiber relays the same information to a large number of PCs, each PC collects diverse inputs from myriad parallel fibers that make synaptic contacts (up to 200,000 in rats, Napper and Harvey, 1988) with the dendritic tree of the individual PCs. The input to the parallel fibers arises from the mossy fibers (MF; see purple lines in *Figure 1a* and *b*), originating from a variety of precerebellar nuclei (such as the pontine nuclei, nucleus reticularis tegmenti pontis, paramedian pontine reticular formation, and other brainstem structures). The former one is special as it is the major gateway for cerebral signals destined for the cerebellum (Thier and Möck, 2006). MFs, originating from these precerebellar nuclei end in the granular layer where their axonal endings terminate in entangled ball-like structures, called cerebellar glomeruli, in which the contact granule cells, give rise to the aforementioned parallel fibers, as well as Golgi cells. While individual PCs receives an indirect stream of afferent information, via the mossy fiber-granule cell-parallel fiber pathway, the same PCs also receive direct input from dedicated climbing fibers (CF; see red lines in *Figure 1a* and *1b*) that originate from neurons in the contralateral inferior olive, located in the lower brain stem. These CFs wrap around the soma and proximal dendrites of a few target PCs, making approximately 300 to 500 synaptic contacts

on each (Hillman, 1969), thus establishing one of the most powerful excitatory synaptic interfaces in the entire brain.

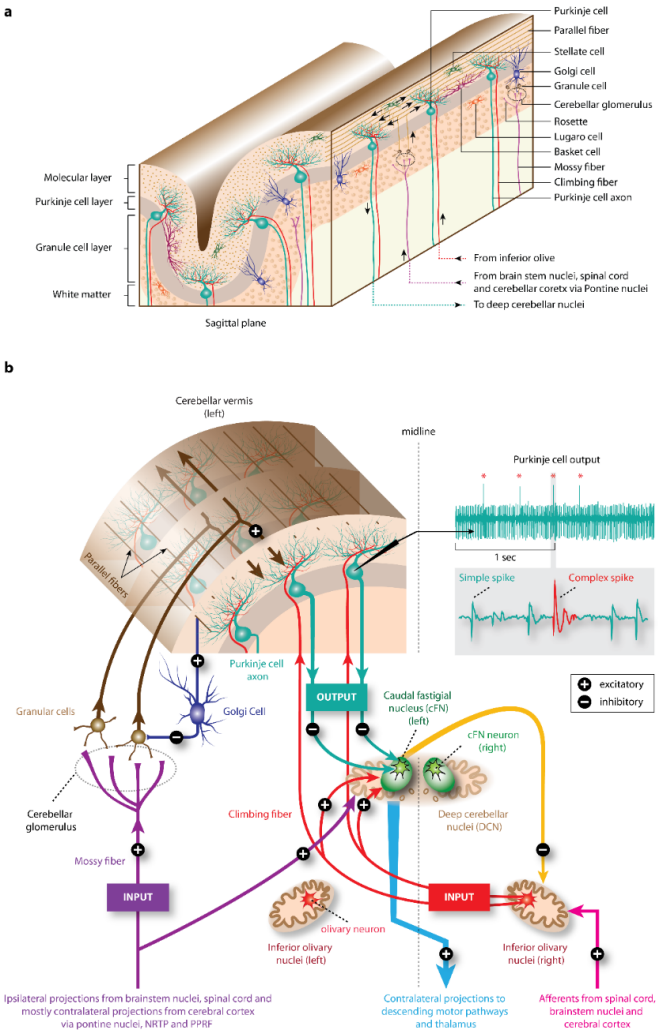

Figure 1. *The architecture of the cerebellar cortex and the canonical microcircuitry (Thier and Markanday, 2019)*

While each PC receives input from only one CF (Eccles et al., 1966)—with a few exceptional cases in which adult PCs have been reported to receive input from more than one CF (Nishiyama and Linden, 2004)—each CF axon may branch before innervating a zone of 5-10 parasagittally aligned PCs (Armstrong et al., 1973; Desclin, 1974; Rosina and Provini, 1983). Together these “microzones” of PCs that share a common CF input, originating from neurons in specific regions of the inferior olivary complex, form elongated "cerebellar modules" (Voogd, 1969) that in turn target specific parts of the deep cerebellar nuclei (DCN). These target DCN neurons that receive inputs from the same CF axons projecting to the specific modules of PCs also send GABAergic inputs back to the source of these CFs in the inferior olivary complex (De Zeeuw et al., 1989). This olivo-cortico-nuclear circuit is the central aspect of these individual cerebellar modules with each module possibly serving a specific cerebellar function (Ruigrok and Voogd, 1990; Ruigrok and Voogd, 2000; Apps et al., 2018), and each microzone residing within these modules acting as a fundamental processing unit. Since a microzone, the site of a canonical circuit, remains uniform throughout the cerebellar cortex, it may seem reasonable to assume that the basic nature of the local computational principle also remains the same throughout the cerebellar cortex. On the other hand, microzones may exhibit different gene expressions (Brochu et al., 1990) and also clear differences in physiological properties (Wadiche and Jahr, 2005; Wang et al., 2011; Xiao et al., 2014). How this might translate into function remains unclear. Within a canonical circuit, significant contributions are also made by a number of interneurons like Golgi cells, stellate cells, and basket cells that liaise interactions between PCs. Yet, it is the large PC processing extracerebellar input and, moreover, the only cerebellocortical neuron with axon leaving the cerebellar cortex, where major cerebellar computations take place thus making them the central building blocks of the canonical microcircuit.

2.3 Purkinje cell discharge: simple spikes and complex spikes

The transformation of the two streams of the information offered by the MF and CF inputs modulate the discharge of PCs (see inset on the top-right in *Figure 1b*), the sole output of the cerebellar cortex, that is further transmitted to the target neurons in the DCN. PC discharge is characterized by the presence of two types of action potentials: simple spikes (SS), and complex spikes (CS). SSs (Eccles et al., 1966), are regular sodium-potassium based action potentials that last only up to a fraction of a millisecond and exhibit a typical bi- or tri-phasic wave morphology when recorded extracellularly (*Figure 1b,* turquoise trace). These short-duration SSs, that reflect the integrated influence of MF-driven parallel fibers and the inhibitory interneurons, can be fired up to several hundred spikes per second.

The SS discharge is briefly interrupted by the occurrence of a CS, driven by a burst of CF action potentials (*Figure 1b,* red trace). The CS causes a huge influx of calcium ions mediated by the voltage-gated calcium channels resulting in a long-lasting depolarization of the target PC. As opposed to their "simpler" counterparts (i.e., SSs), CSs, as the name suggests, display "complex" shapes in extracellular recordings. They are characterized by a fast, back-propagated axonal action potential as the initial spiking component, followed by a slow chain of fluctuating potential shifts that reflect the long-lasting calcium-dependent depolarization (Eccles, 1967; Fujita, 1968; Thach, 1968; Llinás and Sugimori, 1980; Stuart and Häusser, 1994; Davie et al., 2008). In addition to the longer duration polyphasic wave morphology, CSs are also notorious for their perplexingly low firing rates (0.5 to 2 Hz).

2.4 The role of simple spikes in encoding movement kinematics

Ever since the wrist-movements related modulation of PC discharge was first reported in monkeys (Thach, 1968), the role of PC-SSs in controlling single and multi-joint limb movement kinematics has been extensively investigated by a series of follow-up experiments (Thach, 1970b, a; Harvey et al., 1979; Frysinger et al., 1984; Wetts et al., 1985; Fortier et al., 1989; Fortier et al., 1993; Roitman et al., 2005; Ebner et al., 2011). However, even single-joint movements remain demanding when considering the dynamic requirements. Hence, eye movements, not only characterized by limited degrees of freedom but also by less demanding dynamical requirements promised an easier approach to the underpinnings of the cerebellar guidance of movements. In particular, the earlier work on the cerebellar control of eye movements has focused on the parametric adjustment of the vestibuloocular reflex (Robinson, 1976) whose study can rely on fairly simple animal models. On the other hand, in view of their obvious sensitivity to cerebellar disease, early on cerebellar research also addressed slow and fast goal-directed eye movements, smooth-pursuit, and saccades, respectively. For instance, saccades were shown to be impaired as a consequence of surgical lesions (Aschoff and Cohen, 1971; Ritchie, 1976). About the same time, Ron and Robinson (1973) established the first sketch of a cerebellar representation of saccades in its mid-line parts, deploying electrical microstimulation of the monkey cerebellum. Later, resorting to much more sophisticated variants of microstimulation, the Noda laboratory could identify what became known as the oculomotor vermis (OMV), comprising lobules VIc and VIIa of the midline cerebellum as the core saccade-related region (see *Figure 2*). Later, the OMV was shown to also matter for the control of smooth-pursuit eye movements (Suzuki and Keller, 1988b, a; Sato and Noda, 1992; Ohtsuka and Enoki, 1998; Takagi et al., 2000; Dash et al., 2010; Dash et al., 2013; Sun et al., 2017a).

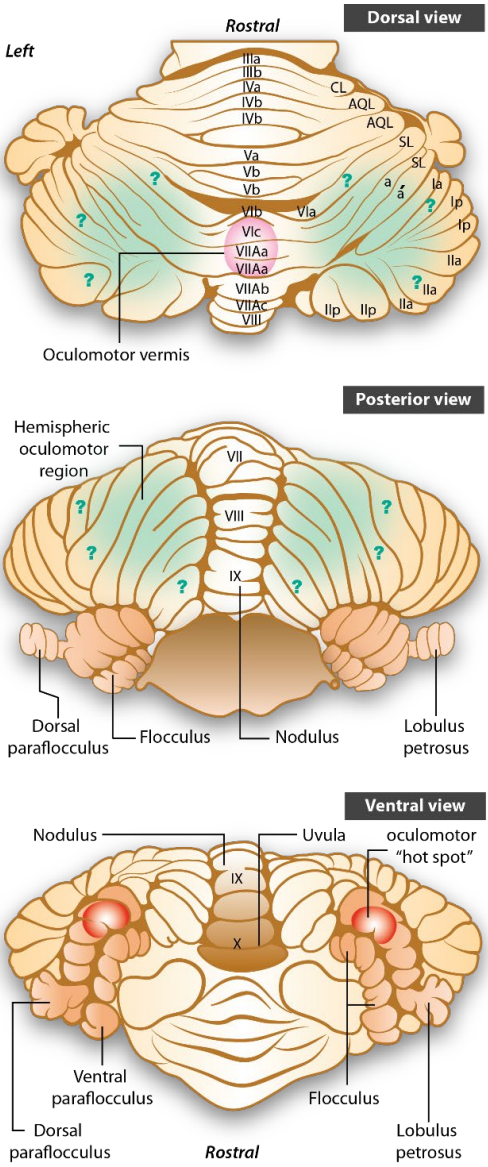

Figure 2. *Three views of the cerebellum showing the topography of different oculomotor representations of eye movements. (a) In the dorsal view, the anterior quadrangular lobule (AQL), the central lobule (CL), and their associated lobules (III, IV, and V) form the anterior*

surface. The oculomotor vermis (OMV), comprising of lobules VIc, VIIAa, and VIIAb, is shaded in pink. (b) In the posterior view, the entire dorsal surface of the cerebellar hemisphere is occupied by the ansiform lobule (crus Ia, Ip, IIa, IIp). Note how the four hemispheric folia of the simple lobule (SL) are connected specifically to the folia of lobules VI and VIIAa. The question marks delineating the hemispheric oculomotor region (HVII; see dorsal and posterior views) centering on hemispheric lobules VII emphasize the uncertainties regarding its exact topography. (c) The oculomotor hot spot, enriched with mostly saccade-related activity, in the dorsal paraflocculus emphasized by Noda & Mikami (1986) is highlighted red in the ventral view of the cerebellum. Figure based on Thier (2011) and Madigan & Carpenter (1971). Acquired from Thier and Markanday, 2019.

Another oculomotor region involved in smooth-pursuit eye movements, albeit not confined to this function, was also found in the flocculus and ventral paraflocculus in monkeys (Stone and Lisberger, 1990a, b; *see Figure 2*), actually congruent with the region responsible for the parametric adjustment of the vestibuloocular reflex. Lesioning the OMV (Vahedi et al., 1995; Takagi et al., 1998; Barash et al., 1999; Takagi et al., 2000; Ignashchenkova et al., 2009; Ohki et al., 2009) results in hypometria, a condition in which saccades fall short of the target location. Hypometria disappears in a couple of weeks after the lesion (Barash et al., 1999). However, what remains–probably forever, is an increased variability of saccade endpoints accompanied by an inability to adapt to short-term changes in target location because of an inability to adjust saccade metrics (Barash et al., 1999). An important question that arises is, what are the neural and behavioral underpinnings of the metric adjustment guaranteed by an intact oculomotor vermis?

One way to change the metric of a saccade is to modify its velocity. In fact, an encoding of saccade velocity has been demonstrated in the PC-SS discharge,

(Herzfeld et al., 2015, 2018) with maximum firing rates increasing linearly with saccade velocity. The metric of a saccade can also be changed by controlling its duration. Precise information on saccade duration is reflected in the duration of the population discharge (Thier et al., 2000; Catz et al., 2008). Further evidence for a role of vermal SSs in the encoding of kinematic parameters of eye movement also comes from studies of smooth-pursuit eye movements (Fukushima et al., 1996; Dash et al., 2013; Sun et al., 2017b, a) where the eyes track a slowly moving target. In such experiments, oculomotor vermal PCs exhibit a modulation of their SS discharge that reflects changes in eye movement speed.

Larger movement vigor may result in shorter movement times and higher velocities. Hence, could it be that changes in SS firing, seemingly related to changes in kinematic parameters such as velocity and duration, are actually a consequence of changes in the forces needed to move the eyes, accommodating changes of eye plant characteristics? This question has been addressed by Prsa et al. (2010) in which they asked monkeys to carry out stereotypic repetitive saccades. Monkeys and humans tested in such paradigms often exhibit a gradual drop in eye velocity not leading to changes in saccade amplitude, because saccade duration is cranked up in a compensatory manner (Brožek, 1949; Bahill et al., Baloh et al., 1975; 1975; Schmidt et al., 1979; Fuchs and Binder, 1983; Straube et al., 1997; Chen-Harris et al., 2008; Xu-Wilson et al., 2009). Prsa and colleagues looked at the abducens nucleus containing the motoneurons driving the muscles responsible for eye movements. It turned out that the relationship between movement kinematics and motoneuronal discharge remained constant throughout the experiment, clearly documenting that the oculomotor plant had not changed. In other words, the observed decrease in the eye velocity—fatigue—must be non-motor, arguably a consequence of a drop in motivation or

attention resulting from changes upstream of the plant and the abducens nucleus. Despite this drop, saccade amplitude remained the same as an intact vermis is able to upregulate saccade duration to an extent that is appropriate in order to compensate for the velocity decline. The evidence implicating the cerebellum in identifying the correct duration comes from lesion experiments: both experimental vermal lesions in rhesus monkeys (Barash et al., 1999) and natural lesions due to disease (Golla et al., 2008) that deteriorates the duration compensation. A fully analogous trade-off mechanism has been shown to compensate for fatigue affecting smooth-pursuit eye movements. In this case, it is the initial eye movement acceleration that exhibits a fatigue-induced decline which is again compensated by an increase in duration. Lesioning the OMV of monkeys destroys this capacity (Dash and Thier, 2013). The precise cerebellar control of movement duration needed to stabilize the metric of a movement is not confined to eye movements. As discussed later, in chapter 3.1 (and Appendix 1), it also holds for fast and precise, goal-directed pointing movements of the index finger of humans, also revealing this velocity–duration trade-off mechanism, which is severely compromised in patients with cerebellar degeneration (Markanday et al., 2018).

2.5 The mysteries and challenges of complex spikes

Unlike SSs, whose role in controlling movement kinematics rather than movement dynamics is supported by a consistent body of evidence, the role of rarely occurring CSs has been quite enigmatic. What information could these rarely occurring spikes characterized by unconventional duration and shapes possibly carry and what might be the best statistical approach to capture this

information? A burning question that has kept researchers busy until the present day.

However, addressing this question is associated with heavy costs, in terms of both effort and time spent in meticulously detecting these rare events hidden in a flood of SSs. It is their scarcity and complex morphology that makes CSs so tempting to study, yet it is exactly these properties that render several spike-sorting approaches unreliable. A slight error in their detection or false rejection may lead to a misinterpretation of their functional roles within the framework of the behavior at stake. Therefore, to avoid this risk, hitherto researchers had to resort to the tedious tasks of manually labeling these CSs. In chapter 3.2 (and Appendix 2), I present a deep neural network-based approach to reliably detect CSs and to measure their duration (Markanday et al., 2019).

2.6 Complex spikes encode error-related information: the classical view

Irrespective of all challenges associated with CS detection, there have been successful attempts to understand their functional role. To begin with, one of the most influential ideas suggesting the role of CSs in error-based learning was proposed by David Marr (1969), later elaborated further by James Albus (1971) and Masao Ito (1972). According to this Marr-Albus-Ito (MAI) hypothesis, motor learning is driven by CSs that serve as "teaching signals" that occur every time an error is experienced; error information is used to adjust the future motor behavior such as to avoid the same error. Mechanistically, the adjustment is based on the coincidence of CF driven CSs–reporting the error–and behavior-

related parallel fiber spikes. As a consequence of the coincidence, the efficacy of parallel fiber-to-PC synapse is downregulated, thereby modifying the PC output which is determined by the sum of all parallel fiber inputs.

One of the paradigms deployed to test the MAI-theory has been saccadic adaptation, elicited by shifting a saccade target during the saccade which results in an unexpected retinal error (McLaughlin, 1967). The direction and size of this error influences the amplitude of the subsequent saccades. In accordance with the basic tenet of the MAI-theory, Soetedjo et al. (2006; 2008a,b) and Herzfeld et al. (2015; 2018) indeed observed that CS fired by saccade-related PCs reflect retinal error, given by the vectorial distance of the image of a saccade target from the fovea. According to Herzfeld et al. (2018), it is mainly the vector´s direction that matters for the CS responses with little influence of its magnitude. The CS´s preferred direction (CS-ON) matters for the SSs fired by PCs. As shown by Herzfeld et al. (2015), the strength of the SS population response of PCs increases linearly with saccade speed. However, this increase was larger in the direction for which CSs did not respond to errors. In a follow-up study (Herzfeld et al., 2018), the same authors examined the influence of individual CSs on subsequent SS discharge rates within the framework of saccadic learning. They found that the presence of a CS, during the brief period between the end of the primary and the beginning of the subsequent corrective saccade, caused a decrease in the SS firing rate that "pulled" the direction of the subsequent saccade towards the CS-ON direction. In contrast, the absence of a CS, causing an increase in the SS activity, "pushed" the upcoming saccade in the opposite direction. This "push-pull" mechanism-based trial-by-trial learning in saccades, which is achieved by distinct modules of PCs sharing similar error information, is fully compatible with the central tenet of the MAI hypothesis. Further support also comes from studies on other forms of motor learning in which the firing of CSs was found to be

influenced by motor errors arising from various types of limb and eye movements (Gilbert and Thach, 1977; Oscarsson, 1980; Kim et al., 1987; Graf et al., 1988; Stone and Lisberger, 1990b; Barmack and Shojaku, 1995; Kitazawa et al., 1998; Kobayashi et al., 1998; Medina and Lisberger, 2008). However, not all findings are fully compatible with this view as discussed in the following chapter.

2.7 Stabilization of motor behavior by complex spikes

Error information conveyed by CSs may indeed explain the acquisition of a modified motor response such as a visually guided saccade of an altered metric. However, one could argue that it is not sufficient to acquire a modified motor skill. Rather the skill needs to be maintained, provided it is useful. In other words, the question is how can a spontaneous, gradual decay of a learned behavior be avoided once the learned behavior is able to minimize the error. Of course, maintenance could be simply passive. However, passive maintenance of a state is not very likely in a biological system in which every element undergoes continuous change. As a matter of fact, the CS may also play a central role in stabilizing the useful modification of motor behavior. This idea emerged from studies on two variants of oculomotor adaptation (Catz et al., 2005; Dash et al., 2010), namely short-term saccadic adaptation (STSA) and smooth-pursuit adaptation (SPA). While STSA stands for a consistent adjustment of saccade amplitude ensuring that the eyes land on target thereby avoiding retinal errors after the saccade, SPA reflects an adjustment of the initial velocity of a smooth pursuit eye movement that helps to minimize retinal velocity errors, i.e. the difference between the speed of the target and the speed of the eyes. Given that CSs are fired when errors occur, one would expect an increased CS firing at the beginning of learning, when errors are maximal, because the movement has not

yet been adapted. In contrast, at the end of adaptation, when errors are minimal, the CS firing should return to its baseline pattern. Contrary to this expectation, in both STSA and SPA, CSs turned out to fire spontaneously at the beginning of the adaptation experiment, followed by a gradual build-up of activity over the course of adaptation, a modulation that reached its maximum at the end of adaptation. According to the authors, these results suggest that in the absence of error, a persistent modulation of CS firing must be responsible for the stabilization of the modified behavior.

2.8 Complex spikes use the information on past errors to predict upcoming errors

A signal sensitive to current error is certainly able to elicit changes promising to avoid future errors. However, why waiting for an error to occur if the error could be predicted much earlier? The ability to predict an error would not only ensure earlier preparation, but also more reliable and robust modifications in case of concordance between the predicted and the actual error. Actually, looking at the repetitive nature of the STSA (Catz et al., 2005) and SPA paradigms (Dash et al., 2010), where predictive probabilities of error increase with time, one may argue that the build-up of CS activity during adaptation might reflect the expectation of future errors based on the evidence accumulated from the probability of occurrence of previous errors. In other words, the assumed ability of the CSs to stabilize the learned behavior in the absence of error may be a consequence of the system to predict that new errors would arise if the modifications were forgotten. This hypothesis is fully supported by a recent study of randomly occurring retinal errors by Junker et al. (2018). They could demonstrate that in a saccade paradigm with random errors, even individual errors had a significant

impact on future saccades made in the same direction. Moreover, their analysis of focusing on the influence of prevailing retinal errors on the subsequent saccades in monkeys pointed out that the direction and amplitude of current saccades can be traced back to errors that occurred up to six trials before. CSs that fired in response to instantaneous errors at the end of saccades were shown to be influenced by the direction of the prevailing retinal errors. The same error also influenced future saccades as reflected by the CS discharge that shifted to a period before the beginning of saccades. Also, recent work on eye-blink conditioning in mice supports this notion (Ohmae and Medina, 2015): in these eye-blink conditioning experiments associations between a conditioned stimulus (LED flashes) and an unconditioned stimulus (an unexpected and unpleasant air-puff) are established based on evidence accumulation. The authors observed that in the beginning CSs were elicited by the unconditioned stimulus. However, paralleling the accumulation of the predictive character of the flashes, the CS responses eventually shifted to the time of the conditioned stimulus that predicted the air-puffs.

2.9 Complex spikes convey information on the rhythmicity and timing of movements

An interesting feature of CSs that was unveiled by Linas and co-workers, was the 8-10 Hz rhythmic and synchronous activity of the climbing fibers. This firing pattern was a consequence of electronic coupling, mediated by the gap junctions (Llinas et al., 1974; Sotelo et al., 1974; King et al., 1976), between the inferior olive neurons and reminiscent of the temporal structure of many forms of motor behavior (Welsh et al., 1995; Leznik and Llinas, 2005), as well as physiological and pathological tremor (Llinás and Volkind, 1973). Together, these findings

suggested that CSs, independent of their influence on SSs, may play an important role in the timing of motor events. In chapter 3.3 (and Appendix 3) I will present findings that link to these earlier ideas that the climbing fiber system might play a key role in the temporal structuring of movements.

2.10 Encoding of reward-related information by complex spikes

In their study focusing on oculomotor fatigue, Prsa and colleagues (2010) proposed that the fatigue, characterized by a gradual decline in the vigor of saccades, must be cognitive in nature since no change in the activity of the oculomotor plant was observed. In line with this idea, several studies have convincingly demonstrated the influence of the subjective value of reward on movement vigor (Xu-Wilson et al., 2009; Reppert et al., 2012; Sedaghat-Nejad et al., 2019; Shadmehr et al., 2019; Muhammed et al., 2020). The ideas discussed by Prsa et al. were developed considering eye movements typically exhibiting a gradual loss of movement vigor. In a recent study requiring many repetitions of fast and accurate goal-directed index finger movements of healthy humans, which is presented in chapter 3.1 of this thesis, we could not see a similar decline. As discussed in detail later, we suggest that the absence of cognitive fatigue in this study was most probably a consequence of the interactive nature of the paradigm, that, by delivering performance feedback at the end of each trial may have sustained the motivation levels. Together, these observations strongly suggest that movement vigor can be considered as a proxy of motivation signals originating in the basal ganglia. Further support comes from studies that demonstrate clear anatomical connections between the cerebellum and the basal ganglia (Bostan and Strick, 2010; Bostan et al., 2013). Although direct glutamatergic projections from the DCNs to the ventral tegmental area with clear

behavioral implications have been recently discovered by Carta et al. (2019), the results of Wagner et al. (2017) establishing the influence of reward expectation at the level of granule cells, also suggest a downstream flow of information. Not only do the reward-related signals approach the cerebellum via the granule cells-parallel fiber pathway, but they are also conveyed via the CF system (Fallon et al., 1984). In a recent achievement, CFs have been shown to convey information on reward expectation, delivery, as well as an unexpected omission. This is achieved by activating specific microzones of PCs, each zone serving a specific function (Kostadinov et al., 2019). Concordant results have also been reported by Larry et al. (2019) by relying on an eye movement study in monkeys in which the size of the expected reward modulated the CS discharge.

Altogether, these findings clearly confirm the reciprocity of information flow between the cerebellum and the dopaminergic system, thereby pointing towards the role of the cerebellum in the processing of cognitive functions that may, directly or indirectly, influence the motor behavior.

2.11 Multiplexing of information by complex spikes

An intriguing aspect of CSs that was unveiled using the eye-blink conditioning paradigm in mice (Ohmae and Medina, 2015), apart from the predictive role of CSs mentioned before, was their ability to flexibly encode different stimuli within a recording session. This was based on the observation that the same CF that responded to an unexpected air-puff (unconditioned somatosensory stimulus) in the beginning, also responded later to a visual LED stimulus (conditioned stimulus) that predicted the air-puff.

A central chapter of this thesis (chapter 3.3, Appendix 3) presents evidence that is directly related to the idea of flexible encoding put forward by Ohmae and Medina (2015). Our own work, (Markanday et. al, 2020, under submission) that was based on exploring the vermal cerebellum of monkeys in a repetitive saccade paradigm suggests that CSs are fully capable of conveying more than one type of information, simultaneously. These results clearly indicate that the rarely firing CSs are fully capable of conveying a wide spectrum of behaviorally relevant information in a multiplexed manner.

3. SUMMARY OF THE SCIENTIFIC FINDINGS

3.1 Study 1

A loss of a velocity-duration trade-off impairs movement precision in patients with cerebellar degeneration

Akshay Markanday, Julian Messner, and Peter Thier

Eur. J. Neurosci. 48:1976–89, 2018

When looking at the patients suffering from cerebellar ataxia, the idea of cerebellar contributions to motor control and coordination becomes directly evident. What is not fully understood are the cerebellar mechanisms underlying motor control and learning. To address these mechanisms, we studied fast and precise, goal-directed index finger movements in cerebellar patients and healthy human subjects. We found an adjustment mechanism that fine-tunes movement durations by using the information on the expected velocity of the upcoming movements. Changes in velocity, that most likely reflect trial-to-trial fluctuations of motivational states, are continuously monitored, and compensated by the cerebellum to ensure movement accuracy. We argue that an increased end-point variability ('motor noise') of movements, the hallmark of ataxia, is a direct consequence of the loss of this velocity-duration trade-off mechanism, which may also explain deficits in learning as well as dysmetria observed in movements.

3.2 Study 2

Using deep neural networks to detect complex spikes of cerebellar Purkinje cells

Akshay Markanday, Joachim Bellet, Marie E. Bellet, Junya Inoue, Ziad M. Hafed, and Peter Thier

J. Neurophysiol., 2020

Several contemporary ideas discussing the role of the cerebellum are centered on complex spikes, arguably one of the most fascinating features of the Purkinje cell discharge. However, owing to their perplexingly low firing rates as well as complex wave morphology, detecting these events reliably becomes a serious challenge, even for well-established spike sorting approaches. With such low firing rates, the consequences of falsely detecting or missing a few spikes can change the entire interpretation of their role. Therefore, to avoid this risk, cerebellum researchers resort to extremely tedious, manual labeling of these events. Here, we present a deep learning algorithm that utilizes information on the high band-passed action potential spectral band and the accompanying low-passed local field potentials band in extracellular records of Purkinje cells activity to detect complex spikes at a much faster speed and an accuracy, comparable to that of human experts. Our algorithm, while outperforming other existing approaches, additionally provides important information on complex spike duration, that may contain relevant information on learning.

3.3 Study 3

Multiplexing of information by cerebellar complex spikes

Akshay Markanday, Junya Inoue, Peter W. Dicke, and Peter Thier

Under submission, 2020

Purkinje cell discharge, the only output of the cerebellar cortex, is characterized by two types of action potentials, high-frequency simple spikes and low-frequency complex spikes. While there is enough evidence that simple spikes convey the information needed to optimize movement kinematics, the functional role of complex spikes is still a burning topic of debate. While initially thought to be specialized in conveying error-related information, serving as a "teaching signal" for the subsequent correction of behavior, several findings have unveiled features of complex spikes that seem to contribute to other aspects of motor behavior as well. Considering such bewildering diversity of findings and views unraveled by highly specific tasks, one may wonder if there is more than just one absolute function, as suggested by the classical error-encoding concept? Or are there distinct pools of PCs with each pool processing a specific stream of information conveyed by climbing fibers resulting in the observed diversity of findings? To address these questions, we recorded complex spikes from the oculomotor vermis of two monkeys tested in a repetitive saccade task that entailed sizable motor errors, as well as microsaccades correcting them. Consistent with the classical view, we observed that complex spikes indeed conveyed error-related information. However, we observed that the same climbing fibers also conveyed information on the metrics of both primary(macro)

and the secondary(micro) saccades. Additionally, we found that complex spikes responded to the onset of trials in a temporally precise manner, that seemed to predict the upcoming events. Furthermore, we also observed clear changes in complex spike duration that seemed to parallel changes in firing rates. To the best of our knowledge, this is the first study that demonstrates such versatility of complex spikes responses, within one paradigm thus pointing towards their role in multiplexing of behaviorally relevant information.

3.4 Study 4

Role of the vermal cerebellum in visually guided eye movements and visual motion perception

Peter Thier and Akshay Markanday

Annu. Rev. Vis. Sci. 5, 247-268, 2019

In this review, we discuss the role of distinct oculomotor regions of the cerebellum with emphasis on the role of the oculomotor vermis in the control of the two variants of visually guided eye movements—visually guided saccades and smooth-pursuit eye movements. In both types of eye movements, information on past retinal errors is used to optimize future oculomotor behavior. While in the case of visually guided saccades this mapping of visual error onto a motor vector is reflected in the amplitude and direction of the subsequent saccades, it is observed as adjustments of velocity in the case of the upcoming smooth-pursuit eye movements. As a consequence of the stereotypic architecture of the canonical microcircuit repeated throughout the cerebellar cortex, the computational principles underlying sensorimotor transformations unraveled by studies of the oculomotor vermis in the control of goal-directed eye movements, most probably, also apply to other forms of movements controlled by other parts of the cerebellum. The review also touches on the neglected role of the cerebellum in visual motion perception as an example of a non-motor function of the human cerebellum and tries to link these non-motor functions to the role of the cerebellum in dealing with ego-motion.

4. CONCLUSIONS AND FUTURE PERSPECTIVES: PUTTING THE PIECES TOGETHER

An important consideration that motivated this dissertation is to appreciate that our current understanding of the cerebellum owes a significant share to the success and failures of various multi-disciplinary approaches adopted in the past. In an attempt to present a "Gestalt view" of the cerebellum, this dissertation relies on results gathered across different approaches, all aimed at understanding the underlying principles of cerebellar function.

In this dissertation, I have proposed a cerebellum-based velocity-duration trade-off mechanism that ensures movement accuracy by continuously updating movement duration in response to trial-by-trial velocity fluctuations. Not only does this result tell us about the functioning of the normal cerebellum, but it also provides an explanation for the increased motor noise observed in patients suffering from cerebellar ataxia. Although some computational models of ataxia have been able to reliably predict consistent metric deviations ('dysmetria') in movements by assuming an inability to correct a systematic bias in internal models (Bhanpuri et al., 2014), they fail to explain motor noise, the hallmark of ataxia. Or to put it differently, ataxia could be understood as a consequence of the loss of a normal cerebellar capacity to mitigate motor noise. Guided by this perspective, future research will have to strive for more sophisticated and realistic models of the cerebellum incorporating the need to predict future performance errors as a way to mitigate motor noise in an adaptive manner. The benefits of such realistic models may have important implications for therapeutic interventions.

The virtue of these computational models notwithstanding, we may still be far from capturing the full spectrum of behavioral deficits associated with cerebellar disorders due to our limited understanding of the cerebellum. Specifically, in the case of CSs, in which a large dissent on their suggested functions instigated Streng et al. (2017) to adopt the metaphor of “complex spike wars” in an attempt to describe the great variety of hardly compatible functions attributed to the climbing fiber system. However, this war does not have a winner. An aspiring scientist who may believe to have identified the holy grail of CS function with all others failing may share the fate of blind men from the old Indian parable who try to grasp the concept of an elephant based on their isolated subjective experiences of a trunk, a tail, an ear, etc. Therefore, rather than proposing an "either-or" role of these CSs, the results of our study provide a unifying framework for these different findings. We suggest that these different views may actually be a subset of one bigger picture—a rather generalized function, in which CSs can flexibly encode a rich spectrum of behaviorally-relevant streams information in a multiplexed manner, useful to optimize goal-directed motor behavior. Our findings have clear implications for the functional architecture of the inferior olive. These findings suggest that the inferior olive realizes a selection mechanism prioritizing the most relevant input information and, that it is able to funnel the prioritized information to any target PC, resorting to dynamically controlled crosstalk at the level of the inferior olive. The latter seems indispensable as the basis of information in the absence of an architecture accommodating dynamic switching at the level of the PC. This would require that quite a few climbing fibers with different functional identities would have access to a given PC. However, unlike the PCs during early stages of development, we know that adult PCs receive input from one climbing fiber only (Eccles et al., 1967).

There is preliminary evidence (Sugihara and Shinoda, 2004) that indeed different types of information arrive in different parts of the olivary nucleus. One may speculate that crosstalk between these different parts could be accommodated by the well-known gap junctions connecting olivary neurons, subject to feedback control from the cerebellar nuclei (Llinas et al., 1974; Sotelo et al., 1974; De Zeeuw et al., 1989; Leznik and Llinas, 2005; Lefler et al., 2020). In other words, flexible control of the electrically coupled olivary gap junctions could be the basis of the assumed multiplexed code. Testing this idea may require paired recordings from olivary neurons belonging to neighboring clusters, with each cluster being a recipient of distinct streams of afferent information.

The blueprint of the cerebellum laid out in Eccles´, Szentagothai´s and Ito´s 'The Cerebellum as a Neuronal Machine', more than 50 years ago, seemed to suggest that we might have reached a pretty much complete understanding of this fascinating part of the brain. However, as always in science, there are no definite answers and any attempt to give a final answer will soon lead to more questions. This also holds for the cerebellum, and arguably its most enigmatic element, the climbing fiber system responsible for the complex spike. Hence, we hardly expect that our idea that the climbing fiber system broadcasts information in a multiplexed manner will turn out to be the ultimate answer to the function of the climbing fiber system. However, we may be confident that this concept will stimulate useful future work. This work will undoubtedly benefit from an important achievement of this dissertation, namely the development of a fully-automated deep learning algorithm for complex spike detection and characterization, significantly reducing the amount of time and effort needed to study these events which have been central to our thinking about the cerebellum, ever since David Marr´s theory of cerebellar cortex.

5. REFERENCES

Albus JS (1971) A theory of cerebellar function. Mathematical Biosciences 10:25-61.

Apps R, Hawkes R, Aoki S, Bengtsson F, Brown AM, Chen G, Ebner TJ, Isope P, Jörntell H, Lackey EP (2018) Cerebellar modules and their role as operational cerebellar processing units. The Cerebellum 17:654-682.

Armstrong D, Harvey R, Schild RF (1973) Cerebello-cerebellar responses mediated via climbing fibres. Experimental Brain Research 18:19-39.

Aschoff JC, Cohen B (1971) Changes in saccadic eye movements produced by cerebellar cortical lesions. Experimental Neurology 32:123-133.

Azevedo FA, Carvalho LR, Grinberg LT, Farfel JM, Ferretti RE, Leite RE, Filho WJ, Lent R, Herculano-Houzel S (2009) Equal numbers of neuronal and nonneuronal cells make the human brain an isometrically scaled-up primate brain. Journal of Comparative Neurology 513:532-541.

Babinski J (1902) Hemiasynergie, lateropulsion et myosis bulbaires avec hemianesthesie et hemiplegie crois ees. Rev Neurol (Paris) 10:358-365.

Bahill AT, Clark MR, Stark L (1975) The main sequence, a tool for studying human eye movements. Mathematical biosciences 24:191-204.

Baloh RW, Sills AW, Kumley WE, Honrubia V (1975) Quantitative measurement of saccade amplitude, duration, and velocity. Neurology 25:1065-1065.

Barash S, Melikyan A, Sivakov A, Zhang M, Glickstein M, Thier P (1999) Saccadic Dysmetria and Adaptation after Lesions of the Cerebellar Cortex. The Journal of Neuroscience 19:10931-10939.

Barmack NH, Shojaku H (1995) Vestibular and visual climbing fiber signals evoked in the uvula-nodulus of the rabbit cerebellum by natural stimulation. Journal of neurophysiology 74:2573-2589.

Bhanpuri NH, Okamura AM, Bastian AJ (2014) Predicting and correcting ataxia using a model of cerebellar function. Brain 137:1931-1944.

Brochu G, Maler L, Hawkes R (1990) Zebrin II: a polypeptide antigen expressed selectively by Purkinje cells reveals compartments in rat and fish cerebellum. Journal of Comparative Neurology 291:538-552.

BroŽek J (1949) Quantitative criteria of oculomotor performance and fatigue. Journal of applied physiology 2:247-260.

Catz N, Dicke PW, Thier P (2005) Cerebellar complex spike firing is suitable to induce as well as to stabilize motor learning. Current Biology 15:2179-2189.

Catz N, Dicke PW, Thier P (2008) Cerebellar-dependent motor learning is based on pruning a Purkinje cell population response. Proceedings of the National Academy of Sciences 105:7309-7314.

Chen-Harris H, Joiner WM, Ethier V, Zee DS, Shadmehr R (2008) Adaptive control of saccades via internal feedback. Journal of Neuroscience 28:2804-2813.

Dash S, Thier P (2013) Smooth pursuit adaptation (SPA) exhibits features useful to compensate changes in the properties of the smooth pursuit eye movement system due to usage. Frontiers in Systems Neuroscience 7.

Dash S, Dicke PW, Thier P (2013) A vermal Purkinje cell simple spike population response encodes the changes in eye movement kinematics due to smooth pursuit adaptation. Frontiers in systems neuroscience 7:3.

Dash S, Catz N, Dicke PW, Thier P (2010) Specific vermal complex spike responses build up during the course of smooth-pursuit adaptation, paralleling the decrease of performance error. Experimental brain research 205:41-55.

Davie JT, Clark BA, Häusser M (2008) The origin of the complex spike in cerebellar Purkinje cells. Journal of Neuroscience 28:7599-7609.

De Zeeuw C, Holstege J, Ruigrok T, Voogd J (1989) Ultrastructural study of the GABAergic, cerebellar, and mesodiencephalic innervation of the cat medial accessory olive: anterograde tracing combined with immunocytochemistry. Journal of Comparative Neurology 284:12-35.

Desclin JC (1974) Histological evidence supporting the inferior olive as the major source of cerebellar climbing fibers in the rat. Brain research 77:365-384.

Ebner TJ, Hewitt AL, Popa LS (2011) What features of limb movements are encoded in the discharge of cerebellar neurons? Cerebellum (London, England) 10:683-693.

Eccles JC (1967) Circuits in the cerebellar control of movement. Proceedings of the National Academy of Sciences of the United States of America 58:336.

Eccles JC, Llinas R, Sasaki K (1966) The excitatory synaptic action of climbing fibres on the Purkinje cells of the cerebellum. J Physiol 182:268-296.

Eccles JC, Ito M, Szentágothai J (1967) The cerebellum as a neuronal machine, 1967. Berlin, New York etc: Springer-Verlag.

Endo H, Hayashi Y, Komiya T, Narushima E, Sasaki M (2001) Muscle architecture of the elongated nose in the Asian elephant (Elephas maximus). Journal of Veterinary Medical Science 63:533-537.

Flourens M-J-P (1824) Recherches experimentales sur les propietes et fonctions due systeme nerveus dans les animaus vertebres. Paris. Polster, MR, Nadel, L, and Schacter, DL (1991) Cognitive neuroscience analysis of memory: A historical perspective Journal of Cognitive Neuroscience 3:95-116.

Fortier PA, Kalaska JF, Smith AM (1989) Cerebellar neuronal activity related to whole-arm reaching movements in the monkey. Journal of Neurophysiology 62:198-211.

Fortier PA, Smith AM, Kalaska JF (1993) Comparison of cerebellar and motor cortex activity during reaching: directional tuning and response variability. Journal of Neurophysiology 69:1136-1149.

Frysinger RC, Bourbonnais D, Kalaska JF, Smith AM (1984) Cerebellar cortical activity during antagonist cocontraction and reciprocal inhibition of forearm muscles. Journal of Neurophysiology 51:32-49.

Fuchs AF, Binder MD (1983) Fatigue resistance of human extraocular muscles. Journal of neurophysiology 49:28-34.

Fujita Y (1968) Activity of dendrites of single Purkinje cells and its relationship to so-called inactivation response in rabbit cerebellum. Journal of Neurophysiology 31:131-141.

Fukushima K, Tanaka M, Suzuki Y, Fukushima J, Yoshida T (1996) Adaptive changes in human smooth pursuit eye movement. Neuroscience Research 25:391-398.

Gilbert P, Thach W (1977) Purkinje cell activity during motor learning. Brain research 128:309-328.

Glickstein M, Strata P, Voogd J (2009) Cerebellum: history. Neuroscience 162:549-559.
Golgi C (1883) Recherches sur l'histologie des centres nerveux.
Golla H, Tziridis K, Haarmeier T, Catz N, Barash S, Thier P (2008) Reduced saccadic resilience and impaired saccadic adaptation due to cerebellar disease. European Journal of Neuroscience 27:132-144.
Graf W, Simpson JI, Leonard CS (1988) Spatial organization of visual messages of the rabbit's cerebellar flocculus. II. Complex and simple spike responses of Purkinje cells. Journal of Neurophysiology 60:2091-2121.
Harvey R, Porter R, Rawson J (1979) Discharges of intracerebellar nuclear cells in monkeys. J Physiol 297:559-580.
Herculano-Houzel S (2009) The human brain in numbers: a linearly scaled-up primate brain. Frontiers in human neuroscience 3:31.
Herzfeld DJ, Kojima Y, Soetedjo R, Shadmehr R (2015) Encoding of action by the Purkinje cells of the cerebellum. Nature 526:439-442.
Herzfeld DJ, Kojima Y, Soetedjo R, Shadmehr R (2018) Encoding of error and learning to correct that error by the Purkinje cells of the cerebellum. Nature Neuroscience 21:736-743.
Hillman DE (1969) Light and electron microscopical study of the relationships between the cerebellum and the vestibular organ of the frog. Experimental Brain Research 9:1-15.
Holmes G (1917) The symptoms of acute cerebellar injuries due to gunshot injuries. Brain 40:461-535.
Ignashchenkova A, Dash S, Dicke PW, Haarmeier T, Glickstein M, Thier P (2009) Normal Spatial Attention But Impaired Saccades and Visual Motion Perception After Lesions of the Monkey Cerebellum. Journal of Neurophysiology 102:3156-3168.
Ito M (1972) Neural design of the cerebellar motor control system. Brain research 40:81-84.
Junker M, Endres D, Sun ZP, Dicke PW, Giese M, Thier P (2018) Learning from the past: A reverberation of past errors in the cerebellar climbing fiber signal. PLoS biology 16:e2004344.
Kim JH, Wang J, Ebner TJ (1987) Climbing fiber afferent modulation during treadmill locomotion in the cat. Journal of Neurophysiology 57:787-802.
King J, Andrezik JA, Falls W, Martin G (1976) The synaptic organization of the cerebello-oiivary circuit. Experimental brain research 26:159-170.
Kitazawa S, Kimura T, Yin P-B (1998) Cerebellar complex spikes encode both destinations and errors in arm movements. Nature 392:494-497.
Kobayashi Y, Kawano K, Takemura A, Inoue Y, Kitama T, Gomi H, Kawato M (1998) Temporal firing patterns of Purkinje cells in the cerebellar ventral paraflocculus during ocular following responses in monkeys II. Complex spikes. Journal of neurophysiology 80:832-848.
Lefler Y, Amsalem O, Vrieler N, Segev I, Yarom Y (2020) Using subthreshold events to characterize the functional architecture of the electrically coupled inferior olive network. Elife 9:e43560.
Leznik E, Llinas R (2005) Role of gap junctions in synchronized neuronal oscillations in the inferior olive. Journal of neurophysiology 94:2447-2456.
Llinas R, Baker R, Sotelo C (1974) Electrotonic coupling between neurons in cat inferior olive. Journal of neurophysiology 37:560-571.

Llinás R, Volkind R (1973) The olivo-cerebellar system: functional properties as revealed by harmaline-induced tremor. Experimental Brain Research 18:69-87.
Llinás R, Sugimori M (1980) Electrophysiological properties of in vitro Purkinje cell dendrites in mammalian cerebellar slices. J Physiol 305:197-213.
Luciani L (1891) Il cervelletto; nuovi studi di fisiologia normale e patologica: Le Monnier.
Madigan JC, Carpenter MB (1971) Cerebellum of the rhesus monkey.
Malacarne V (1776) Nuova esposizione della vera struttura del cervelletto umano di Vincenzo Malacarne: Appresso Giammichele Briolo nella contrada de'guardinfanti.
Markanday A, Messner J, Thier P (2018) A loss of a velocity-duration trade-off impairs movement precision in patients with cerebellar degeneration. European Journal of Neuroscience 48:1976-1989.
Markanday A, Bellet J, Bellet ME, Inoue J, Hafed ZM, Thier P (2019) Using deep neural networks to detect complex spikes of cerebellar Purkinje Cells. Journal of Neurophysiology.
Marr D (1969) A theory of cerebellar cortex. J Physiol 202:437-470.
Marshall LH, Magoun HW (2013) Discoveries in the human brain: Neuroscience prehistory, brain structure, and function: Springer Science & Business Media.
Maseko BC, Spocter MA, Haagensen M, Manger PR (2012) Elephants have relatively the largest cerebellum size of mammals. The Anatomical Record: Advances in Integrative Anatomy and Evolutionary Biology 295:661-672.
McLaughlin SC (1967) Parametric adjustment in saccadic eye movements. Perception & Psychophysics 2:359-362.
Medina JF, Lisberger SG (2008) Links from complex spikes to local plasticity and motor learning in the cerebellum of awake-behaving monkeys. Nature neuroscience 11:1185-1192.
Napper R, Harvey R (1988) Number of parallel fiber synapses on an individual Purkinje cell in the cerebellum of the rat. Journal of Comparative Neurology 274:168-177.
Nishiyama H, Linden DJ (2004) Differential maturation of climbing fiber innervation in cerebellar vermis. Journal of Neuroscience 24:3926-3932.
Noda H, Mikami A (1986) Discharges of neurons in the dorsal paraflocculus of monkeys during eye movements and visual stimulation. Journal of neurophysiology 56:1129-1146.
Ohki M, Kitazawa H, Hiramatsu T, Kaga K, Kitamura T, Yamada J, Nagao S (2009) Role of Primate Cerebellar Hemisphere in Voluntary Eye Movement Control Revealed by Lesion Effects. Journal of Neurophysiology 101:934-947.
Ohmae S, Medina JF (2015) Climbing fibers encode a temporal-difference prediction error during cerebellar learning in mice. Nature neuroscience 18:1798-1803.
Ohtsuka K, Enoki T (1998) Transcranial magnetic stimulation over the posterior cerebellum during smooth pursuit eye movements in man. Brain 121:429-435.
Oscarsson O (1980) Functional organization of olivary projection to the cerebellar anterior lobe. The Inferior Olivary Nucleus:279-290.
Pettigrew JD, Bhagwandin A, Haagensen M, Manger PR (2010) Visual acuity and heterogeneities of retinal ganglion cell densities and the tapetum lucidum of the African elephant (Loxodonta africana). Brain, Behavior and Evolution 75:251-261.
Prsa M, Dicke PW, Thier P (2010) The absence of eye muscle fatigue indicates that the nervous system compensates for non-motor disturbances of oculomotor function. Journal of Neuroscience 30:15834-15842.

Purkinje JE (1837) Neueste Untersuchungen aus der Nerven und Hirn Anatomie. Bericht über die Versammlung deutscher Naturforscher und Aerzte in Prag im September 1883:177-180.

Ramón y Cajal S (1894) The Croonian lecture.—La fine structure des centres nerveux. Proceedings of the Royal Society of London 55:444-468.

Ritchie L (1976) Effects of cerebellar lesions on saccadic eye movements. Journal of Neurophysiology 39:1246-1256.

Robinson DA (1976) Adaptive gain control of vestibuloocular reflex by the cerebellum. Journal of Neurophysiology 39:954-969.

Roitman AV, Pasalar S, Johnson MTV, Ebner TJ (2005) Position, Direction of Movement, and Speed Tuning of Cerebellar Purkinje Cells during Circular Manual Tracking in Monkey. The Journal of Neuroscience 25:9244-9257.

Ron S, Robinson DA (1973) Eye movements evoked by cerebellar stimulation in the alert monkey. Journal of Neurophysiology 36:1004-1022.

Rosina A, Provini L (1983) Somatotopy of climbing fiber branching to the cerebellar cortex in cat. Brain research 289:45-63.

Ruigrok T, Voogd J (1990) Cerebellar nucleo-olivary projections in the rat: An anterograde tracing study with Phaseolus vulgaris-leucoagglutinin (PHA-L). Journal of Comparative Neurology 298:315-333.

Ruigrok T, Voogd J (2000) Organization of projections from the inferior olive to the cerebellar nuclei in the rat. Journal of Comparative Neurology 426:209-228.

Sato H, Noda H (1992) Posterior vermal Purkinje cells in macaques responding during saccades, smooth pursuit, chair rotation and/or optokinetic stimulation. Neuroscience Research 12:583-595.

Schmidt D, Abel L, DellOsso L, Daroff R (1979) Saccadic velocity characteristics- Intrinsic variability and fatigue. Aviation, space, and environmental medicine 50:393-395.

Sereno MI, Diedrichsen J, Tachrount M, Testa-Silva G, d'Arceuil H, De Zeeuw C (2020) The human cerebellum has almost 80% of the surface area of the neocortex. Proceedings of the National Academy of Sciences 117:19538-19543.

Soetedjo R, Fuchs AF (2006) Complex spike activity of purkinje cells in the oculomotor vermis during behavioral adaptation of monkey saccades. Journal of Neuroscience 26:7741-7755.

Soetedjo R, Kojima Y, Fuchs AF (2008a) Complex spike activity in the oculomotor vermis of the cerebellum: a vectorial error signal for saccade motor learning? Journal of neurophysiology 100:1949-1966.

Soetedjo R, Kojima Y, Fuchs A (2008b) Complex spike activity signals the direction and size of dysmetric saccade errors. In: Progress in brain research, pp 153-159: Elsevier.

Sotelo C, Llinás R, Baker R (1974) Structural study of inferior olivary nucleus of the cat: morphological correlates of electrotonic coupling. Journal of neurophysiology 37:541-559.

Stone L, Lisberger S (1990a) Visual responses of Purkinje cells in the cerebellar flocculus during smooth-pursuit eye movements in monkeys. I. Simple spikes. Journal of neurophysiology 63:1241-1261.

Stone L, Lisberger S (1990b) Visual responses of Purkinje cells in the cerebellar flocculus during smooth-pursuit eye movements in monkeys. II. Complex spikes. Journal of Neurophysiology 63:1262-1275.

Straube A, Fuchs AF, Usher S, Robinson FR (1997) Characteristics of saccadic gain adaptation in rhesus macaques. Journal of neurophysiology 77:874-895.

Streng ML, Popa LS, Ebner TJ (2017) Climbing fibers control Purkinje cell representations of behavior. Journal of Neuroscience 37:1997-2009.

Stuart G, Häusser M (1994) Initiation and spread of sodium action potentials in cerebellar Purkinje cells. Neuron 13:703-712.

Sugihara I, Shinoda Y (2004) Molecular, topographic, and functional organization of the cerebellar cortex: a study with combined aldolase C and olivocerebellar labeling. Journal of Neuroscience 24:8771-8785.

Sultan F, Braitenberg V (1993) Shapes and sizes of different mammalian cerebella. s study in quantitative comparative neuroanatomy. Journal fur Hirnforschung 34:79-79.

Sun Z, Smilgin A, Junker M, Dicke PW, Thier P (2017a) The same oculomotor vermal Purkinje cells encode the different kinematics of saccades and of smooth pursuit eye movements. Scientific Reports 7:40613.

Sun Z, Smilgin A, Junker M, Dicke PW, Thier P (2017b) Short-term adaptation of saccades does not affect smooth pursuit eye movement initiation. Journal of Vision 17:19-19.

Suzuki DA, Keller EL (1988a) The role of the posterior vermis of monkey cerebellum in smooth-pursuit eye movement control. II. Target velocity-related Purkinje cell activity. Journal of Neurophysiology 59:19-40.

Suzuki DA, Keller EL (1988b) The role of the posterior vermis of monkey cerebellum in smooth-pursuit eye movement control. I. Eye and head movement-related activity. Journal of Neurophysiology 59:1-18.

Takagi M, Zee DS, Tamargo RJ (1998) Effects of Lesions of the Oculomotor Vermis on Eye Movements in Primate: Saccades. Journal of Neurophysiology 80:1911-1931.

Takagi M, Zee DS, Tamargo RJ (2000) Effects of Lesions of the Oculomotor Cerebellar Vermis on Eye Movements in Primate: Smooth Pursuit. Journal of Neurophysiology 83:2047-2062.

Thach W (1968) Discharge of Purkinje and cerebellar nuclear neurons during rapidly alternating arm movements in the monkey. Journal of neurophysiology 31:785-797.

Thach W (1970a) Discharge of cerebellar neurons related to two maintained postures and two prompt movements. II. Purkinje cell output and input. Journal of Neurophysiology 33:537-547.

Thach W (1970b) Discharge of cerebellar neurons related to two maintained postures and two prompt movements. I. Nuclear cell output. Journal of Neurophysiology 33:527-536.

Thier P (2011) The oculomotor cerebellum. The Oxford handbook of eye movements:173-193.

Thier P, Möck M (2006) The oculomotor role of the pontine nuclei and the nucleus reticularis tegmenti pontis. Progress in brain research 151:293-320.

Thier P, Dicke PW, Haas R, Barash S (2000) Encoding of movement time by populations of cerebellar Purkinje cells. Nature 405:72-76.

Thier, P., & Markanday, A. (2019). Role of the vermal cerebellum in visually guided eye movements and visual motion perception. *Annual review of vision science, 5*, 247-268.

Vahedi K, Rivaud S, Amarenco P, Pierrot-Deseilligny C (1995) Horizontal eye movement disorders after posterior vermis infarctions. Journal of Neurology, Neurosurgery & Psychiatry 58:91-94.

Voogd J (1969) The importance of fiber connections in the comparative anatomy of the mammalian cerebellum. Neurology of Cerebellar Evolution and Development:493-514.

Wadiche JI, Jahr CE (2005) Patterned expression of Purkinje cell glutamate transporters controls synaptic plasticity. Nature neuroscience 8:1329-1334.

Wang X, Chen G, Gao W, Ebner TJ (2011) Parasagittally aligned, mGluR1-dependent patches are evoked at long latencies by parallel fiber stimulation in the mouse cerebellar cortex in vivo. Journal of neurophysiology 105:1732-1746.

Welsh JP, Lang EJ, Suglhara I, Llinás R (1995) Dynamic organization of motor control within the olivocerebellar system. Nature 374:453-457.

Wetts R, Kalaska JF, Smith AM (1985) Cerebellar nuclear cell activity during antagonist cocontraction and reciprocal inhibition of forearm muscles. Journal of Neurophysiology 54:231-244.

Xiao J, Cerminara NL, Kotsurovskyy Y, Aoki H, Burroughs A, Wise AK, Luo Y, Marshall SP, Sugihara I, Apps R (2014) Systematic regional variations in Purkinje cell spiking patterns. PloS one 9:e105633.

Xu-Wilson M, Zee DS, Shadmehr R (2009) The intrinsic value of visual information affects saccade velocities. Experimental Brain Research 196:475-481.

6. APPENDED PAPERS/MANUSCRIPTS

Appendix 1:

Markanday, A., Messner, J., & Thier, P. (2018). A loss of a velocity-duration trade-off impairs movement precision in patients with cerebellar degeneration. *European Journal of Neuroscience*, *48*(4), 1976-1989.

Appendix 2:

Markanday, A., Bellet, J., Bellet, M. E., Inoue, J., Hafed, Z. M., & Thier, P. (2019). Using deep neural networks to detect complex spikes of cerebellar Purkinje Cells. *Journal of Neurophysiology*.

Appendix 3:

Markanday, A., Inoue, J., Dicke, P. W., & Thier, P. (2020). Multiplexing of information by cerebellar complex spikes, Under submission, 2020.

Appendix 4:

Thier, P., & Markanday, A. (2019). Role of the vermal cerebellum in visually guided eye movements and visual motion perception. *Annual review of vision science*, *5*, 247-268.

7. STATEMENT OF PERSONAL CONTRIBUTION

Study 1: Markanday, A., Messner, J., & Thier, P. (2018). A loss of a velocity-duration trade-off impairs movement precision in patients with cerebellar degeneration. European Journal of Neuroscience, 48(4), 1976-1989.

A. M., J. M., and P. T. designed the experiments and worked on the manuscript. A. M. and J.M. conducted the experiments. A.M and J. M. collected the clinical data and A. M. performed the data analysis. A. M. and J. M. contributed equally to this project.

Study 2: Markanday, A., Bellet, J., Bellet, M. E., Inoue, J., Hafed, Z. M., & Thier, P. (2019). Using deep neural networks to detect complex spikes of cerebellar Purkinje Cells. Journal of Neurophysiology.

A.M., J.B., Z.M.H., and P.T. conceived and designed the research. A.M. performed all experiments. A.M., J.B., M.E.B., J.I., Z.M.H., and P.T. interpreted the results of the experiments. A.M., J.B., J.I., Z.M.H., and P.T. prepared the figures. A.M., J.B., M.E.B., J.I., Z.M.H., and P.T. drafted the manuscript. A.M., J.B., M.E.B., J.I., Z.M.H., and P.T. edited and revised the manuscript. A.M., J.B., J.I., Z.M.H., and P.T. approved the final version of the manuscript. J.B., M.E.B., J.I., and A.M. analyzed the data. A. M. and J. B. contributed equally to this project.

Study 3: Markanday, A., Inoue, J., Dicke, P. W., & Thier, P. (2020). Multiplexing of information by cerebellar complex spikes, Under revision, 2020.

A. M. and P.T designed the experiments. A.M., P.D., and P.T., planned and performed the surgical procedures. A.M. performed all experiments. A.M., and J.I analyzed the data. A. M., J. I., and P. T. interpreted the results and drafted the manuscript.

Study 4: Thier, P., & Markanday, A. (2019). Role of the vermal cerebellum in visually guided eye movements and visual motion perception. Annual review of vision science, 5, 247-268.

M. and P.T drafted and edited the manuscript. A.M prepared the figures. A.M and P.T approved the final draft of the manuscript.

8. ACKNOWLEDGMENTS

"No one can whistle a symphony. It takes a whole orchestra to play it." – H.E. Luccock

It is difficult for me to express this ambivalent feeling of "accomplishment" associated with the end of my doctoral journey, especially when I know that my scientific endeavor has just begun. Nevertheless, the contribution of so many people in myriad ways, that helped me achieve this important milestone of my life, has enriched me with so many valuable lessons that the only feeling I can truly express at this point in time is the one of gratitude.

A 'thank you' cannot bear the weight of feelings that I have for my parents, who would sacrifice their own comforts and desires just to catch a glimpse of a smile on my face. The social and moral values that you instilled into my character provides me with clarity of thought and decisions regarding my personal and scientific life. The unconditional love and faith of my sister have been a constant source of all positivity and hope in my life. However, if there is anyone who could tell the number of Purkinje cells recorded in a day, by just looking at my face, is my beloved wife. You have been through all—my highest highs and lowest lows. But your consistent love, motivation, and support continue to provide all the strength and encouragement I need in my life. Every bit of my life and work is dedicated to these three pillars of my life.

To say that this dissertation would not have been possible without my mentor, Peter Thier would only belittle his tremendous contribution towards my scientific, as well as personal development. Your unprejudiced, patient and gentle nature gave me an excellent opportunity to learn and nurture my scientific mind. Your regular lab visits followed by the "anything new?" question, was a daily dose of motivation in times of frustration and failures. The vast knowledge and experience across different walks of life, accompanied by your impeccable eye for

the finest detail, yet the ability to foresee an overall picture is truly inspiring. The knowledge and the experiences that you shared during our discussions, along with your guidance through difficult times in my scientific and personal life are unforgettable. I feel privileged to be your student, and I express my deepest respect and gratitude for all the help, efforts, and time you invested in shaping me into a scientist.

I would like to take this opportunity to sincerely thank Uwe Ilg for all his scientific and personal guidance. Every moment spent with you is a moment of knowledge, joy, and positivity. I also thank Peter Dicke and Friedemann Bunjes for all their help and support that not only made science look easy, but also fun. Your company is a great learning experience. My special thanks to Dagmar Schmerold and Ute Grosshennig who not only took care of all the administrative work but also inspired me through their extremely dedicated, perfectionist yet charming attitude towards work. Here, I would also express my sincere appreciation towards the entire team of veterinarians (especially Mr. Scheurlen and Mrs. Semrau), workshop (Mr. Vollmer), and animal caretakers; especially Manfred Venier, who taught me that only softness and love (not fear!) can win the heart of an animal, and perhaps humans too. I would like to thank all the monkeys (Paco, Popeye, Ebi, Beppo, Ike, Kruemel, and Emil) whose lives were dedicated to this work.

My doctoral endeavor would not be complete without mentioning the share of my colleagues and coworkers whose fruitful discussions and valuable feedback helped in improving my work and expanding my horizon of knowledge. Thank you Joern, Axel, Christine, Nabil, Surya, Artin, Jens, Salah, Marc, Arthur, Christian, Barbara, Oleg, Alexandra, Margarita, Karolina, Kira, Alla, Lu, Peng, Mohammad Khazali, Dan, Silvia, Haian, Shengjun, Hamid, Mohammad Shams, Masih, Ramona, Ian, Marius, Lena, Peter Kraemer, Marie-Sophie, Katerina, Fatemeh, and Matthias.

My special thanks to Julian Messner, Junya Inoue, Joachim and Marie Bellet, and Sungho Hong, for making this collaboration a success.

I would express my sincere appreciation of my thesis advisors for their invaluable time and feedback. Thank you so much Fahad Sultan, for offering your help, guidance, knowledge, and enthusiasm to me. Your generous offer to extract the monkey cerebellum was no less than a private anatomy lecture, a truly memorable experience. I would also like to thank Ziad Hafed, who inspired me with his zeal and tremendous dedication towards science. You were always welcoming and treated me as one of your own lab members. Thank you for all your help, guidance, and generosity. I would like to thank Prof. Hansjoerg Scherberger for his precious time and feedback during our scientific discussions.

Some of the best moments at work were the ones that I spent with my close friends, whose consistent encouragement, support, and advice gave me all the confidence during times of doubt. Thank you, David Mack, for being there and believing in me. I would also like to thank Melanie Höller-Wallscheid, Manuel Roth, and Sad Idrees for all their motivation and help. My heart goes out to my friend Katrin Kutscheidt, whose untimely demise during this journey left a permanent void in my life. You will always be remembered. Finally, I would like to thank all my friends and relatives from India, Germany, and beyond for all the happiness and joy you all brought into my life.

APPENDIX 1

Received: 14 February 2018 | Revised: 6 June 2018 | Accepted: 19 June 2018

DOI: 10.1111/ejn.14062

RESEARCH REPORT

WILEY EJN European Journal of Neuroscience FENS

A loss of a velocity-duration trade-off impairs movement precision in patients with cerebellar degeneration

Akshay Markanday[1†] | **Julian Messner**[1†] | **Peter Thier**[1,2]

[1]Hertie Institute for Clinical Brain Research, Tübingen, Germany

[2]Werner Reichardt Centre for Integrative Neuroscience (CIN), Tübingen, Germany

Correspondence
Peter Thier, Department of Cognitive Neurology, Hertie Institute for Clinical Brain Research, Hoppe-Seyler-Str. 3, 72076 Tübingen, Germany.
Email: thier@uni-tuebingen.de

Funding information
Deutsche Forschungsgemeinschaft, Grant/Award Number: EXC 307

Abstract

Current theories discussing the role of the cerebellum have been consistently pointing towards the concept of motor learning. The unavailability of a structure for motor learning able to use information on past errors to change future movements should cause consistent metrical deviations and an inability to correct them; however, it should not boost "motor noise." However, dysmetria, a loss of endpoint precision and an increase in endpoint variability ("motor noise") of goal-directed movements is the central aspect of cerebellar ataxia. Does the prevention of dysmetria or "motor noise" by the healthy cerebellum tell us anything about its normal function? We hypothesize that the healthy cerebellum is able to prevent dysmetria by adjusting movement duration such as to compensate changes in movement velocity. To address this question, we studied fast goal-directed index finger movements in patients with global cerebellar degeneration and in healthy subjects. We demonstrate that healthy subjects are able to maintain endpoint precision despite continuous fluctuations in movement velocity because they are able to adjust the overall movement duration in a fully compensatory manner ("velocity-duration trade-off"). We furthermore provide evidence that this velocity-duration trade-off accommodated by the healthy cerebellum is based on a priori information on the future movement velocity. This ability is lost in cerebellar disease. We suggest that the dysmetria observed in cerebellar patients is a direct consequence of the loss of a cerebellum-based velocity-duration trade-off mechanism that continuously fine-tunes movement durations using information on the expected velocity of the upcoming movement.

KEYWORDS

cerebellar ataxia, duration adjustment, motor noise, precision

Abbreviations: ADCA, autosomal dominant cerebellar ataxia; ARCA, autosomal recessive cerebellar ataxia; MCP, metacarpophalangeal joint; SAOA, sporadic adult onset ataxia; SCA, spinocerebellar ataxia.

†Both authors contributed equally to this project.

Edited by John Foxe.

All peer review communications can be found with the online version of the article.

1 | INTRODUCTION

Contemporary discussions on the role of the cerebellum have revolved around the concept of motor learning, that is the improvement of motor behaviour based on the experience of past inadequacies (Albus, 1971; Ito, 1982; Marr, 1969). Motor learning should be fast, yet, a certain time of temporal integration ensuring the consistency and reliability of information on past behaviour is indispensable in order to avoid detrimental behavioural adjustments (Shadmehr, Smith, & Krakauer, 2010). This view of the role of the cerebellum that is based on a large body of physiological, theoretical and behavioural investigations is not least supported by the observation of various types of motor learning deficits in patients suffering from cerebellar disease (Donchin et al., 2012; Izawa, Criscimagna-Hemminger, & Shadmehr, 2012; Maschke et al., 2000; Therrien & Bastian, 2015). However, ataxia, characterized by dysmetria of movement as well as less smooth and deviant trajectories, is not readily understandable as a consequence of disturbed motor learning. The reason is that unlike motor learning, ataxia is instantaneous, changing the movement phenotype from one moment to the next or, to put it another way, it is a manifestation of increased motor noise. While attempts to lead ataxia back to biased internal models of movement kinematics or body dynamics (Bhanpuri, Okamura, & Bastian, 2014) thought to be optimized by learning, are able to account for consistent patient-specific aspects of the ataxic phenotype like target overshooting or in other patients target undershooting, they fail to explain the conspicuous increase in endpoint variability. We hypothesize that the increase in endpoint variability that characterizes cerebellar ataxia is the result of the inability of the diseased cerebellum to adjust movement duration such as to compensate changes in movement velocity that are consequences of a variety of noncerebellar influences ("velocity-duration trade-off"). To test this idea, we studied fast goal-directed finger movements in patients with global cerebellar degeneration and in healthy control subjects. We show that the dysmetria of cerebellar patients, the hallmark of their ataxia, is a direct consequence of the loss of a cerebellum-based velocity-duration trade-off mechanism that continuously fine-tunes movement duration using information on the expected velocity of the upcoming movement. In other words, rather than mediating behavioural

TABLE 1 Patients' details

	Sex	Age	Diagnosis	SARA scores	
				Total / 40	Task relevant / 12
P01	Male	27	[a]ARCA1 (with spasticity and polyneuropathy)	5	3
P02	Male	47	Cerebellar ataxia	7	2.5
P03	Male	53	SAOA	11	4
P04	Male	60	ADCA (excluded SCA1, 2, 3, 6, 7, 17)	6.5	2
P05	Male	63	ADCA (excluded SCA1, 2, 3, 6, 8, 10, 12)	10	3
P06	Male	59	SAOA (excluded SCA1, 2, 3, 6, 7, 17)	9	2.5
P07	Female	43	ADCA (excluded SCA1, 2, 3, 6, 7, 17)	5	2
P08	Female	60	ADCA (aetiology unknown)	15.5	6
P09	Female	53	Cerebellar ataxia	20.5	5.5
P10	Male	60	Cerebellar ataxia	5.5	2
P11	Female	56	ADCA type 3 (SCA1, 2, 3, 6, 8, 10, 11, 12, 13, 14, 15, 17, 27 excluded)	18	5
P12	Male	36	[a]ARCA (with pyramidal tract lesion)	10.5	3
P13	Male	32	ARCA	10	4
P14	Male	54	SAOA (SCA1, 2, 3, 6, 7, 8, 12, 14, 17, & FXTAS excluded)	10.5	3
P15	Female	52	SCA 14	12	4

Notes. Task relevant score is based upon the performance during tasks involving upper limb extremities.
ARCA: autosomal recessive cerebellar ataxia; ADCA: autosomal dominant cerebellar ataxia; SCA: spinocerebellar ataxia; SAOA: Sporadic adult-onset ataxia.
[a]Patients with additional noncerebellar damage.

adjustments based on a posteriori information, our findings suggest that an important aspect of cerebellar functioning, which is of utmost relevance for the ataxic phenotype, is the usage of a priori information.

2 | MATERIALS AND METHODS

2.1 | Participants

Fifteen healthy subjects (five females, 10 males, mean age: 51.6 years, range: 33–66 years) and 15 patients (five females, 10 males, mean age: 50.3 years, range: 27–63 years) suffering from different forms of global cerebellar degeneration (for details see Table 1) participated in the main experiment. Thirteen (five females, eight males, mean age: 53.2, range: 32–63 years) out of the 15 patients studied suffered from well-defined genetically determined variants of cerebellar degeneration and are addressed as the group of "cerebellar patients," compared with healthy controls. In these patients, a significant involvement of noncerebellar structures was excluded using standard clinical procedures and the data available from MRI scans and electrophysiological tests, noninvasive approaches that certainly do not exclude more subtle alterations at the microscopic level. The two other patients (P01, P12) had additional extracerebellar pathology and were therefore excluded from the group of cerebellar patients. Nevertheless, the data of patients P01 and P12 are presented in several figures, clearly separable from the other subjects as they may be of interest to those trying to better understand the specific incapacities resulting from such rare diseases. Another group of 10 healthy individuals (four females, six males, mean age: 55.4 years, range: 47–62 years) participated in a "feedback control" experiment. All participants were right-handed and not familiar with the experiment. All participants gave written consent and the Ethical Committee of the Medical Faculty and the University of Tübingen approved the study (verification/project number 413/2015BO2), which was conducted in accordance with the World Medical Association Declaration of Helsinki. Prior to the main experiment, all participants completed a detailed questionnaire exploring the medical history, physical and vocational as well as recreational interests. All patients were examined neurologically among others, carefully considering the items of the Scale for the Assessment and Rating of Ataxia (SARA) (Schmitz-Hubsch et al., 2006).

2.2 | Experimental setup

Subjects were seated comfortably in an upright position on a chair fixed in front of a large screen (width: 160 cm, height: 120 cm) such that the distance between the eye and the screen was approximately 150 cm with the sagittal body axis aligned with the mid-line of the screen. To ensure maximum comfort during the experiment, the subjects' head was not fixed and adopted a convenient position with their right arm on a forearm rest with the hand and the index finger pointing forward (Figure 1a). In order to prevent relevant arm movements during experiments, the forearm and hand/wrist were secured to the rest by Velcro fasteners. As we were interested in fast index finger movements about the finger's base joint (=metacarpophalangeal joint, MCP joint), we blocked significant movement contributions of the two distal finger joints by splinting the index finger distal of the MCP joint using a finger-shaped cast made out of lightweight thermoplastic material. The position of the distal phalanx was measured using the search coil technique by attaching a magnetic search coil (Bechert & Koenig, 1996) to the finger cast axially around the distal phalanx (Figure 1a), sampling the coil signal at a resolution of 1 kHz.

In-house software (NREC), running on a Linux PC (http://nrec.neurologie.uni-tuebingen.de) was used for data collection, stimulus presentation and operations control. All visual stimuli were projected onto the tangent screen by an NEC GT2150 LCD projector (60 Hz, 1280 × 1024 pixels).

2.3 | The main behavioural paradigm

In the main experiment, subjects had to execute rapid, alternating extension and flexion movements of the index finger about the MCP joint needed to keep a white cross-hair shaped cursor (diameter: 4 cm), representing the fingertip's vertical and horizontal position, within a target zone centred on a red dot target (diameter: 1.7 cm), projected onto the screen. The target appeared first in a start position in the screen centre and next jumped unpredictably to one of the two new positions, above and below the start position, respectively, and

FIGURE 1 Experimental setup and paradigm used for measuring fast finger movements. (a) A healthy participant seated comfortably on a chair (left) placed in front of a large projection screen with his right (=preferred) hand resting on a customized ergonomic "mouse" allowing up (mid) and down (right) index finger movements. The index finger was stabilized using a cast. A search coil was placed axially around the middle phalanx, as shown by the dotted black line. (b) Complementary behavioural paradigms. (c) The main behavioural paradigm consisted of 1,700 trials that lasted for around 37 min. (d) Experiment for testing the role of cursor feedback. (e) Position trace during a single downward trial (solid dark grey line). The target jump (dashed grey line) times were randomized within a time window (shaded region) of 100–600 ms from the onset of the trial. (f) Movement onset detection (vertical grey lines) was based on a velocity threshold (horizontal dashed line) of 50 cm/s. Velocity profile (solid dark grey line) of the index finger during a downward movement

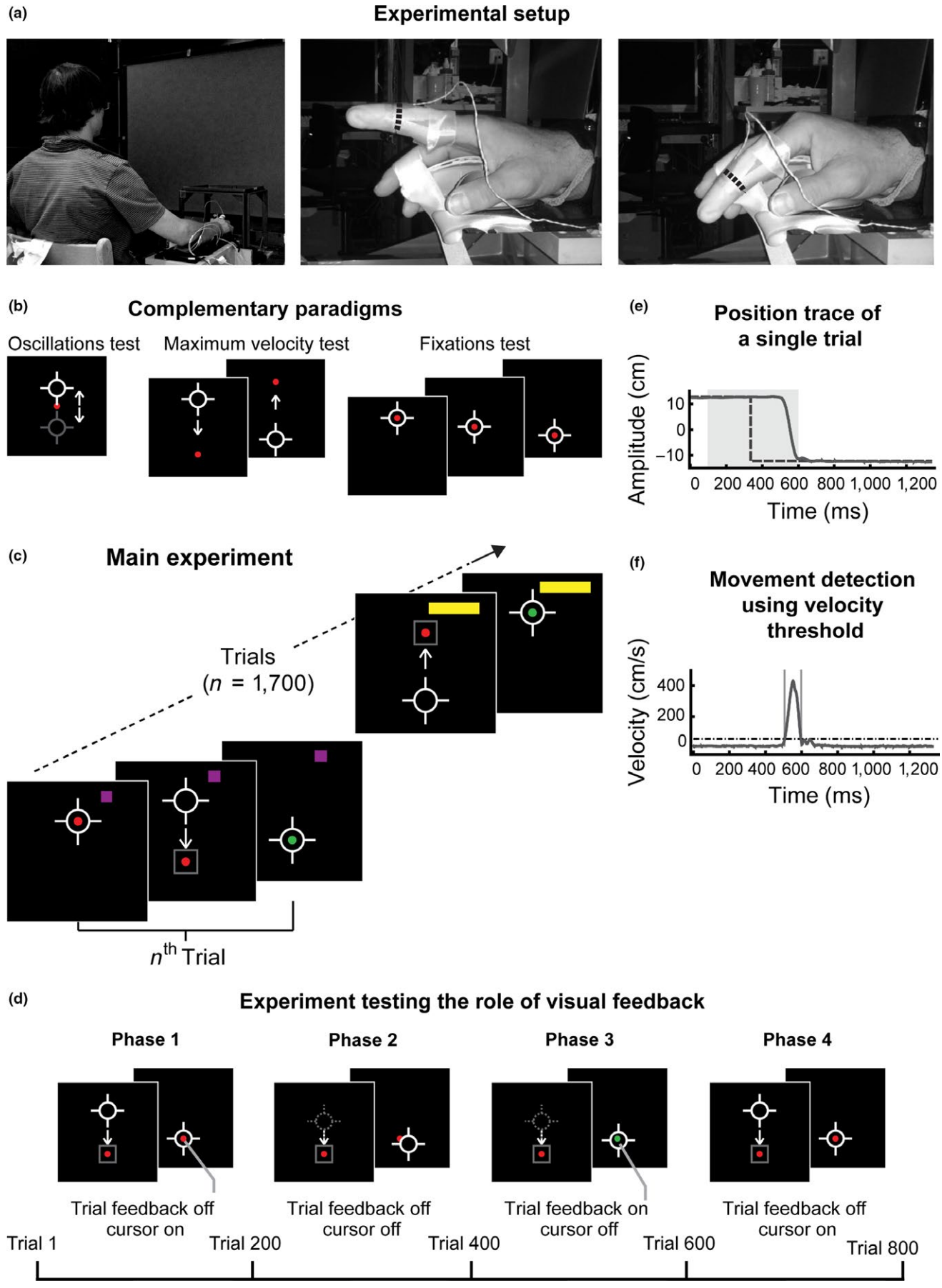
(a)
Experimental setup
(b)
Complementary paradigms
Oscillations test
Maximum velocity test
Fixations test
(c)
Main experiment
Trials
(n = 1,700)
nth Trial
(d)
Experiment testing the role of visual feedback
Phase 1
Phase 2
Phase 3
Phase 4
Trial feedback off
cursor on
Trial feedback off
cursor off
Trial feedback on
cursor off
Trial feedback off
cursor on
Trial 1
Trial 200
Trial 400
Trial 600
Trial 800
(e)
Position trace of
a single trial
Amplitude (cm)
10
0
−10
0 200 400 600 800 1,000 1,200
Time (ms)
(f)
Movement detection
using velocity
threshold
Velocity (cm/s)
400
200
0
0 200 400 600 800 1,000 1,200
Time (ms)

from there alternated between the two. The two target positions were: up: $x = 0$ cm, $y = +12.5$ cm; down: $x = 0$ cm, $y = -12.5$ cm). With a distance between the MCP joint and the screen centre of 110 cm, the 25 cm jump of the target between its two positions evoked an angular rotation of approximately 60° about the MCP joint.

The index finger's resting position was aligned with the middle of the screen in a way that the MCP joint had to be rotated by comparative amounts up and down from the resting position in order to reach the two vertical targets. In order to exclude the possibility that precision might be achieved by merely flexing or extending the index finger to its maximum rotation limit, the amount of angular rotation needed in either direction was kept significantly smaller than the maximal rotation possible. Although all experiments were conducted in a dark room, the weak screen backlight might have allowed some subjects to obtain visual feedback on their moving finger. This is why we used an occluder that prevented watching the hand.

The "Main Experiment" (Figure 1c) required participants to execute long series (~1,700 trials; ~37 min) of fast and precise vertically alternating index finger movements. Each trial lasted approximately 1,300 ms and the target jump times were selected randomly from a variable time window of 100–600 ms from the trial onset to avoid movements based on intuition (Figure 1e). We placed an invisible squared window (4×4 cm) comparable in size to the diameter of the circular ring of the moving cross-hair pointer around the target. The finger movement had to place the cursor into the confines of this window to count as successful. To make sure that the executed movements were fast, we chose a time window of 300 ms that opened 150 ms after the target jump. Any movements executed earlier than the onset of the window or later than 300 ms after the onset, were considered "too early" and "too late" movements, respectively. Only if the movements were fast and precise the target dot turned green, indicating a successful trial. To keep participants motivated throughout the experiment, a horizontal "performance bar" was displayed at the top right corner of the screen that increased in length with every successful trial. Since there was no reference to the maximum length of the bar, no exact estimates of task duration could be inferred from its length. However, near the end of the task, the colour of the bar changed from purple to yellow followed by a beep sound, alarming that only 10% trials were left to finish the task. No other communication was allowed during the experiment.

2.4 | Complementary behavioural paradigms

Before the main experiment, we carried out a series of three short tests (Figure 1b). The first test was the "oscillations test" in which participants were asked to execute rapid, unguided vertically oscillating movements for 10 s, around a red target dot (diameter: 1.7 cm) displayed in the middle of the screen but without an endpoint target. The purpose of this task was to measure the maximum oscillation frequency of the index finger. To this end, subjects were free to choose the movement amplitudes ensuring the highest possible movement frequency. In the second test, the "maximum velocity test," subjects had to execute very fast movements (60 trials; trial duration: 1,400 ms) between two vertically alternating targets. As the main interest of this experiment was to measure the maximum finger velocity possible, precision was not enforced although feedback on the finger position was provided. Finally, in the third test, the "fixation test," subjects had to fixate each of the three target positions (in the order centre: $x = 0$ cm, $y = 0$ cm; up: $x = 0$ cm, $y = +12.5$ cm and down: $x = 0$ cm, $y = -12.5$ cm) with the cursor for 10 s (see Supporting Information Appendix S1 for results).

2.5 | Data analysis

We performed the analysis offline using scripts written in MATLAB (MATLAB, The MathWorks Inc., MA). First, we smoothed the vertical and horizontal components of the finger position records (sampled at a rate of 1 kHz) using a Savitzky–Golay filter (Savitzky & Golay, 1964) (bin size = 10 samples; polynomial degree = 3, derivative = 1), based on a chosen order of derivative. Instantaneous finger velocity and acceleration were derived from the finger position data (Figure 1e). Detection of (primary) finger movements (Figure 1f) was based on a lenient velocity threshold of 50 cm/s that was chosen to eliminate the corrective (secondary) finger movements that resulted from overshooting or undershooting of the cursor relative to the desired target location. We calculated movement amplitude as the absolute difference of vertical finger position at the time of movement onset and offset and duration as the time between on- and offset. Movements lasting for 80–300 ms within an amplitude range of 10–35 cm only were considered for analysis. A significance level of $p < 0.05$ was adopted for statistical interpretations.

3 | RESULTS

3.1 | Main task

The idea behind the "main task" was to scrutinize the relationship between movement velocity and duration on a trial-by-trial basis. Since the peak velocity of a movement is a very sensitive marker of trial-to-trial fluctuations in velocity, we focused our analysis mainly on the peak velocity of finger movements. To examine this relationship, we asked all participants to make long series of fast and precise alternating movements of the index finger of their preferred hand in order to move the cursor up and down such as to achieve the desired target locations displayed on the monitor. We observed

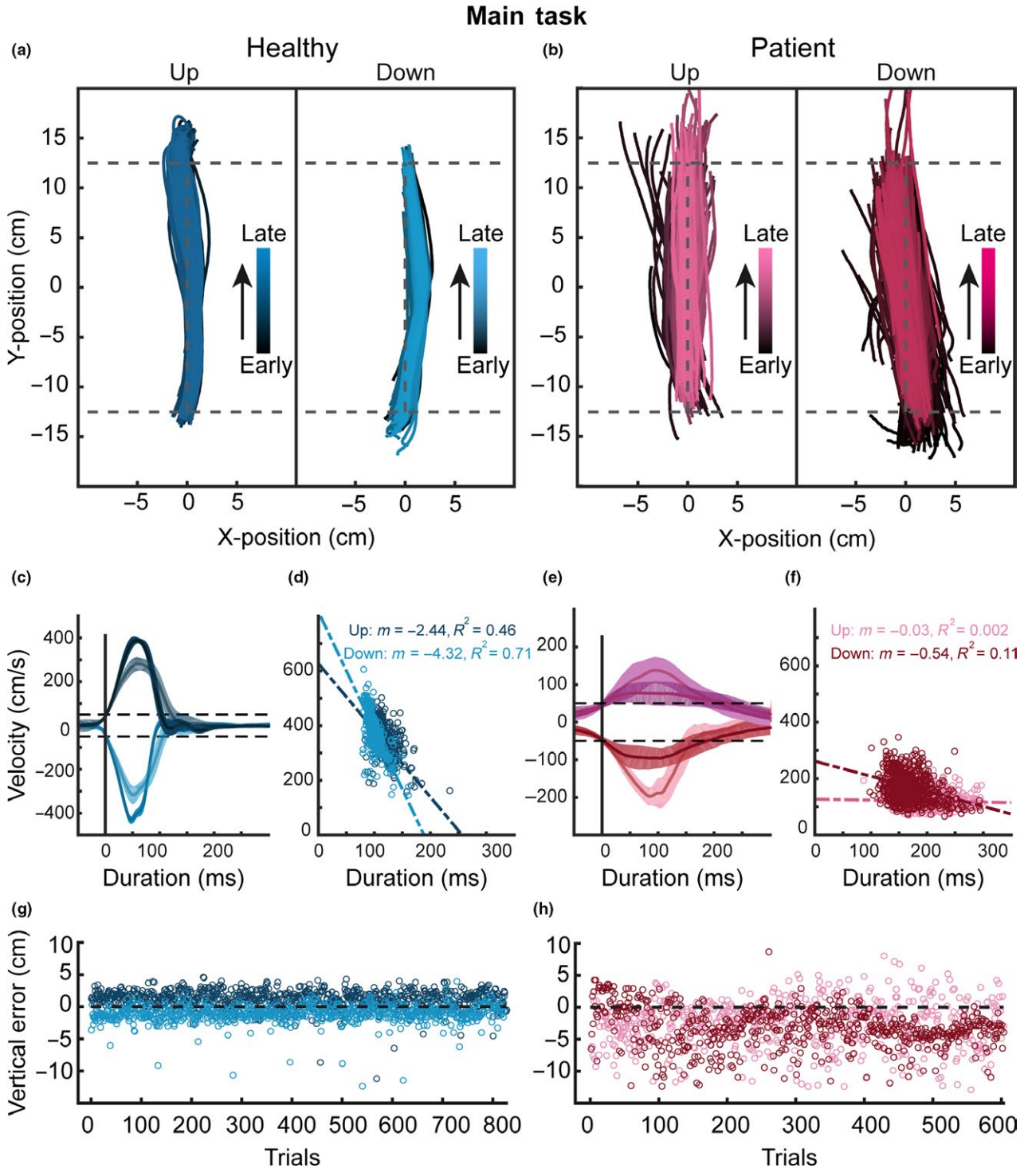

FIGURE 2 Endpoint precision, movement velocity and movement duration in exemplary subjects. (a,b) Movement trajectories of an exemplary healthy subject and cerebellar patient respectively. (c, e) Mean and standard error of mean (*SEM*) of the velocity trace for up and down finger movements with higher and lower peak velocity (100 trials each). (d, f) Velocity-duration trade-off in the healthy subject and patient, respectively, represented by the dashed regression lines fitted to the peak velocity and duration of all up and down trials. Slopes of regression, healthy: $m_{up} = -2.44$; $m_{down} = -4.32$; patient: $m_{up} = -0.03$; $m_{down} = -0.54$. (g, h) Endpoint errors in the up and down movements of the healthy subject and cerebellar patient

that the movement trajectories of the index finger of single healthy participants (Figure 2a) showed much less variability in their general pattern than those of single cerebellar patients (Figure 2b). We also found that individual healthy subjects were able to compensate for changes in the movement velocity (Figure 2c) by making fine adjustments in movement

duration; lower velocity movements were accompanied by higher movement durations and vice-versa. Such clear compensatory adjustment of movement duration in response to changes in peak velocity of finger movements was clearly not seen in individual cerebellar patients (Figure 2e).

The velocity-duration trade-off suggested by the movement trajectories shown in Figure 2a,b is captured by the significant negative slope (m) of the regression lines fitted to plots of peak velocity as a function of movement duration for the two subjects shown in Figure 2d,f. The notion of a disturbed velocity-duration relationship in the patient is supported by two facts disclosed by Figure 2f. Firstly, the quality of the linear fit was poorer in the patient as indicated by significantly smaller coefficients of determination (R^2), (healthy: $R^2_{up} = 0.46$, $R^2_{down} = 0.71$; patient: $R^2_{up} = 0.002$, $R^2_{down} = 0.11$). Secondly, the slope of the regression line was significantly lower in the patient, both for up and for down finger movements (Figure 2d, healthy: $m_{up} = -2.44$; $m_{down} = -4.32$; Figure 2f, patient: $m_{up} = -0.03$; $m_{down} = -0.54$), indicating that a much smaller fraction of the endpoint error that would otherwise result from changes in velocity was compensated in the healthy subject. Consequently, the patient's finger movement trajectories were less smooth and less precise as documented by a larger mean absolute deviation of the finger endpoint from the target and a significantly larger variability of movement endpoints (Figure 2h). The patient not only lacked the high-quality velocity-duration trade-off presented by the healthy subject but in general exhibited smaller movement velocities. However, independent of the clear performance differences between the patient and the control subject, both demonstrated faster downward than upward movements (Figure 2d,f, Supporting information Figure S2a,b). The features distinguishing the exemplary patient and control subject also differentiated the two groups. Healthy participants (Figure 3a,b) had significantly more negative (steeper) values of m (healthy subjects: mean $m_{up} = -1.89$, mean $m_{down} = -2.53$; patients: mean $m_{up} = -0.68$, mean $m_{down} = -0.73$; Wilcoxon rank-sum test, up movements: $z = -4.24$, $p = 2.26 \times 10^{-5}$, down movements: $z = -3.92$, $p = 9.02 \times 10^{-5}$) as well as significantly larger coefficients of determination (healthy subjects: mean $R^2_{up} = 0.5$, mean $R^2_{down} = 0.52$; patients: mean $R^2_{up} = 0.22$, mean $R^2_{down} = 0.13$; Wilcoxon rank-sum test, up movements: $z = 3.41$, $p = 6.52 \times 10^{-4}$; down movements: $z = 4.01$, $p = 6.13 \times 10^{-5}$).

3.2 | Slopes for a matched range of speeds

Since the distribution of the peak velocities of finger movements (Figure 3c, all trials, up and down pooled) of the

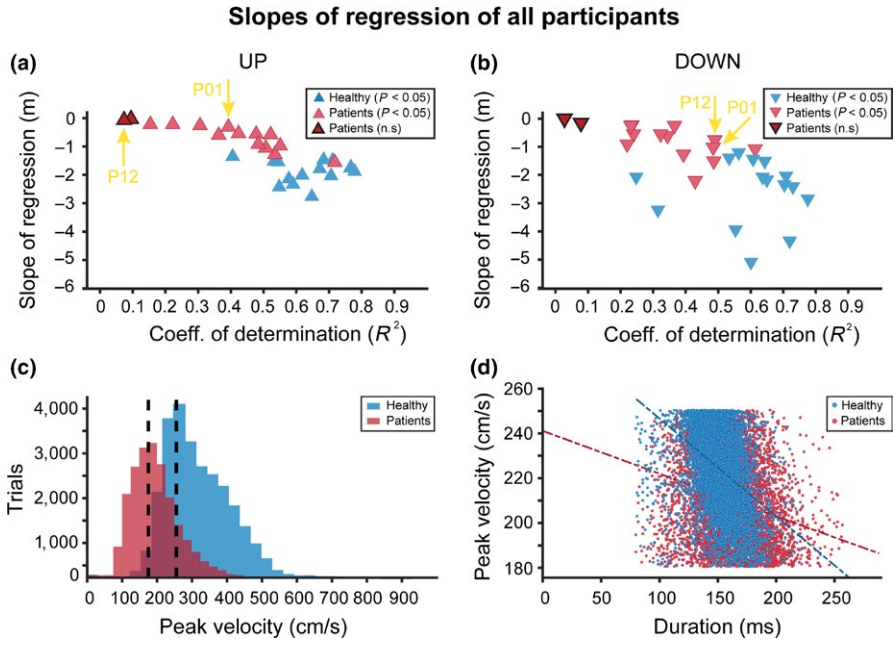

FIGURE 3 Analysis of relationship of movement velocity and movement duration. (a, b) Slopes of regression (m) of movement velocity as function of movement duration for individual subjects as function of associated coefficient of determination (R^2) for up and down finger movements, respectively. Healthy subjects: solid blue triangles; cerebellar patients: solid red triangles. Yellow arrows indicate the patients (P01 and P12) with additional noncerebellar damage (not included in statistical analysis). (c) Peak velocity distribution for all movements (up and down combined) pooled across all healthy subjects and cerebellar patients. Equal numbers of samples were drawn at random from a matched range of peak velocities (180–250 cm/s, dotted black lines) to compute the regression of peak velocity as function of movement duration shown in panel D. (d) Slopes of regression for matched range peak velocities in healthy subjects ($m = -0.44$, $p = 9.53 \times 10^{-234}$, R^2=0.16) and patients ($m = -0.19$, $p = 2.13 \times 10^{-79}$, $R^2 = 0.06$)

cerebellar patients was shifted relative to one of the healthy participants (on average 38.12% lower in patients, Wilcoxon rank-sum test: $z = 130.62$, $p = 0$), one might argue that the poor relationship between movement duration and peak velocity observed in the patient group is an artefact of their lower velocity finger movements rather than a true group difference. To address this objection we restricted the regression analysis to a fixed range of peak velocities (180–250 cm/s) covering the velocity distributions of both groups, drawing at random equal numbers of trials for both groups in order to compute the velocity-duration regressions. Even within this small range of matched velocities, the slopes of regression lines for healthy participants ($m_{\text{healthy}} = -0.44$, $p = 9.53 \times 10^{-234}$) were higher and the corresponding coefficients of determination ($R^2_{\text{healthy}} = 0.16$) larger than in the cerebellar patients ($m_{\text{patients}} = -0.19$, $p = 2.13 \times 10^{-79}$,

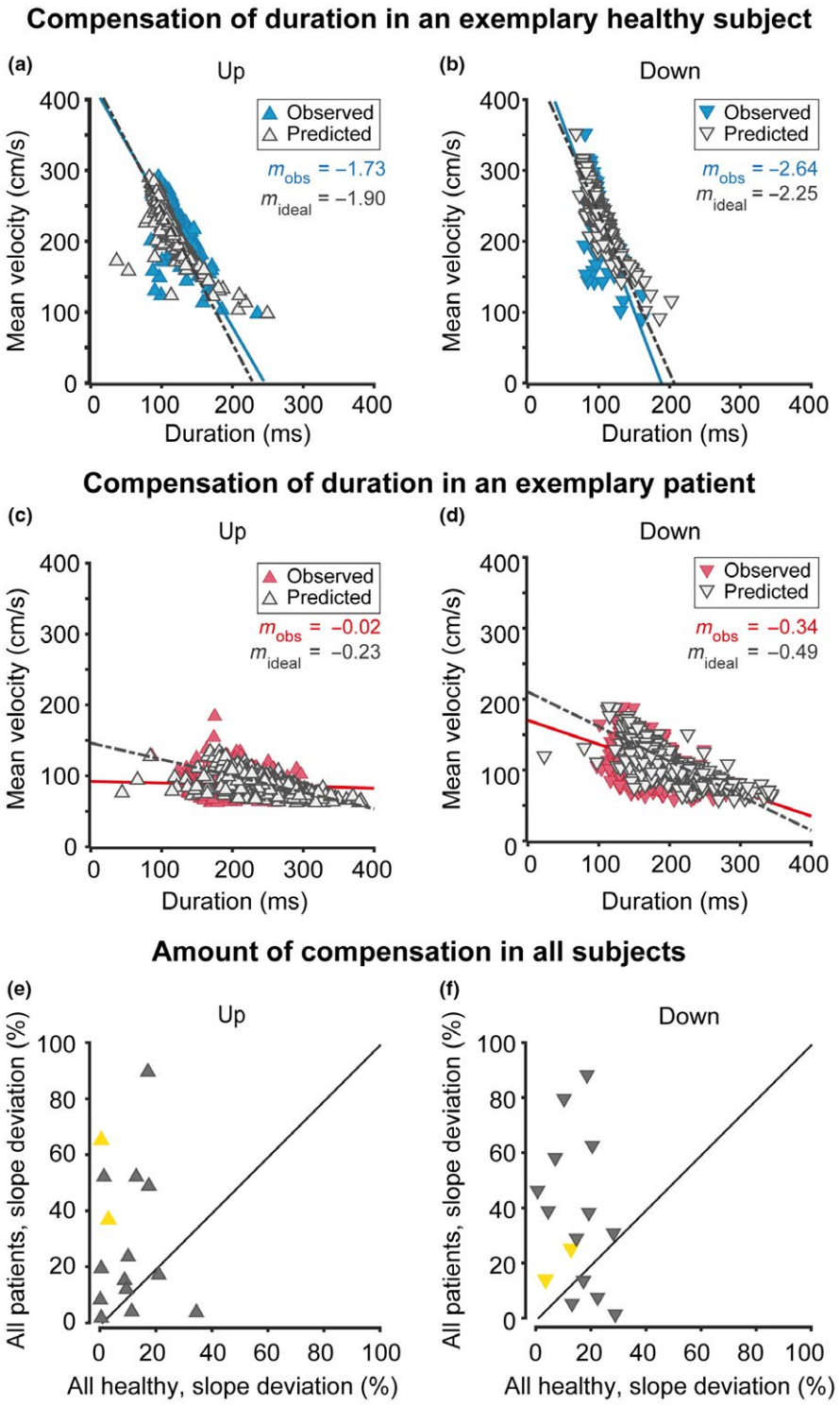

FIGURE 4 Analysis of duration compensation of velocity fluctuations. (a-d) Plots of mean velocities as function of observed durations and ideal durations (see main text for explanation) respectively, for the two exemplary subjects (a, b healthy subject; c, d patient) for up and down movements. Scatter plots and resulting regressions for observed durations are distinguished by colour (red for patients, blue for healthy subjects) from those for ideal durations (light grey). (e, f) Plots of slope deviation coefficients of patients as a function of coefficients of healthy controls. Note that patients exhibited significantly larger slope deviations than healthy subjects (healthy subjects: mean $m_{\text{deviation up}} = 9.9\%$, mean $m_{\text{deviation down}} = 14.75\%$, patients: mean $m_{\text{deviation up}} = 26.73\%$, mean $m_{\text{deviation down}} = 38.47\%$; Wilcoxon rank-sum test, up movements: $z = -2.03$, $p = 0.04$; down movements: $z = -2.40$, $p = 0.01$). Yellow triangles indicate the patients (P01 and P12) with additional noncerebellar damage (not included in statistical analysis)

$R^2_{\text{patients}} = 0.06$, Figure 3d). Finally, although patients' peak velocities were on average slower, measures of velocity variability were not different between groups *SD*, mean $SD_{\text{healthy}} = 60.1$, mean $SD_{\text{patients}} = 54.48$, Wilcoxon rank-sum test, $z = -0.88$, $p = 0.38$). On the other hand, a closer look at the plots of peak velocity as function of duration (Figure 3d) reveals that patients exhibited a larger variability in their movement durations (mean $SD_{\text{healthy}} = 18.84$, mean $SD_{\text{patients}} = 31.74$, Wilcoxon rank-sum test, $z = 4.33$, $p = 1.49 \times 10^{-5}$), ultimately responsible for the poor relationship between movement duration and peak velocity.

3.3 | Quality of velocity-duration trade-off

We next tried to assess the ability of the velocity-duration trade-off to ensure endpoint precision on a trial-to-trial basis. A perfect velocity-duration trade-off would keep the endpoint error zero despite fluctuations in movement velocity when deploying appropriate movement duration. We estimated this ideal movement duration (D_{ideal}) in single trials using the relation,

$$D_{\text{ideal}} = A_{\text{zero}-error}/V \quad (1)$$

where "*V*" is the mean velocity of finger movements and "$A_{\text{zero-error}}$" is the distance between the target and the vertical finger position at the onset of the movement that is, the amplitude required for zero error. We used the mean velocity of individual trials to estimate D_{ideal} rather than peak velocity because it provides a more accurate measure of the consequences of fluctuations in instantaneous velocity for the resulting movement amplitude than peak velocity. We then regressed mean finger velocity as a function of D_{ideal} to compute the ideal slope (m_{ideal}) of the velocity-duration relationship and then compared the slope (m_{ideal}) of the regression line with the slope (m_{observed}) of the regression of mean velocity as a function of observed movement duration. To this end, we calculated a slope deviation coefficient $m_{\text{deviation}}$ expressing how much the observed slope deviated from the predicted one, the latter warranting optimal compensation of velocity fluctuations, according to

$$m_{\text{deviation}} = (m_{\text{ideal}} - m_{\text{observed}})/m_{\text{ideal}} \times 100 \quad (2)$$

The deviation coefficient was clearly smaller in the exemplary healthy individual (Figure 4a,b) ($m_{\text{deviation up}} = 9\%$, $m_{\text{deviation down}} = 17\%$) than in the exemplary patient (Figure 4c,d, $m_{\text{deviation up}} = 91\%$, $m_{\text{deviation down}} = 31\%$). In general, healthy subjects exhibited significantly smaller slope deviations than patients (healthy subjects: mean $m_{\text{deviation up}} = 9.9\%$, mean $m_{\text{deviation down}} = 14.75\%$, patients: mean $m_{\text{deviation up}} = 26.73\%$, mean $m_{\text{deviation down}} = 38.47\%$; Wilcoxon rank-sum test, up movements: $z = -2.03$, $p = 0.04$; down movements: $z = 2.40$, $p = 0.01$), the patients displayed a clear inability to compensate fluctuations in movement velocity paralleled by larger slope deviations that underlies the loss of movement precision in patients (Figure 4e,f).

3.4 | Loss of vigour and hypometria in cerebellar patients

Despite the long and exhausting session it was quite surprising to see that none of the healthy participants showed "fatigue" or loss of their vigour of movement in the main task, in the sense of a gradual steady decline in peak velocity of the finger movements over time. This is the conclusion suggested by comparing the mean peak velocity, duration and amplitude of finger movements (up and down pooled), averaged across all healthy participants (Figure 5 aI,bI,cI) for trials in the early (first 120 trials), late (120 trials before time alarm, i.e. a tone and change in colour of performance bar indicating that 90% of the experiment had been completed) and last (120 trials after time alarm) phase of the main experiment. This comparison showed no significant difference between the three phases (one-way ANOVA for repeated measures, $F = 0.09$, $p = 0.91$). On the other hand, cerebellar patients exhibited a consistent drop (Figure 5 aII) in movement vigour between the early and the late phase (one-way ANOVA for repeated measures, $F = 9.49$, $p = 9.19 \times 10^{-4}$; early vs. late, *t* test: $t = 3.05$, $p = 0.01$). Even the alarm signal indicating 90% task completion did not seem to boost peak velocities (late vs. last, *t* test, $t = 1.31$, $p = 0.22$). As the task difficulty was not adjusted for the patients' group, one potential factor that could possibly account for this loss of movement vigour in patients might have been a decline in motivation over the course of the task. We captured the quality of task performance by gauging the number of successful trials (score) and the instantaneous ratio (ΔS) of successful trials relative to trials executed as proxy of motivation. Both groups exhibited an increase in the number of successful trials (Figure 5 dI,dII) from the early phase (after the first 120 trials: $\text{score}_{\text{healthy}} = 107$, $\text{score}_{\text{patients}} = 70.54$) till the end of the last phase (120 trials after alarm: $\text{score}_{\text{healthy}} = 1{,}444.3$, $\text{score}_{\text{patients}} = 566.54$). Yet, as indicated by the numbers presented, this accumulation was generally slower in patients. Moreover, it took place at a constant rate only in healthy controls. However, in cerebellar patients the quality of task performance (ΔS) declined gradually in the course of the experiment, paralleling the decline in peak velocity. This decline in the vigour of finger movements over trials in the patient group remained uncompensated for duration (Figure 5 bII, one-way ANOVA for repeated measures, $F = 1.99$, $p = 0.16$; early vs. late, *t* test, $t = -1.76$, $p = 0.1$), causing the movement amplitudes to gradually fall short of the desired target location more and more (Figure 5 cII, one-way ANOVA for repeated measures, $F = 7.25$, $p = 0.003$;

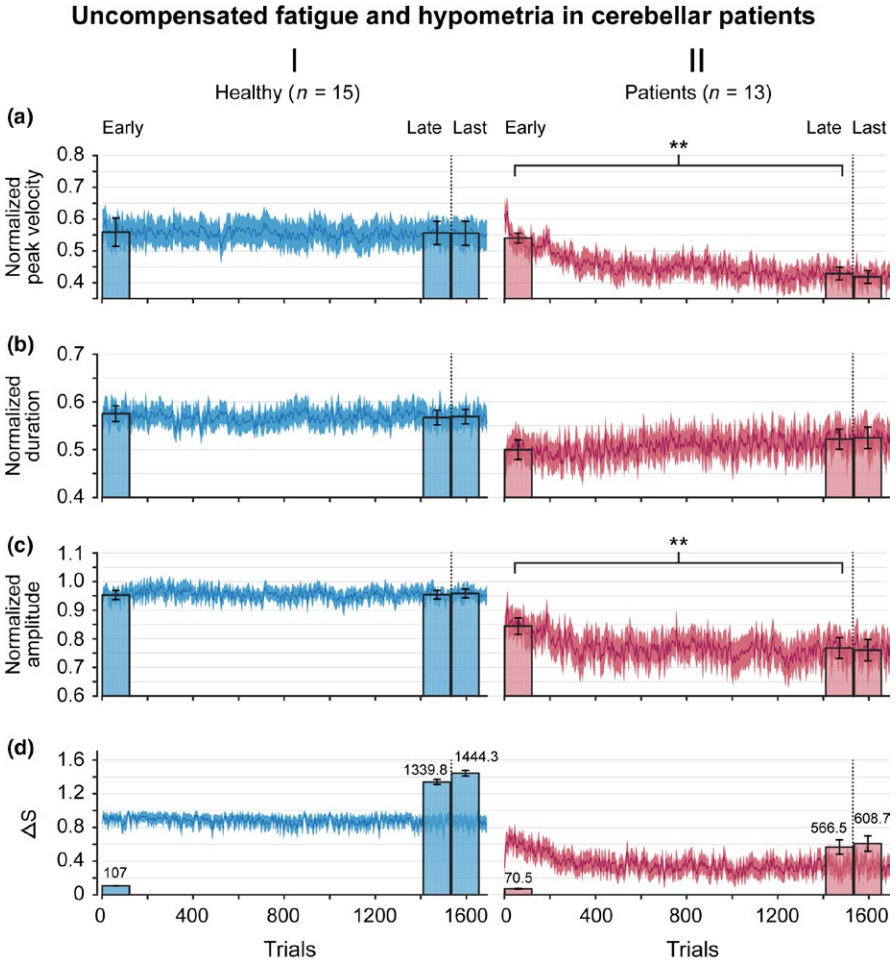

FIGURE 5 Movement velocity, amplitude, duration and task performance as a function of trial number. (aI, bI, cI, aII, bII, cII) Plots showing the mean (±*SEM*) of the normalized peak velocity, duration and amplitude of finger movements (up and down combined) of all healthy participants (blue traces) and patients (red traces) respectively, during the main task. The bars represent the mean (±*SEM*) of the respective kinematic parameter of trials during the "early" (first 120 trials), "late" (120 trials before alarm signal, as indicated by the dotted black line) and "last" phase (120 trials after alarm) of the main task. (dI, dII) The absolute mean score of all healthy participants (blue bars) and cerebellar patients (red bars), respectively, at the end of early, late and last phase of the main task. The average (±*SEM*) instantaneous ratio (ΔS) of successful trials relative to executed trials of all healthy participants and cerebellar patients is shown by the blue and red traces, respectively

early vs. late, *t* test, $t = 2.63$, $p = 0.02$), a condition usually referred to as "hypometria."

3.5 | Experiment testing the role of feedback

The findings reported before suggest that finger movements of healthy controls and patients are subject to velocity fluctuations. Moreover, they indicate that it requires a healthy cerebellum to ensure that the fluctuations are not translated into endpoint errors. This is achieved by an appropriate adjustment of movement duration. Does this adjustment depend on the visual feedback of the ongoing finger movement? This seemed highly unlikely, given the fact that the overall movement duration was usually less than 170 ms (mean + *SD*: 172.9), that the minimal latency of visual feedback would hardly fall below 100 ms and that at least a few 10 ms would be required to capture the initial finger velocity and, based on it, to predict the landing point. Hence, the presence or absence of visual information should if anything impact the final phase of the movement and thereby modulate the overall trajectory. In order to find out if the visual feedback modulated the final movement phase, we tested a new group of 10 naïve healthy right-handed participants in a variant of the main experiment, in which we manipulated not only the availability of visual feedback but also the availability of performance feedback (Figure 1d). This feedback control experiment comprised of four phases, each phase consisting of 200 trials. Participants were instructed to make fast and precise movements. During all four phases, unlike the main experiment, subjects did not see any cumulative score (performance bar) capturing the evolution of the experiment. Although in phase one and phase four cursor feedback on the actual finger position was available, this cursor feedback was partially removed in the second and third phase of the experiment by blanking the cursor during mid-flight as soon as the movement velocity exceeded a threshold of 10 cm/s. The cursor reappeared 500 ms after the detected movement onset, that is well after the completion of a normal movement, which typically took 114.2 (mean-*SD*) to 172.9 (mean + *SD*) ms. Only during the third phase, performance feedback after each trial, indicated by the change of the target colour, was delivered. Had there been an influence of cursor feedback or performance feedback on movement trajectories, one would have expected changes of the typically smooth and continuous, almost bell-shaped velocity profiles of movements (Figure 6) when comparing those in phase one with those during the second or the

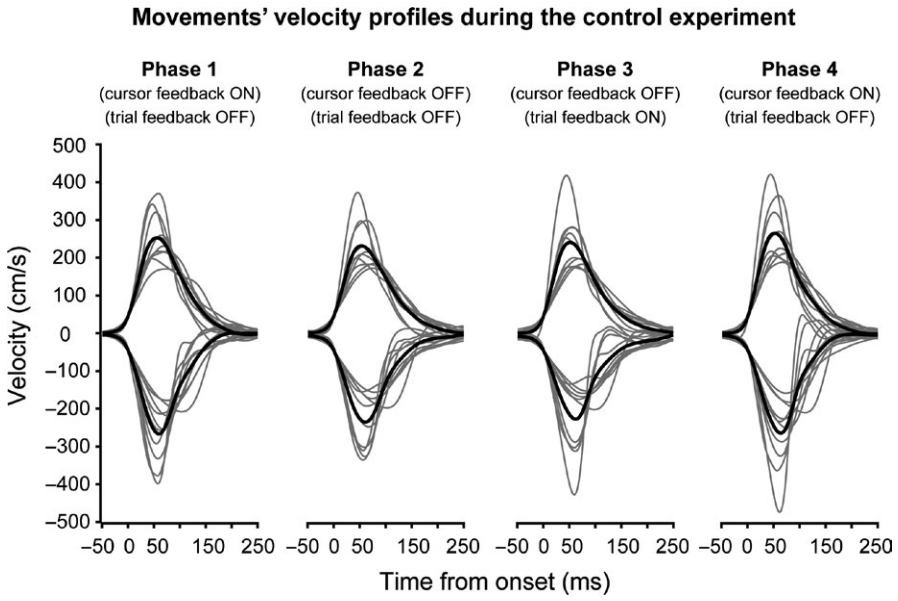

FIGURE 6 The role of cursor feedback. Mean velocity profiles of all up and down movements in healthy control subjects (solid grey lines) during the four phases of control task. Black solid traces indicate the mean of all velocity profiles of up and down finger movements during the four phases. There was no influence of the cursor feedback on the shape of movement velocity profiles

third phase. To detect such changes, we fitted the velocity profile of each trial of all participants by a modified Gamma distribution (Van Opstal & Van Gisbergen, 1987) in order to detect phase-dependent changes in the properties of the fit. The Gamma distribution is given by

$$v(t) = \alpha * [t/\beta]^{\gamma-1} * \exp[-t/\beta] \ldots t \geq 0; \beta > 0; \gamma \geq 1 \quad (3)$$

where $v(t)$ is the movement velocity profile, α and β are scaling constants for velocity and duration, respectively, and γ is the shape parameter that determines the degree of asymmetry to compute skewness ($2/\sqrt{\gamma}$). Gamma functions were able to accommodate the mild deviation from a perfectly symmetric bell-shaped profile, due to the profiles′ slightly steeper ascent than descent. The resulting fits of the velocity profiles of up and down movements were characterized by goodness of fit measures (R^2) typically exceeding 0.94 (median R^2_{up}: Phase 1–4: 0.98, 0.98, 0.98, 0.98 respectively; median R^2_{down}: Phase 1–4: 0.94, 0.92, 0.89, 0.92 respectively), without a significant difference of R^2 and the skewness measure between phase one and phase two (two-way repeated measure ANOVA with the two factors phase and movement direction (i.e. up and down) and post-hoc Tukey-Kramer comparisons between phases with corrections for multiple comparisons; phase 1 vs. 2: skewness, $p = 0.37$; R^2, $p = 0.23$; phase 1 vs. 3: skewness, $p = 0.31$, R^2, $p = 0.09$, tested for multiple comparisons) indicating that there were neither qualitative nor quantitative differences in the shapes of velocity profiles. These results clearly suggest that the selection of movement durations appropriate for the peak velocity reached cannot be based on visual feedback, that is an a posteriori assessment of the velocity reached. Rather they suggest that the system uses a priori knowledge on future peak velocity in order to preselect appropriate movement durations.

4 | DISCUSSION

The aim of this study of fast goal-directed index finger movements was to extend our understanding of the role of the cerebellum in ensuring movement precision. Our results clearly demonstrate that the cerebellum achieves the desired accuracy despite continuous fluctuations in movement velocity by adjusting movement duration accordingly. This precise velocity-duration trade-off depends on the integrity of the cerebellum. This conclusion is based on the fact that patients suffering from a global malfunction of the cerebellum due to degeneration, although in general moving more slowly, exhibit similar variability of finger movement velocities, clearly indicating that this variability is a consequence of extra cerebellar influences. Yet, unlike healthy subjects, the patients are no longer able to deploy compensatory movement durations, an inability that leads to a loss of endpoint accuracy, in other words to dysmetria. This dysmetria is supplemented by less smooth trajectories that often show deviations from a simple "bell-shaped" velocity profile, the manifestation of deviant trajectory components and a relative slowness of movements, problems that in sum make up the cerebellar ataxia of movement.

4.1 | Deviant movement velocities in cerebellar patients

Slower velocities as exhibited by our patients are in accordance with previous observations (Hallett, Shahani, & Young, 1975; Topka, Konczak, Schneider, Boose, & Dichgans, 1998; Wild, Klockgether, & Dichgans, 1996) on the consequences of cerebellar disease. Slower movements could be a useful strategy to cope with the inability

to precisely control movement duration, the key functional disturbance unravelled by this study. The logic here is that the endpoint error resulting from not stopping the movement at the right point in time will decrease with the velocity of the movement. The fact that patients were not only slower in the main task but also in the "maximum velocity task" (see Supporting information Appendix S1), unlike the main task not emphasizing precision, does not necessarily invalidate this interpretation. The reason is that even in the maximum velocity task (Supporting information Figure S2), patients and healthy subjects were still surprisingly accurate. This may suggest that a nonadmitted strategy, ensuring precision, may have still influenced the behaviour. However, a potential alternative—a link to deficiencies of action value assessment—is suggested by a closer look at longer-term velocity changes in the course of the experiment.

It is well established that fast goal-directed eye movements, saccades, when carried out repetitively at short intervals, exhibit a gradual decline in their peak velocity (Bahill & Stark, 1975). This loss of saccadic vigour is a consequence of cognitive fatigue, in particular, a gradual loss of motivation to look at a target that becomes less and less rewarding, rather than a reflection of changes of the oculomotor plant due to usage (Prsa, Dicke, & Thier, 2010; Schmidt, Abel, Dell'Osso, & Daroff, 1979). Against the backdrop of these findings on saccades, we had expected to observe analogous changes in this study of fast finger movements. However, although movement velocity varied in both groups to a similar extent, only the patients showed a consistent decline in movement velocity or fatigue. We suggest that the slower movement velocities of cerebellar patients may be the consequence of lower motivation already early in the experiment and a continuing decline in motivation in its further course. This seems plausible as the subjective load of a task demanding precision must be much higher for subjects suffering from ataxia. The gradual drop in the quality of task performance (ΔS) over the course of the experiment exhibited by the patients (Figure 5 dII) is in line with the assumption of relative overstraining and increasing exhaustion during the experimental session.

4.2 | A cerebellar velocity-duration trade-off ensuring endpoint precision

Subjects in both groups exhibited trial by trial differences in movement velocity. Yet, only healthy subjects were able to compensate differences in velocity by appropriate changes in movement duration to a large extent, thereby substantially narrowing the scatter of finger cursor endpoints around the target. The absence of appropriate duration adjustments in patients clearly indicates that the velocity-duration trade-off is based on cerebellar machinery. Is the choice of appropriate movement duration based on feedback on movement velocity? The fact that the omission of visual feedback did not affect movement trajectories at all (Figure 6), clearly argues against a role of vision in guaranteeing it in healthy subjects. Since the patients were characterized by severe impairments of their velocity duration trade-off, a control experiment trying to assess if visual feedback is needed to implement a trade-off, missing in the patients, seemed inappropriate and was therefore skipped. However, one might argue that the patients–other than healthy controls–might resort to the cursor feedback to mitigate their deficit to some extent. We cannot exclude this possibility with certainty, given the lack of data from the control experiment. Notwithstanding the possibility of different strategies in the two groups, it is safe to conclude that visual feedback of the cursor cannot account for the deteriorated velocity-duration trade-off found in patients. Although a role of cursor feedback within a given trial is not supported by the control experiment, it does not question an important role of feedback in the optimization of an internal model improving the precision of future trials in a feed-forward manner. Indeed patients may exhibit insufficient optimization. This is suggested by the fact that they —unlike healthy subjects— exhibited a gradual decline of their movement amplitudes in the main experiment, compatible with an inability to use error information delivered by the cursor feedback.

With the qualification that the results from the control experiment do not rule out that the velocity-duration trade-off involves much more instantaneous proprioceptive feedback, they might suggest namely that the cerebellum uses a priori information on the velocity of the upcoming movement in order to prepare appropriate movement duration already before movement onset. Such a pre-formed velocity-duration trade-off will only be possible if a reliable estimate of the upcoming velocity is available and it will only be a viable solution if velocity fluctuations cannot be simply avoided from the outset.

Could it be that oculomotor disturbances associated with cerebellar degeneration might explain the poor task performance observed in our patients? In an attempt not to overstrain our subjects, in particular the patients, we had refrained from implementing an explicit control of eye movements. Albeit, one can be certain that the occurrence of the peripheral target triggered a sequence of covert and overt shifts of attention to the target, followed by the finger movement only a few tens of milliseconds later. Hence, the planning of the next finger movement would be dependent on the vision of a target appearing optimally at 10° eccentricity and because of likely dysmetria a bit off, for example at 9 or 11° of eccentricity in the patients. The differences in visual resolution within the range of eccentricities mentioned are probably too small to expect qualitative differences in performance and/

or the selection of strategies differing between two groups. Moreover, also later corrections of dysmetric primary saccades based on secondary saccades would be too late to influence the finger movement. In sum, we suggest that the alterations of the patients′ finger movements are not a consequence of altered eye movements. Rather we would argue that the two motor systems share a common deficiency, namely the lack of an appropriate velocity-duration trade-off.

In previous work on saccadic adaptation of cerebellar patients we demonstrated that the inability of patients to use error feedback to up-regulate their saccade amplitudes was a direct consequence of the failure to adjust saccade durations (Golla et al., 2008). Electrophysiological work on saccadic adaptation of experimental animals suggests that a Purkinje cell simple spike signal controls the adjustment of saccade duration (Catz, Dicke, & Thier, 2008; Thier, Dicke, Haas, & Barash, 2000). Assuming a generic role of the Purkinje cell simple spike firing patterns, the duration adjustment limitations exhibited by the patients in our previous work on eye movements and this study of fast finger movements may be a direct consequence of a loss of the Purkinje cell simple spike control signal that is able to make use of information on the velocity of the ongoing movement.

5 | CONCLUSION

This study has established that the dysmetria of fast finger movements, a central aspect of the ataxia of cerebellar patients, is a direct consequence of the loss of a cerebellum-based velocity-duration trade-off mechanism that fine-tunes movement durations based on information on the expected velocity of the movement. Arguably, deficient temporal control might also explain other aspects of movement deficiencies exhibited by cerebellar patients usually captured by the term ataxia.

ACKNOWLEDGEMENTS

We are grateful to Melanie S. Höller-Wallscheid for her invaluable help in collecting patient data during the experiment and Dr David J. Mack for his encouraging feedback and advice on data analysis. We especially thank Dr Friedemann Bunjes for his technical assistance. This work was supported by the Werner Reichardt Centre for Integrative Neuroscience (CIN) at the Eberhard Karls University of Tübingen. The CIN is an Excellence Cluster funded by the Deutsche Forschungsgemeinschaft (DFG) within the framework of the Excellence Initiative (EXC 307).

CONFLICT OF INTERESTS

The authors have no conflicts of interests to declare.

DATA ACCESSIBILITY

As our data are collected from human subjects, it has still to be discussed with the local Ethics Committee which form is most suitable for public availability.

AUTHOR CONTRIBUTIONS

Akshay Markanday, Julian Messner and Peter Thier designed the experiments and worked on the manuscript. A. M. and J. M. conducted the experiments. J. M. collected the clinical data and A. M. performed the data analysis. Both, A. M. and J. M. contributed equally to this project.

ORCID

Peter Thier http://orcid.org/0000-0001-5909-4222

REFERENCES

Albus, J. S. (1971). A theory of cerebellar function. *Mathematical Biosciences*, *10*, 25–61. https://doi.org/10.1016/0025-5564(71)90051-4

Bahill, A. T., & Stark, L. (1975). Overlapping saccades and glissades are produced by fatigue in the saccadic eye movement system. *Experimental Neurology*, *48*, 95–106. https://doi.org/10.1016/0014-4886(75)90225-3

Bechert, K., & Koenig, E. (1996). A search coil system with automatic field stabilization, calibration, and geometric processing for eye movement recording in humans. *Neuro-Ophthalmology*, *16*, 163–170. https://doi.org/10.3109/01658109609009677

Bhanpuri, N. H., Okamura, A. M., & Bastian, A. J. (2014). Predicting and correcting ataxia using a model of cerebellar function. *Brain*, *137*, 1931–1944. https://doi.org/10.1093/brain/awu115

Catz, N., Dicke, P. W., & Thier, P. (2008). Cerebellar-dependent motor learning is based on pruning a Purkinje cell population response. *Proceedings of the National Academy of Sciences of the United States of America*, *105*, 7309–7314. https://doi.org/10.1073/pnas.0706032105

Donchin, O., Rabe, K., Diedrichsen, J., Lally, N., Schoch, B., Gizewski, E. R., & Timmann, D. (2012). Cerebellar regions involved in adaptation to force field and visuomotor perturbation. *Journal of Neurophysiology*, *107*, 134–147. https://doi.org/10.1152/jn.00007.2011

Golla, H., Tziridis, K., Haarmeier, T., Catz, N., Barash, S., & Thier, P. (2008). Reduced saccadic resilience and impaired saccadic adaptation due to cerebellar disease. *European Journal of Neuroscience*, *27*, 132–144.

Hallett, M., Shahani, B. T., & Young, R. R. (1975). EMG analysis of patients with cerebellar deficits. *Journal of Neurology, Neurosurgery and Psychiatry*, *38*, 1163–1169. https://doi.org/10.1136/jnnp.38.12.1163

Ito, M. (1982). Cerebellar control of the vestibulo-ocular reflex–around the flocculus hypothesis. *Annual Review of Neuroscience*, *5*, 275–297. https://doi.org/10.1146/annurev.ne.05.030182.001423

Izawa, J., Criscimagna-Hemminger, S. E., & Shadmehr, R. (2012). Cerebellar contributions to reach adaptation and learning sensory

consequences of action. *Journal of Neuroscience*, *32*, 4230–4239. https://doi.org/10.1523/JNEUROSCI.6353-11.2012

Marr, D. (1969). A theory of cerebellar cortex. *Journal of Physiology*, *202*, 437–470. https://doi.org/10.1113/jphysiol.1969.sp008820

Maschke, M., Drepper, J., Kindsvater, K., Kolb, F. P., Diener, H.-C., & Timmann, D. (2000). Involvement of the human medial cerebellum in long-term habituation of the acoustic startle response. *Experimental Brain Research*, *133*, 359–367. https://doi.org/10.1007/s002210000417

Prsa, M., Dicke, P. W., & Thier, P. (2010). The absence of eye muscle fatigue indicates that the nervous system compensates for non-motor disturbances of oculomotor function. *Journal of Neuroscience*, *30*, 15834–15842. https://doi.org/10.1523/JNEUROSCI.3901-10.2010

Savitzky, A., & Golay, M. J. (1964). Smoothing and differentiation of data by simplified least squares procedures. *Analytical Chemistry*, *36*, 1627–1639. https://doi.org/10.1021/ac60214a047

Schmidt, D., Abel, L. A., Dell'Osso, L. F., & Daroff, R. B. (1979). Saccadic velocity characteristics: Intrinsic variability and fatigue. *Aviation, Space and Environmental Medicine*, *50*, 393–395.

Schmitz-Hubsch, T., du Montcel, S. T., Baliko, L., Berciano, J., Boesch, S., Depondt, C., … Fancellu, R. (2006). Scale for the assessment and rating of ataxia: Development of a new clinical scale. *Neurology*, *66*, 1717–1720. https://doi.org/10.1212/01.wnl.0000219042.60538.92

Shadmehr, R., Smith, M. A., & Krakauer, J. W. (2010). Error correction, sensory prediction, and adaptation in motor control. *Annual Review of Neuroscience*, *33*, 89–108. https://doi.org/10.1146/annurev-neuro-060909-153135

Therrien, A. S., & Bastian, A. J. (2015). Cerebellar damage impairs internal predictions for sensory and motor function. *Current Opinion in Neurobiology*, *33*, 127–133. https://doi.org/10.1016/j.conb.2015.03.013

Thier, P., Dicke, P. W., Haas, R., & Barash, S. (2000). Encoding of movement time by populations of cerebellar Purkinje cells. *Nature*, *405*, 72–76. https://doi.org/10.1038/35011062

Topka, H., Konczak, J., Schneider, K., Boose, A., & Dichgans, J. (1998). Multijoint arm movements in cerebellar ataxia: Abnormal control of movement dynamics. *Experimental Brain Research*, *119*, 493–503. https://doi.org/10.1007/s002210050365

Van Opstal, A. J., & Van Gisbergen, J. A. (1987). Skewness of saccadic velocity profiles: A unifying parameter for normal and slow saccades. *Vision Research*, *27*, 731–745. https://doi.org/10.1016/0042-6989(87)90071-X

Wild, B., Klockgether, T., & Dichgans, J. (1996). Acceleration deficit in patients with cerebellar lesions. A study of kinematic and EMG-parameters in fast wrist movements. *Brain Research*, *713*, 186–191. https://doi.org/10.1016/0006-8993(95)01514-0

SUPPORTING INFORMATION

Additional supporting information may be found online in the Supporting Information section at the end of the article.

How to cite this article: Markanday A, Messner J, Thier P. A loss of a velocity-duration trade-off impairs movement precision in patients with cerebellar degeneration. *Eur J Neurosci*. 2018;48:1976–1989. https://doi.org/10.1111/ejn.14062

Supporting information

Complementary behavioural paradigms

In addition to the standard clinical procedures for the assessment and rating of ataxia, we asked all our patients and healthy subjects to participate in a series of three short tests (Fig. 1B) focusing on individual aspects of finger movements, before the main experiment, to get more reliable estimates of the symptomatology. The first test was the 'Oscillations test' in which participants were asked to execute rapid, unguided vertically oscillating movements for 10 seconds, around a red target dot (diameter: 1.7 cm) displayed in the middle of the screen but without endpoint target. The purpose of this task was to measure the maximum oscillation frequency of the index finger. To this end, subjects were free to choose the movement amplitudes ensuring the highest possible movement frequency. In the second test, the 'Maximum velocity test', subjects had to execute very fast movements (60 trials; trial duration: 1,400 ms) between two vertically alternating targets. As the main interest of this experiment was to measure the maximum finger velocity possible, precision was not enforced although feedback on the finger position was provided. Finally, in the third test, the 'Fixations test', subjects had to fixate at each of the three target positions (in the order centre: x=0 cm, y=0 cm; up: x=0 cm, y=+12.5 cm and down: x=0 cm, y=-12.5 cm) with the cursor for 10 seconds.

Oscillations test

The patients were much slower when trying to execute fast oscillatory movements around a stationary target centred on the screen, a manifestation of 'adiadochokinesia' (Holmes, 1917). In order to quantify the deficit in patients, we subjected the oscillatory movements of individual

subjects to a fast Fourier analysis, determined the dominating maximal oscillation frequency and calculated averages for the two groups. Overall, healthy participants generated a mean maximal dominating frequency of 5.86 Hz (+/-0.79 sd) of their oscillatory finger movements as compared to 3.23 Hz (+/-0.95 sd) reached by the patients (Fig. S1C**,** group difference significant, Wilcoxon rank-sum test, $z= 3.96$, $p=7.38\times10^{-5}$).

Maximum velocity test

In order to reveal the maximum vigour of movements, we explicitly asked participants in this task to execute up and down movements towards the target as fast as they could, without encouraging accuracy. We observed that healthy participants could generate movements with higher peak velocity (Fig. S2A, S2B, S2D and S2E) as compared to cerebellar patients. The population mean of the peak velocity of all trials pooled across all healthy participants (Fig. S2A, up: $\mu_{pv}=368.7$ cm/s; Fig. S2D**,** down: $\mu_{pv}=411.67$ cm/s) was significantly higher (Wilcoxon rank-sum test, up: $z=13.65$, $p=2.11\times10^{-42}$; down: $z=11.11$, $p=1.16\times10^{-28}$) than in cerebellar patients (Fig. S2A, up: $\mu_{pv}=262.5$ cm/s; Fig. S2D, down: $\mu_{pv}=310.65$ cm/s). Even though the task did not require the movements to be accurate, both groups exhibited trajectories that would bring the movement endpoints close to the target location (Fig. S2C and S2F). While in healthy participants 66.35% of up and 40.27% of down movements landed in an area 2.5 cm above and below the target, the patients could meet the same criteria in only 48.7% and 27.95% for up and down movements, respectively. Moreover, patients exhibited a larger variability in their movement amplitudes, both for up and for down movements (F-Test, $F=0.68$, $p=0.0002$; down, $F=0.76$, $p=0.0064$).

Fixations test

In order to test for movement accuracy, participants had to fixate the cursor with their index finger. The target was turned on at three possible target locations starting from centre (x, y)=(0,0) to top: (x, y)=(0,12.5) and then bottom (x, y)=(0,-12.5) with ample time to move to the target. We observed that both cerebellar patients and healthy participants displayed a consistent tendency to undershoot the target at the top-most location (Fig. S3A and S3C), which was absent around the middle and bottom targets. Independent of this bias of both groups, the patients were less accurate and displayed much larger fixation variability around the target dot, a reflection of dysmetria. On the other hand, healthy participants (Fig. S3A and S3B) were more accurate and showed much less variability around the target (F-test, top, F=0. 03, p=0; mid: F=0.13, p=0; bottom: F=0.05, p=0).

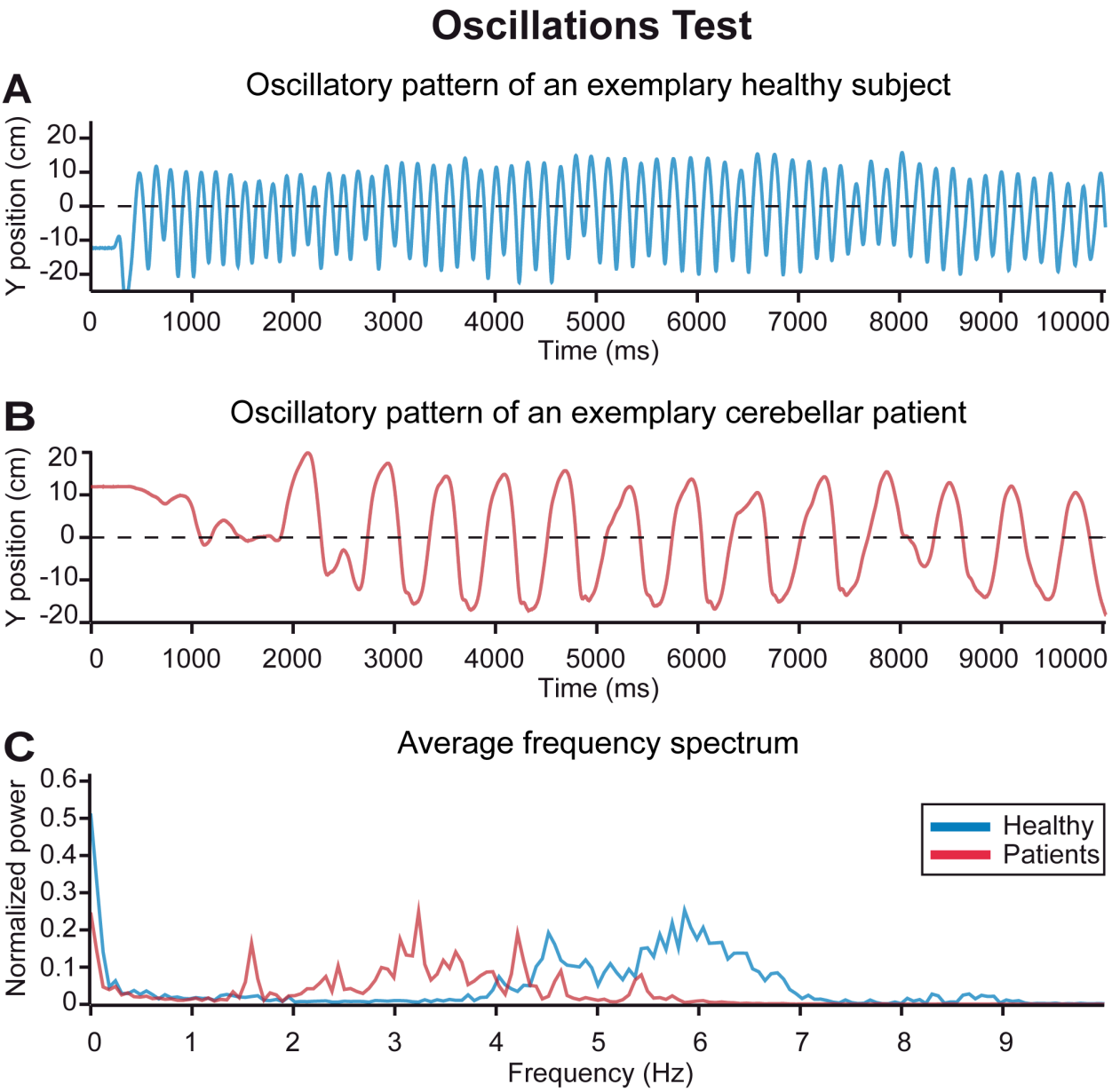

FIG. S1. Test of maximum finger oscillation. (A, B) Position trace of an exemplary healthy participant (solid blue line) and a cerebellar patient (solid red line) respectively, exhibiting rapid oscillatory movements around a stationary red dot, presented at the centre of the screen (black dashed line). **(C)** Average frequency spectrum for all healthy subjects (solid blue line) and

cerebellar patients (solid red line). Patients' maximum oscillation frequency is lower than that of the healthy group.

Maximum velocity test

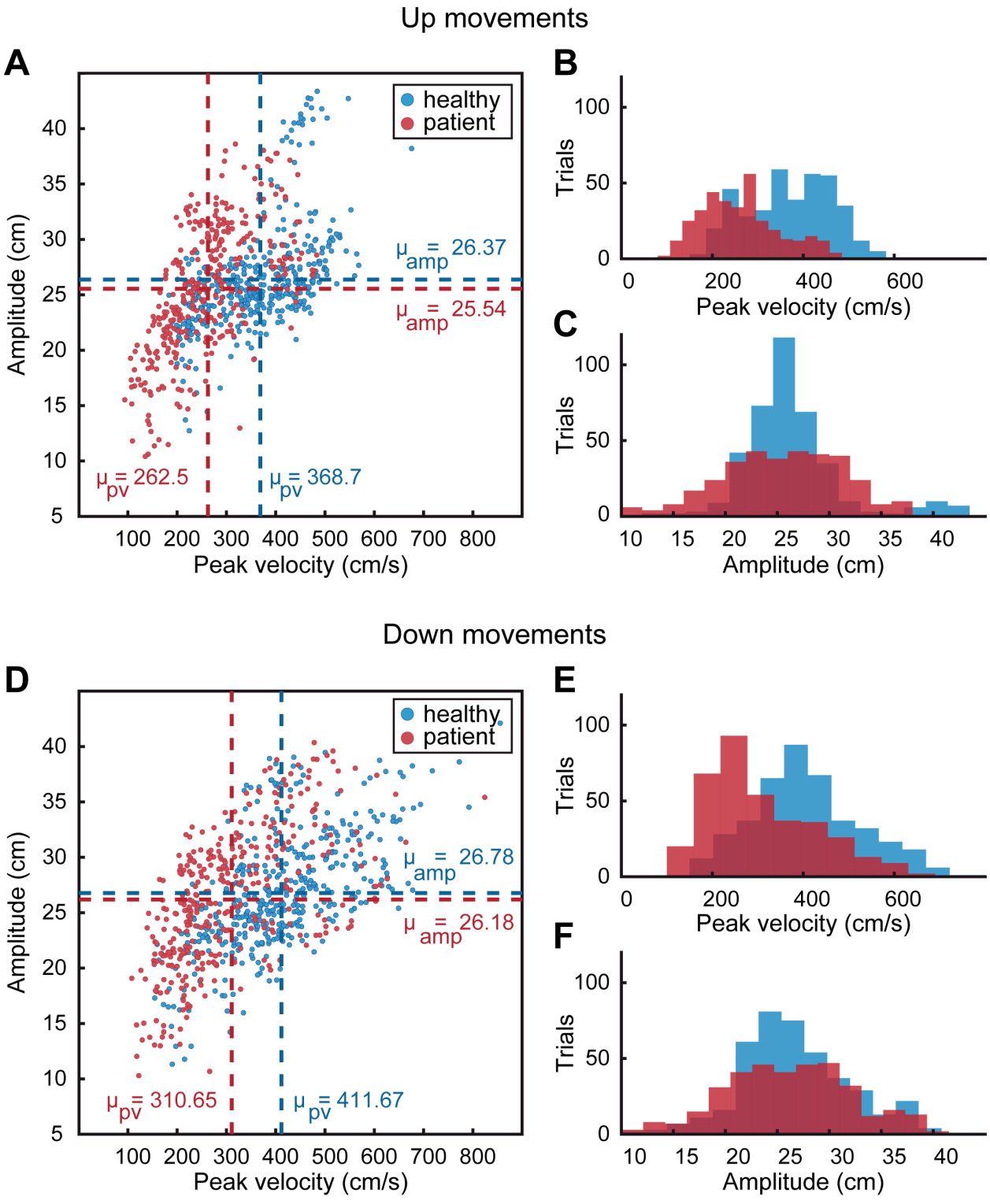

FIG. S2. Maximum velocity test. (A, D) Scatter plots showing peak velocity and amplitude of single trials pooled for all patients (red) and healthy participants (blue) for up and down finger movements, respectively. Population means of amplitudes and peak velocities, for up and down movements are represented by dashed lines. **(B, E** and **C, F)** Peak velocity and amplitude distribution for all trials combined in healthy subjects (blue) and patient group (red), for up and down movements, respectively. Patients generate much slower movements as compared to healthy subjects (Wilcoxon rank-sum test, up: $z=13.65$, $p=2.11\times10^{-42}$; down: $z=11.11$, $p=1.16\times10^{-28}$).

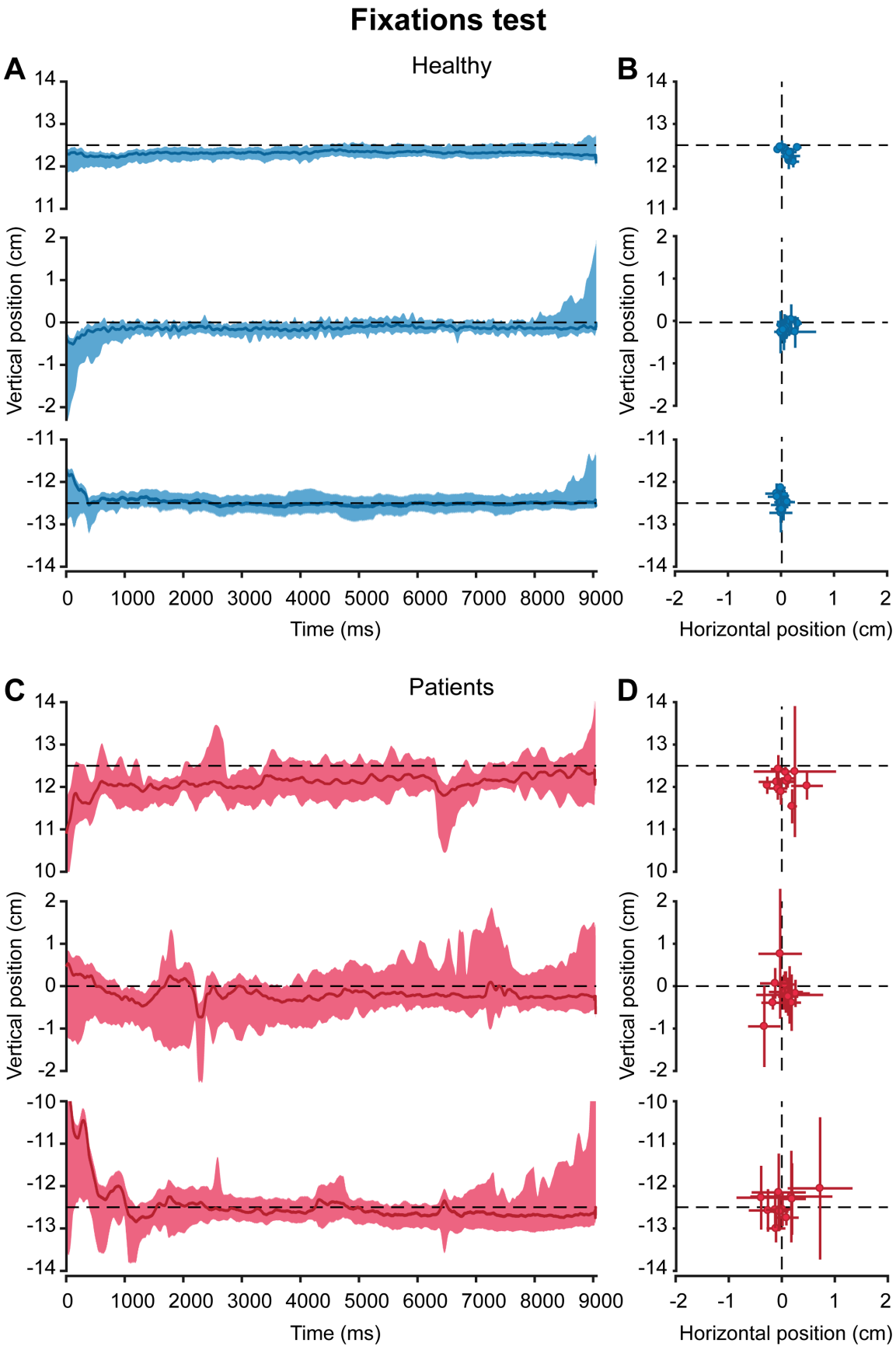
Fixations test
A
Healthy
B
C
Patients
D
Vertical position (cm)
Time (ms)
Horizontal position (cm)

FIG. S3. Fixations test. (A, C) Mean vertical finger positions of all healthy participants (blue line) and patients (red line), respectively, tested at three vertical target locations (dotted black lines) starting from centre (x, y)=(0,0) to top: (x, y)=(0,12.5) and then bottom (x, y)=(0,-12.5). Standard deviation is shown by the shaded regions around the solid lines. **(B, D)** Mean horizontal and vertical finger position of single healthy subjects (solid blue circles) and patients (solid red circles), respectively, was computed for the last 9 seconds of a trial. Standard deviation is shown by error bars. Patients show larger fixation variability as compared to healthy subjects (F-test, top, F=0. 03, p=0; mid: F=0.13, p=0; bottom: F=0.05, p=0).

APPENDIX 2

J Neurophysiol 123: 2217–2234, 2020.
First published May 6, 2020; doi:10.1152/jn.00754.2019.

INNOVATIVE METHODOLOGY

Using deep neural networks to detect complex spikes of cerebellar Purkinje cells

Akshay Markanday,[1,2,3]* Joachim Bellet,[1,2,3]* Marie E. Bellet,[3] Junya Inoue,[1] Ziad M. Hafed,[1,3]* and Peter Thier[1,3]*

[1]*Hertie Institute for Clinical Brain Research, Tübingen, Germany;* [2]*Graduate School of Neural and Behavioral Sciences, International Max Planck Research School, Tübingen University, Tübingen, Germany; and* [3]*Werner Reichardt Centre for Integrative Neuroscience (CIN), Tübingen, Germany*

Submitted 16 December 2019; accepted in final form 4 May 2020

Markanday A, Bellet J, Bellet ME, Inoue J, Hafed ZM, Thier P. Using deep neural networks to detect complex spikes of cerebellar Purkinje cells. *J Neurophysiol* 123: 2217–2234, 2020. First published May 6, 2020; doi:10.1152/jn.00754.2019.—One of the most powerful excitatory synapses in the brain is formed by cerebellar climbing fibers, originating from neurons in the inferior olive, that wrap around the proximal dendrites of cerebellar Purkinje cells. The activation of a single olivary neuron is capable of generating a large electrical event, called "complex spike," at the level of the postsynaptic Purkinje cell, comprising of an initial large-amplitude spike followed by a long polyphasic tail of small-amplitude spikelets. Several ideas discussing the role of the cerebellum in motor control are centered on these complex spike events. However, these events, only occurring one to two times per second, are extremely rare relative to Purkinje cell "simple spikes" (standard sodium-potassium action potentials). As a result, drawing conclusions about their functional role has been very challenging. In fact, because standard spike sorting approaches cannot fully handle the polyphasic shape of complex spike waveforms, the only safe way to avoid omissions and false detections has been to rely on visual inspection by experts, which is both tedious and, because of attentional fluctuations, error prone. Here we present a deep learning algorithm for rapidly and reliably detecting complex spikes. Our algorithm, utilizing both action potential and local field potential signals, not only detects complex spikes much faster than human experts, but it also reliably provides complex spike duration measures similar to those of the experts. A quantitative comparison of our algorithm's performance to both classic and novel published approaches addressing the same problem reveals that it clearly outperforms these approaches.

NEW & NOTEWORTHY Purkinje cell "complex spikes", fired at perplexingly low rates, play a crucial role in cerebellum-based motor learning. Careful interpretations of these spikes require manually detecting them, since conventional online or offline spike sorting algorithms are optimized for classifying much simpler waveform morphologies. We present a novel deep learning approach for identifying complex spikes, which also measures additional relevant neurophysiological features, with an accuracy level matching that of human experts yet with very little time expenditure.

action potentials; cerebellum; complex spikes; convolutional neural networks; local field potentials; simple spikes

INTRODUCTION

The Purkinje cell (PC) output, the sole output of the cerebellar cortex, is driven by two distinct types of responses (Fig. 1*A*), the simple spike (SS) and the complex spike (CS) (Eccles et al. 1966; Thach 1967, 1968). SSs are ordinary sodium-potassium spikes with a simple bi- or triphasic shape in extracellular recordings (Fig. 1*B*). These spikes, lasting only a fraction of a millisecond and firing up to several hundred times per second, reflect the concerted impact of mossy fiber input, mediated via the granule cell-parallel fiber system, as well as inhibitory interneurons. On the other hand, an individual CS (Fig. 1*C*), elicited by a single climbing fiber originating from the inferior olivary nucleus and pervading the proximal dendrites of a PC, is characterized by a polyphasic somatic spike consisting of a first back propagated axonal spike component followed by a series of spikelets riding on a long-lasting, calcium-dependent depolarization (Davie et al. 2008; Eccles and Szentágothai 1967; Fujita 1968; Llinás and Sugimori 1980; Stuart and Häusser 1994; Thach 1968). In addition to an exceptional morphology, CSs also exhibit a perplexingly low firing rate of at most two spikes per second (Fig. 1*A*), which is much lower than the rate of SSs recorded from the same cells. What could these infrequent, yet unique, events possibly tell us about their purpose, and what might be the best statistical tool allowing us to unravel the full extent of information carried by them? These are questions that have kept researchers busy until today.

CSs have originally been hypothesized to play a crucial role in either motor timing (Leznik and Llinás 2005; Llinás 1974) or performance-error based motor learning (Albus 1971; Ito 1972; Marr 1969). While many follow-up experiments seemed to support the latter idea (Herzfeld et al. 2015, 2018; Kitazawa et al. 1998; Medina and Lisberger 2008; Oscarsson 1980), not all findings have been fully compatible with this so-called Marr-Albus-Ito hypothesis, at least not in its original form (Catz et al. 2005; Dash et al. 2010; Junker et al. 2018; Kostadinov et al. 2019; Ohmae and Medina 2015; Streng et al. 2017). As a result, reaching consensus on the diverse views of CS functions would be substantially facilitated by more data on these sparse neural events, collected in conjunction with advanced behavioral paradigms. Yet, it is exactly their unique properties of rarity combined with complex and highly idio-

* A. Markanday and J. Bellet contributed equally to this work. Z. M. Hafed and P. Thier contributed equally to this work.
Correspondence: P. Thier (thier@uni-tuebingen.de).

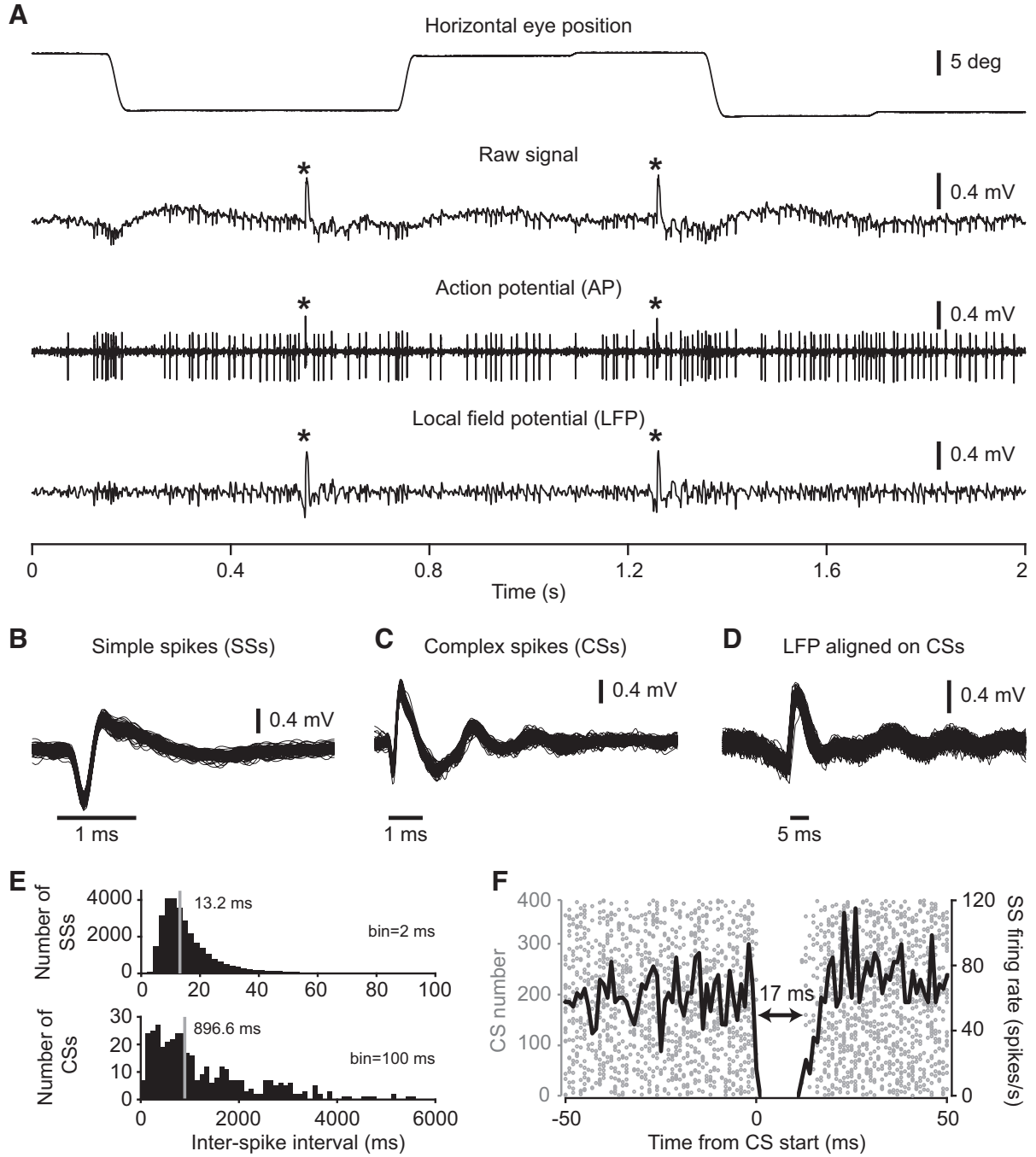

Fig. 1. Characteristics of an exemplary Purkinje cell. *A*; raw signal (wide-band, *2nd row*), action potential (AP; high band-passed, 300 Hz to 3 KHz, *3rd row*), and local field potential (LFP; low passed, 30–400 Hz, *4th row*) activity in relation to horizontal eye movements (*1st row*). *Complex spikes (CSs). *B*: a subset of isolated simple spike (SS) waveforms aligned on SS start. *C*: a subset of isolated CS waveforms aligned on CS start. *D*: a subset of LFP responses aligned to CS start. *E*: histogram of interspike intervals of SSs (*top*) and CSs (*bottom*). Solid gray line depicts the median value. *F*: raster plot showing a 17-ms pause in SS activity caused by the occurrence of a CS. Solid black line represents the mean SS firing rate aligned to CS start.

syncratic spike morphology that have hampered progress. In fact, CS morphology not only differs between individual PCs, but it also often changes over the course of a single recording session from the same PC. This is why standard spike sorting software, which may work well in detecting the much "simpler" and more frequent SSs, turns out to be highly error prone when adapted for detecting CSs. Critically, given the rarity of CSs in relation to their SS counterparts recorded from the same cells, even a few missing or erroneously detected CS events will have a profound impact on conclusions drawn about CS functional roles. Consequently, most researchers either completely shy away from dealing with this problem at all, or they do so by resorting to meticulously labeling CSs manually, possibly prepared by prior coarse predetection by conventional spike-sorting approaches. The manual approach is highly valuable, but it is also exhausting and constrains the amount of experimental data that can be processed. The net result is that in both cases (i.e., either not

addressing CS functions at all, or meticulously labeling CSs using heavy manual loads), the general pace of development in the field is compromised.

In this paper, we present a study of the performance of a convolutional neural network (CNN) developed to dramatically reduce the burden of investigators in identifying CSs. We show that our algorithm is able to learn fast and that it easily matches the performance of an experienced human expert in detecting CSs. We also demonstrate that our approach outperforms an algorithm based on principal component analysis (PCA), which was recently suggested to detect CSs (Zur and Joshua 2019), as well as a commonly used online sorting solution that researchers in the field typically use. Finally, we additionally show that our algorithm is the first, to our knowledge, to provide an accurate estimate of CS duration, a parameter that is supposed to contain critical information for motor learning (Yang and Lisberger 2014).

MATERIALS AND METHODS

Animals, Preparation, Surgical Procedures, and Recording Methods

Two adult male rhesus macaques (*Macaca mulatta*) of age 10 (*monkey K*) and 8 (*monkey E*) yr, purchased from the German Primate Center, Göttingen, were subjects in this study. Initial training of all animals required them to voluntarily enter an individually customized primate chair and get accustomed to the setup environment, a procedure that could last for up to 3 mo. Following initial training, they underwent the first major surgical procedure in which foundations of all implants were fixed to the skull using titanium bone screws and then were allowed to rest for a period of ~3–4 mo to improve the long-term stability of the implant foundations. Then, a titanium-based hexagonal tube-shaped head post was attached to the implanted head holder base to painlessly immobilize the head during experiments, and scleral search coils were implanted to record eye positions using electromagnetic induction (Bechert and Koenig 1996; Judge et al. 1980). Within 2–3 wk of recovery from the eye-coil implantation procedure, the monkeys quickly recapitulated the already learned chair-training protocol and were trained further on their respective behavioral paradigms. Once fully trained, a cylindrical titanium recording chamber, whose position and orientation were carefully planned and confirmed based on pre- and postsurgical MRIs, was finally mounted on the implanted chamber base, tilting backward by an angle of 30° with respect to the frontal plane, right above the midline of the cerebellum. A part of the skull within the chamber was removed to allow precise electrode access to our region of interest, the oculomotor vermis (OMV, lobuli VIc/VIIa), for electrophysiological recordings. All surgical procedures were carried out under aseptic conditions using general anesthesia, and postsurgical analgesics were delivered until full recovery. See Prsa et al. (2010) for full details.

All experiments and surgical procedures were approved by the local animal care authority (Regierungspräsidium Tübingen) and complied with German and European law as well as the National Institutes of Health's *Guide for the Care and Use of Laboratory Animals*. All procedures were carefully monitored by the veterinary service of Tübingen University.

Behavioral Tasks

We collected data from two monkeys generating visually guided saccades, which are known to be associated with CS occurrence (Fig. 1*A*). Each trial started with a red fixation dot (diameter: 0.2°) displayed at the center of a CRT monitor placed 38 cm in front of the monkey. After a short and variable fixation period (400–600 ms from trial onset), the fixation dot disappeared and at the same time, a target, having the same features as the fixation dot, appeared on the horizontal axis at an eccentricity of 15°. In a given session, the target was presented consistently either on the left or right of the central fixation dot. The maximum number of trials (>200) per session depended on the willingness of the monkey to cooperate and on the duration for which a PC could be kept well isolated. Each trial lasted for 1,200 ms. At the end of every correct trial, the monkeys were rewarded with a drop of water.

Electrophysiological Recordings

We recorded extracellular activity with commercially available glass-coated tungsten microelectrodes (impedance: 1–2 MΩ; Alpha Omega Engineering, Nazareth, Israel). Electrode position was controlled using a modular multielectrode manipulator (Electrode Positioning System and Multi-Channel Processor, Alpha Omega Engineering). We targeted the OMV based on the implanted position and orientation of the recording chamber that we used, and we also identified the OMV region based on the characteristic saccade-related modulation of an intense background activity, reflecting multiunit granule cell activity. The wide-band raw signal picked up by our electrode was also clearly modulated by saccadic eye movements (Fig. 1*A*, *2nd row*). The raw signal, sampled at 25 KHz, was band-pass filtered online between 30 Hz and 3 KHz to enable online spike sorting of SSs and CSs based on spike waveform shapes.

Multi Spike Detector: the Online Spike Sorting Algorithm

Single PC units were identified, online, by the presence of a high-frequency SS discharge accompanied by the signatory, low-frequency CS discharge. We used a real-time spike sorter, the Alpha Omega Engineering Multi Spike Detector (MSD), for online unit detection. The MSD, designed for detecting sharp waveforms, uses a template matching algorithm developed by Wörgötter et al. (1986), sorting waveforms according to their shape. The algorithm employs a continuous comparison of the electrode signal against an eight-point template defined by the experimenter to approximate the shape of the spike of interest. The sum of squares of the difference between the template and electrode signal is used as a statistical criterion for the goodness of fit. Whenever the goodness of fit exceeds a threshold, the detection of a spike is reported. The eight-point template can be adjusted manually or, alternatively, run in an adaptive mode that allows it to keep track of waveforms that may gradually change over time.

Online Identification of Simple Spikes and Complex Spikes in Purkinje Cells

As opposed to short duration SSs (Fig. 1*B*), characterized by short interspike intervals (Fig. 1*E*, *top*), the long duration CSs (Fig. 1*C*) are much rarer (Fig. 1*E*, *bottom*, note the different *x*-axis range from the *top*). In addition to the 10- to 20-ms-long pause in SS firing rate following the occurrence of a CS (e.g., Fig. 1*F*, Eccles et al. 1966; Bell and Grimm 1969; Latham and Paul 1971; McDevitt et al. 1982; Thach 1967), the presence of a CS is also indicated by a massive deflection of the local field potential (LFP) signal (30–400 Hz, constructed using a second order Butterworth filter with a sampling frequency of 25 KHz) lasting for the whole duration of the CS (Fig. 1*D*).

Complex Spike Detection Using a Convolutional Neural Network

Overview of our algorithm. Inspired by the architecture of a convolutional neural network (CNN) that was originally designed to segment images ("U-Net"; Ronneberger et al. 2015), our network was initially developed to detect eye movement events in one-dimensional

eye position signals ("U'n'Eye"; Bellet et al. 2019; for the network architecture, see Fig. 2 in that paper, as well as the source code on https://github.com/berenslab/uneye). In the present work, we extended the horizon of our state-of-the-art eye movement algorithm toward the detection of more complex electrophysiological events, such as CSs. The main idea of our approach is to train a classifier to extract relevant features from electrophysiological recordings of PCs and to use these features for identifying CSs. Therefore, we repurposed our existing algorithm to use the LFPs within a frequency band of 30 Hz to 400 Hz (Fig. 1*A*, *4th row*) and high-pass filtered action potential signals (30 Hz to 3 KHz; Fig. 1*A*, *3rd row*), sampled at the same frequency of 25 KHz, as inputs to the network (Fig. 2*A*, *top*). We chose these two inputs because human experts achieve consensus on the presence or absence of a CS, more easily and reliably, if both action potentials and LFPs are simultaneously available. Raw unfiltered signals (potentially containing enough information to detect CSs) are often not analyzed directly, because of a general interest in identifying spiking activity; hence, we focused on using the most commonly used filtered electrophysiological signals in the field. This approach is also consistent with that used by a recent algorithm for CS detection, which we benchmark our algorithm against in the present study (Zur and Joshua 2019). Note that since the fast Fourier transform (FFT) of a CS signal suggests that most of the low-frequency power in CSs lies around ~700 Hz, a wider LFP band than what we used here would have potentially been more optimal. However, the choice of LFP band should not strongly affect the performance of our algorithm with proper training data, and, more importantly, our choice of the LFP band (30–400 Hz) followed Zur and Joshua's recommendation, which was important to allow a fair comparison between the performance of our algorithm and that of these authors.

Because factors such as electrode impedance and distance of the electrode relative to the cell body may potentially result in amplitude

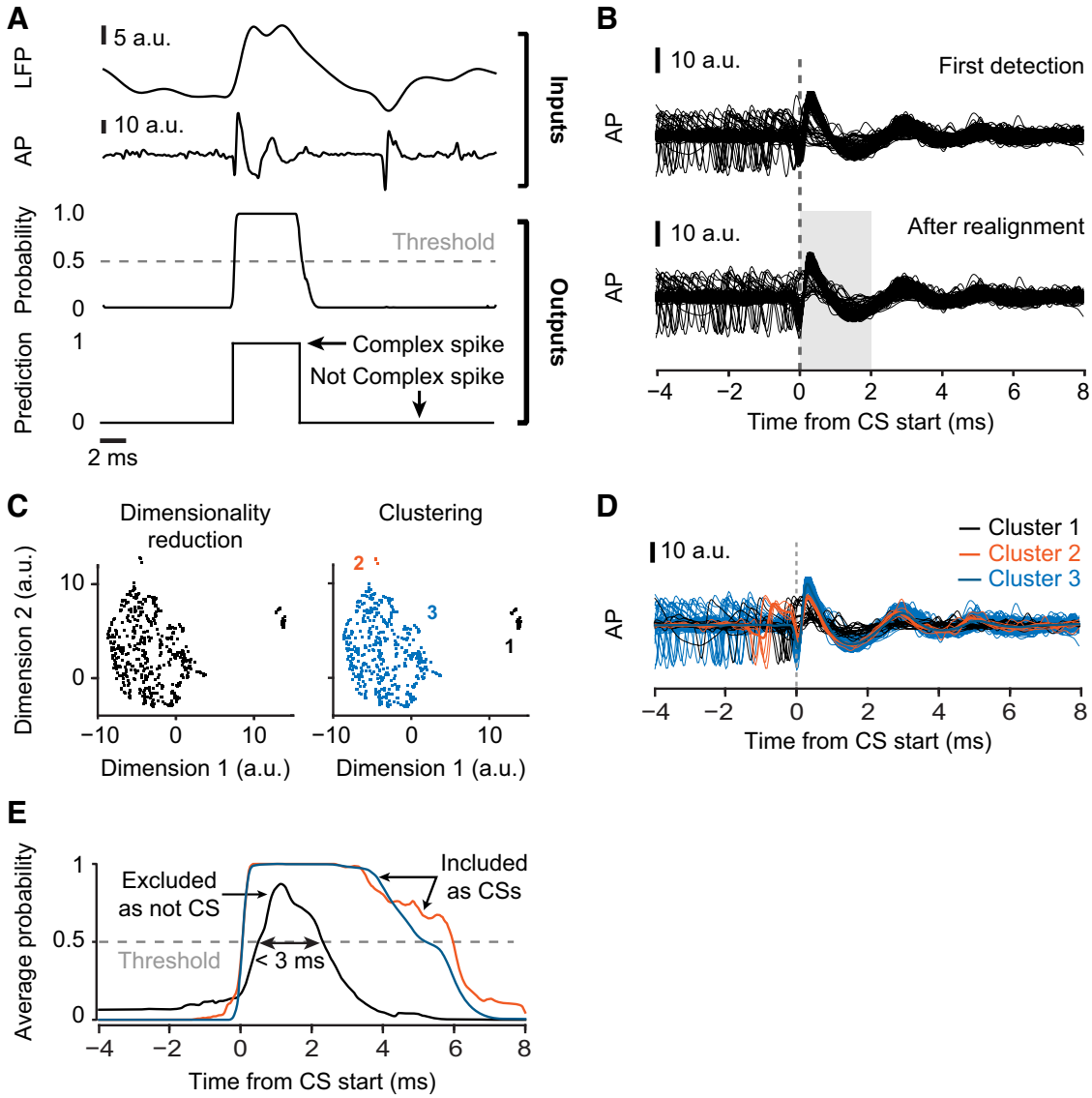

Fig. 2. Pipeline for complex spike (CS) detection. *A*: input to the network [normalized local field potential and action potential signal, labeled as LFP and AP, respectively.] as well as its output (bin-wise predictive probability CSs occurrence and binary CS classification). Dashed gray line signifies the 0.5 probability threshold value; a.u., artificial units. *B*: waveforms aligned to the first detection of start times of all CSs detected by the network (*top*) used for computing an average waveform that served as a template for realigning the waveforms of all detected CS events (*bottom*). *C*: projection of the waveforms during the 2-ms time interval (gray shaded region in *B*, *bottom*) onto a 2-dimensional plane and identification of clusters in this space. Different colors indicate distinct clusters. *D*: waveforms of the clusters in *C*. Note how *cluster 1* clearly violates well-known CS waveform shapes. *E*: average predictive probability output of the network for the events in each cluster. Clusters, whose probability output exceeds the classification threshold of 0.5 (dashed gray line) for <3 ms, are excluded as not representing CSs (*cluster 1*).

scaling of the recorded signals across different recording sessions, we first normalized the LFP and action potential signals by dividing them by the median of the nonnegative signal components. These normalized signals were input to the CNN (Fig. 2*A*, *top*) and combined by the first convolutional layer. The network classified the inputs at every given time point as being either "CS" or "Not CS" (Fig. 2*A*, *bottom*). The classification was achieved by applying a threshold to the result of the final output neuron of the CNN, which may be thought of as providing a predictive probability of the presence of a CS (Fig. 2*A*, *middle*). We picked a threshold of 0.5 on this predictive probability. The prediction for each time bin depended on an interval in the input signal whose size was determined by the size of the max-pooling and convolutional kernels of the CNN. The output was a bin-wise predictive probability of CS occurrence that further underwent a subsequent postprocessing step (described below) to exclude potential false alarms. The details of the network and the steps involved in post processing are explained in more detail in the following sections.

Convolutional neural network details. Our network uses convolutional and max-pooling operations to extract temporal features relevant for distinguishing CSs from the surrounding signal. Max-pooling is an operation that down-samples the input signal to reduce the dimensionality of its representation in the network. It filters the input with a certain window size and extracts only the maximum value. It then steps further on the input, repeating the same operation on the next time window. Convolutional layers extract relevant features of the input signal by learning the parameters of its convolutional kernel during training. The total number of parameters used in the model was 31,482. We chose the size of the max-pooling (mp) and convolutional kernels (c) as seven and nine bins, respectively. These influence the signal interval (SI) taken into account for labeling one time bin in the output, as described by the formula

$$\mathrm{SI} = \frac{(c+1)mp^2 + (c-1)mp + 2(c-2)}{2}$$

The formula for this SI was determined analytically by applying the kernels of the network layers in a chain. In our case, the SI corresponds to 281 time bins centered around each classified bin containing a predicted CS event. As our sampling rate was 25 kHz, a CS of 10-ms duration would span 250 time bins. This means that the network was often using information surrounding CS events (281 vs. 250 time bins) to classify CSs. In applications with different sampling rates than ours, the choice of SI can be adjusted to match our strategy of using information surrounding individual CS events.

Training and testing procedures. To prepare the training set, we asked a human expert, experienced in the visual classification of PC spikes, to identify CS events and manually label their start and end points. The expert did this for a total of 159 recorded PCs. For this, the expert used small segments of action potential and LFP recordings, without having access to eye movement data. For each PC, 24 segments, each 250-ms long, were manually labeled. Due to the probabilistic nature of CS occurrence, a recording segment could either contain a CS or not. This resulted in 250-ms-long "labeled input" segments with binary values; 1, between the start and end points of the manually labeled CSs, and 0 elsewhere. For our training set, we only considered those recording segments that contained at least one CS.

For every PC tested for CS detection, we trained a separate network excluding the currently tested PC from the training set. This "leave-one-out" approach allowed us to test how well the network generalized to new data sets, on which it had not been trained, and it also allowed us to have multiple performance tests on our algorithm. Therefore, the training set always comprised the remaining 158 PCs not being currently tested. Depending on which PC was excluded from the set, due to the "leave-one-out" approach, our training set consisted of 2,160–2,192 recording segments that corresponded to a total duration of 540–548 s. Other parameters of network training, such as loss function, learning rate, batch size, and early stopping criterion, were chosen as described in Bellet et al. (2019) for U'n'Eye.

We also performed one more performance test of our and other algorithms, which was concerned with establishing consistency with expert labeling. For seven PCs (out of 159), we asked our human expert to manually label CSs in the entire records and not just a small training subset within each of them. This allowed us to directly compare the labeling of the entire records of these seven PCs by all algorithms that we considered in this study and the human expert. The choice of these seven PCs was based on how well isolated the units were, which allowed the other algorithms to perform at their best capacities in detecting CSs, thus posing a tough competition to our algorithm. Our algorithm in this case was based on training the network on segments from the remaining 158 PCs (other than the currently tested one), as described above.

Postprocessing. We implemented three automated postprocessing steps to enhance the quality of CS detection by our algorithm, for example, to minimize false alarms. First, time shifts between the detected start points of all CSs fired by a particular PC were corrected by realigning them. To this end, we computed the average waveform from the first detection of start times of all detected CSs (Fig. 2*B*, *top*). This average-waveform template was then used as a reference to realign each waveform within a ±2-ms window around CS start so that the cross correlation was maximized (Fig. 2*B*, *bottom*). Second, action potential and LFP waveforms, occurring within 2 ms after CS start, were projected onto a two-dimensional plane (Fig. 2*C*, *left*) using the Uniform manifold approximation and projection (UMAP) dimensionality reduction technique (McInnes et al. 2018). The waveform clusters after dimensionality reduction represented potential candidates for CSs of the recorded PC. Some of these candidates needed to be excluded. For example, if the network in the first step mistakenly classified non-CS events as CSs, then the clustering method would help to refine the classification. This was achieved by using a third postprocessing step (Fig. 2*C*, *right*) to cluster waveforms into suitable CSs and unsuitable ones. For example, among the CS events erroneously detected by the network, there might be SSs that are revealed by a separate cluster in the two-dimensional space (Fig. 2, *C*, *right*, and *D*, black vs. orange and blue). In this third step, groups of waveforms were identified (Fig. 2*D*) using HDBSCAN, a hierarchical clustering algorithm (Campello et al. 2013) that builds a tree to describe the distance between data points. The algorithm minimizes the spanning size of the tree and further reduces the complexity of the tree to end up with a minimum number of leaf nodes, corresponding to the clusters. We used the default parameters for HDBSCAN with the option to find only one cluster. Waveforms were excluded if they belonged to a cluster for which the average predictive probability output from the network remained above 0.5 for less than 3 ms, which was deemed too brief to be an appropriate duration of CS waveform (Fig. 2*E*). Not only non-CS events might have contributed to a distinct cluster separated from the main CS cluster, but true CSs with slightly deviant waveforms (Fig. 2*D*, orange vs. blue) might also have led to separate clusters in the two-dimensional space (Fig. 2*C*, orange vs. blue). For all CS clusters that met the defined threshold criterion on predictive probability (Fig. 2*E*, *cluster 1* and *2*), CS timing and corresponding cluster IDs allowed the user to carefully inspect each cluster and decide whether to include clusters with deviant, yet true, CSs or not.

Optional postverification. After receiving the final output from our algorithm, comprising of CS start and end times, embedding dimensions, as well as cluster IDs, users can optionally add a postverification step to track secondary effects that they may be interested in investigating (e.g., gradual drift in cell position relative to the electrode). To do this in our own analyses, we visually verified the authenticity of the detected CSs. For this, we relied on the shape of the averaged CS waveforms belonging to each cluster as well as the pause induced by the same cluster (putative PC) in SS firing. Similar CSs, albeit grouped under a separate cluster (possibly due to a modified

shape of their waveform), induced pauses of similar duration in SS firing. On the other hand, false positives were excluded based on their inability to match the above criteria. Although not embedded in our automated algorithm, this manual "postverification" step can provide added confidence regarding the performance of our algorithm, and at a minimal cost of time investment. Indeed, all results in this paper (except those in Fig. 10) describe the performance of our algorithm without any manual postverification.

Complex Spike Detection Using Zur and Joshua's PCA-Based Algorithm

To compare the performance of our algorithm to the recently developed PCA-based algorithm (Zur and Joshua 2019), we used the graphical user interface (GUI) provided by the authors at https://github.com/MatiJlab/ComplexSpikeDetection. The code was adjusted to open our data (i.e., .mat files), but we otherwise followed all instructions provided by the authors. To have a fair comparison with our fully automated algorithm, we excluded (from our algorithm) the last "postverification" step based on visual selection of each putative CS.

Quality Metrics

We evaluated the performance of all three algorithms (ours, the PCA-based approach, and the MSD) in detecting CSs using the so-called F1 score (Dice 1945; Sorensen 1948), which compares the consistency of CS labels predicted by the algorithm with the "ground-truth" labels provided by the human expert. The F1 score is the harmonic mean of recall (the ratio of true positive detections and all true CS labels) and precision (the ratio of true positive detections and all CS labels predicted by the algorithm), as given by the following equation:

$$\mathrm{F1} = \frac{2 \times \mathrm{recall} \times \mathrm{precision}}{\mathrm{recall} + \mathrm{precision}}$$

In our case, an F1 score of 1 would suggest that the CSs predicted by our algorithm perfectly matched the "ground-truth" labels provided by the human expert. However, a lower F1 score may suggest that CSs were either erroneously missed or falsely detected. For quality assessment, we also computed the post-CS firing rate of SSs, a signatory feature immune to labels detected by the human expert, which served as a reliable and objective criterion for the identification of a CS. Finally, the resulting CS waveforms were scrutinized by visual inspection.

RESULTS

Our goal in this study was to develop an algorithm for CS detection that matches human-level performance while at the same time minimizing the amount of effort needed in manual labeling and inspection. We achieved this by utilizing a machine learning approach in which a human expert manually labels a very small training data set, which is then used to train a CNN for feature extraction (Fig. 2). We also added additional postprocessing (but still automated) steps that significantly increased the robustness of our algorithm. To establish the utility of our approach for the wider community, we also compared its performance to that of two established methods from the literature. In what follows, we summarize the objective measures of our algorithm's performance. As we show, our algorithm currently outperforms the existing methods in CS detection. Our code and data sets are both available freely for adaptation to individual laboratories' needs and with step-by-step tutorials on use.

Objective Quality Measure Confirms Identity of Complex Spikes

It is well-established that SS firing rate decreases during 10–20 ms after the emission of a CS (Bell and Grimm 1969; Eccles et al. 1966; Latham and Paul 1971; McDevitt et al. 1982; Thach 1967; Fig. 1*F*). This physiological feature, which is independent of the subjective assessment of the human expert, provided us with an important means for objectively measuring the CS labeling quality of our CNN-based algorithm. For 159 PCs, we evaluated SS firing rates before and after the occurrence of CSs detected by our algorithm. As depicted in Fig. 3, CSs identified by our algorithm were followed by a clear and significant decrease in the neurons' SS firing rates (Fig. 3*A*). In the pre-CS period of 3–8 ms, the median SS firing rate of the 159 PCs was 54.9 spikes/s; this dropped to 1.8 spikes/s in the post-CS period of 3–8 ms (Fig. 3*B*, Wilcoxon signed-rank test: $P = 2.1 \times 10^{-35}$). Also, this effect was clearly visible at the level of single neurons (Fig. 3, *B* and *C*), suggesting that the overall suppression of SS firing rate across all PCs (Fig. 3, *A* and *B*) was not merely a consequence of contributions made only by a fraction of the PCs. In the next section, this drop in median firing rate will be compared with that obtained when other algorithms were applied to the same data to demonstrate that our algorithm performs significantly better and with much fewer false positives.

Our Algorithm Outperforms Existing Algorithms

To demonstrate the efficiency of our algorithm, we compared its performance to two other existing approaches. The first approach, the MSD (see MATERIALS AND METHODS), is an online spike sorting application that was based on a template matching algorithm suggested by Wörgötter et al. (1986). Although initially designed to detect fast spiking events such as SSs, the potential of the MSD was quickly realized by several laboratories to detect events with more complex morphological waveforms such as CSs (e.g., Catz et al. 2005). Specifically, the approach with the MSD in terms of CS detection has traditionally been to use this application as an initial "coarse" detector of potential CSs, which was then followed by extensive manual labeling by experts. The second method that we compared our algorithm to was the recent one by Zur and Joshua (2019), which was based on PCA to separate CSs from SSs. This particular algorithm is important to compare with because, like ours, it takes advantage of the deflection in LFP signals occurring at the time of CSs. It is also the latest algorithm available in the literature.

We first investigated the proportion of CSs identified by our algorithm in addition to those found by the other approaches. Across the 159 PCs, our algorithm found a median of 32% additional CSs as compared with the MSD and 5.9% additional CSs as compared with the PCA-based algorithm. In contrast, the additional CSs detected exclusively by the MSD approach but not by our algorithm were significantly less (1.9%; $P = 1.4 \times 10^{-20}$ Wilcoxon signed-rank test; Fig. 4*A*), and the ones found exclusively by the PCA-based algorithm but not by our algorithm were also less (4.3%; $P = 0.097$; Wilcoxon signed-rank test; Fig. 4*D*).

Our algorithm also led to significantly less false positives than both the MSD- and PCA-based algorithms. To demon-

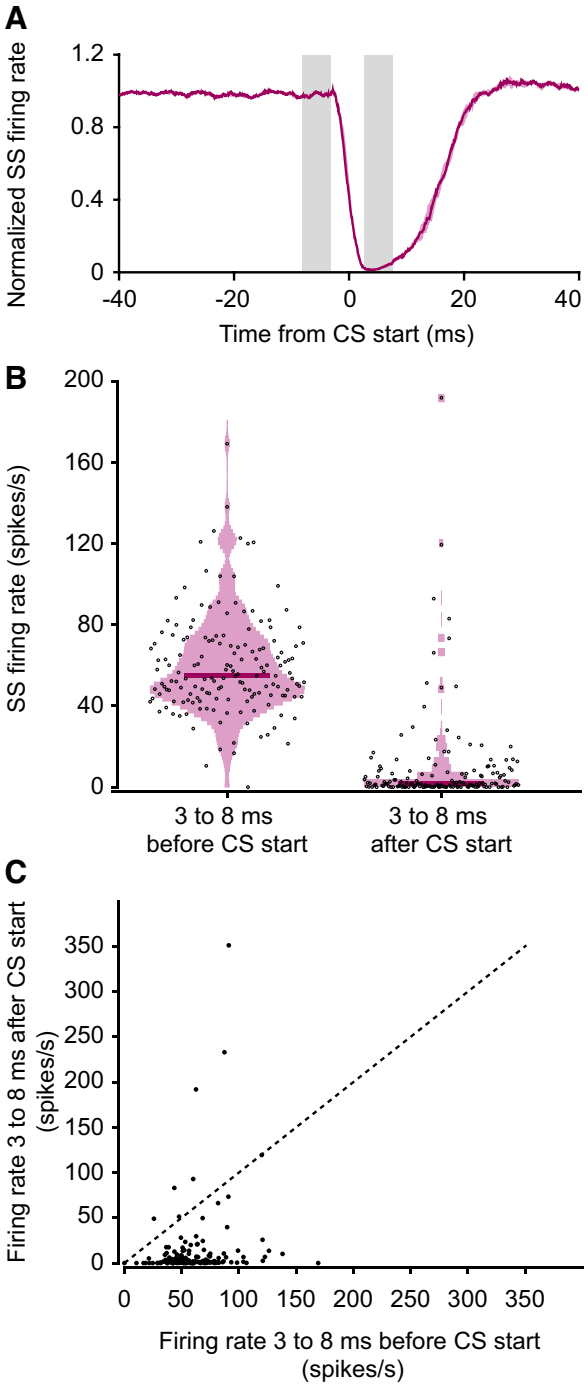

Fig. 3. Decrease of simple spike (SS) rate after complex spikes (CSs). *A*: baseline-normalized median SS firing rate aligned to the start of CSs detected by our algorithm. Data show median ± confidence intervals (obtained by bootstrapping) over 159 Purkinje cells (PCs). Gray shaded regions correspond to the period of 3 to 8 ms before and after CS start that are used for comparing SS firing rates before and after CS start, respectively. *B*: violin plots showing SS firing rate 3 to 8 ms before and after CS start. Each dot represents the average SS firing rate aligned to start time of all CSs corresponding to their respective PCs predicted by our algorithm. Thick lines indicate the median SS firing rate of all PCs. *C*: scatter plot comparing the SS firing rate of each cell (black dots), aligned to CS start, 3 to 8 ms before and after CS start. Dashed back line is the unity line.

strate this, we measured SS firing rate during a post-CS period (3–8 ms after the start times of putative CSs). We did so specifically for CSs that were found exclusively by each algorithm but not the others. A lack of sufficient pause in SS firing provided an objective physiological measure of a falsely identified CS (a true CS should have a pause in SS firing after its occurrence). In Fig. 4*B*, we found that there was a reliable pause in SS firing rate for CSs that were detected by both our algorithm and the MSD (Fig. 4*B*, gray). However, the MSD approach clearly had more false positives than our algorithm because the CSs detected exclusively by the MSD method (and not by our algorithm) had much higher SS firing rates after "putative" CS start times than true detected CSs (Fig. 4*B*, online sorter only data). These exclusively detected CSs were therefore most likely false detections. In contrast, for CS events detected exclusively by our algorithm but not by the MSD, there was still a strong pause in SS firing rate after CS event detection (Fig. 4*B*, our algorithm only data). This means that there were genuine CSs that were missed by the MSD method. The same conclusions could also be reached when we compared our algorithm to the one based on PCA (Fig. 4*E*). Therefore, our algorithm had fewer false positives than both of the other algorithms.

A closer look at the time courses of SS firing rates aligned to the start times of CSs detected exclusively by each algorithm revealed the scenarios that may explain the differential performance across algorithms (and our algorithms' overall superior performance). Specifically, Fig. 4, *C* and *F*, displays the median of normalized SS firing rate aligned to the start times of putative CSs from the pool of 159 PCs. The probability of SS occurrence for CSs detected by the MSD algorithm only (but not ours) resembled a typical autocorrelation function reflecting the refractory period of well-isolated SSs (Fig. 4*C*, dashed green curve). This suggests that the MSD algorithm tended to falsely report a CS at the time of a SS. The MSD approach also often missed CSs when SSs occurred less than 5 ms before their start times (Fig. 4*C*), which is a scenario that is known to modify the shape of CS waveforms (Servais et al. 2004). These waveforms were missed by the MSD algorithm as they differed from the template defined by the experimenter. However, our algorithm did not miss these CSs with modified waveforms (also see Fig. 10). It is the accumulation of SSs occurring just before these CSs detected exclusively by our algorithm (and not by the MSD algorithm) that explains the sharp increase in SS firing rate (Fig. 4*C*) that we observed ~3 ms before the start times of CSs. That is, because this figure shows only the CSs exclusively detected by our algorithm and not the MSD, and because SSs near CS onset modify CS shape, the CSs exclusively detected by our algorithm were ones in which SSs were so close to CS onset that they modified CS waveforms enough for the MSD to completely miss them. Interestingly, the additional CSs only detected by the PCA-based algorithm (and missed by our algorithm) also resulted in a peak in SS firing (Fig. 4*F*). At first glance, one might erroneously argue in favor of the PCA-based algorithm for being more sensitive than ours in detecting CSs. However, a closer look at the much weaker pause in SS firing rate that follows the peak clearly suggests that these additional CSs were actually not real CSs (Fig. 4*F*). They were likely false detections due to potential artifactual LFP modulations around SS events (Fig. 4*F*, *inset*).

To further demonstrate the performance differences among all three algorithms, Fig. 5 shows explicit example "CS" waveforms from five PCs with averaged LFP and action potentials. For each

cell in this figure, we show the average CS waveforms that were detected exclusively by one of the algorithms only but not by the other two. In summary, our algorithm was both more sensitive and less error prone than the online sorting application (MSD) as well as the PCA-based algorithm.

Our CNN Approach Reaches Human Expert-Level Performance

We also evaluated to what extent the predictions from the three approaches agreed with labels from a human expert. To this end, we computed the F1 score (see MATERIALS AND

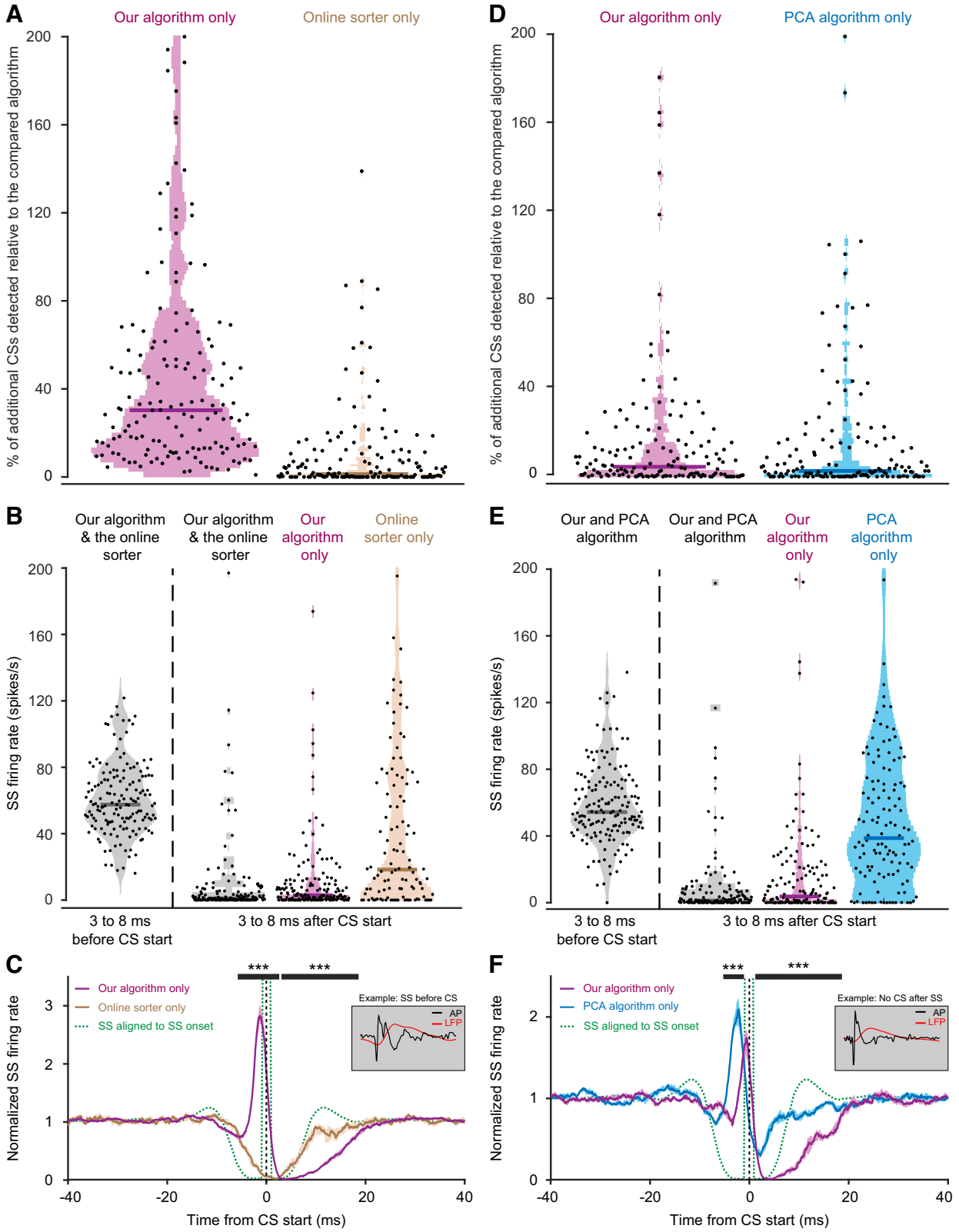

METHODS) on short recording segments from the same 159 neurons; each currently tested neuron was excluded from the training set. For these segments, we had "ground-truth" labels from the human expert. The F1 score is a measure of consistency in performance between an algorithm and the human expert. As shown in Fig. 6*A*, our algorithm agreed best with the human expert on all CS labels, reflected by an F1 score of 1 or near 1 (Fig. 6*A*). A comparison of F1 scores between our algorithm and the PCA algorithm (Fig. 6*B*, *top*), as well as our algorithm and the online sorter MSD (Fig. 6*B*, *middle*), clearly reveals that for a majority of PCs (52% in the first comparison and 79% in the latter) our algorithm achieved overall higher F1 scores than the other approaches. Comparing the F1 scores of the PCA-based algorithm to the ones achieved by the MSD (Fig. 6*B*, *bottom*), suggests that the former approach also outperformed the latter in a majority (64%) of PCs. In sum, the predictions by our approach were more "human-like" than the ones labeled by the MSD and PCA-based algorithms.

Our algorithm also did not need extensive training sets to achieve good performance in terms of the F1 score. To show this, we plotted the performance of our algorithm as a function of the amount of training data that we used to optimize the CNN's weights (Fig. 6*C*). With a training set of ~35 s, our algorithm already led to better median F1 score performance than both the PCA-based and MSD approaches ($P = 1.2662 \times 10^{-5}$and $P = 7.2048 \times 10^{-10}$ respectively, Wilcoxon signed rank test) (Fig. 6*C*).

We also summarized the performance of our algorithm against the two other algorithms using confusion matrices in Fig. 6*D*. The total number of truly detected CSs (true positives) relative to the human expert was highest in the case of our algorithm (2,053) as compared with the other algorithms (1,908 for PCA and 1,578 for MSD). Similarly, the sum of our algorithm's false positive and false negative rates was the lowest. It should be noted here that, in this context, true positive, false positive, and false negative rates are always reported relative to the human expert labels, unlike our use of these terms in our analysis of SS pauses across different algorithms (Fig. 4).

Finally, for seven PCs, we asked our human expert to fully label the entire recorded data for each neuron, instead of only a subset (MATERIALS AND METHODS). We then compared the CS labels of the three algorithms to the ones placed by the human expert on the entire records of the neurons (spanning a time range of ~8–14 min of neural recording). Overall, the predictions of our algorithm agreed very well with the human labeling (Fig. 7, see "Expert vs. Our algorithm"). A few events were identified as CSs by our algorithm but not by the human expert. However, also the waveforms of these events matched the waveforms of CSs that were labeled by the human expert (Fig. 7, *cells 3*, *5*, and *6*), indicating that the CSs ignored by the expert were indeed genuine CSs (they were probably reflecting mental lapses during manual labeling by the expert). For one of the PCs, the waveforms of additionally detected CSs indicated that our algorithm mistakenly labeled some SSs as CSs (Fig. 7, *cell 7*). These false positive detections, whose average predictive probability remained above the threshold (0.5) for more than 3 ms and were not removed during automatic postprocessing, however, would appear as isolated clusters after dimensionality reduction (Fig. 2*C*). Hence, such false detections could be easily removed post hoc by inspecting the properties of the CSs in the respective isolated cluster. For false positive labels, the average duration of the SS pause (i.e., 15–20 ms) after these events would also be reduced to the average refractory period of SSs in this recording. As compared with the human expert, the PCA-based algorithm resulted in more false positives (Fig. 7, see "Expert vs. PCA algorithm," *cells 1*, *3*, *4*, and *7*) and false negatives (*cells 3* and *5*). The MSD made mistakes mostly because of false negatives (Fig. 7, see "Expert vs. Online sorter").

The comparison with human labels further showed that our algorithm reliably identified the ends of CSs and, considering the knowledge of CS start, provided a quantitative estimate of CS duration. For the recording segments from the 159 PCs, we compared the end times of all CSs that were detected by both our algorithm and the human expert. Correspondingly, average CS durations per cell predicted by our algorithm and the human expert were highly correlated ($\rho = 0.89$, $P = 6.15 \times 10^{-41}$, Spearman correlation; Fig. 8*A*). In light of a possible CS duration code supplementing a CS rate code (Herzfeld et al. 2015, 2018; Junker et al. 2018; Warnaar et al. 2015; Yang and Lisberger 2014), it is important to precisely identify the end times of CSs and to track changes in CS duration in conjunction with behavioral changes even within individual PCs, a particularly tedious task for the expert who has to scrutinize the data. Our algorithm was indeed capable of identifying small variations in CS duration similar to the expert. This is indicated by a strong correlation ($\rho = 0.5$, $P = 2.09 \times 10^{-102}$, Spearman correlation; Fig. 8*B*) of the residuals of human-labeled and algorithm-labeled CS end times of the selected 159 PCs,

Fig. 4. Comparison of complex spike (CS) detection by our algorithm, the principal component analysis (PCA)-based algorithm and the online sorter application Multi Spike Detector (MSD). *A*: violin plots showing the percentage of additional CSs detected exclusively by our algorithm and the online sorter. The percentage of additional CSs detected by an algorithm was calculated using the formula: (CSs detected by algorithm − CSs detected by both/CSs detected by both) × 100, where 100% corresponds to the number of CSs detected by both methods. Our algorithm detected significantly more CSs than the MSD. *B*: violin plots showing simple spike (SS) firing rate aligned to the start of the CSs predicted by both algorithms (gray) or of the events additionally labeled as CSs by either our algorithm (pink) or the online sorter (beige). The decrease in SS firing after CSs, predicted by our algorithm but not by the online sorter, indicates a higher sensitivity of our algorithm. *A* and *B*: each dot represents the average SS firing rate aligned to all CSs for the recording of 1 neuron. Thick lines indicate the median. *C*: pause in the baseline normalized median (±confidence intervals) SS firing rate following a CS. The sharp increase in SS firing rate ~3 ms before CS start (vertical dashed line in black), observed only for CSs detected by our algorithm (pink), and not the MSD (beige), suggests that these SSs occurring shortly before the start of CSs might have altered their waveform. Note how the pause in the SS firing due to CSs detected by the MSD (beige) resembles the SS autocorrelation (green dashed line). Only our algorithm was sensitive enough to detect such CSs with altered waveforms. Black bars on *top* show (with ***) intervals with a significant difference between the 2 traces (random permutations cluster corrected for multiple comparisons). AP, action potential. *C*, *inset*: an example of such a waveform. *D*, *E*, and *F*: Same as in *A*, *B*, and *C*, except now the comparison is made to the PCA-based algorithm (cyan). The sharp increase in SS activity just before the start of CSs detected by the PCA-based algorithm may suggest that their algorithm was also sensitive enough to capture changes in CS waveform. However, unlike the pause in SS firing induced by CSs detected by our algorithm, the pause observed in their case was much weaker. This suggests that the additional events detected by the PCA algorithm were not real CSs but rather other events like SSs paralleled by deflections in the local field potential (LFP) signal. *F*, *inset*: an example of such false detection.

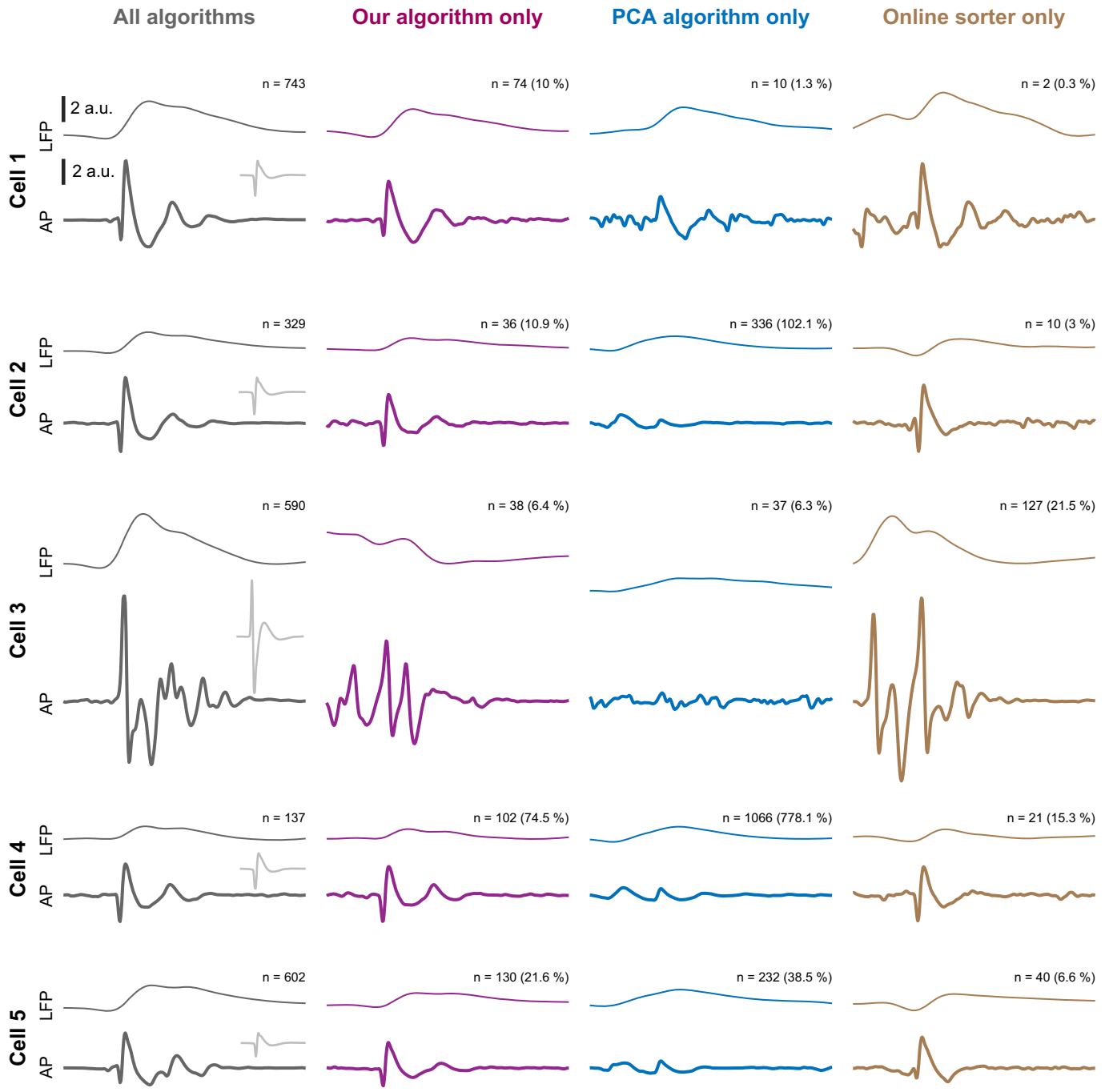

Fig. 5. Waveforms of events labeled as complex spikes (CSs) by our algorithm, the principal component analysis (PCA)-based algorithm, and the online sorting application Multi Spike Detector (MSD). Examples from 7 neurons showing the average waveform in the local field potential (LFP) and action potentials of CSs detected exclusively by all 3 methods: our algorithm only (pink), the PCA-based algorithm only (cyan), and the online sorter only (beige). CSs detected commonly by all 3 algorithms are shown in gray. Averaged simple spike waveforms (light gray) of each Purkinje cell (PC), scaled down by 50% relative to the CSs, are shown in *column 1*, *insets*.

obtained by subtracting the mean CS duration of the respective PC (Fig. 8*C*). As shown in Fig. 8*C*, the estimate of CS end times provided by our algorithm and the human expert differed only very slightly.

Practical Considerations for Using Our Algorithm

Our CNN-based algorithm uses the LFP and action potential signals simultaneously as input signals that pass through a series of steps to deliver CS start and end times as the final output. These steps have been summarized in Fig. 9. In short, the workflow of our algorithm can be divided into three main stages. The first stage, "Network training" (Fig. 9*A*), requires segments of manually labeled inputs as well as action potential and LFP signals. These act as the training set. The second stage, "CS detection" (Fig. 9*B*), is fully automated (including automated postprocessing) and utilizes the network weights learned during training to detect CS events among recordings of new sets of PCs. For this stage, the action potential and LFP

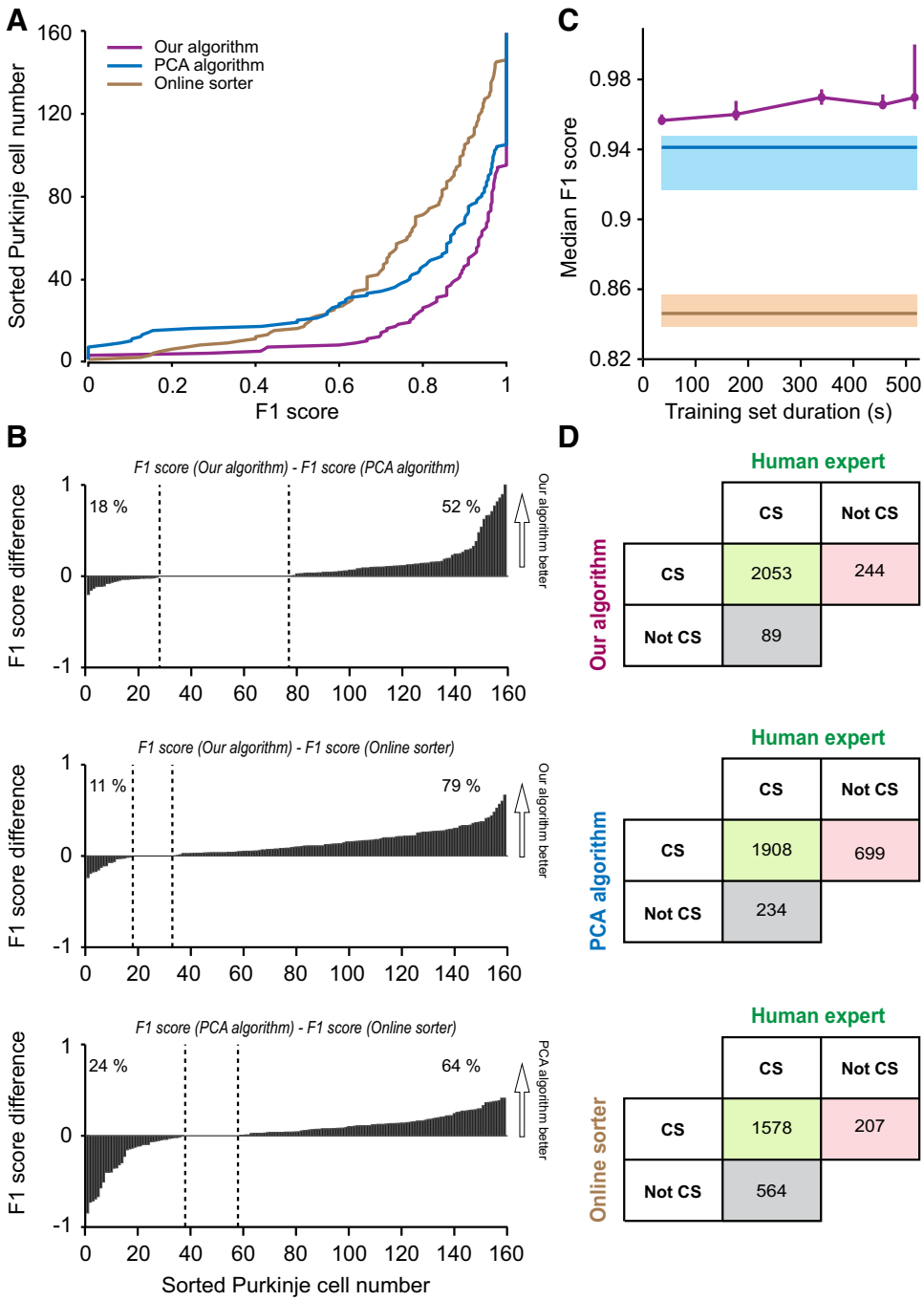

Fig. 6. Classification agreement of our algorithm, the principal component analysis (PCA)-based algorithm, and the online sorter application (MSD) with a human expert. *A*: distribution of F1 scores of our algorithm (pink), the PCA-based algorithm (cyan), and the online sorter (beige) computed by comparing complex spike (CS) labels with the human expert. Data from 159 neurons. *B*: difference between F1 scores obtained by our algorithm and the PCA-based algorithm (*top*), our algorithm and the online sorter (*middle*), and the PCA-based algorithm and the online sorter (*bottom*). *C*: F1 score of our algorithm as a function of the total duration of the training set (pink). Filled circles indicate the median, and error bars represent the 95% confidence interval of the median obtained by bootstrapping. As a reference, the F1 score achieved by the online sorter (beige) and by the PCA-based algorithm (cyan) are also displayed. Thick lines indicate the median and the shaded area represents 95% confidence interval of the median obtained by bootstrapping. *D*: confusion matrixes summarizing the CS detection performance of all 3 algorithms relative to the human expert. Green boxes represent the correctly detected CSs (true positives), gray boxes represent the falsely missed CSs (false negatives), and the red boxes represent the falsely detected CSs (false positives).

signals from an entire recording can be passed to the algorithm in one shot without the need for segmentation, which is automatically implemented by the algorithm.

One of the key requirements for correct CS classification is the quality of the recorded PC signal, which may naturally depend on several factors. For example, subtle drifts between electrode tip and the cell body during a recording session can lead to sudden or gradual changes in the signal-to-noise ratio of the PC signal and potentially change the morphology of the CS waveform. Also, several SSs firing in close proximity to each other might lead to complex waveforms that may erroneously be detected as CS events. Furthermore, there is also a possibility of CS waveforms being modified by the presence of preceding SSs (Servais et al. 2004; Zang et al. 2018). For our algorithm to be more resilient to such influences, it utilizes the three automatic postprocessing steps at the output of the CNN (see *Postprocessing* in MATERIALS AND METHODS). These postprocessing steps allow easy optimization of our algorithm's output.

The very final stage, "Postverification" (Fig. 9*C*), allows users to scrutinize every PC one last time to confirm whether the events marked by the algorithm were real CSs or just false positives.

We now summarize how to handle the few cases in which special care may be warranted when using our algorithm. Specifically, while in most cases our algorithm performed accurately in labeling true events, there were some cases in which distinct clusters of events were detected. During post-

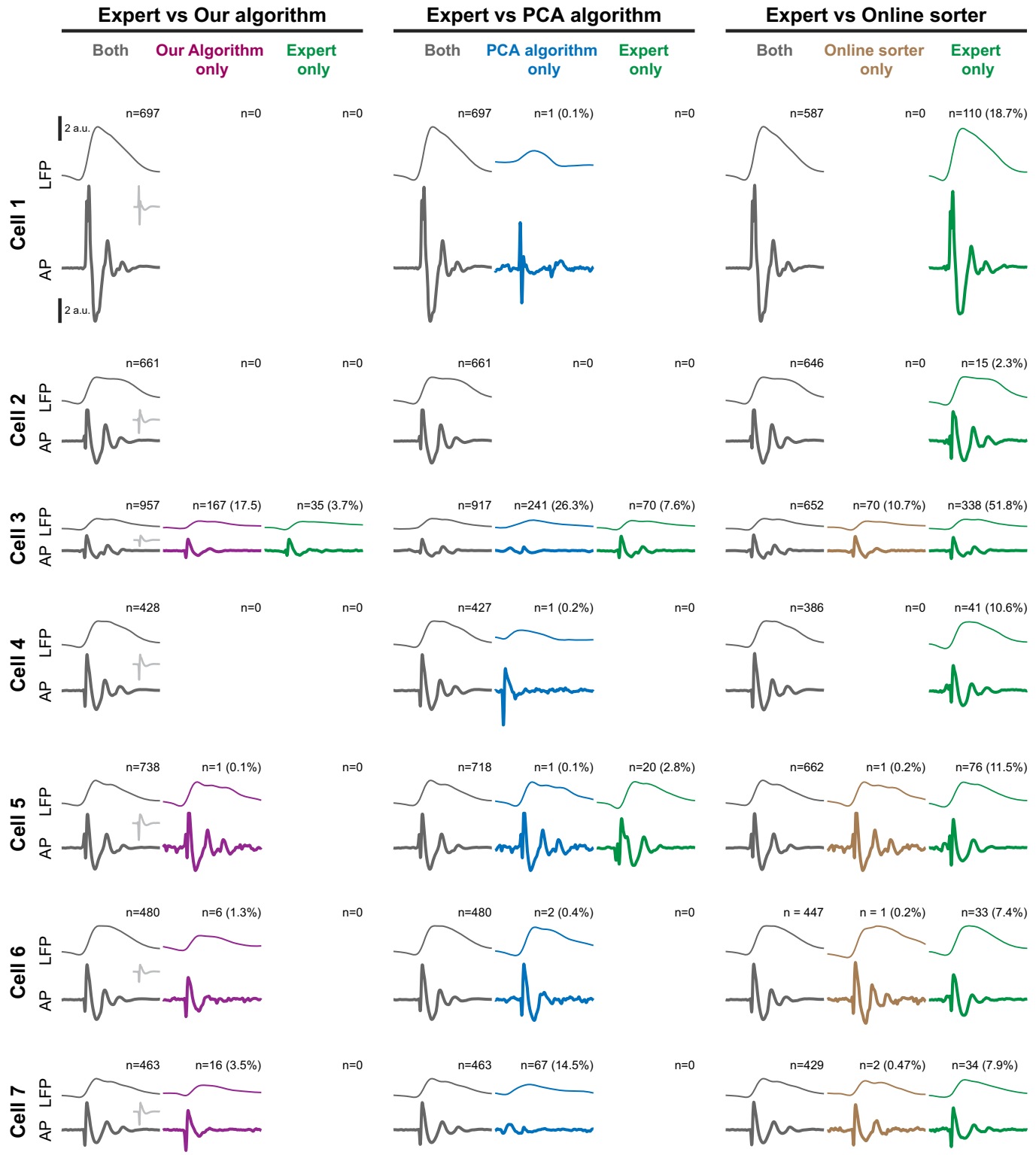

Fig. 7. Comparison of waveforms of events labeled as complex spikes (CSs) by all 3 algorithms with the human expert. Examples from 7 neurons showing the average CS waveforms in the local field potential (LFP) and action potentials (APs). PCA, principal component analysis. Expert vs. Our algorithm: CSs detected by the expert and our algorithm (*left*), our algorithm only (*middle*), and the expert only (*right*). Expert vs. PCA algorithm: CSs detected by the expert and the PCA algorithm (*left*), PCA algorithm only (*middle*), and expert only (*right*). Expert vs. Online sorter: CSs detected by the expert and online sorter (*left*), online sorter only (*middle*), and expert only (*right*). *Insets*, *1st column*: the averaged simple spike waveforms (light gray) of the corresponding Purkinje cells (PCs), scaled down by 50% relative to the CSs.

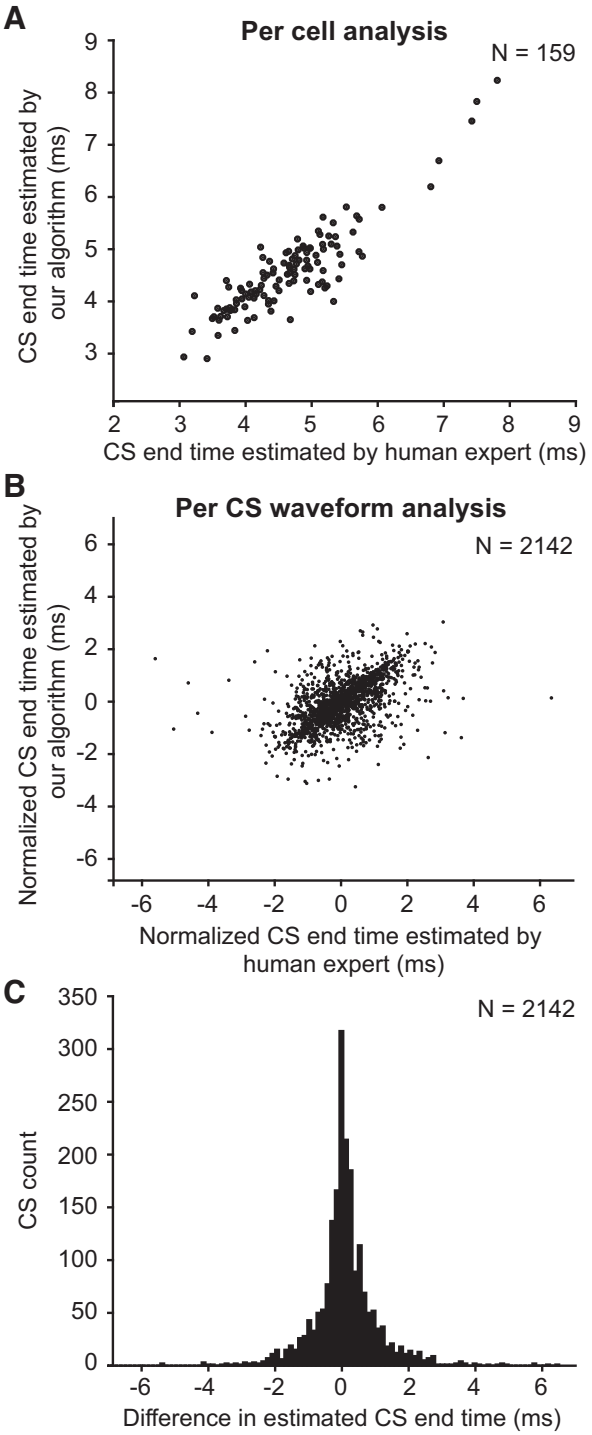

Fig. 8. Comparison of complex spike (CS) end times estimated by our algorithm and by the human expert. *A*: correlation of CS end times estimated by our algorithm and the human expert. Each dot shows the average end time of all CSs from 1 neuron. *B*: correlation of all CS end times pooled across the 159 neurons. The end time of each CS was normalized by subtracting the average end time of the respective neuron. *C*: distribution of difference in CS end times labeled by our algorithm and by the human expert. Data show all CSs detected by both our algorithm and the human expert in short recording segments from 159 neurons.

verification, a closer look at the waveforms of those distinct clusters with separate IDs revealed that these events were true CSs having their waveforms somehow modified. One such possibility is depicted in Fig. 10, *A* and *B*, where the amplitude of CS waveform is reduced gradually over time, most probably due to subtle position shifts between the tip of the recording electrode and the targeted neuron. These modified waveforms, seen as separate clusters (Fig. 10*A*), were in fact separated by time as seen in the raster plot of SSs aligned to CS start time (Fig. 10*B*): the CSs with *cluster ID 1* (red) appeared early during the recording session, while the ones with *cluster ID 3* (cyan) appeared later. Plotting the mean CS waveforms of *cluster 1* (early) and *cluster 3* (late) on top of each other (Fig. 10*B*, *top*) clearly shows a reduction in amplitude of LFP and action potential signals over time.

Also, it is likely that there can be interactions between SS occurrence and CS waveform appearance. Specifically, and as mentioned earlier, a study on PCs in nonanesthetized mice has demonstrated that the shape of the CS waveform can be altered by preceding SSs (Servais et al. 2004). Furthermore, recently conducted experiments on climbing fiber responses in PCs have revealed that the potassium currents, by means of voltage gating in a branch-specific manner, can regulate the climbing fiber driven calcium ion influx leading to changes in CS waveform amplitude (Zang et al. 2018). This may explain why the additional CSs detected by our algorithm might have potentially deceived other algorithms. An example of CS waveforms being modified by the presence of preceding SS is shown in Fig. 10, *C* and *D*, yellow trace. The genuine nature of the additional CSs detected by our algorithm in all cases was confirmed with the help of another prominent physiological marker: the pause in spontaneous firing activity of SSs 10–20 ms right after the occurrence of a CS. Although we observed this pause in the vast majority (92%) of PCs, there was only a small subset of PCs where the suppression of SS activity during the post-CS period was either very weak or missing (Fig. 3*C*). This may allow us to question the credibility of this physiological marker in confirming the presence of a CS. However, it is very unlikely since the lack of this SS pause may simply be an artifact of the poor signal-to-noise ratio of the recorded PCs that potentially led to falsely detected SS events by the online sorter MSD. In this study, we focused on SSs that were detected using the MSD. However, in principle, other CNN based approaches designed specifically for detection of fast spiking events (Rácz et al. 2020) could also be paired with our method.

DISCUSSION

This study proposes a largely automated approach to CS detection as a sensitive and reliable alternative to tedious and experience-dependent manual labeling. After training with surprisingly little data, our algorithm outperformed a widely used spike sorter as well as the latest PCA-based algorithm designed exclusively for CS detection. Moreover, our algorithm also easily caught up with the performance of an experienced human expert. Searching manually for rare events like CSs, amidst a sea of high-frequency SS signals, not only requires several weeks of tedious effort but, as demonstrated by research on visual search (Evans et al. 2011; Wolfe et al. 2005), is also error prone, even among experts. Our network renders CS detection not just feasible but, also, more objective and systematic. Steps describing the general workflow of our algorithm are summarized in Fig. 9.

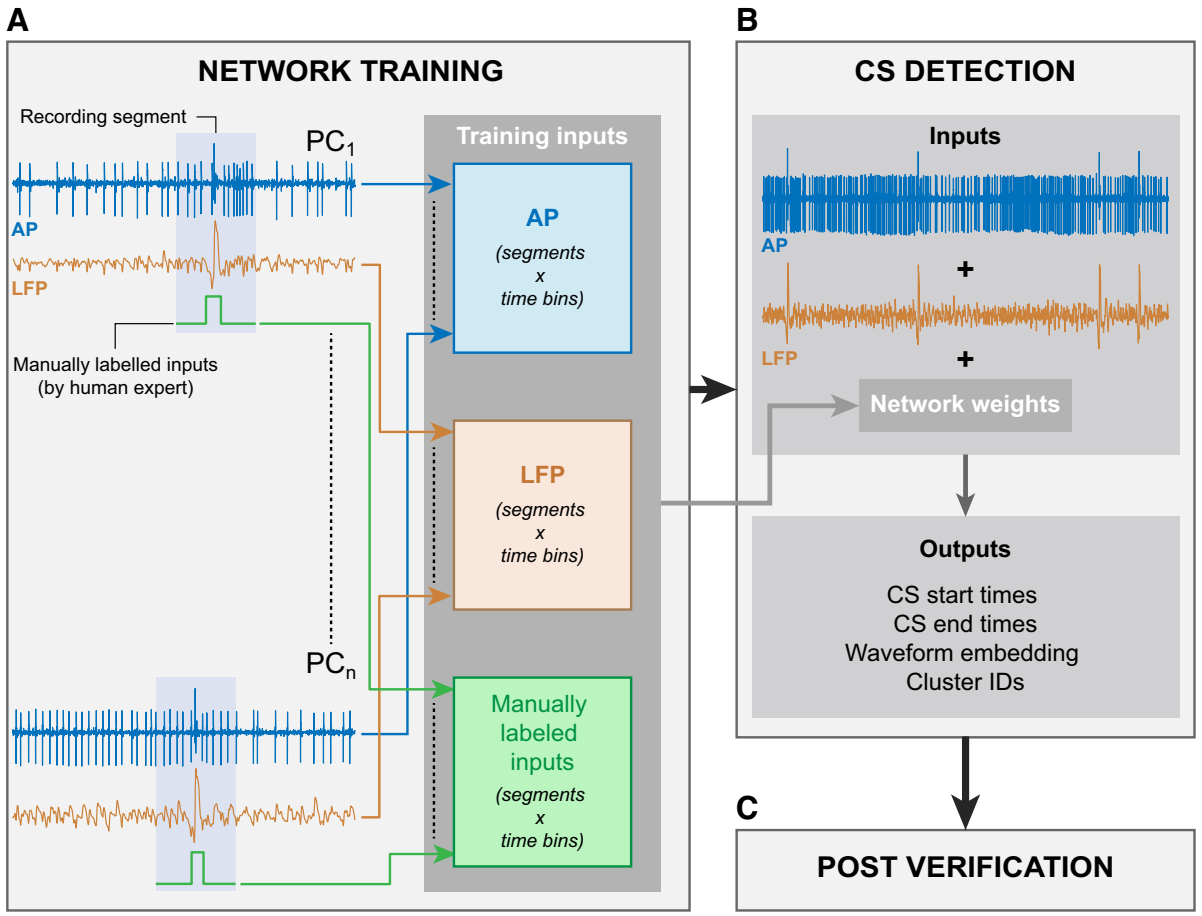

Fig. 9. Workflow for using our algorithm. *A*: the experimenter selects small segments of signal containing at least 1 complex spike (CS) each. Each segment is fed into the neural network in the form of 3 matrixes containing the action potentials (APs), the local field potentials (LFPs), and the labels separately. After training, the network outputs a set of weights. *B*: the weights are used for evaluating new signals. The output of the algorithm delivers information about CS start and end times, their IDs, and waveform shape. *C*: this information can be used by the analysts to manually verify the CS labels during postverification. PC, Purkinje cell.

Challenges Associated with Complex Spike Detection

When looking at the raw trace of a well-isolated PC neuron, like the one in Fig. 1*A*, one might argue that the problem of CS detection is rather trivial; a simple voltage-threshold-based detection could easily solve this problem. However, no matter how well isolated a PC may be, there may be fluctuations of the raw signal being recorded, which can occur at different time scales (whether fast or due to gradual drifts in the position of the neuron relative to the electrode). These fluctuations necessarily modify the start and end times of detected events using simple voltage thresholds. Therefore, even when clean signals can sometimes allow simple detection with thresholds for some applications, the relevance of CSs in the field of cerebellum research extends beyond "mere detection." Precise characterization of CSs and their overall durations, as well as the characterization of their morphology, may matter a great deal for function (Herzfeld et al. 2015, 2018; Junker et al. 2018; Warnaar et al. 2015; Yang and Lisberger 2014).

The major challenge that any approach for detecting CSs meets is the polymorphic complexity and rarity of these neural events (Warnaar et al. 2015). Experienced human experts may in principle reach a high level of agreement by using visual search to identify CS events. However, this approach is very tedious and therefore inevitably associated with fluctuations of attention, which jeopardizes the analyst's performance (Wolfe et al. 2005). The tediousness of the manual detection approach is increased even further if attempts are made to pinpoint the times of CS start and end or to identify distinct features of the CS morphology such as its spikelet architecture (Warnaar et al. 2015). Therefore, conventional spike sorters based on template matching (Catz et al. 2005; Dash et al. 2010; Herzfeld et al. 2015, 2018; Junker et al. 2018) or even simpler voltage-threshold crossings can be useful to facilitate visual inspection. However, the need to double check detected CS events will forestall gains in investments of time and effort only minimally.

Our Algorithm Is More Sensitive and Performs Better than Other Existing Approaches

Although initially designed to detect fast spiking events like SSs, the use of MSD was extended by cerebellum researchers to detect CSs (Catz et al. 2005). However, the challenges associated with CS detection made it difficult for the MSD to be used as a tool for CS detection and also limited its use in assisting visual inspection. To highlight these challenges, we compared the performance of our algorithm to that of the MSD, and clearly, our algorithm was better.

In a very recent publication, a PCA-based algorithm (Zur and Joshua 2019), designed exclusively for detecting CS

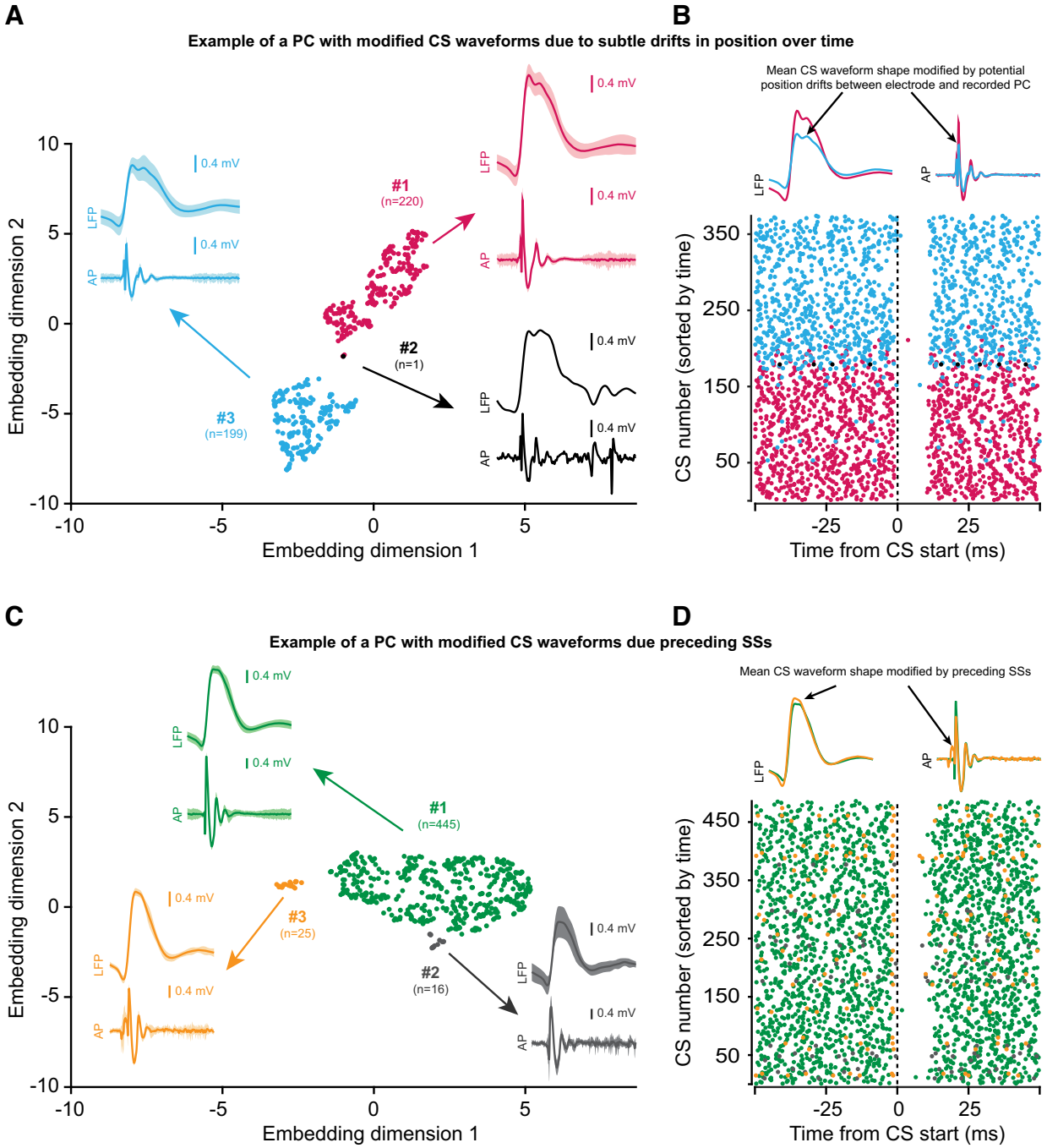

Fig. 10. Postverification of complex spikes (CSs) with modified waveforms. *A* and *B*: example of a Purkinje cell (PC) where the shape of the CS waveform was modified potentially due to subtle drifts between the position of the recording electrode tip and the targeted neuron over time. *A*: CSs detected by our algorithm based on their waveform shape appear as distinct clusters (*1–3*) with separate IDs in a 2-dimensional feature space. *Insets*: averaged CS waveforms ± SD in local field potential (LFP) and action potential for each cluster. *B*: raster plot showing simple spike (SS) activity aligned to all CSs detected by our algorithm sorted by time. Note how the clusters separated in feature space appear early (red) and late (cyan) during the recording session when sorted by time. The LFP and action potential signals of these late waveforms were clearly smaller in amplitude as compared with the earlier waveforms. Nevertheless, the pause induced in SS firing by both clusters was the same, suggesting that the CSs belonging to these clusters were the same. *C* and *D*: example of a PC where the shape of the CS waveform was modified by the presence of preceding SSs. Note how the presence of SSs just before the CSs, seen as large SDs around the averaged action potential waveform (*C*, *insets*), modified the average shape of the CS waveform as compared with that of the main (green) cluster (*D*, *top*). Also, as seen in the raster plot, the pause induced by these distinct CS clusters in SS firing was the same.

events by utilizing the LFP and action potential frequency bands, demonstrated improved sorting of CSs. Since our CNN-based algorithm was also trained on both frequency bands, we adapted our PC data as per the PCA-based algorithm's requirements to directly compare its performance with ours. The virtue of the PCA-based approach notwithstanding, a comparison of F1 scores reveals that it is clearly outperformed by our network-based method. Unlike the PCA-based approach that relies on an arbitrary threshold initially set by the user and may not capture all CSs in situations where oscillations may occur

in the LFP signal, our CNN-based algorithm uses the UMAP dimensionality reduction technique, thus making it more resistant to such changes. Moreover, our algorithm also extracts a number of key parameters on CS timing and morphology in a regularized and systematic manner that are not provided by the PCA-based approach, which are, as stated earlier, potentially important for understanding the functional role of CSs.

Not only was our algorithm more sensitive in detecting CSs, but it also rejected more false CSs, as compared with the other algorithms. This can best be seen in the example of Fig. 2*C*. In Fig. 2*C*, the *cluster 1* waveforms, despite sharing a similar shape of the initial spike component with the genuine CSs in *cluster 3*, appeared as a clearly separated group in our dimensionality reduced space. These erroneous waveforms were therefore safely rejected. On the other hand, waveforms belonging to *cluster 2*, neighboring the main *cluster 3*, were still accepted due to close resemblance of their features to the genuine ones.

It is well established (Eccles and Szentágothai 1967) that individual adult PCs, unlike PCs during early stages of development, usually receive input from only one climbing fiber. Only in rare cases also adult PCs have been found to be innervated by more than one climbing fiber (Nishiyama and Linden 2004). Consequently, it is usually very unlikely to find a second CS with completely different properties in addition to the first CS in records of individual PCs. However, we found a subset of nine (out of 159) PCs for which the CNN delineated a completely separate, large cluster of CSs in addition to the main cluster, suggesting input from more than one climbing fiber. The ability of our algorithm to identify such PCs is yet another demonstration of the high sensitivity and selectivity of our approach.

To test whether our algorithm could really take over the burden of labeling CSs manually, we made a one to one comparison of the performance of the CNN and the human expert on records of seven PCs for which all CSs had been labeled manually. Indeed, our algorithm's performance matched the human-level expertise in detecting CSs in all PCs, except for one in which additional CSs were detected by our algorithm (Fig. 7, *cell 7*). The location of these CSs in a distinct cluster in a two-dimensional feature space allowed the experimenter to easily evaluate the validity of the identification of the waveform as a potential CS and, in this case, to conclude that it was spurious. A similar comparison of the PCA-based algorithm's performance to that of the human expert yielded spurious detections in more cases, suggesting that the performance of our algorithm was closest to the performance of the human expert.

Our Algorithm Detects Start and End Points of CSs with Human-Level Performance

The prevailing idea of CSs serving as the "teaching-signal" for postsynaptic PCs (Albus 1971; Marr 1969), for which the occurrence of each CS event might be the only source of relevant information (Gellman et al. 1985; Rushmer et al. 1976), has been challenged by studies that demonstrated that the duration of action potential bursts fired by olivary neurons may vary and that this may be reflected by changes in the duration and the spikelet architecture of CSs (Bazzigaluppi et al. 2012; De Gruijl et al. 2012; Llinás and Yarom 1981; Maruta et al. 2007; Mathy et al. 2009; Rasmussen et al. 2013; Ruigrok and Voogd 1995; Zang et al. 2018). These observations have suggested that not only the occurrence of a CS but also its duration may be relevant for motor learning. Addressing this possibility requires experimenters to invest even more time to manually label the start and end times of CS waveforms in addition to just detecting the events themselves. Not surprisingly, given the amount of time and effort involved, only a handful of attempts have been made to test this idea (Herzfeld et al. 2015, 2018; Junker et al. 2018; Yang and Lisberger 2014) with inconsistent results. To achieve consensus, larger data sets collected under more diverse conditions would have to be explored, a necessity that researchers have been reluctant to meet because of the hassles of the manual timing analysis. Since our CNN-based approach is able to effortlessly follow the performance of the human expert in detecting the start and end of the CS waveforms, by applying the expert's "mental rules" learned during training, quantifying task-related changes in the architecture of CSs collected at different times in an experiment will become much more feasible in the future.

Deep Learning as a Research Tool

More broadly, deep learning allows modeling nonlinear relationships between input and output for which no analytical solutions may exist. It is exactly this property of deep learning that explains why this machine learning approach has recently emerged as a potentially powerful research tool, which can tremendously reduce the workload of scientists (Bellet et al. 2019; Cireşan et al. 2012; Havaei et al. 2017; Oztel et al. 2017). In light of recent developments, in which deep learning has been successfully utilized to not only design stimuli with controlled higher order statistics (Gatys et al. 2015), but also to model nonlinear relationships in neural data (Ecker et al. 2018), it is not hard to imagine that the full potential of deep learning will significantly boost the pace of neuroscientific research in the coming years. Certainly, in the case of cerebellar neurophysiology, we believe that our use of deep learning to detect the rare, but relevant, CS events will allow much renewed investigation of the contentious functional role of these highly peculiar spikes in motor control and beyond.

Conclusion

So far, all analysis involving CSs has been based on extremely laborious, manual, or semiautomated methods. This enormously slows down the pace of developments in the field. Our deep learning approach can reverse this reality. For example, for a database like ours (159 PCs), our approach requires the human expert to invest only 2–3 h of CS labeling for training purposes and another 3–4 h to later verify the results. Given that it takes a comparable time to manually label all CSs found in recordings of just one PC, this investment in time is negligible compared with the alternative of manually labeling all recorded PCs. Moreover, our automated algorithm performs this task on par with human experts, and it renders more systematic valuable information about the timing and morphology of CS waveforms. The algorithm has been made available for use via an open source implementation at https://github.com/jobellet/detect_CS with provisions for retraining the network to new users' own measurements. The data from all 159 PCs are available for download at https://figshare.com/articles/

Extracellular_recording_of_cerebellar_Purkinje_cells_and_labels_of_complex_spikes_from_expert/11872227. We strongly believe that the gains in time and reliability that our tool offers may substantially facilitate the quest for the functional role of the still largely mysterious CSs.

GRANTS

Supported by Deutsche Forschungsgemeinschaft (DFG) Research Unit 1847 "The Physiology of Distributed Computing Underlying Higher Brain Functions in Non-Human Primates" Projects FOR 1847-A3 (TH 425/13-2) and FOR 1847-A6 (HA 6749/2-1). Z.M.H. was also supported by DFG Collaborative Research Centre 1233 "Robust Vision" (Project No. 276693517).

DISCLOSURES

No conflicts of interest, financial or otherwise, are declared by the authors.

AUTHOR CONTRIBUTIONS

A.M., J.B., Z.M.H., and P.T. conceived and designed research; A.M. performed experiments; A.M., J.B., M.E.B., J.I., Z.M.H., and P.T. interpreted results of experiments; A.M., J.B., J.I., Z.M.H., and P.T. prepared figures; A.M., J.B., M.E.B., Z.M.H., and P.T. drafted manuscript; A.M., J.B., M.E.B., Z.M.H., and P.T. edited and revised manuscript; A.M., J.B., J.I., Z.M.H., and P.T. approved final version of manuscript; J.B., M.E.B., J.I., and A.M. analyzed data.

ENDNOTE

At the request of the authors, readers are herein alerted to the fact that additional materials related to this manuscript may be found at the institutional website of one of the authors, which at the time of publication they indicate is for the electrophysiological signals and labels (No Behavior): https://figshare.com/articles/Extracellular_recording_of_cerebellar_Purkinje_cells_and_qjlabels_of_complex_spikes_from_expert/11872227; for the training set: https://figshare.com/articles/CS_detect_training_set/11891283; and for every network weights: https://figshare.com/articles/detect_CS_network_weights/11788833. These materials are not a part of this manuscript, and have not undergone peer review by the American Physiological Society (APS). APS and the journal editors take no responsibility for these materials, for the website address, or for any links to or from it.

REFERENCES

Albus JS. A theory of cerebellar function. *Math Biosci* 10: 25–61, 1971. doi:10.1016/0025-5564(71)90051-4.

Bazzigaluppi P, De Gruijl JR, van der Giessen RS, Khosrovani S, De Zeeuw CI, de Jeu MT. Olivary subthreshold oscillations and burst activity revisited. *Front Neural Circuits* 6: 91, 2012. doi:10.3389/fncir.2012.00091.

Bechert K, Koenig E. A search coil system with automatic field stabilization, calibration, and geometric processing for eye movement recording in humans. *Neuroophthalmology* 16: 163–170, 1996. doi:10.3109/01658109609009677.

Bell CC, Grimm RJ. Discharge properties of Purkinje cells recorded on single and double microelectrodes. *J Neurophysiol* 32: 1044–1055, 1969. doi:10.1152/jn.1969.32.6.1044.

Bellet ME, Bellet J, Nienborg H, Hafed ZM, Berens P. Human-level saccade detection performance using deep neural networks. *J Neurophysiol* 121: 646–661, 2019. doi:10.1152/jn.00601.2018.

Campello RJ, Moulavi D, Sander J. Density-based clustering based on hierarchical density estimates. In: *Pacific-Asia Conference on Knowledge Discovery and Data Mining*. New York: Springer, 2013, p. 160–172.

Catz N, Dicke PW, Thier P. Cerebellar complex spike firing is suitable to induce as well as to stabilize motor learning. *Curr Biol* 15: 2179–2189, 2005. doi:10.1016/j.cub.2005.11.037.

Cireşan D, Meier U, Schmidhuber J. Multi-column deep neural networks for image classification (Preprint). *arXiv* 12022745, 2012.

Dash S, Catz N, Dicke PW, Thier P. Specific vermal complex spike responses build up during the course of smooth-pursuit adaptation, paralleling the decrease of performance error. *Exp Brain Res* 205: 41–55, 2010. doi:10.1007/s00221-010-2331-2.

Davie JT, Clark BA, Häusser M. The origin of the complex spike in cerebellar Purkinje cells. *J Neurosci* 28: 7599–7609, 2008. doi:10.1523/JNEUROSCI.0559-08.2008.

De Gruijl JR, Bazzigaluppi P, de Jeu MT, De Zeeuw CI. Climbing fiber burst size and olivary sub-threshold oscillations in a network setting. *PLOS Comput Biol* 8: e1002814, 2012. doi:10.1371/journal.pcbi.1002814.

Dice LR. Measures of the amount of ecologic association between species. *Ecology* 26: 297–302, 1945. doi:10.2307/1932409.

Eccles JC, Llinás R, Sasaki K. The action of antidromic impulses on the cerebellar Purkinje cells. *J Physiol* 182: 316–345, 1966. doi:10.1113/jphysiol.1966.sp007826.

Eccles JC, Szentágothai J. *The Cerebellum as a Neuronal Machine*. Oxford, UK: Springer-Verlag, 1967.

Ecker AS, Sinz FH, Froudarakis E, Fahey PG, Cadena SA, Walker EY, Cobos E, Reimer J, Tolias AS, Bethge M. A rotation-equivariant convolutional neural network model of primary visual cortex (Preprint). *arXiv* 180910504, 2018.

Evans KK, Cohen MA, Tambouret R, Horowitz T, Kreindel E, Wolfe JM. Does visual expertise improve visual recognition memory? *Atten Percept Psychophys* 73: 30–35, 2011. doi:10.3758/s13414-010-0022-5.

Fujita Y. Activity of dendrites of single Purkinje cells and its relationship to so-called inactivation response in rabbit cerebellum. *J Neurophysiol* 31: 131–141, 1968. doi:10.1152/jn.1968.31.2.131.

Gatys LA, Ecker AS, Bethge M. A neural algorithm of artistic style (Preprint). *arXiv* 150806576, 2015.

Gellman R, Gibson AR, Houk JC. Inferior olivary neurons in the awake cat: detection of contact and passive body displacement. *J Neurophysiol* 54: 40–60, 1985. doi:10.1152/jn.1985.54.1.40.

Havaei M, Davy A, Warde-Farley D, Biard A, Courville A, Bengio Y, Pal C, Jodoin P-M, Larochelle H. Brain tumor segmentation with deep neural networks. *Med Image Anal* 35: 18–31, 2017. doi:10.1016/j.media.2016.05.004.

Herzfeld DJ, Kojima Y, Soetedjo R, Shadmehr R. Encoding of action by the Purkinje cells of the cerebellum. *Nature* 526: 439–442, 2015. doi:10.1038/nature15693.

Herzfeld DJ, Kojima Y, Soetedjo R, Shadmehr R. Encoding of error and learning to correct that error by the Purkinje cells of the cerebellum. *Nat Neurosci* 21: 736–743, 2018. doi:10.1038/s41593-018-0136-y.

Ito M. Neural design of the cerebellar motor control system. *Brain Res* 40: 81–84, 1972. doi:10.1016/0006-8993(72)90110-2.

Judge SJ, Richmond BJ, Chu FC. Implantation of magnetic search coils for measurement of eye position: an improved method. *Vision Res* 20: 535–538, 1980. doi:10.1016/0042-6989(80)90128-5.

Junker M, Endres D, Sun ZP, Dicke PW, Giese M, Thier P. Learning from the past: a reverberation of past errors in the cerebellar climbing fiber signal. *PLoS Biol* 16: e2004344, 2018. doi:10.1371/journal.pbio.2004344.

Kitazawa S, Kimura T, Yin P-B. Cerebellar complex spikes encode both destinations and errors in arm movements. *Nature* 392: 494–497, 1998. doi:10.1038/33141.

Kostadinov D, Beau M, Blanco-Pozo M, Häusser M. Predictive and reactive reward signals conveyed by climbing fiber inputs to cerebellar Purkinje cells. *Nat Neurosci* 22: 950–962, 2019. [Erratum in *Nat Neurosci* 23: 468, 2020. 10.1038/s41593-020-0594-x.] doi:10.1038/s41593-019-0381-8.

Latham A, Paul DH. Spontaneous activity of cerebellar Purkinje cells and their responses to impulses in climbing fibres. *J Physiol* 213: 135–156, 1971. doi:10.1113/jphysiol.1971.sp009373.

Leznik E, Llinás R. Role of gap junctions in synchronized neuronal oscillations in the inferior olive. *J Neurophysiol* 94: 2447–2456, 2005. doi:10.1152/jn.00353.2005.

Llinás R. Eighteenth Bowditch lecture. Motor aspects of cerebellar control. *Physiologist* 17: 19–46, 1974.

Llinás R, Sugimori M. Electrophysiological properties of in vitro Purkinje cell dendrites in mammalian cerebellar slices. *J Physiol* 305: 197–213, 1980. doi:10.1113/jphysiol.1980.sp013358.

Llinás R, Yarom Y. Electrophysiology of mammalian inferior olivary neurones in vitro. Different types of voltage-dependent ionic conductances. *J Physiol* 315: 549–567, 1981. doi:10.1113/jphysiol.1981.sp013763.

Marr D. A theory of cerebellar cortex. *J Physiol* 202: 437–470, 1969. doi:10.1113/jphysiol.1969.sp008820.

Maruta J, Hensbroek RA, Simpson JI. Intraburst and interburst signaling by climbing fibers. *J Neurosci* 27: 11263–11270, 2007. doi:10.1523/JNEUROSCI.2559-07.2007.

Mathy A, Ho SS, Davie JT, Duguid IC, Clark BA, Häusser M. Encoding of oscillations by axonal bursts in inferior olive neurons. *Neuron* 62: 388–399, 2009. doi:10.1016/j.neuron.2009.03.023.

McDevitt CJ, Ebner TJ, Bloedel JR. The changes in Purkinje cell simple spike activity following spontaneous climbing fiber inputs. *Brain Res* 237: 484–491, 1982. doi:10.1016/0006-8993(82)90460-7.

McInnes L, Healy J, Melville J. UMAP: Uniform manifold approximation and projection for dimension reduction (Preprint). *arXiv* 180203426, 2018.

Medina JF, Lisberger SG. Links from complex spikes to local plasticity and motor learning in the cerebellum of awake-behaving monkeys. *Nat Neurosci* 11: 1185–1192, 2008. [Erratum in *Nat Neurosci* 12: 808, 2009.] doi:10.1038/nn.2197.

Nishiyama H, Linden DJ. Differential maturation of climbing fiber innervation in cerebellar vermis. *J Neurosci* 24: 3926–3932, 2004. doi:10.1523/JNEUROSCI.5610-03.2004.

Ohmae S, Medina JF. Climbing fibers encode a temporal-difference prediction error during cerebellar learning in mice. *Nat Neurosci* 18: 1798–1803, 2015. doi:10.1038/nn.4167.

Oscarsson O. Functional organization of olivary projection to the cerebellar anterior lobe. In: *The Inferior Olivary Nucleus: Anatomy and Physiology*, edited by Courville J, de Montigny C, Lamarre Y. New York: Raven Press, 1980, p. 279–290.

Oztel I, Yolcu G, Ersoy I, White T, Bunyak F. Mitochondria segmentation in electron microscopy volumes using deep convolutional neural network. In: 2017 IEEE International Conference on Bioinformatics and Biomedicine (BIBM). Piscataway, NJ: IEEE, 2017, p. 1195–1200.

Prsa M, Dicke PW, Thier P. The absence of eye muscle fatigue indicates that the nervous system compensates for non-motor disturbances of oculomotor function. *J Neurosci* 30: 15834–15842, 2010. doi:10.1523/JNEUROSCI.3901-10.2010.

Rácz M, Liber C, Németh E, Fiáth R, Rokai J, Harmati I, Ulbert I, Márton G. Spike detection and sorting with deep learning. *J Neural Eng* 17: 016038, 2020. doi:10.1088/1741-2552/ab4896.

Rasmussen A, Jirenhed D-A, Zucca R, Johansson F, Svensson P, Hesslow G. Number of spikes in climbing fibers determines the direction of cerebellar learning. *J Neurosci* 33: 13436–13440, 2013. doi:10.1523/JNEUROSCI.1527-13.2013.

Ronneberger O, Fischer P, Brox T. U-net: Convolutional networks for biomedical image segmentation. In: International Conference on Medical Image Computing and Computer-Assisted Intervention. New York: Springer, 2015, p. 234–241.

Ruigrok TJ, Voogd J. Cerebellar influence on olivary excitability in the cat. *Eur J Neurosci* 7: 679–693, 1995. doi:10.1111/j.1460-9568.1995.tb00672.x.

Rushmer DS, Roberts WJ, Augter GK. Climbing fiber responses of cerebellar Purkinje cells to passive movement of the cat forepaw. *Brain Res* 106: 1–20, 1976. doi:10.1016/0006-8993(76)90069-X.

Servais L, Bearzatto B, Hourez R, Dan B, Schiffmann SN, Cheron G. Effect of simple spike firing mode on complex spike firing rate and waveform in cerebellar Purkinje cells in non-anesthetized mice. *Neurosci Lett* 367: 171–176, 2004. doi:10.1016/j.neulet.2004.05.109.

Sorensen TA. A method of establishing groups of equal amplitude in plant sociology based on similarity of species content and its application to analyses of the vegetation on Danish commons. *Biol Skar* 5: 1–34, 1948.

Streng ML, Popa LS, Ebner TJ. Climbing fibers control Purkinje cell representations of behavior. *J Neurosci* 37: 1997–2009, 2017. doi:10.1523/JNEUROSCI.3163-16.2017.

Stuart G, Häusser M. Initiation and spread of sodium action potentials in cerebellar Purkinje cells. *Neuron* 13: 703–712, 1994. doi:10.1016/0896-6273(94)90037-X.

Thach WT Jr. Somatosensory receptive fields of single units in cat cerebellar cortex. *J Neurophysiol* 30: 675–696, 1967. doi:10.1152/jn.1967.30.4.675.

Thach WT. Discharge of Purkinje and cerebellar nuclear neurons during rapidly alternating arm movements in the monkey. *J Neurophysiol* 31: 785–797, 1968. doi:10.1152/jn.1968.31.5.785.

Warnaar P, Couto J, Negrello M, Junker M, Smilgin A, Ignashchenkova A, Giugliano M, Thier P, De Schutter E. Duration of Purkinje cell complex spikes increases with their firing frequency. *Front Cell Neurosci* 9: 122, 2015. doi:10.3389/fncel.2015.00122.

Wolfe JM, Horowitz TS, Kenner NM. Cognitive psychology: rare items often missed in visual searches. *Nature* 435: 439–440, 2005. doi:10.1038/435439a.

Wörgötter F, Daunicht WJ, Eckmiller R. An on-line spike form discriminator for extracellular recordings based on an analog correlation technique. *J Neurosci Methods* 17: 141–151, 1986. doi:10.1016/0165-0270(86)90067-1.

Yang Y, Lisberger SG. Purkinje-cell plasticity and cerebellar motor learning are graded by complex-spike duration. *Nature* 510: 529–532, 2014. doi:10.1038/nature13282.

Zang Y, Dieudonné S, De Schutter E. Voltage- and branch-specific climbing fiber responses in Purkinje cells. *Cell Reports* 24: 1536–1549, 2018. doi:10.1016/j.celrep.2018.07.011.

Zur G, Joshua M. Using extracellular low frequency signals to improve the spike sorting of cerebellar complex spikes. *J Neurosci Methods* 328: 108423, 2019. doi:10.1016/j.jneumeth.2019.108423.

APPENDIX 3

Multiplexing of information by cerebellar complex spikes

Abbreviated title: Multiplexing of information by complex spikes

Akshay Markanday[1,2], Junya Inoue[1], Peter W. Dicke, Peter Thier

[1]Hertie Institute for Clinical Brain Research, Tübingen, Germany
[2]Graduate School of Neural and Behavioral Sciences, International Max Planck Research School, Tübingen University, Tübingen, Germany

Correspondence
Peter Thier
Department of Cognitive Neurology,
Hertie Institute for Clinical Brain Research,
Hoppe-Seyler-Str. 3, 72076
Tübingen, Germany.
Email: thier@uni-tuebingen.de

Conflict of interest: The authors declare no competing financial interests

Acknowledgments: Supported by DFG Research Unit 1847 "The Physiology of distributed computing underlying higher brain functions in non-human primates".

Abstract

Purkinje cell (PC) discharge, the only output of cerebellar cortex, involves two types of action potentials, high-frequency simple spikes (SSs) and low-frequency complex spikes (CSs). While there is consensus that SSs convey information needed to optimize movement kinematics, the function of CSs, determined by the PC´s climbing fibre input, remains controversial. While initially thought to be specialized in reporting information on motor error for the subsequent amendment of behavior, CSs seem to contribute to other aspects of motor behavior as well. When faced with the bewildering diversity of findings and views unraveled by highly specific tasks one may wonder if there is just one true function with all the other attributions wrong? Or is the diversity of findings a reflection of distinct pools of PCs, each processing specific streams of information conveyed by climbing fibres? With these questions in mind we recorded CSs from the monkey oculomotor vermis deploying a repetitive saccade task that entailed sizable motor errors as well as microsaccades, correcting them. We demonstrate that in addition to conveying error related information, CSs carry information on the metrics of both primary and small corrective saccades in a time specific manner, with changes in CS firing probability coupled with changes in CS duration. Furthermore, we also found CS activity that seemed to predict the upcoming events. Hence PCs receive a multiplexed climbing fibre input that merges complementary streams of information on the behavior, separable by the recipient PC because they are staggered in time.

Introduction

The first and arguably the most influential concept on the role of the climbing fibre input to Purkinje cells (PCs) in cerebellar cortex, originally proposed by David Marr (Marr, 1969) and subsequently further elaborated by others (Albus, 1971; Ito, 1972), has been its assumed role in reporting motor errors. Information on motor error is used to drive motor learning by implementing amendments necessary for avoiding the future reoccurrence of an error. Within the framework of the Marr-Albus-Ito (MAI) theory, it is the cerebellocortical Purkinje cell (PC) whose output is changed under the influence of error reports provided by its climbing fibre input. PCs are unique in that they fire two types of action potentials, high-frequency simple spikes (SSs) and low-frequency complex spikes (CSs). SSs, that represent the integrated influence of information mediated via the mossy fibre-parallel fibre system and modulatory influences of interneurons, are fired at frequencies high enough to have an impact on target neurons outside the cerebellar cortex. They are thought to be the sole carrier of information allowing extracerebellar structures to optimize movement kinematics. CSs, on the other hand, are local manifestations of the second stream of input information conveyed by climbing fibres impinging onto target PCs. The strong excitatory influence of these CSs is thought to drive long-term plasticity at parallel fibre-to-PC synapses that is responsible for the integration of the two separate streams of information conveyed by the climbing fibre system and the mossy fibre-parallel fibre system. It is this adjustment of the impact of the parallel fibre input under the control of CSs that is thought to underlie the adjustment of the PC´s SS output.

Several studies have used the CS as a proxy of climbing fibre activity to get a handle on the role of this system in controlling behavior. While many of them have been able to lend support to the assumed role of CSs in signaling information on motor error (Barmack and Shojaku, 1995; Gilbert

and Thach, 1977; Graf et al., 1988; Herzfeld et al., 2015, 2018; Kim et al., 1987; Kitazawa et al., 1998; Kobayashi et al., 1998; Medina and Lisberger, 2008; Oscarsson, 1980; Soetedjo et al., 2008), others have unveiled features, not to be expected within the framework of the classical MAI-concept. An early example is the demonstration of the clock-like regularity and precision of the firing of neurons in the inferior olive (the source of climbing fibres) by Llinas and coworkers, convincing them to suggest a role of CSs in the temporal segmentation of movement (Leznik and Llinas, 2005; Llinas et al., 1974; Llinás and Volkind, 1973). Since then, many more observations on CS signaling have been made that require adaptations of the classical concept or even alternatives to it. For instance, studies on oculomotor adaptation in monkeys have suggested that climbing fibre activity, gauged by measuring CS discharge may not only initiate learning as posited by the classical MAI-concept but, moreover, help to stabilize learning by reverberating information on past errors (Catz et al., 2005; Dash et al., 2010; Junker et al., 2018). Fully compatible with this idea, also experiments on eye blink conditioning in mice have demonstrated that the same CSs that initially encode unexpected errors are able to predict future errors by responding to a conditioned stimulus reflecting information on past errors that serves as proxy of future errors (Ohmae and Medina, 2015). Support for a role of CS in encoding movement kinematics in addition to representing position errors comes from manual tracking experiments on monkeys (Streng et al., 2017). Finally, more recently, yet another non-classical role of CSs has been put forward, namely one in conveying information on reward signals in a reactive and predictive manner, a view that is supported by visuomotor tracking experiments in mice and the study of smooth pursuit eye movements in monkeys (Kostadinov et al., 2019; Larry et al., 2019).

It is a remarkable irony that CSs, notorious for extremely low discharge rates (Davie et al., 2008; Eccles, 1967; Fujita, 1968; Llinás and Sugimori, 1980; Stuart and Häusser, 1994; Thach, 1968),

hardly suitable to carry rich information, should accommodate such a diversity of behaviorally relevant signals. An answer how this might eventually be feasible is the possibility that not only the CS event as such might matter, but also the CS´s morphology, characterized by varying duration and versatile patterns of spikelets (Warnaar et al., 2015). Yang and Lisberger (2014, 2017) have argued that CS duration may indeed mediate error information instructing smooth-pursuit adaptation and suggested that instructive signals may adapt the spikelet architecture in a graded manner during motor learning. Hence, although there may be a basis for accommodating richer information, one may still wonder if there is just one true function of CS with all the other attributions wrong? And perhaps, we are still missing the one, true function of CS. Could it be that we cerebellar physiologists share the fate of the blind monks in the ancient Indian parable, examining different parts of an elephant, each mistaking the respective part felt for the whole elephant? Alternatively, the diversity of findings on CSs might reflect distinct pools of PCs, each processing specific streams of information conveyed by climbing fibres? With these questions in mind we recorded CSs from the monkey oculomotor vermis deploying a repetitive saccade task. We demonstrate that probably every PC receives multiplexed climbing fibre input that merges different and complementary streams of information on the behavior at stake, potentially separable by the recipient PC because they are staggered in time.

Materials and Methods

Animals, preparation, surgical procedures and recording methods

All neural and behavioral data used in this study was collected from two adult male rhesus macaques (*Macaca mulatta*), monkey K (age: 10 years) and monkey E (age: 8 years) that were

purchased from the German Primate Center, Göttingen. All training, experiments and surgical procedures abided by the rules set by German and European law as well as the National Institutes of Health's *Guide for the Care and Use of Laboratory Animals* and were approved by the local authority (Regierungspräsidium Tübingen) for animal care. All procedures were carefully supervised by the veterinary service of Tübingen University.

Animals were trained to voluntarily enter an individually customized primate chair and get accustomed to the setup environment. After successful chair training, that could last for up to three months, the first major surgical procedure was conducted. During this procedure titanium foundations of all implants were attached to the skull with titanium bone screws and allowed to rest under the subsequently re-closed skin for a period of approximately 3-4 months to ensure the long-term stability of the implant foundations. For the commencement of head fixation and experimental training, a titanium-based hexagonal tube-shaped head post was fixed to the base of the implanted head holder via the locally opened skin that allowed us to painlessly immobilize the head during experiments. At the same time, we implanted magnetic scleral search coils (Judge et al. 1980; Bechert and König, 1996) to record eye position with high precision. After 2-3 weeks of recovery from the surgical procedures, monkeys were trained further on the tasks at stake. Once proficient, we opened the skin above the already implanted chamber foundation in order to attach the upper part of the cylindrical titanium recording chamber, tilting backwards by an angle of 30° with respect to the frontal plane, right above the midline of the cerebellum and trepanated the skull within the confines of the chamber. The position and orientation of the chamber had been carefully planned based on pre-surgical MRI and was later confirmed by post-surgical MRI. This allowed reliable electrode access to our region of interest, the oculomotor vermis (OMV, lobules VIc/VIIA). All surgical procedures were performed under aseptic conditions using general

anesthesia (see Arnstein et. al., 2015 for more details). All vital physiological parameters (blood pressure, body temperature, heart rate, pO_2 and pCO_2) were closely monitored. After surgery, analgesics (buprenorphine) were delivered to ensure painless recovery. Regular ethograms were recorded to keep track of monkeys´ progress until full recovery.

Behavioral task

We trained the two monkeys on a fatigue inducing repetitive fast eye movements (saccades) task (Fig. 1A). A trial was initiated whenever the monkeys moved their eye gaze into an invisible fixation window (2x2°) centered on a red fixation dot of diameter 0.2° that was displayed at the center of a CRT monitor, placed at a distance of 38 cm in front of the subject. After a short fixation period varying from 400 to 600 ms relative to trial onset, the fixation dot disappeared and at the same time, a target appeared (go-signal) either on the left or–in other sessions–on the right at 15° eccentricity with features, matching the one of the fixation dot. In response, the monkey made a fast eye movement (saccade) towards the new target location which was considered correct only if the eye gaze landed within an invisible fixation window (2x2°) centred on the target. Every centre-out (= centrifugal) saccade (CF), made correctly towards the target was rewarded with an instantaneously delivered drop of water. Approximately 700-900 ms after the go-signal, the peripheral target disappeared, and the central fixation dot reappeared. In order to proceed with the next CF trial, the monkeys readily executed short-latency back saccade from the peripheral target location to the fixation dot - centripetal saccades (CP) - although these CP saccades were not rewarded. As shown in Fig. 1B-D, the metric and kinematic structure of CP and CF saccades were very similar, their opposite directions non-withstanding, and both exhibited saccadic fatigue as described by Prsa et al. (2010), characterized by a gradual drop in peak velocity, compensated by

171 an increase of duration, keeping saccade amplitude stable. The maximum number of trials per
172 session varied (on average 300) depending on the motivation of the monkey to perform the task as
173 well as on the time for which a PC could be kept well isolated. The duration of each trial was 1200
174 ms. Linux based in-house software, NREC (http://nrec.neurologie.uni-tuebingen.de) was used to
175 control the experiment and to collect and preprocess data.
176
177 *Electrophysiological recordings of Purkinje cells in the oculomotor vermis*
178 We performed extracellular recordings from PCs using glass-coated tungsten microelectrodes
179 (impedance: 1-2 MΩ) that were purchased from Alpha Omega Engineering, Nazareth, Israel. The
180 position of the electrodes, that were targeted towards the OMV, was controlled using a modular
181 multi-electrode manipulator (Electrode Positioning System and Multi-Channel Processor, Alpha
182 Omega Engineering). The identity and the exact coordinates of the OMV predicted by the MRI
183 scans were confirmed by physiological criteria, that is, the presence of a dense saccade related
184 background activity, reflecting multi-unit granule cells activity. To differentiate action potentials
185 from the underlying LFP signals, extracellular potentials, recorded at the sampling rate of 25 KHz,
186 were high band-pass filtered (300 Hz - 3 KHz) and low-pass filtered (30 Hz- 400 Hz), respectively.
187 A total of 160 PCs were recorded out which 151 were considered for analysis.
188
189 *Identification and detection of simple spikes and complex spikes*
190 The final identification of individual PC units relied on the demonstration of the two types of
191 actions potentials they fire, the high-frequency SS discharge and the low-frequency CS discharge,
192 and the verification that both originated from the same cell by documenting a 10-20 ms pause in
193 SS firing following the occurrence of a CS (Bell and Grimm, 1969; Latham and Paul, 1971;

McDevitt et al., 1982). Following a preliminary separation and characterization of CS and SS carried out online using Alpha Omega Engineering´s Multi Spike Detector (MSD), needed to direct the experimental approach, the definitive analysis was based on an offline approach as described in detail in Markanday et al. (2019). In short, a deep neural network was trained to use relevant features of PC recordings that allow fast and reliable identification of CSs as well as characterization of their morphology including the detection of their start and end times. The algorithm relies on dividing the record into a high-pass spectral band (300 Hz- 3 KHz) suitable for the characterization of action potentials recordings and a lower frequency band (30 Hz- 400 Hz) for the characterization of LFP signals.

Data analysis

Saccade detection

All primary saccades of sizes between 13 to 17 degrees were detected with the help of a velocity threshold criterion of 30 deg/s. In order to detect corrective microsaccades with amplitudes varying from 0.2 to 2 deg, we used a more lenient velocity threshold of 10 deg/s in conjunction with the requirement of a duration longer than 10 ms.

Estimating the preferred direction and population response of complex spikes

Since saccades were only made horizontally left or rightwards, the directions were binned into two broad classes having a size of 180° each. Interestingly, we did not observe the expected CS discharge in response to the large retinal error caused by the initial target jump. However, in most PCs, and as also reflected by the population response (Supplementary Fig. 1A), we observed the strongest modulation in CS activity developing around the time of saccade end. We therefore

determined CS's preferred primary saccade direction based on the probability of CS firing for each direction by calculating the total number of CSs fired during the *'early post-saccadic period'* of 0 to 100 ms after saccade end and dividing them by the total number of saccades made in each direction. The direction with a higher mean probability of CS firing was defined as the preferred direction of the CS unit. For determining the preferred direction of corrective saccades, we calculated the firing probability during the *'post-corrective saccadic period'* of 0 to 100 ms from corrective saccade offset. To determine each PC's preferred direction of performance errors we used the *'pre-corrective saccadic period'* of -200 to 0 ms from corrective saccade onset.

For computing the average discharge rate, we convolved each CS with a normalized Gaussian kernel of 5 ms standard deviation. CS population responses were estimated using a bootstrapping technique to estimate the variance of the population discharge as suggested by Herzfeld et al. 2018. Assuming that 50 cells project onto a single cFN neuron, we calculated the CS population discharge based on 50 CS units drawn at random with replacement from the population. We repeated this process 50 times, and calculated the population mean and 95% confidence intervals.

Determining peak and trough times of CS firing rate

To capture the effects of saccade duration on the timing of CSs, we relied on the timing of the peak CS firing rate, as well as the timing of the trough. To calculate the peak time of the CS response, we randomly chose 50 PCs, each PC containing at least 10 trials for each duration bin and calculated the mean firing rate and the time of the peak firing rate. By repeating this process 1000 times, mean time of the peak and its 95% confidence intervals were estimated.

To estimate the time of the trough, that was well aligned to the end of saccades and marked the beginning of CS modulation (Supplementary Fig. 1A), we randomly selected 1000 trials of each

duration bin across all cells and computed the mean discharge rate. Then, we fitted a second order polynomial to the baseline period (-200 ms to 0 ms from saccade onset), and a linear function from the time of the peak back to -45 ms to the trough (Supplementary Fig. 1B). The intersection of these two functions gave us an estimate of the trough time for each iteration. This process was repeated 1000 times and the mean timing of the trough and its 95% confidence interval were estimated.

Results

Differences in saccadic vigor

In this study, we trained two rhesus monkeys to execute long series of saccades towards a fixed target, and back to the central starting location. We then looked at the resulting performance errors arising from the natural endpoint variability on top of a gradual decline in saccade peak speed during sessions. This decline was most probably a consequence of the need to make stereotypic eye movements separated by short intertrial intervals of only 100 ms, arguably causing a gradual loss of interest in the task resulting in a decline of saccadic vigor over the course of trials (Fig. 1B, left and right upper panel). This "cognitive fatigue" (Prsa et al., 2010), slowing down the pace of saccades was compensated by an upregulation of saccade duration (Fig. 1B, left and right middle panel) sufficient to keep saccade endpoints (Fig.1B, left and right lower panel) within the required range of $\pm 2°$ around the target location at 15° eccentricity. A comparison of the first 30 (early; CF saccades: dark red; CP saccades: dark blue) and the last 30 (late; CF saccades: light red; CP saccades: light blue) trials in a single behavioral session clearly reveals this speed-duration "trade-off" mechanism (Fig. 1C; upper and lower panel) characterized by a drop of the median peak speed

by 28.3% (early: 616.9 deg/s; late: 444.4 deg/s; Wilcoxon signed rank test, $p<0.001$) and 21.5% (early: 723.4 deg/s; late: 567.9 deg/s; Wilcoxon signed rank test, $p<0.001$) in CP and CF directions, respectively. This reduction in the peak speed was compensated by an upregulation of median duration by 27.1% (early: 43 ms; late: 59 ms; Wilcoxon signed rank test, $p<0.001$) and 17.8% (early: 37 ms; late: 45 ms; Wilcoxon signed rank test, $p<0.001$) for CP and CF saccades, respectively. Consequently, the resulting median amplitudes did not change for CF saccades (early: 15.8 deg; late: 15.5 deg; Wilcoxon signed rank test, $p=0.06$) and only slightly for CP saccades (early: 15.8 deg; late: 15.2 deg; Wilcoxon signed rank test, $p=0.002$). The effect of fatigue in the later part of the trials in the CF (light red) and CP (light blue) saccades can be seen as the "widening" (i.e. longer duration) of the inverted bell-shaped velocity profiles of saccades in conjunction with a reduction of the peak (Fig. 1C, lower panel). As indicated by the position trace (Fig. 1C, upper panel), the end positions of saccades did not change.

Across all 160 recording sessions we observed consistent effects as indicated by the averages (Fig. 1D). Compared to the early trials, the median peak speed of both CF and CP saccades (Fig. 1D, left panel) in the late trials declined by 8.2% and 12.6% across all sessions, respectively (CF: early: 632.8 deg/s, late: 580.9 deg/s, Wilcoxon signed rank test, $p<0.001$, $Z=10.7$; CP: early: 583.3deg/s, late: 509.7 deg/s, Wilcoxon signed rank test, $p<0.001$, $Z=10.8$). These changes were compensated by an increase of duration (Fig. 1D, middle panel) of CF and CP saccades by 9.7% and 19.3%, respectively (CF: early: 39.9 ms, late: 43.8 ms, Wilcoxon signed rank test, $p<0.001$, $Z= -10.7$; CP: early: 43.3 ms, late: 51.7 ms, Wilcoxon signed rank test, $p<0.001$, $Z= -10.8$), thus stabilizing saccade amplitudes (Fig. 1D, Right panel; CF: early: 14.7 deg, late: 14.6 deg, Wilcoxon signed rank test, $p=0.02$, $Z= 2.2$; CP: early: 14.8 deg, late: 14.9 deg, Wilcoxon signed rank test, $p=0.03$, $Z= 2.1$). The influence of cognitive fatigue on saccade speed and its compensation of a speed vs.

duration trade-off can also be seen in the scatter plots of individual sessions. Figure 1E (left) plots late saccade speed as function of early saccade speed across individual sessions. In this plot, which distinguishes CF (red dots) and CP (blue dots) saccades, the vast majority (CF:94.4%, CP: 96.3%) of data points lie below the unity line. On the other hand, the data points in the corresponding plot of late saccade duration as function of early saccade duration lie above the unity line (Fig. 1E, middle panel) whereas those in the plot of late saccade amplitude as function of early saccade amplitude do not deviate from it (Fig. 1E, right panel).

Independent of the influence of the fatigue task, we observed a clear difference between CF and CP saccades (Fig. 1D and 1E): CF saccades were not only faster than the CP saccades (early: CF: 632.8 deg/s, CP: 583.3 deg/s, Wilcoxon signed rank test, $p<0.001$, $Z= 8.5$; late: CF: 580.9 deg/s, CP: 509.7 deg/s, Wilcoxon signed rank test, $p<0.001$, $Z= 9.8$), but also exhibited shorter durations (early: CF: 39.9 ms, CP: 43.3 ms, Wilcoxon signed rank test, $p<0.001$, $Z= -8.9$; late: CF: 43.8 ms, CP: 51.7 ms, Wilcoxon signed rank test, $p<0.001$, $Z= -10.1$). On the other hand, their amplitudes did not differ (early: CF: 14.7 deg, CP: 14.8 deg, Wilcoxon signed rank test, $p=0.17$, $Z= -1.3$; late: CF: 14.6 deg, CP: 14.9 deg, Wilcoxon signed rank test, $p=0.11$, $Z= -1.5$). Also, the influence of fatigue, seen as the amount of reduction in peak speed, was stronger in the CP direction (12.6%) as compared to that of CF saccades (8.2%). Note that rewards followed the successful execution of CF saccades, whereas CP saccades were needed to get ready for a new trial, yet not followed by an immediate reward. Hence, the higher speed and shorter duration of CF saccades, their larger vigor, may be a consequence of more immediate reward expectations.

Complex spikes carry/provide information on the direction, amplitude and duration of the primary saccade

When comparing the CS firing rate for CF and CP saccades, we found clear direction dependent differences. As exemplified by the example PC shown in Fig. 2A saccades to the right, that happened to be CP saccades, were followed by a sharp increase in the CS firing during the post-saccadic period (0 to 100 ms after saccade end). Also, saccades in the opposite direction, CF saccades, were followed by an increased discharge. Yet, this increase was significantly weaker (peak firing rate ± s.e.m: CP= 5.97 ± 1.0 spikes/s; CF= 1.69 ± 0.5 spikes/s; Wilcoxon rank sum test, $p<0.001$, $z=4.20$). The notion that this difference was a reflection of direction rather than a preference for centripetal saccades is indicated by the fact that other PCs could fire more CSs for CF saccades with no consistent preference for centripetal or centrifugal saccades in our sample (peak firing rate ± s.e.m: CF=1.33 ± 0.09 spikes/s; CP= 1.45 ± 0.10 spikes/s; Wilcoxon signed rank test, $p = 0.99$, $z=9.38$, Supplementary Fig. 2). We used CS discharge rate in the *'early post-saccadic period'* of the primary saccade, 0-100 ms relative to saccade offset, to identify the preferred direction of CSs (PD_{ps}; subscript *ps: primary saccade*) and the opposite as the anti-preferred direction (PD_{ps}+180°). The overall CS firing across all 151 PCs in their PD_{ps} was clearly larger (Fig. 2B, left) than to saccades made in the anti-preferred direction (peak firing probability ± s.e.m: PD_{ps}= 1.76 ± 0.11 spikes/s; PD_{ps}+180°= 1.07 ± 0.08 spikes/s; Wilcoxon signed rank test, $p<0.001$, $z=6.38$). One may argue that trying to assess a preferred direction based on just two opposite horizontal directions may fail in many cases because of insufficient sensitivity. Yet, as demonstrated by the scatter plot of individual PCs' CS mean firing rate in the antipreferred direction as a function of the CS mean firing rate in the preferred direction (Fig. 2C, left), this was clearly not the case, with just a handful of CSs lying on the unity line. On the other hand, a plot of

postsaccadic CS firing for right vs. left saccades (CF and CP combined; Fig. 2C right) did not yield consistent preferences (Fig. 2B, right; peak firing probability ± s.e.m: Left= 1.34 ± 0.10 spikes/s; Right= 1.46 ± 0.10 spikes/s; Wilcoxon signed rank test, p=0.43, z=0.78 and Fig. 2C, right).

It could also be objected that the strong CS discharge observed in the early post-saccadic period might be a consequence of the large retinal error generated by the target jumps. However, in the vast majority of PCs (83%) we did not observe any significant modulation during the period between 50 ms from target jump time to the time of primary saccade whereas – as said before – we typically observed a clear response closely following the end of the saccade, suggesting that the observed CS discharge was related to the primary saccade itself.

We next explored the effects of saccade amplitude on the firing probability of CSs. To this end, we exploited the natural variability of saccade endpoints within the fixation window of ± 2 deg centered on the target location (for CF saccades) and the fixation point (for CP saccades). Saccades with amplitudes ranging between 13 to 16 deg were divided into equally spaced bins (bin size: 0.5 deg) and pooled across PD_{ps} and PD_{ps}+180° (i.e., CP and CF saccades in both left and right directions). As shown in Figure 3A, the maximum CS firing during the *'early post-saccadic period'* turned out to increase linearly with saccade amplitude (R-sq: 0.97; p=<0.001). To test the influence of saccade duration on CSs, we sorted the same pool of saccades into duration bins (range: 35-65 ms; bin size: 5 ms) and saw that longer duration saccades were associated with later population peak responses (Fig. 3B; R-sq: 0.95; p=0). Since the amplitude increased with the duration of saccades, we also observed an increase in the CS firing for long duration saccades. When aligning the CS population response to saccade offset (Supplementary Fig. 1A), we found that the postsaccadic increase in CS firing was preceded by a trough, a decrease in CS firing relative to the baseline level that at first glance seemed to indicate saccade end. This was indeed

353 the case because also the timing of the trough (see methods for details, Supplementary Fig. 1B)
354 proved to depend on saccade duration with trough times shifting with increasing saccade duration
355 relative to saccade end (Supplementary Fig. 1C, R-sq: 0.86, p=0.007). Surprisingly, considering
356 the tight behavioral relationship between saccade velocity and duration, the firing probability of
357 CSs turned out to be independent of saccadic peak velocity (Fig. 3C; R-sq: 0; p=0.99). In sum,
358 CSs in our sample carried information on the direction of the primary saccade, its amplitude and
359 duration, yet not saccade velocity.

360

361 *Complex spikes carry information on corrective eye movements*

362 As a consequence of the inherent variability of saccade endpoints, saccades only rarely landed
363 exactly on target. Rather they usually 'undershot' or 'overshot' by small and variable amounts and
364 were followed by occasional secondary, corrective eye movements (amplitude: 0.2-2 deg) made
365 towards the target location. As a matter of fact, we observed that the influence of these corrective
366 saccades on the firing of CSs was similar to the one on primary saccades. Figure 4A demonstrates
367 the responses of an exemplary PC neuron (same PC as in Fig. 2A) around the time of corrective
368 saccades made during a single behavioral session. Trials, aligned with corrective saccade onset,
369 were sorted according to the direction of the corrective saccade (left panels: corrective saccades to
370 the left, right panels: to the right) regardless of their starting positions, and the latter distinguished
371 by color (CF primary saccades: red, CP primary saccades: green). No matter if the preceding
372 primary saccade had been CP or CF, the CS firing rate increased within a period of about 100 ms
373 after the corrective saccade ("*post-corrective-saccadic period*"). This is clearly depicted in the
374 case of the exemplary PC with a rightward preference for corrective saccades (Fig. 4A) as

exhibited by a strong discharge (peak firing rate: ± s.e.m: 6.25 ± 1.56 spikes/s) during the '*post-corrective-saccadic period*' (Fig. 4A, middle and bottom right panel), regardless of the preceding CF (red) or CP (green) saccades. In contrast, no clear modulation in CS firing was observed following corrective saccades to the left, the unit´s non-preferred direction (peak firing rate ± s.e.m: 1.32 ± 0.92 spikes/s). Note, however, the increase in CS probability in the error period between primary saccade offset and corrective saccade onset (Fig. 4A, middle and bottom left panel), we will consider in more detail later.

We compared the CS firing for corrective saccades made to the left and to the right in the '*early post-corrective-saccadic period'*, chosen analogously to the window for the characterization of primary saccade related firing, in order to define their preferred and the anti-preferred direction (PD_{cs} and PD_{cs}+180° respectively, subscript *cs: corrective saccades*). We did this for each CS unit. The preferred direction of the corrective saccades corresponded to the preferred direction for primary saccades in only 42% of the PCs, i.e. a percentage that is close to the one to be expected in case of a random relationship of preferred directions for primary and for corrective saccades. Figure 4B depicts the population responses for corrective saccades made in the preferred and the anti-preferred direction directions. Similar to the CS population response for primary saccades made into their preferred direction, we observed a clear peak of CS firing in the PD_{cs} (peak firing probability ± s.e.m: PD_{cs}= 2.33 ± 0.14 spikes/s; PD_{cs}+180° =0.93 ± 0.07 spikes/s; Wilcoxon signed rank test, $p<0.001$, $z=7.74$) during the 100 ms period from corrective saccade offset (gray shaded region in Fig. 4B). However, in contrast to the CS population response to primary saccades in PD_{ps}+180° (Fig. 2B, left column) the CS population response to corrective saccades in the PD_{cs}+180° direction exhibited a broader discharge during the *'pre-corrective-saccadic period'* of 200 ms from corrective saccade onset (Fig. 4A, middle and bottom left panels, and Fig. 4B). We

398 will discuss the basis of the CS modulation during this period in detail later after having first
399 considered the amplitude tuning of the post-corrective saccade CS response.

400 To this end, we sorted all corrective saccades from all sessions in amplitude bins (bin size: 0.5
401 deg), pooling corrective saccades made in the PD_{cs} and PD_{cs}+180° and plotted the CS peak firing
402 rate as a function of corrective saccade amplitude. As shown in figure 5A, this resulted in a clear
403 post-corrective saccade peak whose size depended linearly on the amplitude (R-sq: 0.97, p=0.01).
404 This was also true when looking at the CS population responses separately for the PD_{cs} and
405 PD_{cs}+180° (Supplementary Fig. 3A and B). Sorting corrective saccades based on duration we
406 observed that the peak of the CS population response occurred the later, the longer the corrective
407 saccade took (Fig. 5B; R-sq: 0.98, p=0.08), a relationship which corresponds to the one for primary
408 saccades. Further investigating the PD_{cs} and PD_{cs}+180° individually for effects of saccade duration
409 on the CS timing revealed similar patterns in both cases (Supplementary Fig. 4). Moreover, even
410 the timing of modulation onsets ('troughs') shifted with saccade durations (Supplementary Fig. 4).

411 Our results on corrective saccades clearly indicate that CSs carry precise information on corrective
412 saccade amplitudes and timing in the *'post-corrective-saccadic period'* in a manner that is very
413 similar to information on primary saccades in the '*early post-saccadic period'*.

414

415 *Complex spikes convey error related information*

416 As mentioned in the previous section, we also observed a pre-corrective saccade increase in CS
417 firing for corrective saccades in the PD_{cs}+180° direction -200 to 0 ms before corrective saccade
418 onset (Fig. 4).

We wondered if this modulation was related to retinal error resulting from imprecise primary saccades prompting subsequent corrective saccades. To explore this possibility, we sorted all primary saccades recorded for a given PC according to the direction of the retinal error, i.e. the vector pointing from the saccade end towards the target location resulting from imprecise primary saccades, ignoring saccade direction and starting point. The error direction for which higher CS firing was observed in the *'pre-corrective-saccadic period'* was labeled PD_{error} and the opposite direction PD_{error}+180°. For each PC, we calculated CS responses to primary saccades that were made in the direction of PD_{error} and PD_{error}+180° respectively and combined them to compute CS population responses for these two directions. As shown in figure 6A the population averages differed in this *'early post-saccadic period'* with the average in the preferred error direction characterized by a "burst-tonic" profile, starting to deviate from the population average for the opposite direction a few 10 ms after saccade offset, exhibiting a peak firing rate about 50 ms after saccade offset and staying elevated until well after 200 ms. Note that also the profile for the opposite direction showed an early peak while lacking the later tonic response component.

When sorted by the preferred direction of primary saccades, the population averages exhibited an early peak, significantly larger in the preferred saccade direction (compare Fig. 6B). Yet, the averages for the preferred and the antipreferred directions lacked any difference later, during the *'late post-saccadic period'* of 50-250 ms from primary saccade offset, falling back to baseline level already after only 113 ms. The contrast between the population averages sorted by retinal error as opposed to the averages sorted by primary saccade direction becomes particularly apparent when comparing the respective difference plots for the preferred and the anti-preferred directions (Fig. 6C), clearly demonstrating that the later modulation of CS firing is error-specific and independent of the metric of the primary saccade. But what about the early peak, at least

qualitatively similar in all population averages, no matter if they were based on error or primary saccade direction. Could it be that the discharge in the '*early post-saccadic period*' reflects error rather than saccade direction and amplitude? In this case, saccades made into the same direction and with similar amplitudes but different error directions should give rise to qualitatively different discharge patterns in this '*early post-saccadic period*'. However, as shown by the exemplary neuron depicted in supplementary figure 5, this was clearly not the case. The early post-saccadic CS burst evoked by saccades in this unit´s preferred direction to the right (Supplementary Fig. 5, left) was the same, no matter if the calculation of the average discharge pattern was based on pooled hypo- or hypermetric saccades, i.e. saccades with oppositely directed retinal errors (Supplementary Fig. 5, middle: leftward error saccades; rightward error saccades). In fact, the CS response obtained by averaging across all saccades in PD_{ps} and PD_{ps}+ 180° with leftward and rightward errors only reduced the sensitivity of the CS discharge observed as a reduction in the size of the peak CS response in '*early post-saccadic period'* in both cases (Supplementary Fig. 5, dark gray traces at the bottom, middle and right panels).

The conclusion that the early postsaccadic response is dominated by sensitivity to primary saccade metrics rather than just error is fully supported by the population analysis summarized in supplementary figure 6. Here we compared population responses of all large and small saccades (mean amplitude: 16.3 deg and 13.6 deg, respectively), regardless of the direction of resulting errors, which resulted in a significant difference between CS responses only during the early 20-85 ms period from saccade end (Supplementary Fig.6, left panel; running t-test: $p<0.001$). Large saccades were mostly hypermetric saccades that overshot the target in 95% of trials considered. In 47% of PCs these saccades were associated with retinal errors in PCs´ preferred error direction ($PD_{error)}$, and in 53% with errors in the opposite direction (PD_{error}+180°). The corresponding

numbers for small amplitude (i.e. hypometric) saccades: 92% undershoots, PD_{error}: 50%, PD_{error}+180°: 50%. Pooling across error directions resulted in the cancellation of the overall error (mean error for large and small amplitude saccades: 0.3 deg and 0.2 deg, respectively) and consequently cancelled the differences between CS responses in the *'late post-saccadic period'*. The difference during the late period of 29-248 ms from saccade end (running t-test: $p<0.001$) becomes evident only when saccades of comparable sizes (mean amplitudes: 14.4 deg and 14.9 deg) were sorted by equally sized errors (mean error: 1.3 deg) in opposite directions, although the "spilling over" of error related effects can also observed during the early period. To ensure that this early response indeed conveyed information on primary saccades we further compared population responses computed from a subset of all large and small amplitude saccades that resulted in equal error sizes in the PCs' preferred and anti-preferred error directions (Supplementary Fig. 6C and D). The mean error sizes resulting from large (mean amplitude: 16.4 deg) and small saccades (mean amplitude: 13.5 deg) made in PD_{error}+180° were 1.36 deg and 1.4 deg, respectively, while those resulting from large and small amplitude saccades (mean amplitude: 16.4 deg and 13.5 deg) made in PD_{error} were 1.36 deg and 1.4 deg, respectively. Since, both large and small amplitude saccades resulted in equally sized errors the stronger CS discharge for large amplitude saccades relative to the small ones (running t-test: $p<0.001$; Bonferroni corrected for multiple comparisons) in the '*early post-saccadic period*' clearly suggests a saccade related response. In sum, this analysis establishes a clear influence of the metric of the primary saccade on CS firing. Error information influences CS firing over a longer period of time after the primary saccade, most probably adding to the early metrics related firing.

We wondered if the undeniable influence of error on the CS firing is graded, reflecting not only an influence of direction but also of error amplitude. To find an answer we sorted the CS population

responses for corrective saccades into retinal error magnitude bins (bin size: 0.5 deg; Fig. 7A, left) calculated for the *'pre-corrective saccadic period'* (200 msec before corrective saccade onset). As shown in Fig. 7A, right, the mean firing rate of CSs decreased with error magnitude in the PD_{error}. Moreover, it dropped further with increasing error magnitude in the PD_{error}+180° (Fig. 7A, right). We observed a similar pattern of CS firing rates during the *'late post-saccadic period'* of primary saccades, when sorted by error magnitude (Supplementary Fig. 7), clearly indicating that the *'pre-corrective-saccadic period'* and *'late post-saccadic period'* shared the same error related information and establishing that error influences CS firing in a graded manner.

As demonstrated earlier, primary saccade amplitude modulates CS firing in the '*early post-saccadic period'*. However, unlike the influence of error magnitude which is opposite for errors in the preferred and the anti-preferred direction, it turned out to be the same in the case of saccade related firing as measured in the '*early post-saccadic period'*. For both primary saccades (Fig. 7B) and for corrective saccades (Fig.7C), discharge increased with amplitude, no matter if saccades were made in the preferred or the anti-preferred direction, respectively. However, note that the amplitude tuning cannot be graded across the whole range of amplitudes considered. This is clearly indicated by the fact that in absolute terms, the CS firing associated with corrective saccades was clearly not weaker than the firing associated with the much larger primary saccades. Hence, in addition to direction and amplitude, the discharge in the '*early post-saccadic period'* is also determined by saccade type.

Complex spike duration encodes error and saccade related information

It has been argued earlier that not only the probability of CSs firing but also systematic changes in CS duration, the latter being dependent on the 'state' of the olivary neurons determining the strength of the climbing fibre input (Bazzigaluppi et al., 2012; Mathy et al., 2009), carry behaviorally relevant information necessary to drive motor learning (Yang and Lisberger, 2014, 2017). To test the relevance of CS duration in our task, we measured the duration of individual CSs fired by each PC as the time between CS start and end, deploying an interactive deep neural network approach described in detail in Markanday et al. (2020). As shown for an exemplary PC neuron (Fig. 8A), we found a bimodal distribution of CS durations for a single behavioral session. Taking a closer look at the CSs in the two modes revealed that the longer duration CSs (mean duration of CS: 6 ms) were characterized by a waveform with an additional spikelet at the end, not exhibited by CSs in the short duration mode (mean duration of CS: 4.2 ms). There was no change in the shape of the initial fast spiking component (Fig. 8B).

To investigate task related changes in CS duration we computed a running average (bin size: 50 ms) of percentage change in CS duration relative to mean CS duration of an individual PC and estimated a population-based percentage change in CS duration. This population measure showed a conspicuous drop relative to baseline (peak change from baseline: 7.5%) in the perisaccadic period. In the subsequent phase the population CS duration increased again, reaching a maximum value of 1.6% about 100 ms after primary saccade end, When comparing the trajectory of duration changes with the one for CS firing rate (Supplementary Fig. 8) it became clear that the two were obviously yoked with decreases in duration paralleling decreases in CS probability and vice versa.

When distinguishing saccades smaller than 15 deg from those larger than this value, it became apparent that the CS duration changes for larger amplitude saccades (mean amplitude: 16.4 deg) differed from those for smaller amplitude saccades (mean amplitude: 13.7 deg) in the post-saccadic period, a difference that started approximately 50 ms after saccade offset (Fig. 8C). As shown in figure 8D, the percentage change in CS duration during the post-saccadic period increased with primary saccade amplitude (bin size: 1 deg), independent of saccade direction, a pattern very similar to the amplitude tuning obtained for CS firing rates (Fig. 7B). Distinguishing primary saccades based on their preferred error direction (i.e. PD_{error} vs. PD_{error}+180°; Fig. 8E), we observed that CS duration grew in the error period for saccades causing larger errors in the preferred error direction and dropped in the opposite direction (Fig. 8F), a pattern reminiscent of the one observed for CS firing rates in response to error magnitudes (Fig. 7A). Similar to the dependence of CS firing on the size of corrective saccades, we found that CS durations increased with corrective saccade amplitude, regardless of their direction (i.e. PD_{cs} and PD_{cs}+180°; Fig. 8G, H). Finally, the influence of error magnitude on CS duration before corrective saccade (Fig. 8 I, J) was similar to the one for primary saccades in preferred and anti-preferred error directions.

Together, these findings clearly suggest that CSs convey saccade and error related information by duration changes that parallel changes in CS firing rates.

Trial onset evoked responses of complex spikes

When analyzing CSs of individual PCs, we found that in a subset of PCs (N=73 out of 151), the probability of CS firing increased more strongly before an upcoming saccade when aligned to the appearance of the central fixation dot as compared to aligning trials to the onsets of the preceding

CP saccades. Figure 9A shows an example of one of those few PCs (N=27) that could be held long enough to record CSs in both left and right CF directions, in separate sessions. This cell fired CSs following left but not right CF saccades (Fig. 9A; left column). In the case of CP saccades (Fig. 9A; middle column), we observed only a very weak modulation during the post-saccadic period. However, the CS firing rate was clearly enhanced when aligning trials with CP saccades to the onset of the upcoming CF trials (marked by the appearance of the central fixation dot) with a relatively sharp peak in CS firing at 200 ms after trial onset, regardless of direction (Fig. 9A; right column; peak firing probability ± s.e.m: left= 3.40 ± 0.39 spikes/s; right= 2.40 ± 0.46 spikes/s; Wilcoxon signed rank test p=0.40, z=0.83). Considering the large temporal scatter of the preceding CP saccade end points relative to the onset of the upcoming CF trial onset, the temporal precision of this CS discharge, resulting in a sharp peak, clearly argues against the possibility that it might be a late reflection of the preceding CP saccades. Could it be a response to the large visual error due to the appearance of the central fixation dot relative to the position of eyes at the end of CF saccades? This possibility can be safely ruled because of the lack of directional specificity of the CS peak discharge (Fig. 9A, right column), assuming that any sensitivity to retinal error should be directional. We pooled CS responses of all 27 PCs (Fig. 9B), from which data on both left and right CF (and CP) saccades were available, and found no difference between the size of the CS peak discharge rates in the trial onset aligned CS population responses for the two directions (peak firing probability ± s.e.m: left= 1.51 ± 0.18 spikes/s; right= 1.67 ± 0.20 spikes/s; Wilcoxon signed rank test, p=0.37, z=0.89). If these peaks were related to the CP saccades preceding the upcoming trial one might expect to see an influence of CP saccades on all task related CSs fired at about the time at which we observed the CS peaks tentatively related to trial onset. Moreover, this influence would be expected to be CP saccade amplitude related. This was clearly not the case as

documented by a consideration of pooled CS responses of all 151 task-related PCs. Although their CSs firing probability clearly modulated with CP saccade amplitudes (Fig. 9C, R-sq=0.89, $p<0.01$) when aligned to CP offset during the *'early post-saccadic period'*, the same CSs when aligned to trial onset exhibited no clear relationship to CP saccade amplitudes made towards the central fixation dot (Fig. 9C, R-sq=0.12, p=0.5). Finally, we sorted the CP saccades according to their arrival times relative to the time of the onset of the upcoming trial (Fig. 9E). As shown in figure 9F and G, the "onset" peaks were absent in the case of late CP saccades that arrived only shortly before the next jump of the target to an eccentric position. On the other hand, the peaks were maximal in the case of early CP saccades with a gradual change between these two extremes (Fig. 9G; R-sq=0.97; p=0.016). In sum, these results indicate that the increase in CS firing around 200 ms after trial onset is neither related to retinal error, nor to the kinematics of the preceding CP saccade. Rather, it may reflect a prediction of the upcoming event, i.e., the time of the target jump and/or a preparation of the behavior required.

Discussion

The purpose of this study was to investigate if CSs are capable of conveying different streams of behaviorally relevant information in a multiplexed manner. By scrutinizing if CS responses evoked in a demanding saccade paradigm causing cognitive fatigue are related to different events, we were able to demonstrate that many seemingly "spontaneously firing" CSs actually transport information on several behaviorally relevant parameters.

Complex spikes encode saccade related parameters

When aligning the CS discharge to primary saccades, we observed a strong and temporally precise accumulation of CSs within a 100 ms period starting precisely at the end of saccades. This strong modulation was clearest for saccades made in one of two horizontal directions, specific to the respective PC. Since we tested CF and CP saccades in only left and right horizontal directions, it is important to note, that our consideration of the directionality of the saccade related CS responses must be very coarse. Therefore, in some cases (36 PCs) in which we did not find clear differences between CS responses in the two saccade directions, we probably missed the preferred direction because it may have deviated too much from the horizontal. In any case, CS firing increased linearly with the amplitude of the saccade made in our admittedly coarse estimate of the preferred direction. The subtle changes in saccade duration due to fatigue were paralleled by shifts in the latency of the peak of the modulation and by shifts in the onset of this modulation. At first glance, one may feel tempted to argue that CSs occurring during this *'early post saccadic period'* may only convey error related information and that the observed increase in the CS firing in response to saccade amplitudes may simply be a reflection of retinal errors emerging from imprecise saccades possibly growing with saccade amplitude. However, there are several reasons to discard this interpretation. First, we found a strong relationship between the end of the primary saccade and the onset of CS modulation with increases in saccade duration associated with later modulation onset. Second, in population averages in which the two error directions were balanced, we still found clear saccade-related responses in this *'early post-saccadic period'*. Moreover, these responses were saccade amplitude dependent. On the other hand, changes during the '*late period post-saccadic period'* only appeared when CSs were sorted by error direction. Third, also corrective saccades (< 2 deg) exhibited an increased CS firing within a 100 ms period from saccade

offset that showed a saccade amplitude and duration dependence fully analogous to the one for primary saccades. Assuming that corrective saccades will finally lead to target fovealization one would not expect any discharge due to a remaining directional retinal error. Hence, we are confident that the CS response during the '*early post-saccadic period*' reflects the metric and the kinematics of saccades rather than the retinal error. This notion is in accordance with previous work on reaching arm movements of monkeys demonstrating an influence of movement direction and kinematics on CSs (Fu et al., 1997; Kitazawa et al., 1998) and work on saccadic adaptation (Catz et al., 2005) that demonstrated the build-up of CS modulation with changes in saccade amplitude paralleling the disappearance of error.

Complex spikes encode error related information

The fact that we found clear non-visual saccade related responses does not refute the idea that CSs encode retinal errors. We could clearly identify error direction dependent changes in CS firing at the level of individual PCs. However, they occur later than the ones related to saccade kinematics with some overlap notwithstanding. In CS population averages the error related influence started around 50 ms after saccade offset and lasted for more than 200 ms, i.e. at corrective saccade onset. In fact, this is the same period in which Herzfeld et. al (2015; 2018) reported error related CS activity. We observed a linear increase in the CS firing rate with error magnitude within a small range of magnitudes (<2 deg) in the preferred direction while previous studies reported an absence of error magnitude tuning (Soetedjo and Fuchs, 2006; Soetedjo et al., 2008). However, this is not necessarily inconsistent as we did not consider larger errors for which the tuning we describe might exhibit saturation.

643 *Encoding of saccade and error related information by complex spike duration*

644 The duration and morphology of CS are determined by the duration and temporal structure of
645 action potential bursts fired by olivary climbing fibres. The latter reflect the state of the inferior
646 olive as set by gap junctions controlling the communication between neighboring cells. Longer
647 duration axonal bursts, that are thought to translate into CSs with more spikelets and overall longer
648 duration, (Eccles, 1967; Latham and Paul, 1971; Mathy et al., 2009; Warnaar et al., 2015).
649 Increasing the duration of CS will lead to more influx of calcium, boosting long-term depression
650 at parallel fibre-PC synapses, believed to be the major basis of cerebellar learning (Yang and
651 Lisberger, 2014, 2017). In accordance with this framework, Yang and Lisberger (2014) could
652 demonstrate that smooth-pursuit adaptation, a variant of oculomotor learning, was accompanied
653 by changes in CS duration. In contrast, attempts to identify corresponding correlations between
654 CS duration and saccadic adaptation have failed (Herzfeld et al., 2018; Junker et al., 2018). This
655 inconsistency, and in general the paucity of relevant data on the role of CS duration is most
656 probably a consequence of the fact that so far the analysis of CSs required a tedious and error-
657 prone manual approach (Herzfeld et al., 2018; Junker et al., 2018; Warnaar et al., 2015; Yang and
658 Lisberger, 2014, 2017). In our study, we could take advantage of a new approach deploying a deep
659 learning network that greatly facilitated the identification of the individual CSs, including the
660 quantification of their duration and morphology, and yet warranting the sensitivity and specificity
661 of the analysis of a human expert (Markanday et al., 2019). In accordance with previous findings
662 (Warnaar et al., 2015; Yang and Lisberger, 2017), we could indeed establish clear saccade-related
663 changes in CS duration accompanying changes in CS firing rates. Yoked changes in CS rate and
664 duration reflected both information on saccade metric and saccade related retinal errors. CS
665 duration changes were typically based on the addition or omission of terminal spikelets. These

findings support the notion that the control of PC calcium levels underpinning synaptic plasticity deploys concerted changes in CS rate and duration.

Changes in saccade-related CS firing were not only confined to increases in rates, accompanied by changes in CS duration, but also involved a conspicuous decreased component around the time of the saccade. The phenomenology of this pause in CS firing, accompanied by a drop in CS duration, is particularly intriguing as its time course is strikingly similar to the time course of saccadic suppression of perception with both spanning a peri-saccadic period of approximately -75 to +85 ms relative to saccade onset. Saccadic suppression is thought to have a neural correlate in the superior colliculus (SC), where neurons in the intermediate SC exhibit a suppression of their discharge that parallels the perceptual phenomenon (Hafed and Krauzlis, 2010). Given that climbing fibres in the oculomotor vermis receive their visual input probably primarily from the superior colliculus (Frankfurter et al., 1976; Harting, 1977; Huerta and Harting, 1984; Kojima and Soetedjo, 2018; Kyuhou and Matsuzaki, 1991; Szentágothai and Rajkovits, 1959), we speculate that the peri-saccadic suppression of CS activity might be handed over from the SC for whatever purpose.

Complex spikes predict upcoming events

We found that a large proportion of task-related PCs showed a sharp increase in CS firing around 200 ms after trial onset, i.e. at a time the monkey got ready for a new target-directed centrifugal saccade. Our analysis of a subset of PCs, for which data on CF and CP saccades in both left and right directions was available, revealed that this CS "burst" was insensitive to the direction or amplitude of preceding centripetal saccades. Aligning these responses to different events other

than the onset of the new trial only compromised the strength of the CS response, supporting the link to trial onset, marked by the reappearance of the central fixation dot. The reappearance of the fixation dot was followed by target jumps 400 to 600 ms later, to which the monkeys responded with target directed saccades after varying delays. The longer it took the monkey to execute the saccade, the smaller the magnitude of the CS signal, tentatively linked to trial onset, got. This dependency may suggest a role of the trial onset related CS signal in predicting the upcoming target jump. The rationale is that reaction times should be the shorter the better the ability to predict the timing of the preceding target jump is. A role of the CS in predicting the time of target-directed saccades is in accordance with previous work on eye-lid conditioning in mice (Ohmae and Medina, 2015), in which CS bursts elicited by the conditioned stimulus predict the time of occurrence of the unconditioned stimulus. The assumed role of the CS in predicting saccades may also open a fresh perspective on the building up of the CS discharge modulation during short-term saccadic adaptation, paralleling the gradual disappearance of performance errors (Catz et al., 2005). Here, the CS signal might serve as prediction of the persisting need to adjust saccade amplitudes once error information, initially driving the adjustment is no longer available.

Multiplexing of different streams of information by complex spikes

In this study, we could demonstrate that individual PCs are influenced by different types of task related information that mark distinct elements in the sequence of events relevant for the behavior at stake. These different streams of information are multiplexed by individual climbing fibres in a manner that ensures the required precise alignment of information and behavioral events. How could this be accomplished and for what purposes? As to the latter question, a speculative answer

might be a revision of the classical Marr-Albus-Ito theory of cerebellar learning (Albus, 1971; Ito, 1972; Marr, 1969) in which the role of the climbing fibre system is confined to providing information on performance errors driving learning. In the case of saccadic learning, the relevant error signal is the retinal error resulting from a dysmetric saccade. Undeniably, information on error feedback is extremely important for optimal motor control, and as documented once again in this study is conveyed by the climbing fiber system and reflected in the pattern of PC CSs. Yet, error feedback arrives late which is why earlier information useful to judge the quality of the behavior is pertinent. Such information is provided by the climbing fibre system serving saccades by reflecting the metric of the executed saccades already immediately after its execution well before the arrival of retinal feedback. Independent of whether this early information reflects proprioceptive feedback or efference copy it may allow the system to jump start corrections well before the arrival of information on retinal error. As demonstrated, useful information may become available even earlier if experience allows the system to predict future motor needs, allowing it to get ready. In the same vein, Junker et al. (2018) could show that saccadic learning is shaped by information on past errors, leaving a signature in the CS firing, able to stabilize adjustments of the metric of saccades even at times error information might be no longer available (Catz et al., 2005). As said earlier, the idea that the climbing fibre system is able to tap different sources of information useful for optimal behavioral control is well in line with recent thinking about the underpinnings of eye lid conditioning (Ohmae and Medina, 2015).

The idea that optimal control may rely on dynamic encoding of more than one source of information by CSs (Ju et al., 2019; Streng et al., 2017), always relying on the most promising ones, is a concept that has clear implications for the functional architecture of the olivary system: it would not be sufficient for the inferior olive to have separate access to different sources of task

related information. Rather these different streams of information must converge at the level of individual neurons and, moreover, the system should have means to prioritize or select distinct streams. The limited anatomical data available suggests that olivary afferents from different sources contact different parts of an olivary nucleus (Sugihara and Shinoda, 2004). Hence, convergence of information at the level of individual olivary neurons or groups of neurons would require crosstalk within a nucleus. A possible basis might be provided by opening gap junctions allowing the exchange of information. In other words, the availability of multiplexed information at the level of PCs pertinent for learning might be based on the flexible control of olivary gap junctions.

Figures and figure legends

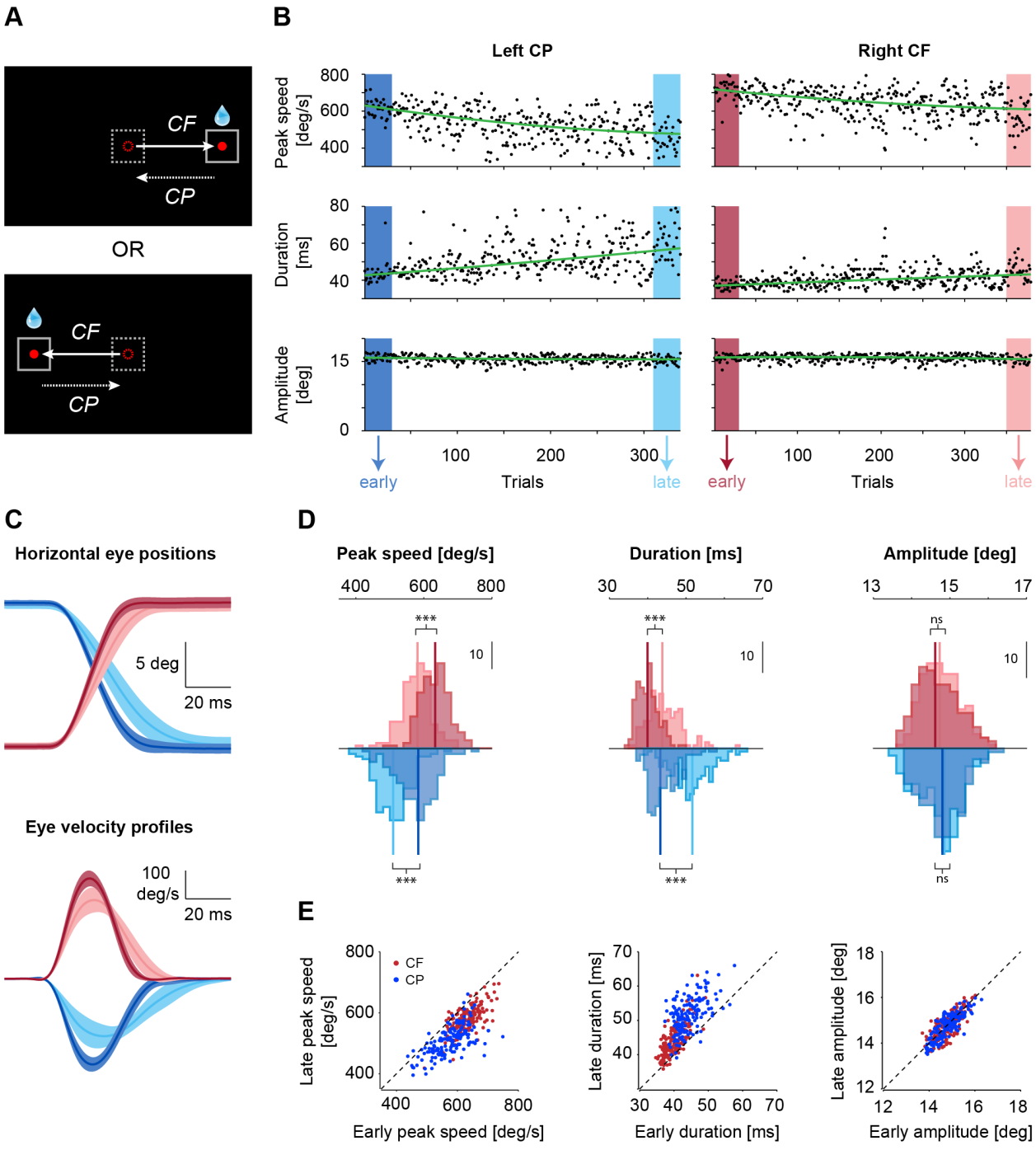

Figure 1. A. Experimental paradigm showing two separate sessions in which the rewarded centrifugal (CF) saccades were made either towards right (top panel) or left (bottom panel). The resulting centripetal (CP) saccades were naturally made in the opposite direction. **B**. Behavioral results from a single experimental session showing a gradual decline in saccade peak speed (top panels) , paralleled by increasing duration (middle panels) to maintain saccade amplitudes (bottom panels) in case of both CF (right column) and CP (left column) saccades. Solid green lines show the trend using a second order polynomial fit. Dark and bright shaded regions in blue and red represent the early and late 30 trials, respectively. **C**. Horizontal eye position (upper panel) and velocity profiles of CF (red) and CP(blue) of early and late 30 trials from the same session as shown in **B**. **D**. Histograms comparing peak speed (left), duration (middle) and amplitude (right) of early and late, CF and CP saccades, pooled across 160 sessions. Solid vertical lines represent the median values. Vertical scale bars represent the number of sessions. **E**. Scatter plots showing the effect of the paradigm on peak speed (left), duration (middle) and amplitude (right) of early and late, CF (red dots) and CP (blue dots) saccades, at the level of individual sessions. Each dot represents the mean value of early and late 30 trials in an individual session. Dotted lines represent the unity line.

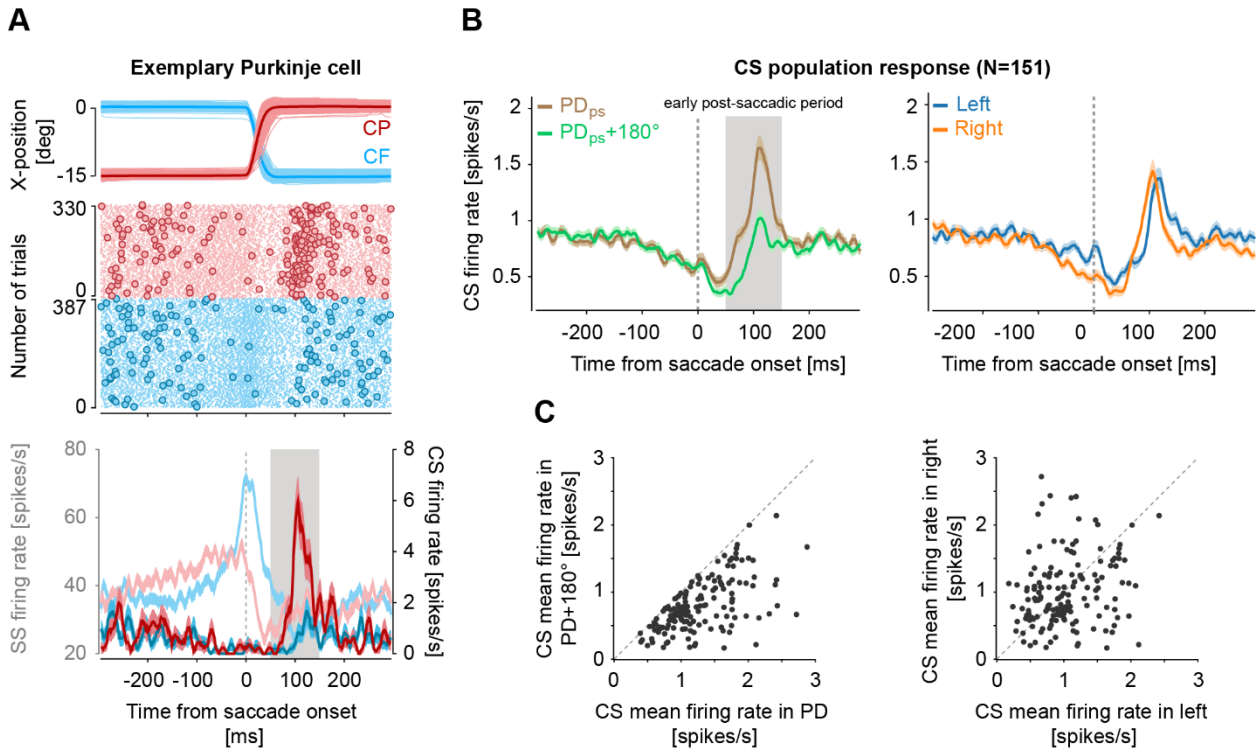

Figure. 2. A. Response of an exemplary Purkinje cell (PC) to left CF (blue) and right CP (red) saccades (upper panel). Raster plot (middle panel) of Simple spikes (SSs, dots) and Complex spikes (CSs, circles) and their corresponding mean (± s.e.m) firing rates (bottom panel) are shown in faded and bright colors, respectively. Note how the probability of CS occurrence increases during the *'early post-saccadic period'* (gray shaded region, 0-100 ms from saccade end) for the rightward but not leftward saccades, suggesting that the PC's preferred direction for primary saccades (PD_{ps}) pointed in the rightward direction. All data are aligned to saccade onset (dashed gray line). **B.** CS population response (mean ± s.e.m; N=151 PCs) in PC's preferred (PD_{ps}) and anti-preferred (PD_{ps}+180°) direction (regardless of left, right, CF and CP) of primary saccades (left panel) reveals a strong difference during the *'early post-saccadic period'* (gray shaded region), as compared to CS responses for primary saccades made in the left and right direction (right panel),

790 regardless of CF and CP saccades. All data are aligned to saccade onset (dashed gray line). **C.**
791 Scatter plot showing individual differences between the PD_{ps} and PD_{ps}+180° (left panel), and left
792 and right directions (right panel). Each dot represents the mean of CS firing probability calculated
793 during the *'early post-saccadic period'* for each PC. Gray dashed lines are the unity lines.

794

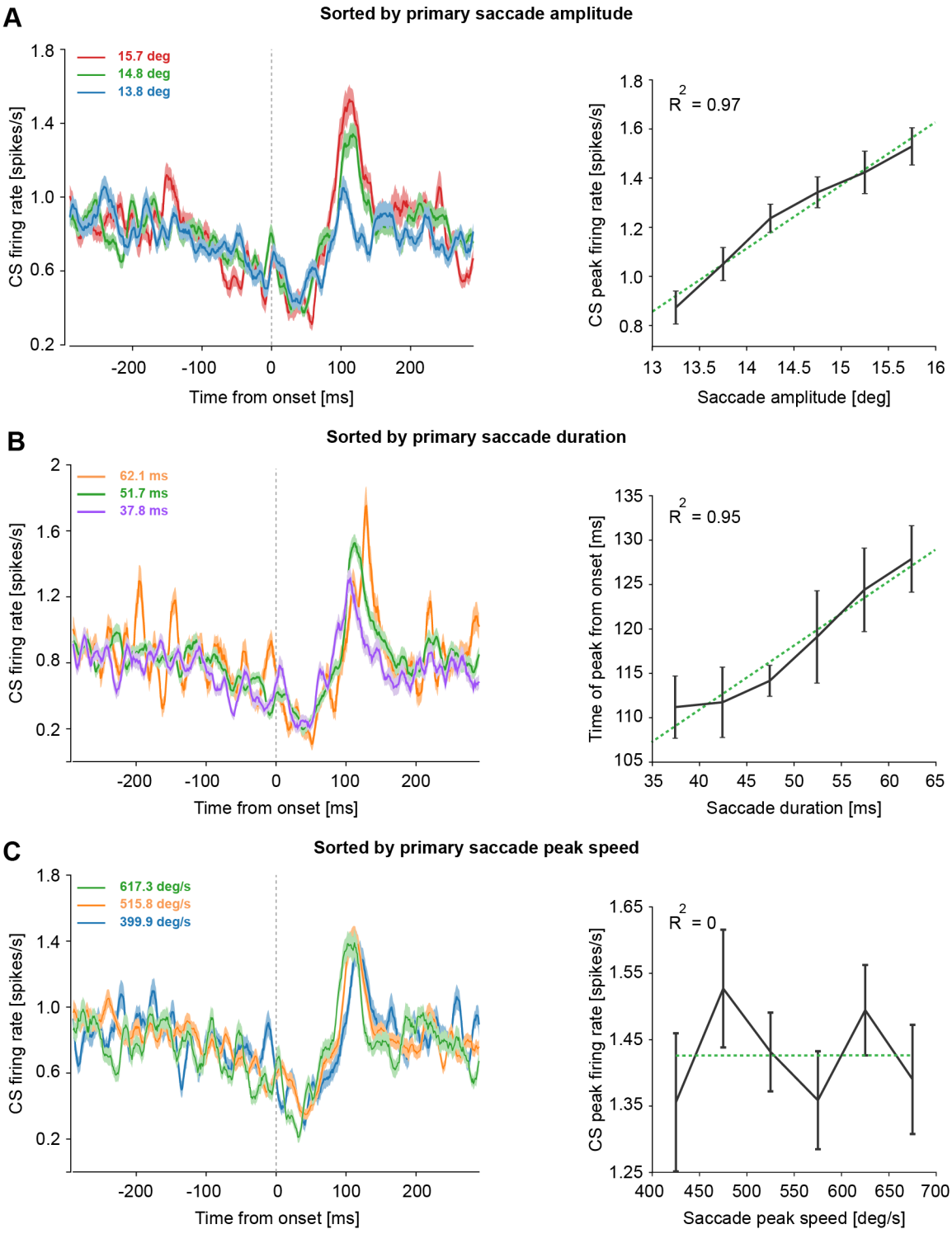
A
Sorted by primary saccade amplitude
15.7 deg
14.8 deg
13.8 deg
CS firing rate [spikes/s]
Time from onset [ms]
CS peak firing rate [spikes/s]
R2 = 0.97
Saccade amplitude [deg]
B
Sorted by primary saccade duration
62.1 ms
51.7 ms
37.8 ms
CS firing rate [spikes/s]
Time from onset [ms]
Time of peak from onset [ms]
R2 = 0.95
Saccade duration [ms]
C
Sorted by primary saccade peak speed
617.3 deg/s
515.8 deg/s
399.9 deg/s
CS firing rate [spikes/s]
Time from onset [ms]
CS peak firing rate [spikes/s]
R2 = 0
Saccade peak speed [deg/s]

795

796

Figure. 3. A. CS population response (bootstrapped mean ± confidence intervals) aligned to the onset of all primary saccades (PD_{ps} and PD_{ps}+180° combined) sorted by different amplitudes (left panel). The relationship between saccade amplitudes and peak firing probability of CSs is demonstrated with the help of a simple linear regression (right panel). **B.** Population response to saccades sorted by durations (left). The relationship between the timing of peak response and saccade duration is shown on the right. **C.** Population response to saccades with different speeds (left) and the corresponding regression plot (right). Green dotted lines represent the regression fits.

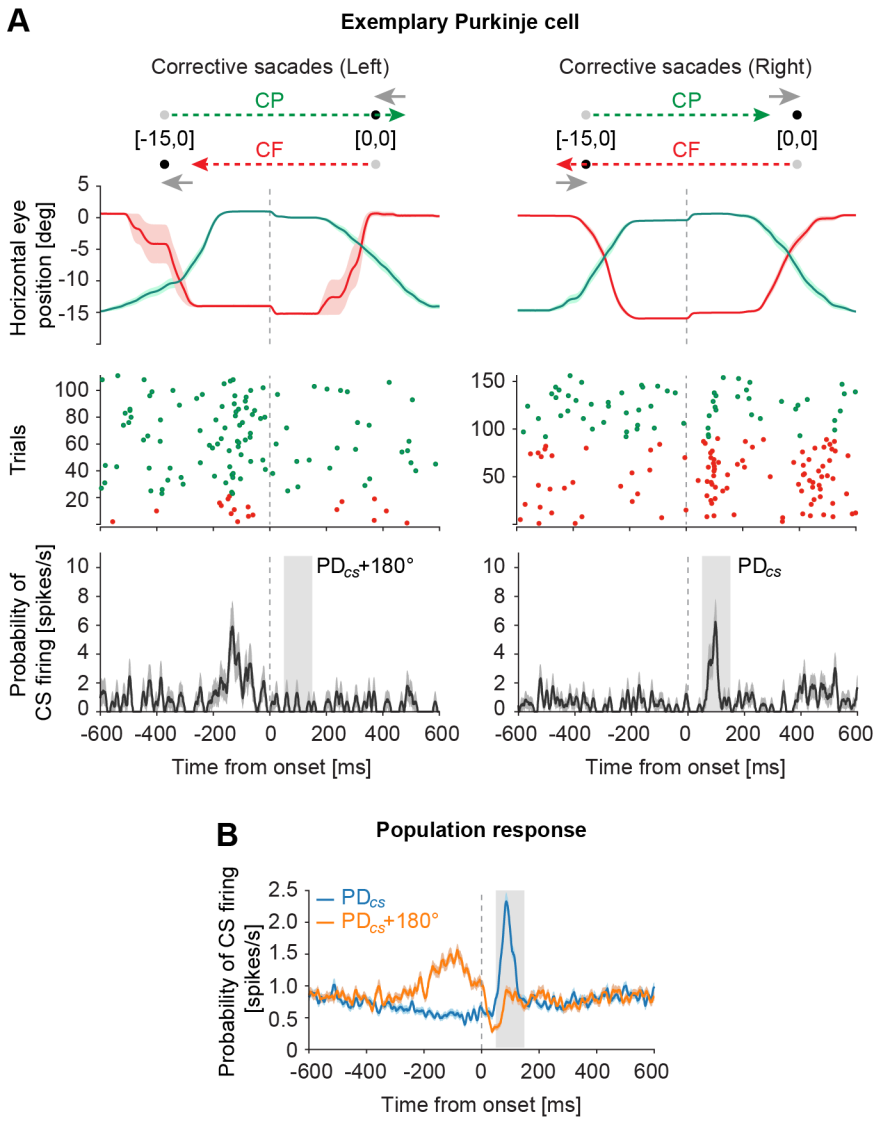

805

806

807 **Figure. 4. A.** CS response of an exemplary PC to corrective saccades in leftward (left panels) and rightward
808 direction (right panels). As illustrated by the schematic diagram on the top, supported by averaged (± s.e.m)
809 saccade trajectories underneath, an experimental session with left CF (red) and right CP (green) saccades
810 resulted in leftward corrective saccades that were made to correct the leftward error arising from CP
811 saccades that "overshot" the fixation dot, and CF saccades that "undershot" the target location (left panel).
812 The start and end position of these corrective saccades were naturally different. Similarly, rightward
813 corrective saccades resulted from overshooting CF and undershooting CP saccades (right panel). As seen

in raster plots (middle panels) and the mean (± s.e.m) firing response of all trials (bottom panel), the peak firing probability of CSs was much larger for rightward (right panel) as compared to the leftward (left panel) corrective saccades during the *'early post-corrective saccadic period'* of 0-100 ms from corrective saccade end (gray shaded region). For each PC, CS's preferred direction for corrective saccades (PD_{cs}) was based on this period. Note that neither different starting positions of corrective saccades, nor the direction of preceding primary saccades influenced the CS firing. **B.** CS population response (mean ± s.e.m; N=151 PCs) sorted by PC's preferred (PD_{cs}) and anti-preferred (PD_{cs}+180°) direction (regardless of left, right, CF and CP) of corrective saccades based on *'early post-corrective saccadic period'* (gray shaded region). Note, that the CS activity during the *'pre-corrective saccadic period'* of approximately -200 to 0 ms from corrective saccade onset was used for determining the CS's preferred direction of errors (PD_{error}).

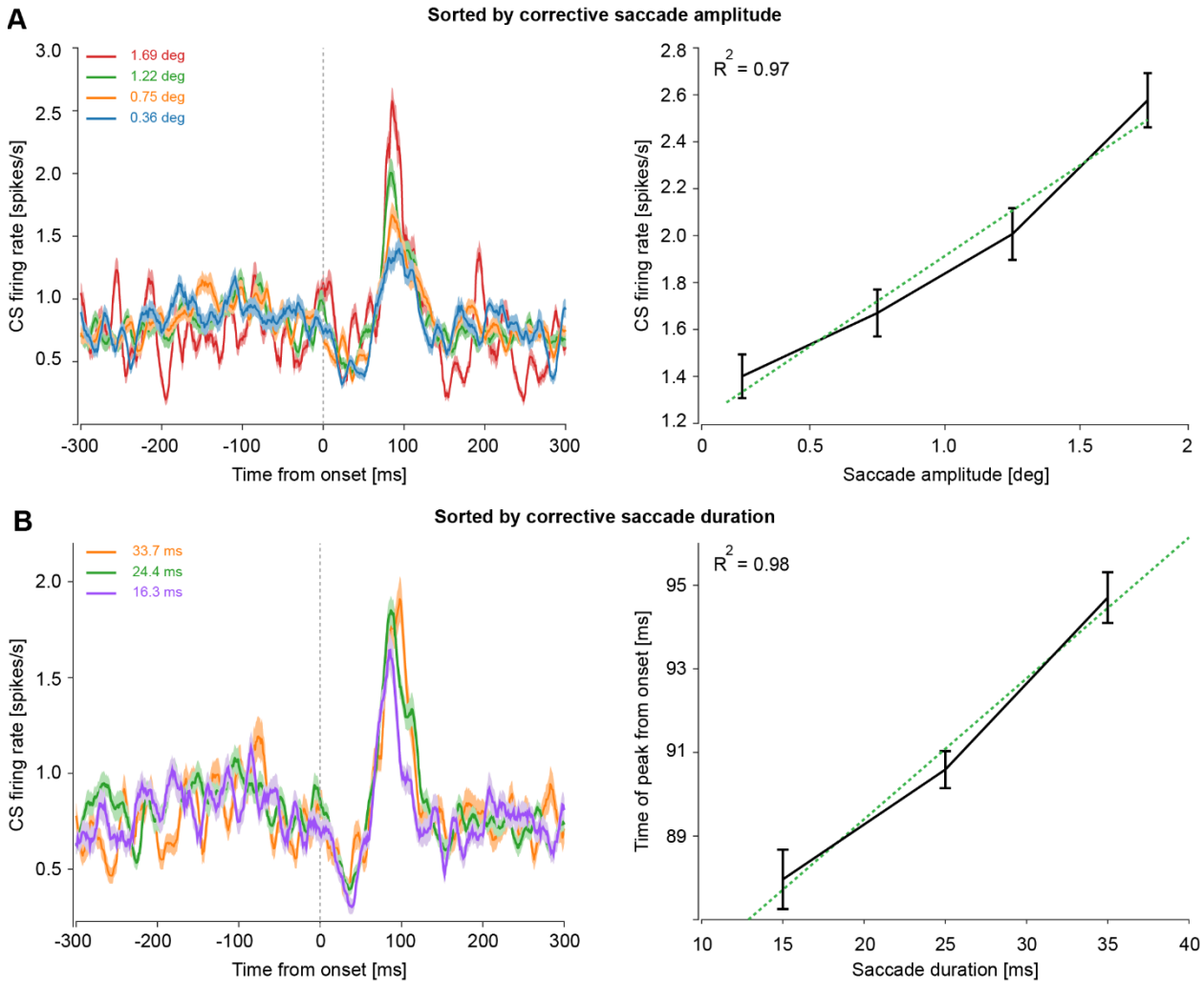

828

829

830 **Figure. 5. A.** CS population response (bootstrapped mean ± confidence intervals) aligned to the
831 onset of all corrective saccades (PD_{cs} and PD_{cs}+180° combined) sorted by different amplitudes
832 (left panel). The relationship between saccade amplitudes and peak firing probability of CSs is
833 shown on the right. **B.** CS response to corrective saccades of different durations (left) and the
834 corresponding relationship between the timing of peak response and saccade duration (right).
835 Green dotted lines represent the regression fits.

836

837

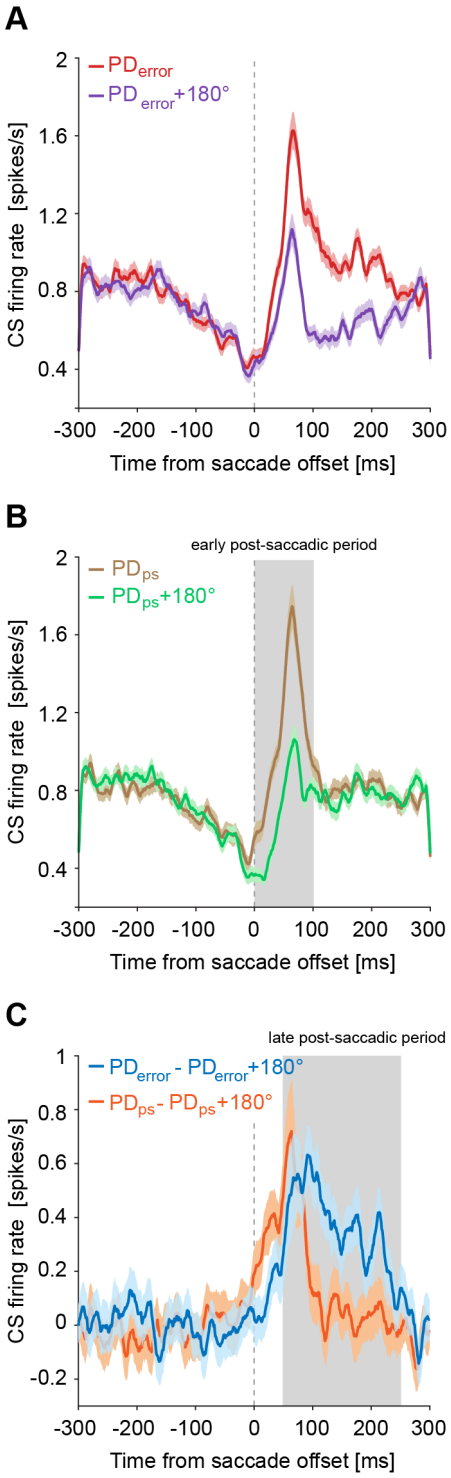

838

839 **Figure. 6. A.** CS population response (mean ± s.e.m) aligned to the offset of primary saccades

840 made in the preferred (PD_{error}, red) and anti-preferred direction (PD_{error}+180°, purple) to errors

841 that resulted from the natural variability in saccade endpoints. PD_{error} was estimated based on the

differences between CS probability during the *'pre-corrective saccadic period'*. **B.** CS population response aligned to the offset of primary saccades made in the preferred (PD_{ps}, brown) and anti-preferred direction (PD_{ps}+180°, green) of primary saccades. Note, the differences in the two responses are confined to the *'early post-saccadic period'* (gray shaded region). **C.** Difference between the CS responses in PD_{error} and PD_{error}+180° (blue), and PD_{ps} and PD_{ps}+180° (orange). The influence of sorting CSs by PD_{error} can be seen as the separation of the curves during the *'late post-saccadic period'* of 50 -250 ms from saccade offset (gray shaded region).

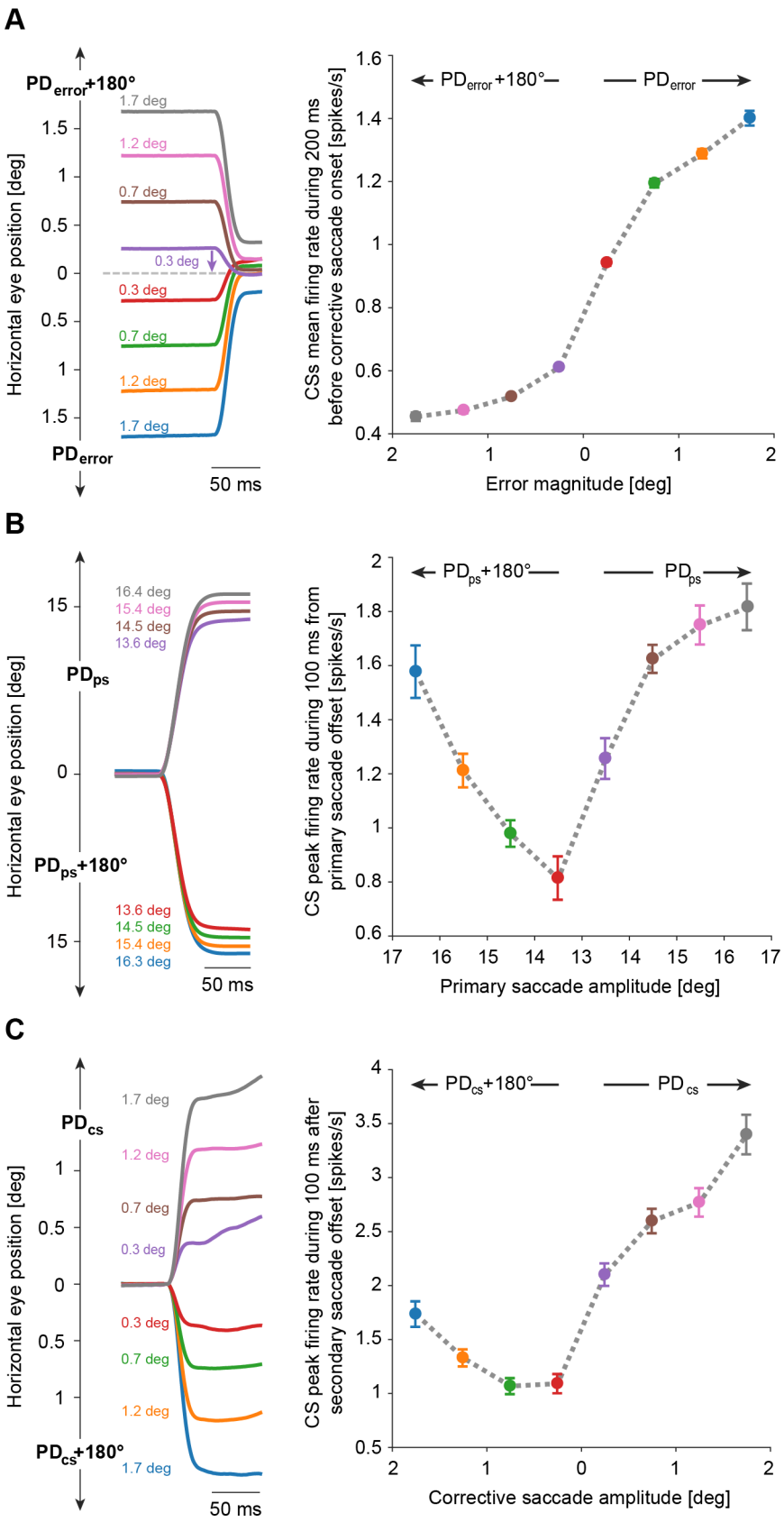
A
PD error+180°
1.7 deg
1.2 deg
0.7 deg
0.3 deg
0.3 deg
0.7 deg
1.2 deg
1.7 deg
PD error
50 ms
Horizontal eye position [deg]
PD error+180°
PD error
CSs mean firing rate during 200 ms before corrective saccade onset [spikes/s]
Error magnitude [deg]
B
16.4 deg
15.4 deg
14.5 deg
13.6 deg
PDps
PDps+180°
13.6 deg
14.5 deg
15.4 deg
16.3 deg
50 ms
Horizontal eye position [deg]
PDps+180°
PDps
CS peak firing rate during 100 ms from primary saccade offset [spikes/s]
Primary saccade amplitude [deg]
C
PDcs
1.7 deg
1.2 deg
0.7 deg
0.3 deg
0.3 deg
0.7 deg
1.2 deg
PDcs+180°
1.7 deg
50 ms
Horizontal eye position [deg]
PDcs+180°
PDcs
CS peak firing rate during 100 ms after secondary saccade offset [spikes/s]
Corrective saccade amplitude [deg]

850

Figure. 7. A. Average eye trajectories showing corrective saccades that were made to correct errors (vector pointing from corrective saccade onset towards target location for CF saccades and fixation dot for CP saccades, both centered at 0 deg) of different sizes in PD_{error} and PD_{error}+180° (left panel) and their respective influence on CS firing probability (bootstrapped mean ± confidence intervals) during the *'pre-corrective saccadic period'* (right). Note how the mean firing probability decreases monotonously from PD_{error} to PD_{error}+180°, despite an increase in the error magnitude in the opposite direction. **B.** Primary saccades of different amplitudes in PD_{ps} and PD_{ps}+180° (left), and their corresponding influence on the peak firing probability (bootstrapped mean ± confidence intervals) during the *'early post-saccadic period'* (right). **C.** Corrective saccades of different amplitudes in PD_{cs} and PD_{cs}+180° (left), and their corresponding influence on the peak firing probability (bootstrapped mean ± confidence intervals) during the *'early post-corrective saccadic period'* (right).

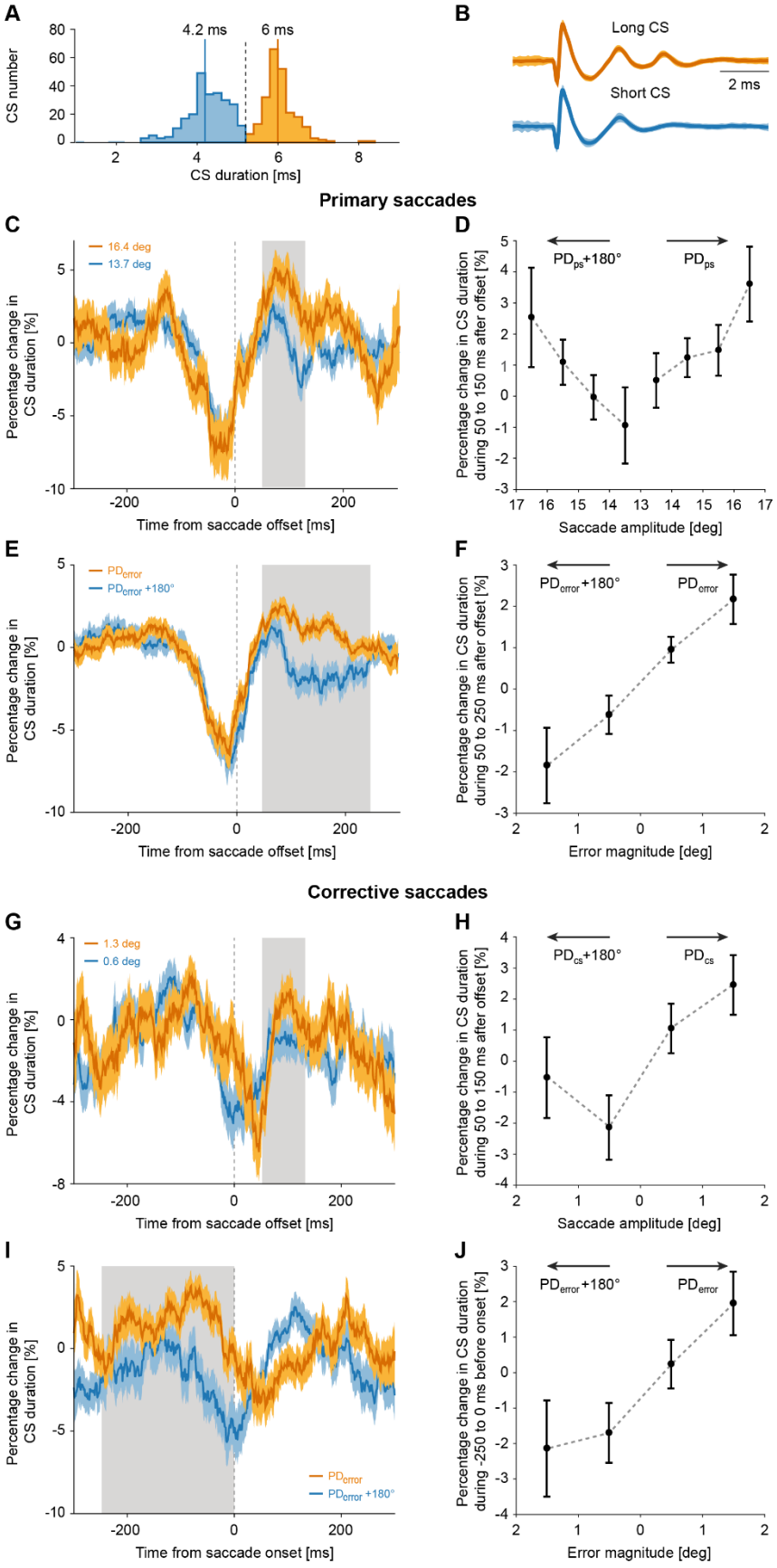
A
4.2 ms
6 ms
CS number
CS duration [ms]
B
Long CS
Short CS
2 ms
Primary saccades
C
16.4 deg
13.7 deg
Percentage change in CS duration [%]
Time from saccade offset [ms]
D
PDps+180°
PDps
Percentage change in CS duration during 50 to 150 ms after offset [%]
Saccade amplitude [deg]
E
PDerror
PDerror +180°
Percentage change in CS duration [%]
Time from saccade offset [ms]
F
PDerror+180°
PDerror
Percentage change in CS duration during 50 to 250 ms after offset [%]
Error magnitude [deg]
Corrective saccades
G
1.3 deg
0.6 deg
Percentage change in CS duration [%]
Time from saccade offset [ms]
H
PDcs+180°
PDcs
Percentage change in CS duration during 50 to 150 ms after offset [%]
Saccade amplitude [deg]
I
PDerror
PDerror +180°
Percentage change in CS duration [%]
Time from saccade onset [ms]
J
PDerror+180°
PDerror
Percentage change in CS duration during -250 to 0 ms before onset [%]
Error magnitude [deg]

864

Figure. 8. A. Histogram showing a bimodal distribution of CS durations in an exemplary PC. For illustration purposes, we separated the distribution into long and short duration CSs by eye. Solid vertical lines represent the median value of short (blue) and long (dark yellow) duration CSs. **B.** Averaged (± s.e.m) waveforms of long and short duration CSs. **C.** Population response (mean ±s.e.m) showing percentage change in CS duration, for large (dark yellow) and small (blue) amplitude saccades. Population response was obtained from running averages of percentage change in CS duration, computed for every 50 ms bins, relative to the mean CS duration of each PC. **D.** Percentage change in CS duration during the 50-150 ms period from primary saccade offset (gray shaded region in C) relative to saccade amplitudes in PD_{ps} and PD_{ps}+180°. **E.** Percentage change in CS duration for primary saccades made in PD_{error} and PD_{error}+180°. **F.** Percentage change in CS duration relative to error magnitudes in PD_{error} and PD_{error}+180° during the 50-250 ms period from saccade offset. **G and H.** Same as C and D, except for corrective saccade. **I.** Percentage change in CS duration for corrective saccades in PD_{error} and PD_{error}+180°. **J.** Percentage change in CS duration relative to error magnitudes in PD_{error} and PD_{error}+180° during the -250-0 ms period from saccade onset. Error bars represent the s.e.m.

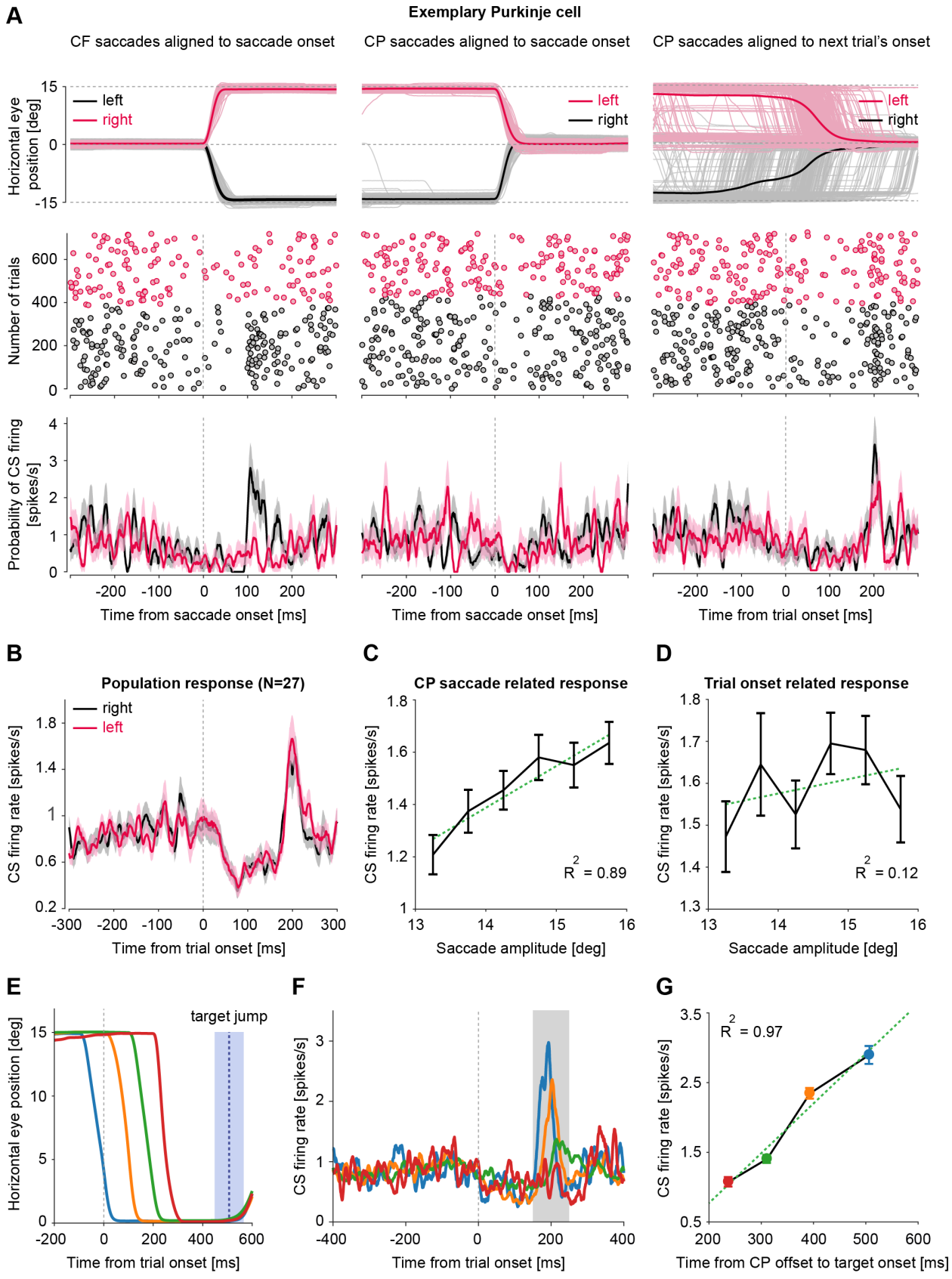
A
Exemplary Purkinje cell
CF saccades aligned to saccade onset
CP saccades aligned to saccade onset
CP saccades aligned to next trial's onset
Horizontal eye position [deg]
left
right
Number of trials
Probability of CS firing [spikes/s]
Time from saccade onset [ms]
Time from trial onset [ms]
B
Population response (N=27)
CS firing rate [spikes/s]
C
CP saccade related response
Saccade amplitude [deg]
R2 = 0.89
D
Trial onset related response
R2 = 0.12
E
target jump
F
G
R2 = 0.97
Time from CP offset to target onset [ms]

882

Figure. 9. A. CS response of an exemplary PC neuron tested in both, left and right, CF (left column) and CP (middle column) directions. Data are aligned to saccade onset. CP saccades and the CS responses aligned to the onset of the next trial are shown in the rightmost column. Despite the variability of saccades, note how precisely CS are accumulated around 200 ms from trial onset. Upper row: individual saccades are shown as thin lines. Thick lines represent average saccade trajectories. Middle row: Raster plot of CSs. Lower row: Mean (± s.e.m) CS response for each condition. **B.** Trial onset evoked CS response (mean ± s.e.m) of all PCs (N=27) tested for saccades in both directions. Red and black traces correspond to the left and right position of the trial onset related fixation dot relative to the eye position at the end of the previous CF saccade, respectively. **C.** Change in peak firing probability of CS population response (N=151), aligned to CP saccade onset, relative to changes in CP saccade amplitudes. **D.** Change in peak firing probability of CS population response (N=151), aligned to next trial's onset, relative to changes in CP saccade amplitude. Note how the same CSs lose information on saccade amplitudes when aligned to trial onset. **E, F and G.** CP saccades (average trajectories) sorted by their time of arrivals at the fixation dot, relative to the time of target jump and corresponding changes in peak firing probability of the CS population response. Mean ± s.e.m of target jump times is represented by the blue vertical dotted line and shaded region in blue, respectively. Error bars represent ± confidence intervals around the bootstrapped mean. Dotted green line represents the linear regression fit.

References

Albus, J.S. (1971). A theory of cerebellar function. Mathematical Biosciences 10, 25-61.

Arnstein, D., Junker, M., Smilgin, A., Dicke, P.W., and Thier, P. (2015). Microsaccade control signals in the cerebellum. Journal of Neuroscience 35, 3403-3411.

Barmack, N.H., and Shojaku, H. (1995). Vestibular and visual climbing fiber signals evoked in the uvula-nodulus of the rabbit cerebellum by natural stimulation. Journal of neurophysiology 74, 2573-2589.

Bazzigaluppi, P., De Gruijl, J.R., Van Der Giessen, R.S., Khosrovani, S., De Zeeuw, C.I., and De Jeu, M.T. (2012). Olivary subthreshold oscillations and burst activity revisited. Frontiers in neural circuits 6, 91.

Bell, C.C., and Grimm, R. (1969). Discharge properties of Purkinje cells recorded on single and double microelectrodes. Journal of Neurophysiology 32, 1044-1055.

Catz, N., Dicke, P.W., and Thier, P. (2005). Cerebellar complex spike firing is suitable to induce as well as to stabilize motor learning. Current Biology 15, 2179-2189.

Dash, S., Catz, N., Dicke, P.W., and Thier, P. (2010). Specific vermal complex spike responses build up during the course of smooth-pursuit adaptation, paralleling the decrease of performance error. Experimental brain research 205, 41-55.

Davie, J.T., Clark, B.A., and Häusser, M. (2008). The origin of the complex spike in cerebellar Purkinje cells. Journal of Neuroscience 28, 7599-7609.

Eccles, J.C. (1967). Circuits in the cerebellar control of movement. Proceedings of the National Academy of Sciences of the United States of America 58, 336.

Frankfurter, A., Weber, J., Royce, G., Strominger, N., and Harting, J. (1976). An autoradiographic analysis of the tecto-olivary projection in primates. Brain research 118, 245-257.

Fu, Q.-G., Mason, C.R., Flament, D., Coltz, J.D., and Ebner, T.J. (1997). Movement kinematics encoded in complex spike discharge of primate cerebellar Purkinje cells. Neuroreport 8, 523-529.

Fujita, Y. (1968). Activity of dendrites of single Purkinje cells and its relationship to so-called inactivation response in rabbit cerebellum. Journal of Neurophysiology 31, 131-141.

Gilbert, P., and Thach, W. (1977). Purkinje cell activity during motor learning. Brain research 128, 309-328.

Graf, W., Simpson, J.I., and Leonard, C.S. (1988). Spatial organization of visual messages of the rabbit's cerebellar flocculus. II. Complex and simple spike responses of Purkinje cells. Journal of Neurophysiology 60, 2091-2121.

Hafed, Z.M., and Krauzlis, R.J. (2010). Microsaccadic suppression of visual bursts in the primate superior colliculus. Journal of Neuroscience 30, 9542-9547.

Harting, J.K. (1977). Descending pathways from the superior colliculus: an autoradiographic analysis in the rhesus monkey (Macaca mulatta). Journal of comparative neurology 173, 583-612.

Herzfeld, D.J., Kojima, Y., Soetedjo, R., and Shadmehr, R. (2015). Encoding of action by the Purkinje cells of the cerebellum. Nature 526, 439-442.

Herzfeld, D.J., Kojima, Y., Soetedjo, R., and Shadmehr, R. (2018). Encoding of error and learning to correct that error by the Purkinje cells of the cerebellum. Nature Neuroscience 21, 736-743.

Huerta, M.F., and Harting, J.K. (1984). Connectional organization of the superior colliculus. Trends in Neurosciences 7, 286-289.

Ito, M. (1972). Neural design of the cerebellar motor control system. Brain research 40, 81-84.

Ju, C., Bosman, L.W., Hoogland, T.M., Velauthapillai, A., Murugesan, P., Warnaar, P., van Genderen, R.M., Negrello, M., and De Zeeuw, C.I. (2019). Neurons of the inferior olive respond to broad classes of sensory input while subject to homeostatic control. J Physiol 597, 2483-2514.

Junker, M., Endres, D., Sun, Z.P., Dicke, P.W., Giese, M., and Thier, P. (2018). Learning from the past: A reverberation of past errors in the cerebellar climbing fiber signal. PLoS biology 16, e2004344.

Kim, J.H., Wang, J., and Ebner, T.J. (1987). Climbing fiber afferent modulation during treadmill locomotion in the cat. Journal of Neurophysiology 57, 787-802.
Kitazawa, S., Kimura, T., and Yin, P.-B. (1998). Cerebellar complex spikes encode both destinations and errors in arm movements. Nature 392, 494-497.
Kobayashi, Y., Kawano, K., Takemura, A., Inoue, Y., Kitama, T., Gomi, H., and Kawato, M. (1998). Temporal firing patterns of Purkinje cells in the cerebellar ventral paraflocculus during ocular following responses in monkeys II. Complex spikes. Journal of neurophysiology 80, 832-848.
Kojima, Y., and Soetedjo, R. (2018). Elimination of the error signal in the superior colliculus impairs saccade motor learning. Proceedings of the National Academy of Sciences 115, E8987-E8995.
Kostadinov, D., Beau, M., Pozo, M.B., and Häusser, M. (2019). Predictive and reactive reward signals conveyed by climbing fiber inputs to cerebellar Purkinje cells. Nature Neuroscience 22, 950-962.
Kyuhou, S.-I., and Matsuzaki, R. (1991). Topographical organization of the tecto-olivo-cerebellar projection in the cat. Neuroscience 41, 227-241.
Larry, N., Yarkoni, M., Lixenberg, A., and Joshua, M. (2019). Cerebellar climbing fibers encode expected reward size. Elife 8, e46870.
Latham, A., and Paul, D. (1971). Spontaneous activity of cerebellar Purkinje cells and their responses to impulses in climbing fibres. J Physiol 213, 135-156.
Leznik, E., and Llinas, R. (2005). Role of gap junctions in synchronized neuronal oscillations in the inferior olive. Journal of neurophysiology 94, 2447-2456.
Llinas, R., Baker, R., and Sotelo, C. (1974). Electrotonic coupling between neurons in cat inferior olive. Journal of neurophysiology 37, 560-571.
Llinás, R., and Sugimori, M. (1980). Electrophysiological properties of in vitro Purkinje cell dendrites in mammalian cerebellar slices. J Physiol 305, 197-213.
Llinás, R., and Volkind, R. (1973). The olivo-cerebellar system: functional properties as revealed by harmaline-induced tremor. Experimental Brain Research 18, 69-87.
Markanday, A., Bellet, J., Bellet, M.E., Inoue, J., Hafed, Z.M., and Thier, P. (2019). Using deep neural networks to detect complex spikes of cerebellar Purkinje Cells. Journal of Neurophysiology.
Marr, D. (1969). A theory of cerebellar cortex. J Physiol 202, 437-470.
Mathy, A., Ho, S.S., Davie, J.T., Duguid, I.C., Clark, B.A., and Häusser, M. (2009). Encoding of oscillations by axonal bursts in inferior olive neurons. Neuron 62, 388-399.
McDevitt, C.J., Ebner, T.J., and Bloedel, J.R. (1982). The changes in Purkinje cell simple spike activity following spontaneous climbing fiber inputs. Brain research 237, 484-491.
Medina, J.F., and Lisberger, S.G. (2008). Links from complex spikes to local plasticity and motor learning in the cerebellum of awake-behaving monkeys. Nature neuroscience 11, 1185-1192.
Ohmae, S., and Medina, J.F. (2015). Climbing fibers encode a temporal-difference prediction error during cerebellar learning in mice. Nature neuroscience 18, 1798-1803.
Oscarsson, O. (1980). Functional organization of olivary projection to the cerebellar anterior lobe. The Inferior Olivary Nucleus, 279-290.
Prsa, M., Dicke, P.W., and Thier, P. (2010). The absence of eye muscle fatigue indicates that the nervous system compensates for non-motor disturbances of oculomotor function. Journal of Neuroscience 30, 15834-15842.
Soetedjo, R., and Fuchs, A.F. (2006). Complex spike activity of purkinje cells in the oculomotor vermis during behavioral adaptation of monkey saccades. Journal of Neuroscience 26, 7741-7755.
Soetedjo, R., Kojima, Y., and Fuchs, A.F. (2008). Complex spike activity in the oculomotor vermis of the cerebellum: a vectorial error signal for saccade motor learning? Journal of neurophysiology 100, 1949-1966.

Streng, M.L., Popa, L.S., and Ebner, T.J. (2017). Climbing fibers control Purkinje cell representations of behavior. Journal of Neuroscience 37, 1997-2009.
Stuart, G., and Häusser, M. (1994). Initiation and spread of sodium action potentials in cerebellar Purkinje cells. Neuron 13, 703-712.
Sugihara, I., and Shinoda, Y. (2004). Molecular, topographic, and functional organization of the cerebellar cortex: a study with combined aldolase C and olivocerebellar labeling. Journal of Neuroscience 24, 8771-8785.
Szentágothai, J., and Rajkovits, K. (1959). Ueber den Ursprung der Kletterfasern des kleinhirns. Zeitschrift für Anatomie Und Entwicklungsgeschichte 121, 130-141.
Thach, W. (1968). Discharge of Purkinje and cerebellar nuclear neurons during rapidly alternating arm movements in the monkey. Journal of neurophysiology 31, 785-797.
Warnaar, P., Couto, J., Negrello, M., Junker, M., Smilgin, A., Ignashchenkova, A., Giugliano, M., Thier, P., and De Schutter, E. (2015). Duration of Purkinje cell complex spikes increases with their firing frequency. Frontiers in cellular neuroscience 9, 122.
Yang, Y., and Lisberger, S.G. (2014). Purkinje-cell plasticity and cerebellar motor learning are graded by complex-spike duration. Nature 510, 529-532.
Yang, Y., and Lisberger, S.G. (2017). Modulation of Complex-Spike duration and probability during cerebellar motor learning in visually guided Smooth-Pursuit eye movements of monkeys. Eneuro 4.

Supplementary figures and figure legends

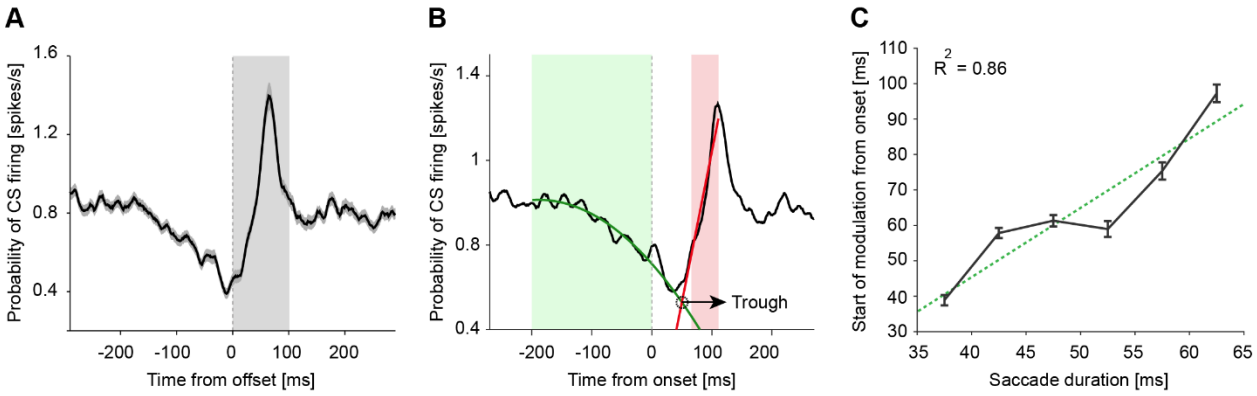

Supplementary Figure 1. A. CS population response aligned to primary saccade offset. Note how the trough that marks the beginning of large modulation (gray shaded region), occurs at the time of saccade end (dotted gray line). **B.** A schematic illustration demonstrating the estimation of modulation onset (trough times). Solid green line represents the second order polynomial fit to data during -200 to 0 ms from saccade onset (light green shaded region). Solid red line represents the linear fit to data, 45 ms from the time of peak firing towards saccade onset. The intersection of these two curves estimates the time of trough. **C.** The dotted green line demonstrates the linear relationship (R^2=0.86, p=0.007) between saccade duration and modulation onset (trough time).

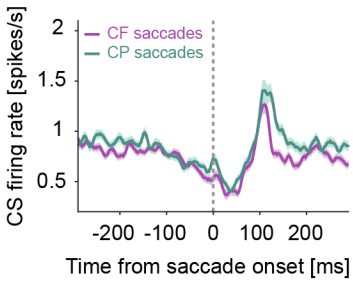

Supplementary Figure 2. CS population response (mean ± s.e.m) aligned to the onset of primary saccades made in the CP (green) and CF direction (purple).

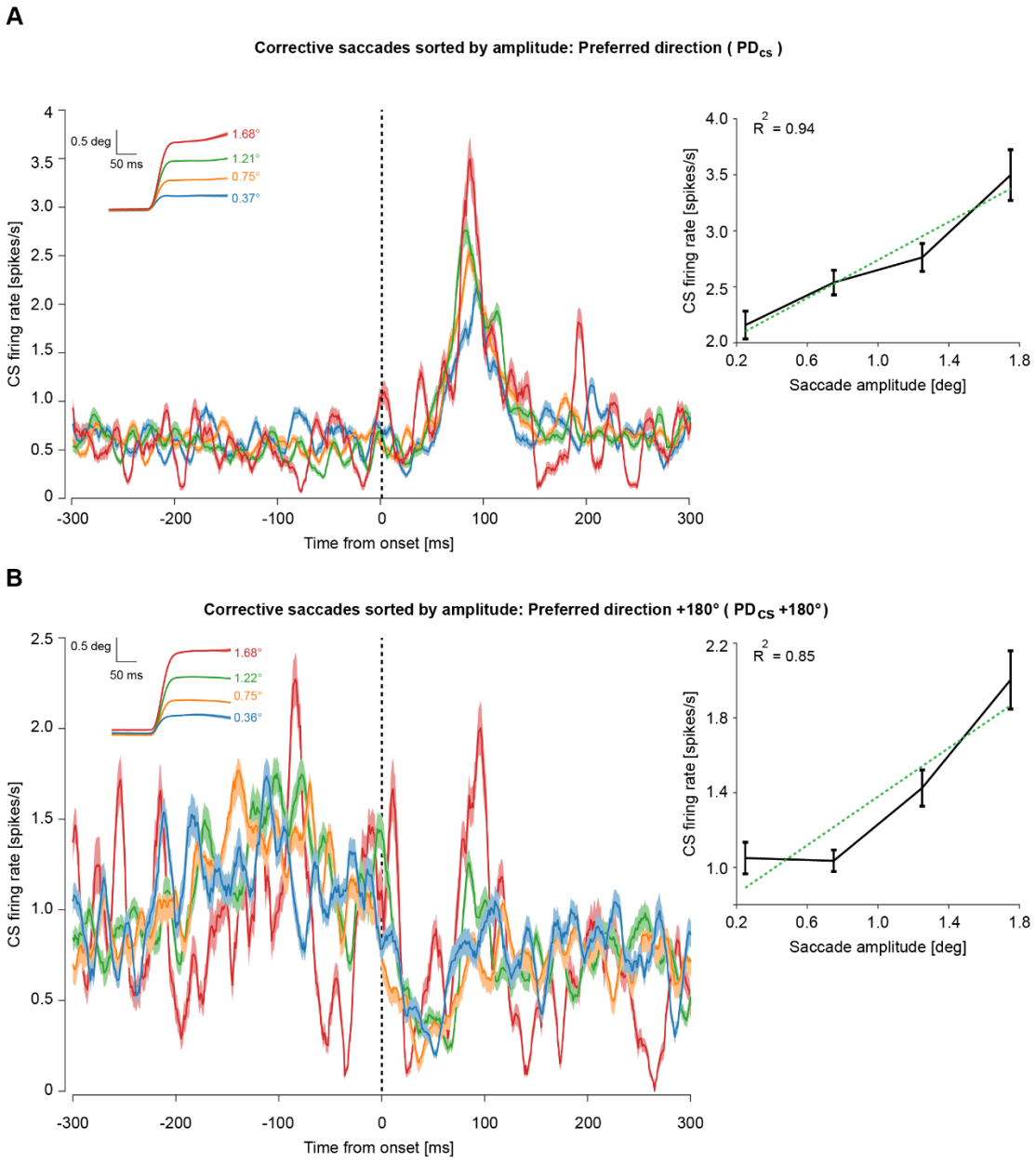

Supplementary Figure 3. A. CS population response aligned to the onset of corrective saccades, sorted by amplitudes (insets; left panel), made in PD_{cs}. The corresponding relationship between CS peak firing probability and corrective saccade amplitude is shown on the right. Linear regression fit is given by the dotted green line (R^2=0.94, p=0.02). **B.** Same as A, except corrective saccades were made in PD_{cs}+180° (R^2=0.85, p=0.07). Error bars represent the bootstrapped mean ± confidence intervals.

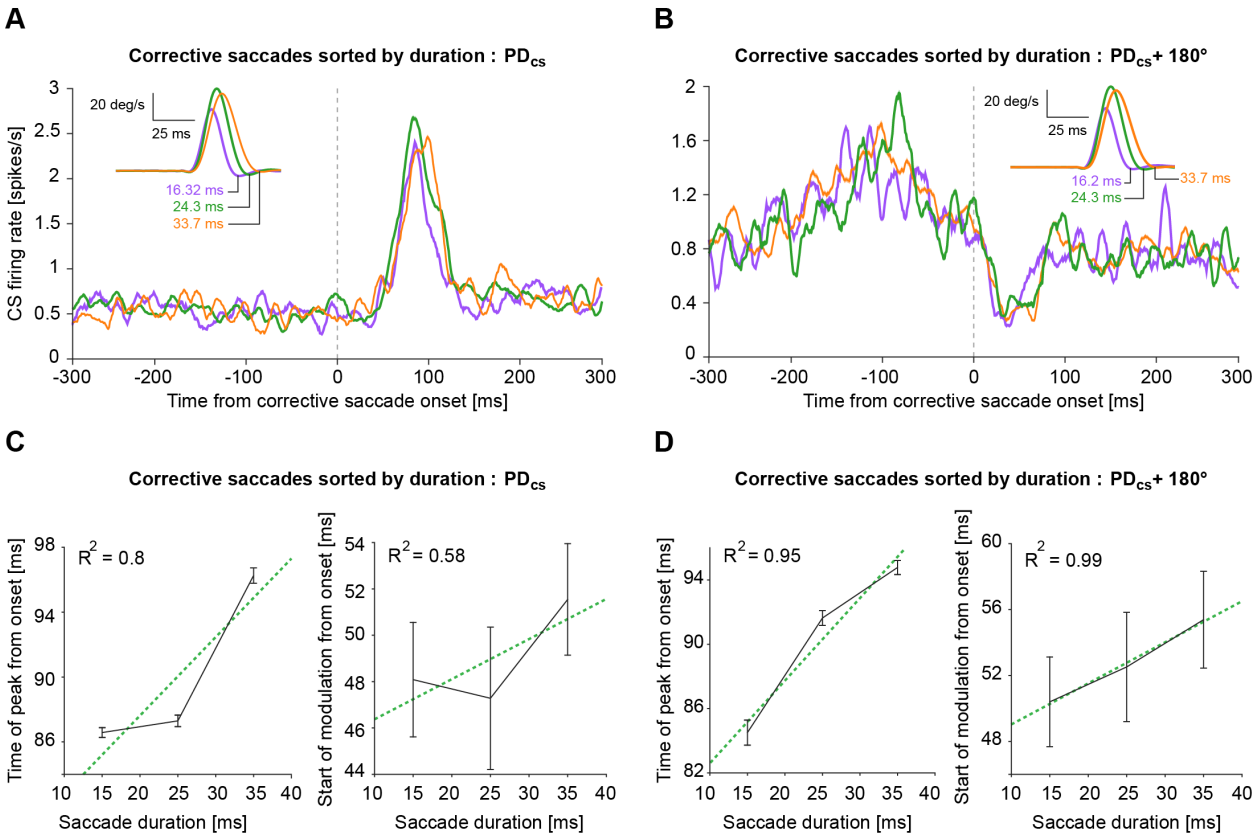

Supplementary Figure 4. A and B. CS population response aligned to the onset of corrective saccades, sorted by durations (insets), made in PD_{cs} and PD_{cs}+180°. **C and D.** The corresponding relationship between the peak timing of the CS response and corrective saccade duration (left panels, PD_{cs}: R^2=0.8, p=0.29; PD_{cs}+180°: R^2=0.95, p=0.14) and modulation onset and saccade duration (right panels, PD_{cs}: R^2=0.58, p=0.45; PD_{cs}+180°: R^2=0.99, p=0.06). Dotted green lines represents the fits derived from simple linear regressions. Error bars represent the bootstrapped mean ± confidence intervals.

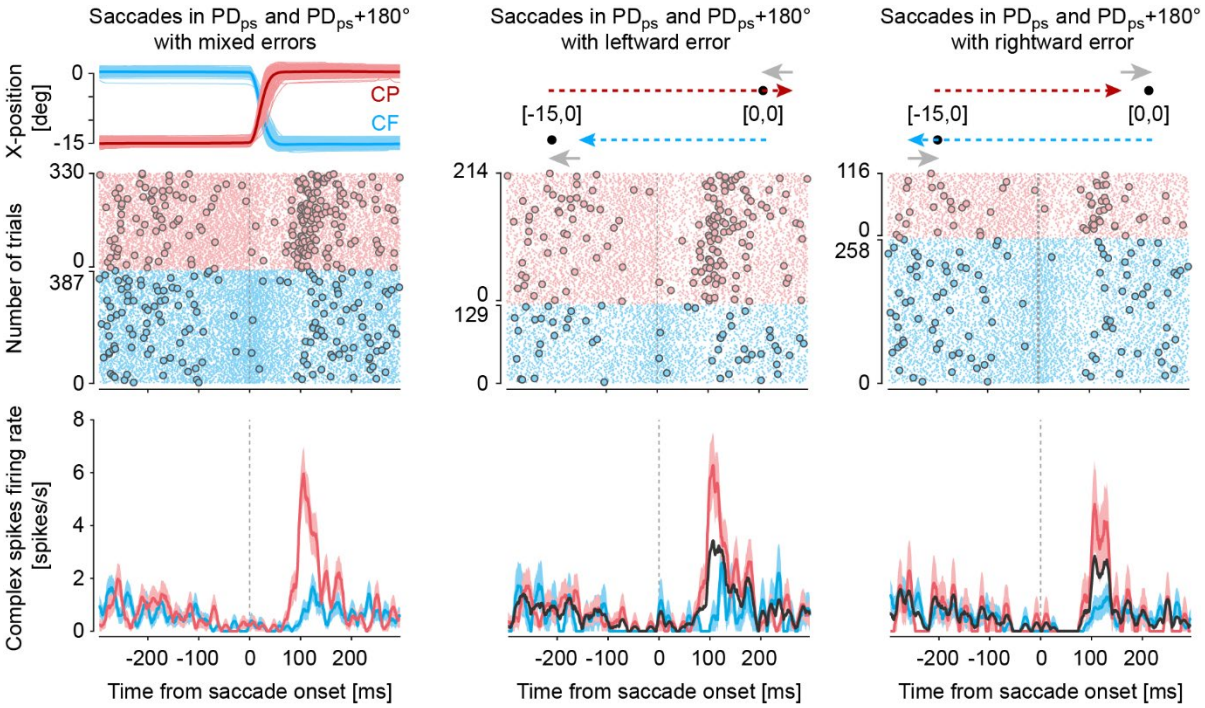

Supplementary Figure 5. CS response of an exemplary PC to primary saccades in CF (PD_{ps}+180°, in blue) and CP (PD_{ps}, in red) saccades are shown in the left column. When saccades are sorted according to the direction of errors, as illustrated by the schematic diagram on the top, the overall response of saccades with leftward error (solid gray trace, lower middle panel) looks very similar to the response for all saccades with rightward errors (solid gray trace, lower right panel). Middle row: Raster plots showing CS response to CF (blue circles) and CP (red circles) saccades. Bottom row: Average (± s.e.m) firing response of all trials in each condition. Data are aligned to saccade onset.

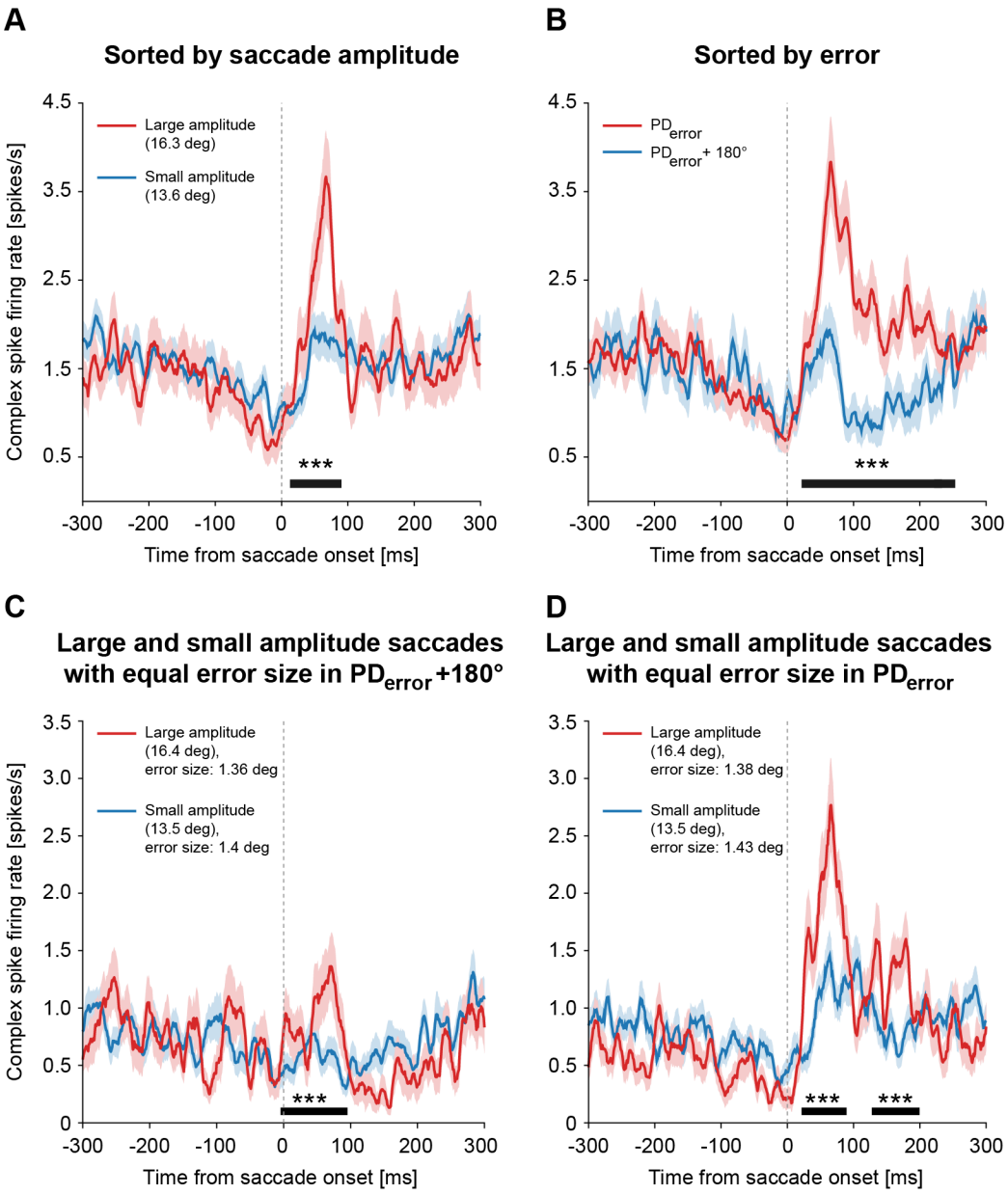

Supplementary Figure 6. Comparison of CS population responses (mean ± s.e.m) sorted by saccade amplitudes (A, large amplitude: red, small amplitude: blue) and preferred directions of error (B, PD_{error}: red, PD_{error}+180°: blue). C and D shows the comparison of all large and small amplitude saccades resulting in equally sized errors in preferred and anti-preferred error

directions, respectively. Black horizontal bars denote the period for which a significant difference ($p<0.001$; marked by asterisks) between the CS responses was observed.

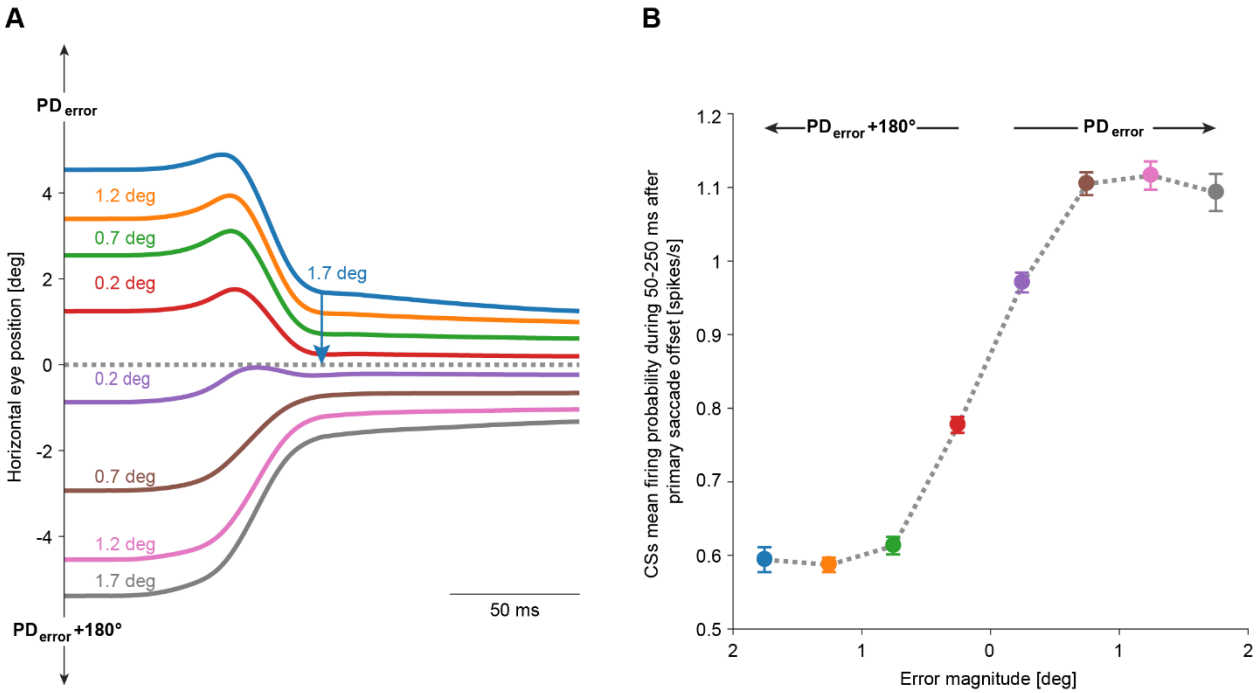

Supplementary Figure 7. A. Average eye trajectories showing different magnitudes of errors resulting from variability in primary saccade ends relative to target location (CF saccades) and fixation dot (CP saccades), both centered at 0 deg (horizontal dashed line), in PD_{error} and PD_{error}+180° (left panel). **B.** Influence of error magnitudes in PD_{error} and PD_{error}+180° on CS mean firing probability (bootstrapped mean ± confidence intervals) during the *'late post-saccadic period'* of 50-250 ms from saccade offset.

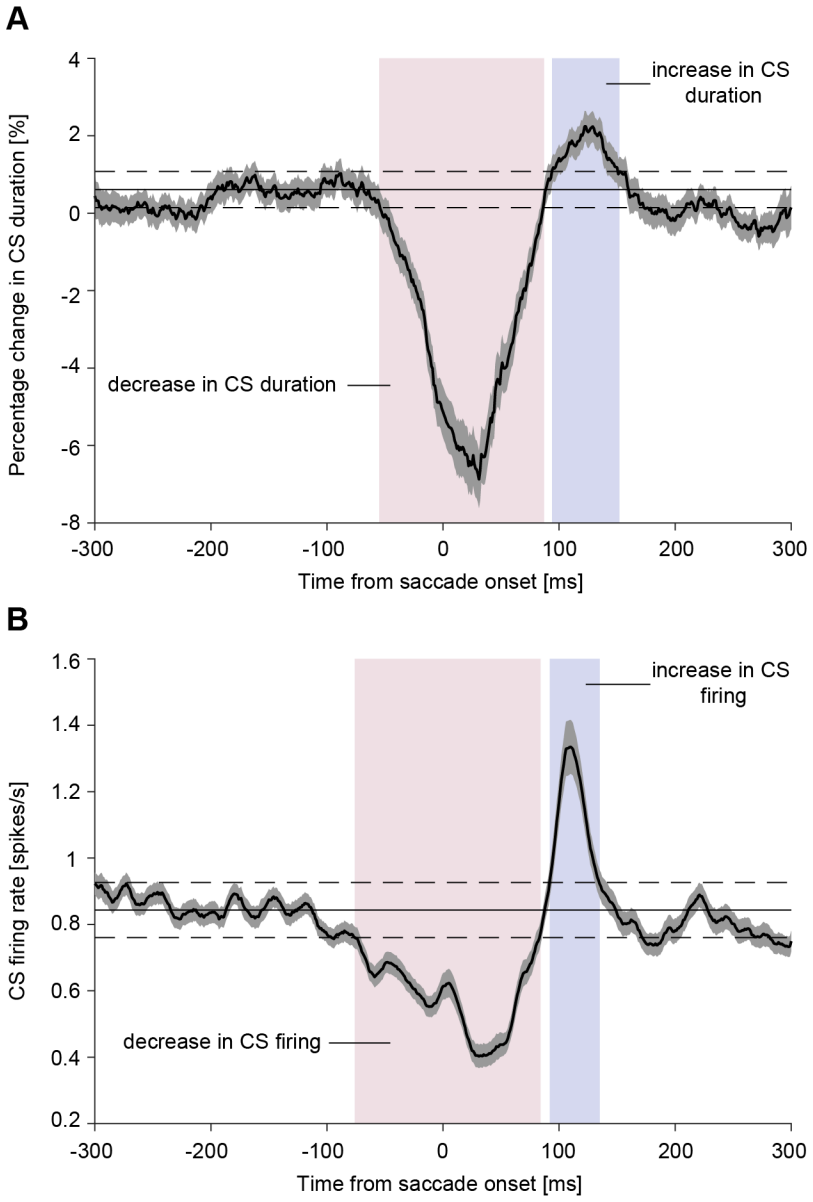

Supplementary Figure 8. A. Population percentage change in CS duration (mean ± s.e.m) aligned to primary saccade onset. The period of decrease (-55 to 87 ms from saccade onset, shaded region in light red) and increase (94 to 152 ms from saccade onset, light blue shaded region) in CS duration were estimated whenever the response crossed the threshold. **B.** Population firing response of CSs (mean ± s.e.m) aligned to primary saccade onset. The period of decrease (-76 to 84 ms from saccade onset, shaded region in light red) and increase (92 to 134

ms from saccade onset, light blue shaded region) in CS firing probability were estimated whenever the response crossed the threshold. Solid horizontal lines in A and B represent the mean values during the baseline period (-200 to -100 ms from saccade onset) and horizontal dashed lines represent the threshold (3×s.d around the mean). Note how the regions of decrease and increase in CS duration and firing probability, respectively, largely overlap.

APPENDIX 4

ANNUAL REVIEWS

Annual Review of Vision Science

Role of the Vermal Cerebellum in Visually Guided Eye Movements and Visual Motion Perception

Peter Thier and Akshay Markanday

Department of Cognitive Neurology, Hertie Institute for Clinical Brain Research, University of Tübingen, 72076 Tübingen, Germany; email: thier@uni-tuebingen.de

Annu. Rev. Vis. Sci. 2019. 5:247–68

First published as a Review in Advance on July 12, 2019

The *Annual Review of Vision Science* is online at vision.annualreviews.org

https://doi.org/10.1146/annurev-vision-091718-015000

Keywords

oculomotor vermis, simple spike, complex spike, saccade, smooth-pursuit, visual motion perception

Abstract

The cerebellar cortex is a crystal-like structure consisting of an almost endless repetition of a canonical microcircuit that applies the same computational principle to different inputs. The output of this transformation is broadcasted to extracerebellar structures by way of the deep cerebellar nuclei. Visually guided eye movements are accommodated by different parts of the cerebellum. This review primarily discusses the role of the oculomotor part of the vermal cerebellum [the oculomotor vermis (OMV)] in the control of visually guided saccades and smooth-pursuit eye movements. Both types of eye movements require the mapping of retinal information onto motor vectors, a transformation that is optimized by the OMV, considering information on past performance. Unlike the role of the OMV in the guidance of eye movements, the contribution of the adjoining vermal cortex to visual motion perception is nonmotor and involves a cerebellar influence on information processing in the cerebral cortex.

1. ARCHITECTURE OF THE CEREBELLUM

The cerebellum, Latin for "little brain," is small only if we regard its volume. It is actually quite large if we consider the number of its neurons, which account for 85% of all neurons in the human brain (Herculano-Houzel 2009). However, admittedly, most of them—the so-called granule cells—are small, supporting scanty dendrites. Therefore, individually they most probably make only relatively modest computational contributions. A distinct difference between the cerebellum and the other cortical structure of the mammalian brain, the cerebrum, is the lack of association fibers connecting different regions of the cortical surface. Hence, cerebellar computations are much more local, based on a canonical circuit that transforms input offered by two types of afferents, mossy fibers (MFs) and climbing fibers (CFs), into output provided by the axons of the cerebellar Purkinje cells (PCs) that contact brain stem target neurons, assembled in the deep cerebellar nuclei (DCNs). Because the canonical circuit is the same throughout the cerebellum, we may safely assume that the transformations this canonical circuit supports are also the same independent of the part of the cerebellum considered. Distinct functions arise as a consequence of a standard transformation applied to different sources of input and the results are broadcasted to distinct target structures. The central element in this canonical circuit is the PC. Its large and planar dendritic tree samples input from myriad parallel fibers (PFs) (up to 200,000 in rats) (Napper & Harvey 1988), the axons of granule cells that run perpendicular to the PC's dendritic tree (**Figure 1*a*,*b***). Granule cells are contacted by MFs, originating from numerous precerebellar nuclei. The most important nuclei are the pontine nuclei (PNs), the major cerebellar gateway for information from the cerebral cortex (Thier & Möck 2006). Other precerebellar nuclei relevant for oculomotor regions of the cerebellum are the nucleus reticularis tegmenti pontis, a dorsal extension of the dorsomedial PNs, and the paramedian pontine reticular formation and other brain stem structures for the immediate premotor control of eye movements (Büttner & Büttner-Ennever 2006). The second type of afferent, the CF, is emitted by neurons in the inferior olive (IO) in the lower brain stem that receives eye movement–related input from the accessory optic system and the superior colliculus, with the latter also serving the MF system by way of the PNs and the nucleus reticularis tegmenti pontis. An individual PC receives input from one CF that wraps around its soma and proximal dendrites, making approximately 300 to 500 synaptic contacts (Hillman 1969). The circuit is completed by various types of interneurons, such as Golgi cells, acting at the level of the mossy fiber–granule cell stage or by stellate and basket cells mediating interactions between PCs (**Figure 1*a***). Studying how this canonical circuit controls eye movements and other forms of sensory guided behavior is substantially facilitated by the fact that many of its elements have distinct electrophysiological signatures. The most intriguing example is arguably the complex spike (CS) (Thach 1968) generated by PCs as a consequence of a single CF spike impinging on a PC, causing a massive calcium influx via voltage-gated calcium channels and, consecutively, a long-lasting depolarization (see **Figure 1*b***). CSs that appear polyphasic in extracellular recordings are fired at perplexingly low frequencies of around 1 per second and less and can last many milliseconds. They are complemented by PC simple spikes (SSs) (Eccles et al. 1966), which are ordinary sodium-potassium spikes, fired at conventional rates that reflect the integrated influence of PFs and interneurons on PCs. The few action potentials contributed by CSs at the PC axon terminal are indistinguishable from those by SSs, which heavily outnumber CSs (Monsivais et al. 2005). Hence, the SS carries information that influences extracerebellar circuitry controlling motor functions, whereas the CS plays a role at the level of the PC, where it modulates the cell's response to coincident PF input (Albus 1971, Ito 1972).

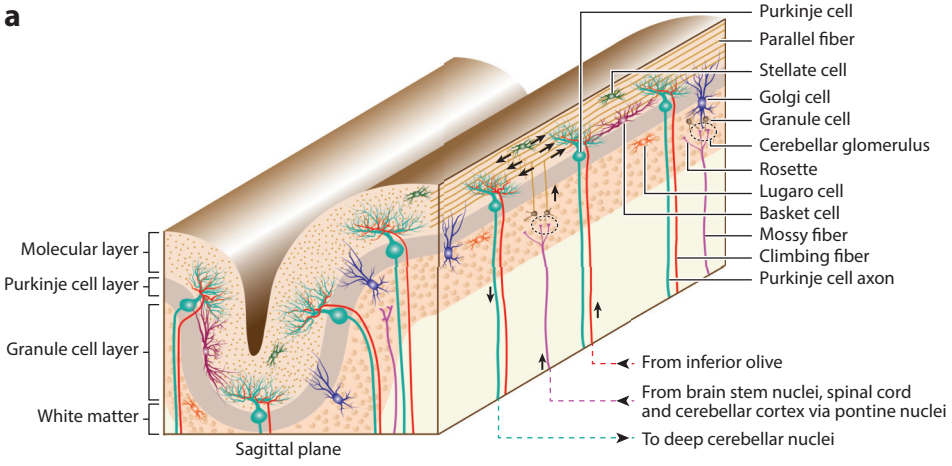

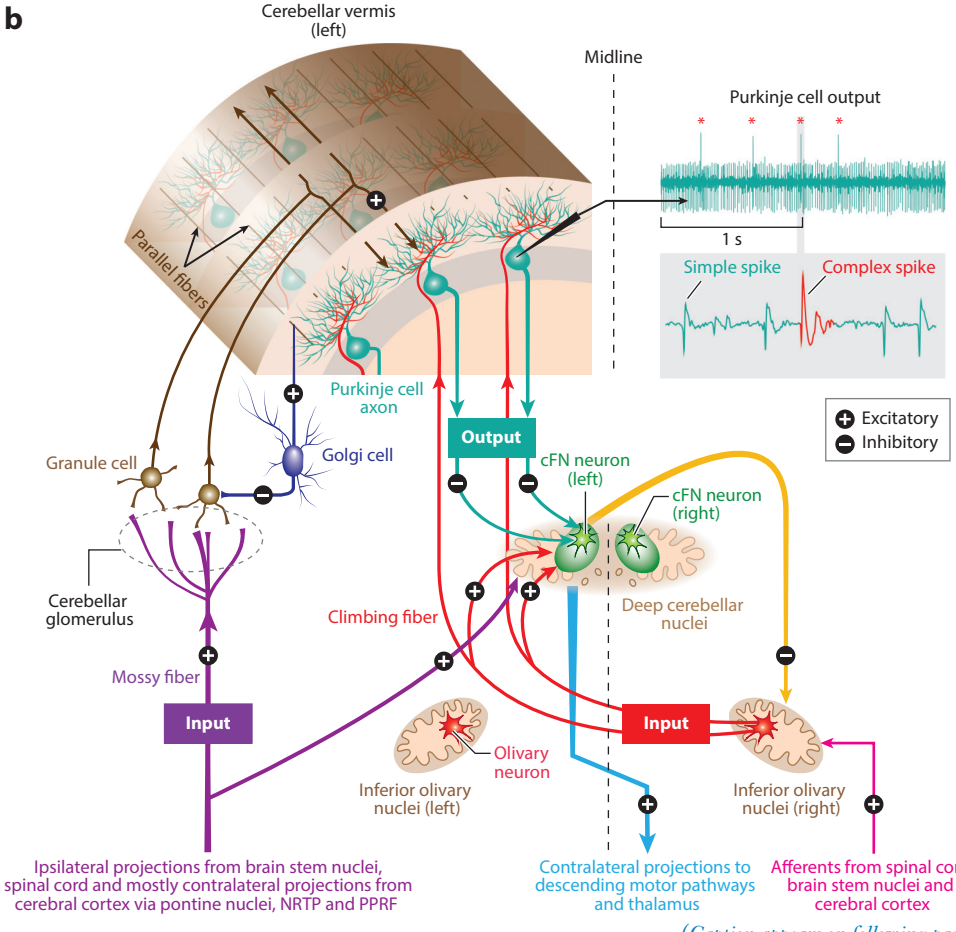

(*Caption appears on following page*)

Figure 1 (*Figure appears on preceding page*)

Cerebellar cortex and the canonical cerebellar circuitry. (*a*) The architecture of the cerebellar cortex and its key structural elements. The cerebellar cortex is anisotropic with three layers and two distinct axes, the left-right axis defined by parallel fibers aligned with the coronal axis (corresponding to the lateral wall of the tissue block shown) and the flat dendritic trees of Purkinje cells, which are perpendicular to the parallel fiber axis and aligned with the sagittal plane. (*b*) The canonical cerebellar circuit integrating afferent information provided by the two types of afferents, mossy fibers and climbing fibers, and impacting target neurons in the deep cerebellar nuclei by way of the axons of Purkinje cells. The inset at the upper right depicts an exemplary Purkinje cell spike train consisting of simple spikes, which are conventional sodium-potassium action potentials reflecting the collective influence of mossy fiber/parallel fiber activity and various interneurons, and the much rarer and longer-lasting complex spikes, which are released by climbing fiber input from the inferior olive. Abbreviations: cFN, caudal fastigial nucleus; NRTP, nucleus reticularis tegmenti pontis; PPRF, paramedian pontine reticular formation.

2. OCULOMOTOR REGIONS OF THE CEREBELLAR CORTEX

Several distinct oculomotor regions are distinguishable in the cerebellar cortex (**Figure 2**). The first region corresponds to the archicerebellum, or vestibulocerebellum, the oldest part of the cerebellum in evolutionary terms. It comprises the flocculus, including the adjoining ventral paraflocculus, the uvula, and the nodulus. It uses information on self-motion, derived from the vestibular nuclei and the accessory optic system, to optimize image-stabilizing oculomotor reflexes (see Dash & Thier 2014 for a review). Surprisingly, in primates this phylogenetically ancient part of the cerebellum is not confined to this function. Rather, the flocculus and ventral paraflocculus also contribute to a much more recent phylogenetic achievement, smooth-pursuit eye movements (SPEMs). SPEMs allow the observer to stabilize the image of an object of interest within the confines of the fovea, serving high-acuity fovea (Stone & Lisberger 1990), inevitably entailing self-induced retinal slip of the background image. However, unlike retinal slip of the background image elicited by head or body movements, retinal slip elicited by SPEMs should not evoke an opposing (optokinetic) eye movement reflex for stabilizing the background, because it would annihilate the desired tracking movement. Likewise, vestibularly driven eye movements need to be suppressed in case the observer moves relative to the world while fixating on a world stationary object, causing a smooth-pursuit-like eye movement relative to the head. Hence, the integration of SPEM-related information may reflect the need to dynamically adjust ocular reflexes required by the emergence of a fovea.

The second major region is the oculomotor vermis (OMV), which comprises the caudal part of lobule VI (VIc) and the rostral part of neighboring lobule VII (VIIA), key structures in the control of visually guided, goal-directed eye movements. The dorsal paraflocculus, although it adjoins the flocculus/ventral paraflocculus, is not part of the vestibulocerebellum. Like the OMV, it is part of the phylogenetically more recent neocerebellum or pontocerebellum that is characterized by a dominance of input from the cerebral cortex, mediated by the PNs. Also, the dorsal paraflocculus seems to be involved in the control of goal-directed eye movements, in particular saccades (Noda & Mikami 1986), although its role is less clear compared with that of the OMV. A final cerebellar area involved in eye movements and eye movement–related vision is the hemispheric oculomotor region (HOR). It is a relatively large region that adjoins the OMV and centers on the hemispheric parts of the simple lobule. The caudal end of the HOR, whose exact boundaries have not been determined, may abut the dorsal paraflocculus. The HOR has been implicated in the control of both saccades and SPEMs (see Thier 2011 for further details). Unfortunately, the sparsity of relevant data has thus far precluded an identification of a specific contribution to these goal-directed eye movements. We come back briefly to the HOR in Section 10, when discussing the role of the cerebellum in visual motion perception.

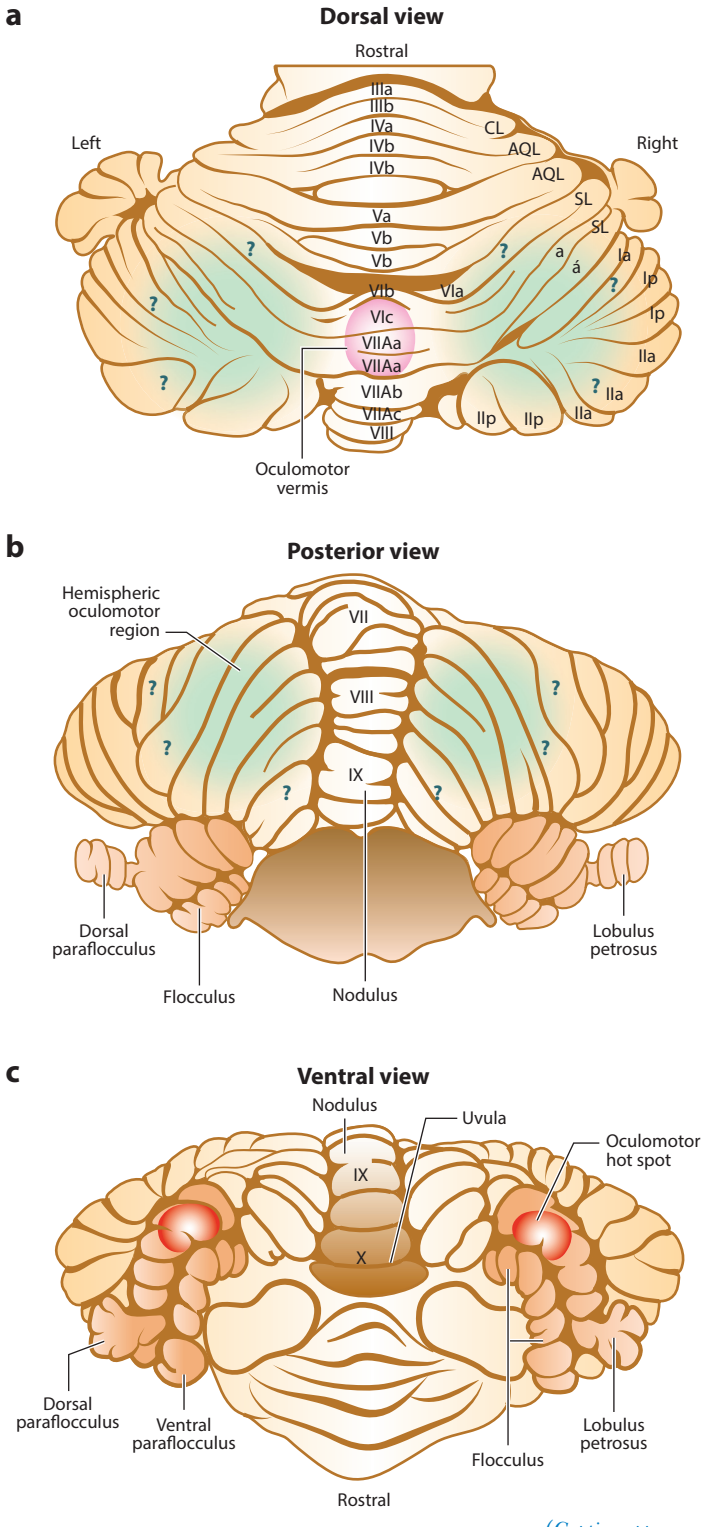

(*Caption appears on following page*)

Figure 2 (*Figure appears on preceding page*)

Three views of the cerebellum illustrating the topography of the various oculomotor representations of eye movements. (*a*) In the dorsal view, the anterior quadrangular lobule (AQL), the central lobule (CL), and their associated lobules (III, IV, and V) form the anterior surface. (*b*) Posteriorly, the entire dorsal surface of the cerebellar hemisphere is occupied by the ansiform lobule (crus Ia, Ip, IIa, IIp). Note how the four hemispheric folia of the simple lobule (SL) are connected specifically to the folia of lobules VI and VIIAa. The question marks delineating the hemispheric oculomotor region (HVII; see dorsal and posterior views) centering on hemispheric lobules VII emphasize the uncertainties regarding its exact topography. Note that BOLD activity found in work on the perception of eye movement–related visual motion probably coincided with parts of HVII. (*c*) The oculomotor hot spot, enriched with mostly saccade-related activity, in the dorsal paraflocculus emphasized by Noda & Mikami (1986) is highlighted red in the ventral view of the cerebellum. Figure based on Thier (2011) and Madigan & Carpenter (1971). Abbreviation: BOLD, blood-oxygen-level-dependent.

3. SIGNIFICANCE OF THE OCULOMOTOR VERMIS FOR OCULOMOTOR LEARNING

3.1. Kinematic Adjustments During Short-Term Saccadic Adaptation

A contribution of the posterior vermis and neighboring parts of the hemispheres to visually guided eye movements was first suggested by the consequences of surgical lesions in monkeys, characterized by the fact that visually guided saccades became dysmetric (i.e., lacking the proper amplitude) (Aschoff & Cohen 1971, Ritchie 1976). As reported later, similar disturbances are exhibited by patients with pathology in this region (e.g., Bötzel et al. 1993). Further support for a role in saccades came from Ron & Robinson (1973), who demonstrated that electrical stimulation of the posterior vermis and neighboring parts of the hemispheres evoked saccades. Without doubt, this early work overestimated the size of the saccade-related region in the posterior cerebellum, a consequence of the large size of the lesions, arguably also encroaching on saccade-related parts of the DCNs, and the comparatively high currents used in the early stimulation work. As shown later by Noda and coworkers (Fujikado & Noda 1987, Noda & Fujikado 1987b, Noda et al. 1990, Yamada & Noda 1987), a small saccade-related core zone confined to adjoining parts of lobules VI and VII (VIc, VIIA)—the OMV—can be distinguished by its exquisite sensitivity to electrical microstimulation. In the OMV, currents of less than 10 μA are sufficient to evoke saccades. The stimulation effect is a consequence of activating PC axons originating from the OMV rather than of antidromically activating saccade-related brain stem nuclei by way of their MF projections to the OMV (Fujikado & Noda 1987; Noda & Fujikado 1987a,b). The OMV as defined by microstimulation is congruent with a zone characterized by clear saccade-related background activity in the granule cell layer and a high density of PCs and other types of neurons showing saccade-related activity.

Lesions confined to the OMV cause hypometric saccades (i.e., visually guided saccades that undershoot the target) (Barash et al. 1999; Ignashchenkova et al. 2009; Ohki et al. 2009; Takagi et al. 1998, 2000; Vahedi et al. 1995). A few weeks to months after the lesion the experimental animals exhibit complete recovery from hypometria (Barash et al. 1999). What persists for at least a year is an increased variability of saccade end points and an inability to modify saccade metrics on a short timescale [short-term saccadic adaptation (STSA)]. For instance, in experiments that require subjects to adjust the amplitude of visually guided saccades, the target guiding the saccade is displaced in a consistent manner to a new location during the saccade. Because the eyes will land at the original location of the target, the addition of a second, corrective saccade is needed to acquire the target. Since the intrasaccadic target steps and the resulting performance errors are consistent, the saccadic system adapts the amplitude of the primary saccade to bring the eyes closer to the final position of the target, thereby reducing the need for corrective secondary saccades (McLaughlin 1967). In an analogous manner, changing the angular coordinate of the target during

the primary saccade prompts learned changes of the direction of this saccade (Chen-Harris et al. 2008, Noto et al. 1999, Xu-Wilson et al. 2009a).

3.2. Kinematic Adjustments During Smooth-Pursuit Adaptation

Microstimulation and lesion experiments have clearly established that the OMV also contributes to SPEMs. Whether microstimulation of the OMV gives rise to SPEMs or saccades seems to be determined by the particulars of the oculomotor protocol and the choice of the stimulation parameters (Krauzlis & Miles 1998) and not by the site of microstimulation. Lesions of the OMV not only compromise visually guided saccades but also impair SPEMs, in particular the initial, open-loop response phase of the SPEMs (Dash & Thier 2013, Takagi et al. 2000). In this initial phase, the eyes move under the guidance of a target whose image slip on the retina is not yet reduced by the eye movement that is delayed relative to the onset of the target movement. Following a lesion, eye velocity in this open-loop period is too low to catch up with the target and it can no longer be adapted to expected changes in target velocity [smooth-pursuit adaptation (SPA)]. SPA is demonstrated by asking monkeys or humans to pursue a moving target whose position changes in a ramp-like fashion, and velocity changes in a step-wise manner, at the time the open-loop phase ends. If the velocity step is consistent from trial to trial and therefore predictable, healthy subjects will adjust their open-loop SPEM velocity to ensure that the eyes will move at the velocity corresponding to the target velocity after the velocity step (Fukushima et al. 1996, Kahlon & Lisberger 1996). As a consequence of the lesion, this ability to act preemptively is compromised, for at least three months after the lesion (Takagi et al. 2000, Zee et al. 1981).

SPA and STSA can be understood as examples of short-term adjustments that modify the parameters that describe how specific sensory information is mapped onto a motor vector. For instance, in the case of saccades this is a vector defining the location of the target in a retinal frame of reference, determining the amplitude and direction of the foveating saccade. Only when the optimal mapping parameters are used will the saccade shift the target image into the fovea. Likewise, optimally mapping the target acceleration and velocity onto the eye movement is the precondition for keeping the image of a moving target within the fovea.

3.3. The Vestibulo-Ocular Reflex as Another Example of Parametric Adjustment

Another well-known example of parametric adjustment is the adaptation of the vestibulo-ocular reflex, which is dependent on the flocculus. This reflex uses vestibular information about head movements to evoke opposing eye movements (for a review, see Dash & Thier 2014, Lisberger & Fuchs 1974). Choosing the optimal mapping between the two ensures that the retinal image of the visual world remains still despite the head movement. In all three cases parametric adjustment secures optimal vision, helping deploy the fovea in the case of saccades and SPEMs and stabilizing the visual background in the case of the vestibulo-ocular reflex. Selecting the right parameters is essential, as the feedback on the visual consequences of the eye movement would be too late to tune the ongoing movement. Because of the long visual latencies, the role of visual feedback must be confined to shaping the parameters for the future manifestations of the movements.

3.4. Parametric Adjustments for Reducing Trial-by-Trial Errors

In the standard adaptation paradigms described above, dozens to hundreds of repetitions of consistent target displacements are typically deployed to reveal clear and consistent adaptation of saccades and SPEMs. However, on closer scrutiny it appears that even the experience of only one insufficient movement response leaves a highly specific mark on the future behavior. This is the

conclusion suggested by recent work in which we tested monkeys in a random error paradigm (Junker et al. 2018). In this experiment, the animals were asked to make saccades to visual targets presented randomly in one out of eight directions relative to straight ahead. Unpredictably, during a saccade, the target could step farther out, away from the center of the screen, step back toward the center, or stay put (**Figure 3*e***). In the first case, the saccades fell short of the final target location, causing a retinal error in the outward direction. In the second case, they overshot the target, leading to an inward error, whereas in the third case, consistent errors were absent. We investigated the effect that the retinal error in a certain direction in a given trial n had on the amplitude of the saccade in the next trial n_{future} made in the same direction, which was separated from trial n by on average six trials. This analysis showed that a retinal error not only caused a corrective saccade in trial n but also led to significant changes in the metrics of the saccade in trial n_{future}, increasing the amplitude of the primary saccade in the case of an outward error and, conversely, decreasing it in the case of inward errors (**Figure 3*f***). That is, the amplitude changes observed in trial n_{future} reduced the size of the retinal error in trial n_{future} had it been subject to the same intrasaccadic target shift as in trial n.

4. SIGNIFICANCE OF THE OCULOMOTOR VERMIS FOR THE PREVENTION OF PRECISION LOSS DUE TO FATIGUE

STSA is typically understood as a means to ensure that the relationship between the retinal error or vector (i.e., the vector connecting the fovea with the retinal target image) and the saccade vector can be readjusted if developmental or disease-related changes such as the development of refractive errors distort the mapping. However, these processes take time. Why then is STSA fast, having an impact from one saccade to the next? Without questioning a role of STSA in helping deal with the longer-term functional consequences of development and disease, we suggest that its primary role is to compensate for errors prevailing on a much shorter timescale (e.g., due to fatigue). Visually guided saccades, when performed repetitively, often exhibit a decline in peak velocity, which is taken as sign of fatigue (Bahill & Stark 1975, Brožek 1949, Chen-Harris et al. 2008, Fuchs & Binder 1983, Schmidt et al. 1979, Straube et al. 1997, Xu-Wilson et al. 2009b). In such cases, the required end point precision is nevertheless ensured by a compensatory upregulation of movement duration. The loss of peak velocity is not a consequence of changes of the oculomotor plant, as the relationship between the activity of oculomotor neurons and the resulting movement remains constant despite the development of fatigue (Prsa et al. 2010). Hence, saccadic fatigue must be a consequence of changes in the central saccade commands driving the oculomotor neurons, arguably due to a loss of motivation and attention but possibly also due to neuronal adaptation. Patients with vermal pathology show the same loss of peak velocity as healthy controls. Yet, unlike the healthy controls, the patients are unable to compensate for the velocity loss by upregulating saccade duration (Golla et al. 2008). Consequently, their saccade amplitude tends to decrease along the sequence of saccades. These patients are also unable to upregulate their saccade amplitudes in a typical gain-increase STSA experiment in which the saccade target is stepped farther out during the saccade. The reason is that the patients are unable to upregulate saccade duration in the face of only minor changes of saccade peak velocity. It is the upregulation of saccade duration that allows healthy subjects to increase saccade amplitude in the gain-increase STSA experiment. Finally, the residual gain-decrease STSA exhibited by patients is basically uncompensated fatigue, a loss in velocity not counteracted by changes in saccade duration. In sum, fatigue has a central, nonmotor origin, not involving the cerebellum, causing a loss in saccade velocity. The cerebellum—and most probably the OMV—ensures saccadic precision by adjusting the duration of the saccade, arguably deploying the same duration control mechanism that is also

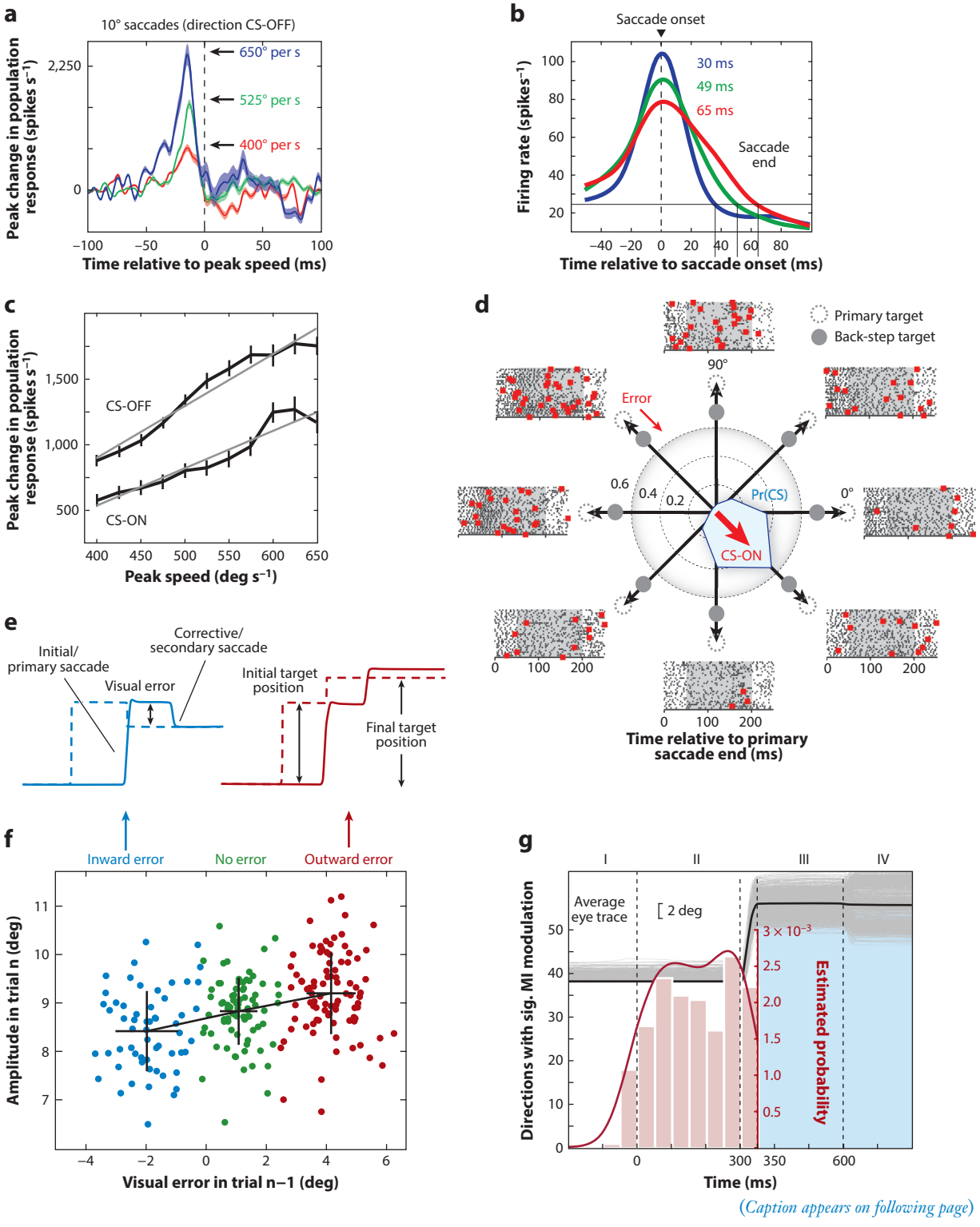

(Caption appears on following page)

Figure 3 (*Figure appears on preceding page*)

The role of OMV PC CSs and SSs in encoding and modifying saccade metrics and kinematics. (*a*) Saccade-related population activity of OMV (PC-SS) units for visually guided saccades of different speeds made in the CS-OFF direction. (*b*) Saccade-related PC-SS population activity for saccades of varying amplitudes and durations. Note that the end of the signals coincides with the end of the saccades. Panel *b* adapted from Thier et al. (2000) with permission. (*c*) Peak discharge rate of the population of PC-SS increases linearly with speed in both CS-ON and CS-OFF directions, albeit with higher gain in the CS-OFF direction. (*d*) Raster plots showing PC-SSs and PC-CSs fired by an exemplary PC for retinal errors (induced by using McLaughlin's intrasaccadic backstep paradigm) in different directions to determine its preferred error direction identified by a maximal probability of CS firing (as shown by the *red arrows*). Panels *a*, *c*, and *d* adapted from Herzfeld et al. (2015) with permission. (*e*,*f*) Exemplary eye movement traces evoked in a random error paradigm. (*e*) Monkeys performed visually guided saccades in eight randomly chosen directions in the frontoparallel plane, and in each trial the target could either stay put (not shown), jump back toward the center (*left panel*, *blue trace*), or jump farther out (*right panel*, *red trace*). If the target jumped during the primary saccade, the eyes missed the target, causing either an inward or an outward visual error and a second, corrective saccade followed. (*f*) Plot of saccade amplitude in a given trial preceded by a trial in the same direction with an inward error (*blue circles*), no error (*green circles*), or an outward error (*red circles*). Note that subsequent trials in the same direction were separated by on average 6.04 trials in other directions. Data are from an exemplary session of one monkey. Crosses give the means and standard deviation of each cluster. The means were significantly different (ANOVA, $p < 0.01$), indicating that the experience of only a single error had a clear impact on the later recapitulation of the same behavior. (*g*) CS modulation in a given trial is influenced by the presence and the type of visual error in past trials made in the same direction. The histogram maps the distribution of times of maximally significant trial-by-trial modulation of mutual information of CS units, on the basis of a comparison of three cases, inward versus outward error, inward error versus no error, and outward error versus no error, in a normalized saccade trial. The resulting plot shows a clear accumulation of information on past errors right before the primary saccade (*red area*). The significant mutual information at later times can no longer be unambiguously associated with an influence of past errors because of the confounding presence of a new visual error resulting from the primary saccade. Panels *f* and *g* adapted from Junker et al. (2018) with permission. Abbreviations: CS, complex spikes; OMV, oculomotor vermis; PC, Purkinje cell; SS, simple spike.

responsible for the behavioral responses in gain-increase STSA experiments (Thier et al. 2000). That is, we suggest that a major biological function of the machinery studied in STSA experiments is to compensate for the loss of precision due to fatigue.

The idea that cerebellum-dependent duration control helps compensate for short-term kinematic changes in an attempt to maintain precision turns out to be useful also for other types of movements. For instance, smooth-pursuit initiation, the early open-loop part of the movement, is characterized by a gradual loss in peak acceleration over consecutive trials. Its impact on velocity is mitigated by an upregulation of the duration of the acceleration pulse. This compensatory upregulation of duration is lost after experimental lesions of the monkey OMV (Dash & Thier 2013). Also, fast and precise target-directed pointing movements of the finger exhibit a speed–duration trade-off. It is lost in patients with cerebellar degeneration (Markanday et al. 2018). As the patients are unable to compensate for the fluctuations in velocity by adjusting movement duration, they present increased end point variability (i.e., movement ataxia). Can we attribute the loss of the velocity (acceleration)–duration trade-off to the loss of a well-adjusted SS output signal? Unfortunately, the data available do not allow a definite answer.

5. ROLE OF OCULOMOTOR VERMIS SIMPLE SPIKES IN CONTROLLING EYE MOVEMENT KINEMATICS

SSs recorded from the OMV exhibit eye movement–related activity. The early work described the responses as either saccade- or SPEM-related, with the demonstration of occasional dual SSs responding to both saccades and SPEMs (Sato & Noda 1992, Suzuki & Keller 1988). We established that these dual SSs are by no means oddities. Rather, most PC units in the OMV are dual, sensitive to both types of goal-directed eye movements, although surprisingly their directional preferences for eye movements in the frontoparallel plane seem to be unrelated (Sun et al. 2017).

A quantitative analysis of the eye movement–related responses of these dual SSs showed that the relative significance of eye position, velocity, and acceleration for the prediction of SS trains

differed for saccades and SPEMs. Whereas both saccade- and SPEM-related SS trains were influenced by all three kinematic variables in a multiple linear regression of discharge rate as a function of eye movement kinematics, the relative weights of the three variables depended on the type of goal-directed eye movement performed. In the case of SPEMs, eye velocity was the most important kinematic variable, whereas eye position was the most important in the case of saccades (Sun et al. 2017). However, a higher weight of the eye velocity term has been suggested by a previous population analysis of SSs (**Figure 3*a***) tested only for saccades (Herzfeld et al. 2015). This difference notwithstanding, one might argue that the notion that the OMV controls eye position in the case of saccades and eye velocity in the case of SPEMs is in good accordance with key assumptions of well-established models of saccade and SPEM generation. These models try to accommodate the need to integrate latency-free estimates of relevant state variables. In the case of saccades, the key state variable is the current eye position that is compared with the desired target position, the difference between the two positions telling the system how much farther to move the eyes (Robinson 1973, Scudder 1988). In the case of SPEM, models usually assume a prediction of eye velocity, avoiding the detrimental delay of visual feedback on the pursuit eye movement (Fukushima et al. 1996, Kahlon & Lisberger 1996).

6. SITE OF SACCADIC LEARNING

A saccade is accurate if the eyes land on the target, and conversely, SPEMs are optimal if the eyes are able to keep pace with the moving target. As stated above, the correction of deviations from optimal performance depends on the integrity of the OMV and entails changes of its SS output, the latter thought to be responsible for the behavioral changes. How does the information on performance errors reach the OMV and how does it lead to pertinent changes of the SS output? According to the Marr–Albus–Ito theory of cerebellar learning (Albus 1971, Ito 1972, Marr 1969), error information, assumed to be mediated by olivary CFs (**Figure 1*b***), causes changes of the synaptic weights of PF synapses, changes that in turn translate into changes of the SS output (Kojima et al. 2010; for a review, see Prsa & Thier 2011). That is, the assumption is that learning-based changes are first implemented at the level of PCs. In fact, in accordance with this view, we could not observe any learning-related changes in the discharge of Golgi cells tested in a standard paradigm of STSA (Prsa et al. 2009). However, although Golgi cells are clearly downstream of PCs in the architectural hierarchy of the cerebellar cortex, they are not elements of the direct pathway to PCs consisting of mossy fibers–granule cells–parallel fibers and may therefore stay unaffected by input changes. As recordings from MFs in awake monkeys are typically short-lived, attempts to test whether MFs undergo changes of their spiking pattern in standard adaptation paradigms involving many hundreds of trials have hitherto failed. However, the discovery that the major biological function of short-term oculomotor learning is to compensate for fatigue has recently allowed us to readdress the possibility of learning-related changes at a pre-PC level. In a recent unpublished study, we evoked saccadic fatigue, characterized by a gradual loss in saccade peak velocity, compensated by an increase in saccade duration that ensured the maintenance of end point precision. To this end, we asked monkeys to carry out a large number of repetitive, stereotypic saccades, building on a paradigm introduced by Prsa et al. (2010). One may have expected that MFs convey information on an ideal default velocity and duration not affected by the kinematic changes characterizing saccadic fatigue. Contrary to this expectation, the MF discharge patterns exhibited changes that perfectly reflected the kinematic changes (A. Markanday, P.W. Dicke & P. Thier, unpublished data). Yet this result speaks by no means against the view that learning takes place only at the level of the PC. Rather it may be an inevitable consequence of the fact that the MFs are elements in a closed loop in which all elements are affected by the impact of the PC

output. Hence, MF recordings, in which SS feedback on the brain stem machinery is prevented, will be needed to decide whether learning takes place before the level of PC. Unfortunately, this experiment is not straightforward. The reason is that—as we see below—blocking SS feedback by globally switching off the DCNs would inevitably affect the processing of error-related information processed in the IO. That MFs offer a precise description of the kinematic changes due to fatigue, involving a reflection of both velocity and movement time, is interesting with regard to supposedly divergent views on the relevant saccade parameters controlled by PCs. When we first suggested SS population coding as the major control principle (Thier et al. 2000), we argued that the population signal determined the end of the saccade, a conclusion supported by the observation that the end of the SS population signal correlated with the end of the saccade (**Figure 3*b***) in the cases of both normal and adapted visually guided saccades (Catz et al. 2008, Thier et al. 2000). This view is in line with the behavioral finding that cerebellar lesions compromise the ability to select the movement duration needed to ensure end point precision irrespective of changes in movement velocity (Golla et al. 2008). Conversely, the Shadmehr laboratory (Herzfeld et al. 2015) has argued that a SS population signal controls saccade velocity, a view suggested by the observation that peak firing rates of the population signal grew with peak velocity (**Figure 3*a***) (see also Section 7). However, the MF results alluded to above clearly indicate that, at the level of the input to PCs, precise information about both velocity and time is available. This fact may suggest that the SS population might actually encode both kinematic parameters (i.e., velocity and duration) rather than selectively caring for only one or the other.

7. COMPLEX SPIKES CONVEY INFORMATION ON THE PREVAILING RETINAL ERROR

One of the biggest challenges in studies of the role of CSs has been their extremely low firing rate. What could these rare bouts of activity possibly tell us about the sensory guidance of behavior and what might be the best statistical tool able to detect relevant information in CS trains? Addressing this question requires careful detection of these scarce events, as even slight errors of falsely omitting or detecting CSs can cause misinterpretations of their functional role. Because the existing spike sorting approaches cannot fully reliably handle the rarity and complex morphology of CSs, researchers have relied on tedious manual labeling of CSs to avoid errors in their detection. Only recently, a supervised deep-learning-based fully automated approach (Markanday et al. 2019) has been able to offer a fast and reliable solution to this problem that will allow researchers to obtain better control over the statistics of CS events.

Whereas an individual PC is contacted by a single CF, the individual CF uses collateral branches to supply several PCs, hereby sharing information originating from the IO (see **Figure 1*b***). Moreover, these PCs with common CS input—when located in the OMV—collectively project onto a single nucleus neuron in the caudal fastigial nuclei. Against this backdrop, it becomes understandable that a recent study showed that indeed PC units recorded from the OMV of monkeys shared a common CS property, namely similar tuning for the direction of retinal error, when tested in a McLaughlin's intrasaccadic backstep paradigm (Herzfeld et al. 2015). The backstep induces a retinal error and forces the monkey to make a second saccade, correcting the retinal error. Herzfeld et al. (2015) labeled the error direction for which the highest probability of CS firing was observed (the preferred error direction) as the CS-ON direction, while the opposite direction with the lowest probability of CS firing (i.e., nonpreferred error direction) was labeled CS-OFF (**Figure 3*d***). Populations of PCs, comprising comparable numbers of pausing and bursting SS units that were pooled separately for the CS-ON and CS-OFF directions, exhibited a SS population discharge whose strength increased with increasing saccade speeds for both

CS-ON and CS-OFF directions (**Figure 3*a*,*c***); however, the gain was larger for the CS-OFF pool. Unlike error direction, the magnitude of retinal error had no influence on the probability of CS firing. But the error magnitude affected the CS timing—experiencing a larger error increased the likelihood of a CS to be fired within 75–150 ms after saccade termination (Herzfeld et al. 2018). Although the duration of CSs found within this period was longer than that of CSs found elsewhere, this increase did not account for changes in behavior, suggesting that indeed CS timing rather than duration played a critical role in conveying information on the visual error needed to adjust the upcoming behavior. The occurrence of a CS in the period between primary and corrective saccades biased the direction of the next saccade toward the CS-ON direction. Conversely, without a CS, the next saccade was pushed more in the opposite direction. CSs are followed by a transient depression of SS activity 10–20 ms later (see below). Correspondingly, the contribution of the population of SSs fired by CS-ON PCs exhibited a decrease in the discharge rate. By contrast, the population of SSs fired by CS-OFF PCs exhibited a significant increase. The basis of this increase relative to the baseline firing rate of CS is less clear. Assuming that PCs whose CS-ON is to the right are located in the left OMV and vice versa, experiencing an error in either direction would result in a shift in balance between the left and the right OMV SS outputs. This then would translate into a shift in balance of the motoneuron drive between the agonist and antagonist eye muscles, moving the eyes toward the error direction and thereby causing a saccade gain change.

The evidence presented by Herzfeld et al. (2018) is in full accordance with the central tenet of Marr's theory of cerebellar cortex (Marr 1969), in which the CF system broadcasts an error signal that allows PCs to optimize the motor behavior, a view also supported by previous work on the role of the floccular complex in vestibulo-ocular reflex and SPA (Stone & Lisberger 1990). The reciprocal relationship between an increased CS probability and a decrease in SSs, which in turn is associated with decreased movement vigor, might be a consequence of CS causing long-term depression of PF synapses, thereby reducing the excitatory drive to PCs as posited by the Marr–Albus–Ito theory of cerebellar learning. However, as the dip in SS firing following a CS may also be a consequence of the recruitment of inhibitory interneurons and of the activation of calcium-dependent potassium channels of PCs (Kakizawa et al. 2007, Mathews et al. 2012), these findings do not necessarily demand long-term depression.

8. COMPLEX SPIKES STABILIZE OCULOMOTOR BEHAVIOR

Not all observations of the OMV PC firing patterns studied during cerebellum-based oculomotor learning are readily compatible with the view that the primary role of the CS is it to broadcast the current visual error. For instance, Catz et al. (2005) failed to detect a significant CS modulation by error in conjunction with two variants of STSA, one using stereotypic backsteps of the target, thereby evoking gain-decrease STSA, and the other conversely evoking gain-increase STSA by stepping the target farther out. Given the fact that the retinal errors are maximal early in the series of adaptation trials, one might have expected a higher probability of significant CS discharge modulation early in the series. Yet, in contrast to this expectation, CSs were fired at random in the beginning and a significant CS saccade-related signal built up gradually in parallel with the gradual decrease in the size of the retinal error over the course of adaptation. This building up of CS discharge reached its maximal and stable expression at the end of the adaptation series: At a point, an optimal adaptation of the primary saccade was able to prevent the occurrence of a visual error. While gain-increase adaptation was associated with a pause in the CS population response peaking 10 ms before the end of the primary saccade, a CS burst associated with gain-decrease adaptation peaked 23 ms before the end of the primary saccade. In a study of SPA, Dash et al. (2010) observed similar changes of the CS discharge pattern. In this study of macaque monkeys,

gain-decrease SPA was induced, repeatedly over many trials, by abruptly reducing the velocity of the pursuit target 100–200 ms after the onset of its ramp-like target movement. Conversely, in order to evoke gain-increase SPA adaptation, the target velocity was abruptly upregulated. Because the visual system takes a long time to extract the new velocity, the eyes typically keep moving for approximately 100–150 ms according to the target velocity before the target velocity steps, over- and undershooting the target, thereby causing a substantial retinal velocity error. Adaptation gradually adjusts the initial eye velocity to the level of target velocity after the velocity step, thereby reducing the error. That is, depending on the occurrence and direction of the velocity step, the same initial target velocity may cause different eye velocities at the time of the target velocity step in order to optimally prepare for the predicted target velocity. Again, CSs occurred at random early in the adaptation series. However, paralleling the gradual buildup of adaptation (i.e., the modification of the initial eye velocity), the CS units developed a clear modulation. During gain-decrease SPA, the probability of CSs increased with a decrease in pursuit velocity in 0–100 ms relative to pursuit onset and conversely decreased with gain-increase SPA. In both cases, the CS modulation was concomitant with changes in eye velocity, rather than the errors, and stable at the end of the adaptation series. Both studies, fully consistent with each other, demonstrate that the CS signal runs parallel to the behavioral changes. This suggests that CSs play a role in stabilizing the adaptive changes of the behavior.

9. COMPLEX SPIKES CONVEY AN ERROR PREDICTION REFLECTING THE PAST

One might argue that the probability and the size of the behavioral change studied by Catz et al. (2005) and Dash et al. (2010) are determined by the certainty that these changes are needed. If this were true, the buildup of the CS signal could be understood as a reflection of the buildup of knowledge on the probability of future errors (i.e., an error prediction rather than information on the current error). This intriguing speculation is in line with conclusions drawn from recent work on eye blink conditioning (Ohmae & Medina 2015). Air puffs applied to the eye, experienced as unpleasant, evoke transient eyelid closure, a short-latency reflex yielding protection. If this unconditioned stimulus is repetitively paired with a harmless, neutral second sensory event such as a flash of light, the latter—the conditioned stimulus—develops the ability to evoke an eyelid closure at the time the air puff is expected. CSs are elicited by the delivery of an air puff early during eye blink conditioning, when the air puff is still unexpected. Yet, later, once the flash of light has become predictive of the air puff, the CS shifts to the time of the flash as if predicting the subsequent occurrence of the air puff. While supporting a role of the CS in predicting the necessity of a particular motor adaptation accords with the studies of oculomotor adaptation by Catz et al. (2005) and Dash et al. (2010), this work on eye blink conditioning also demonstrates a sensitivity to unexpected current errors, emphasized by Herzfeld et al. (2015, 2018) yet not seen in the experiments of Catz et al. and Dash et al. We think that recent work from our laboratory (Junker et al. 2018) reconciles the somewhat divergent views by demonstrating that oculomotor learning involves information on both current and predicted errors, and, moreover, suggests how the former might be used to derive the latter. As stated above, random saccade errors are able to evoke noticeable changes of future saccades. Resorting to an analysis of mutual information with Bayesian binning (Endres & Foldiak 2005) of CS units of PCs recorded in parallel with the behavior, we found that the discharge of many CSs was influenced by the direction of the prevailing retinal error. There are two adjacent periods in which the target image does not fall on the fovea: before the primary saccade and between the end of the primary saccade and the beginning of the second, or corrective, saccade. The time of the maximal modulation of the CS discharge scattered

widely between target onset and the execution of the secondary saccade, with an emphasis on the interval between the primary and the secondary saccades. Irrespective of the timing, sensitivity to a prevailing retinal error accords with the assumption that the CS encodes the direction of the visual error. However, the error influenced the CS discharge not only during its acute presence in trial n but also much later in trial n_{future}, before a primary saccade to a target presented in the same direction as the one responsible for the original error in trial n. This was indicated by significant mutual information on the type of error in trial n before the primary saccade in trial n_{future}. This influence of past error can be seen even in individual CS units (**Figure 3*g***). A few hundred milliseconds before the primary saccade ($t = 0$), the probability of CS firing is significantly lower for trials preceded by outward error trials. A fraction of the PCs tested showed significant changes in their SS discharge around the time of the upcoming primary saccade, preceding CS reverberation modulation, which is most probably responsible for the changes of saccade amplitudes in trials n_{future}, evoked by trial n errors. This change of SS activity was usually too late to be responsible for the CS reverberation signal. As the SS activity occurred later than the CS reverberation activity, it could not have evoked the latter. However, the temporal relationship between the CS and SS signals might be compatible with the former causing the latter, on the basis of long-term depression of PF–PC synapses, suppression of SS firing following CS due to the recruitment of inhibitory interneurons and the activation of calcium-dependent potassium channels of PCs, or both (see above). But how might the CS reverberation activity be generated in the first place? We suggest that performance error–related CS activity leads to changes of the SS population output, which is then fed back to the IO by nucleo-olivary projection neurons in the DCNs (see **Figure 1*b***), inducing a state change of neurons of the IO. Extracerebellar information on the intention to prepare a new saccade may then trigger the conversion of the state change to the changes of the firing of CFs responsible for the CS reverberation signal. The putative olivary state change—and correspondingly the change of CF activity—should be the larger, the stronger the change of the SS population signal is. However, larger SS changes result from consistent error input, characteristic of saccadic adaptation paradigms, with stereotypic target shifts as used, for example, by Catz et al. (2005). Consequently, CS modulation before an upcoming saccade will grow, whereas CS modulation between the end of the primary saccade and the beginning of the corrective saccade, reflecting the current error, will decrease because the growing behavioral changes will reduce the error. Finally, the hypothesized positive-feedback character of the IO–PC–IO loop entails a persistence of the CS modulation even in the absence of fresh error. It reflects the certainty that a particular behavioral adjustment should be maintained in the absence of eventually countermanding new error information.

10. ROLE OF THE CEREBELLUM IN VISUAL MOTION PERCEPTION

Traditionally the cerebellum has been seen as a part of the brain devoted to motor behavior, and correspondingly, for a long time, the motor cortex was considered the only cortical recipient of cerebellar output. This picture has changed. We now know that large parts of the cerebral cortex, probably more than 80% in primates, project to the cerebellum and in turn that these cerebrocortical areas, which include large parts of sensory cortices, receive feedback from the cerebellar cortex, mediated by the DCNs and specific thalamic nuclei (Bostan et al. 2010, Hoshi et al. 2005, Mathews et al. 2012, Middleton & Strick 2001, Sultan et al. 2000). Given the fact that the vast stretches of cerebral cortex that are interconnected with the cerebellum do not have a role in the immediate control of motor behavior, it is not surprising that the cerebellum has been implicated in numerous nonmotor functions (Ivry & Diener 1991, Jokisch et al. 2005, Kelly & Strick 2003, Nawrot & Rizzo 1995, Schmahmann & Sherman 1998, Strick et al. 2009). It may be difficult to

identify a sensory, cognitive, or affective function that has not been associated with the cerebellum (Schmahmann 1991, 2004; Schmahmann & Sherman 1998). Yet many of these claims are problematic because they are based on studies of patients suffering from disease of the cerebellum, conditions in which an involvement of extracerebellar structures often seems conceivable. This applies in particular to patients suffering from one of the many variants of spinocerebellar degeneration, which inevitably also affect, albeit to varying degrees, noncerebellar parts of the brain. Another problem has often been the lack of appropriate efforts to control for disturbances of eye fixation and, more generally, the lack of consideration of the sensory and cognitive consequences of the inability to move precisely and reliably. The claim that pathology affecting the OMV and possibly also the neighboring parts of the posterior vermis leads to disturbances of visuospatial attention is a case in point. This hypothesis was guided by the obvious formal correspondence between covert and overt shifts of attention and the well-established role of the OMV in ensuring the precision of overt shifts of attention (Akshoomoff & Courchesne 1992, 1994; Townsend et al. 1996, 1999). Yet more carefully controlled studies of patients with relatively widespread cerebellar pathology and of monkeys with experimental lesions of the posterior vermis have not been able to support the idea of a dysmetria of attention (Golla et al. 2005, Helmuth et al. 1997, Ignashchenkova et al. 2009, Nixon & Passingham 1999, Schoch et al. 2004, Thier et al. 1999). The same subjects that exhibited disturbed overt shifts of attention showed completely normal covert shifts of attention (Golla et al. 2005, Ignashchenkova et al. 2009).

By contrast, a key example of a nonmotor function of the cerebellum that has withstood all attempts to question it is the perception of visual motion. Impaired visual motion perception in patients suffering from global cerebellar pathology was first reported by Ivry & Diener (1991). Although this early study also suffered from some of the methodological problems mentioned above, better controlled experiments with more carefully selected patients have fully supported the existence of a visual motion perception deficit in cerebellar patients suffering from midline pathology. The visuoperceptual deficit is indeed specific to visual motion perception. Visual acuity and the ability to discriminate spatial positions are unaffected (see **Figure 4*a*,*b***). Moreover, the motion perception deficit (**Figure 4*b***) cannot be explained by disturbances of visual fixation (Nawrot & Rizzo 1995, 1998; Thier et al. 1999). Evidence supporting this conclusion (summarized in **Figure 4*c***) demonstrates normal fixation performance of patients vis-à-vis a clear motion perception deficit (H. Scherer, P. Thier & T. Haarmeier, unpublished data). Similar deficits have been observed in nonhuman primates following experimental lesions of the vermis emphasizing lobules VIII (Ignashchenkova et al. 2009). Visual motion processing is cerebellum dependent because the cerebellum provides an essential resource for the processing of visual motion in the parieto-occipital cortex. This is the conclusion suggested by a study of patients with cerebellar lesions but intact cerebral cortex. Using magnetoencephalography (MEG), we recorded cortical responses in the patients and healthy controls while the subjects tried to extract the direction of motion in a random dot kinematogram with varying coherence during controlled stationary fixation (Händel et al. 2009). The patients showed a significant impairment in global motion discrimination despite normal fixation behavior. Moreover, this deficit was paralleled by quantitative differences in MEG activity recorded from the parieto-temporal cortex, including a reduced responsiveness to coherent visual motion. Across all subjects, the perceptual thresholds correlated with the representation of motion strength in the MEG signals on a single-subject basis, with the patients contributing the segment of the regression line characterized by a particularly poor motion perception and weakly distinctive MEG activity. Why does visual motion perception require cerebellar input? We think the reason is the inferential nature of visual motion perception. In order to arrive at a veridical percept of visual motion, the visual system has to eliminate those parts of the retinal motion input that are a consequence of the self-motion in order to filter out

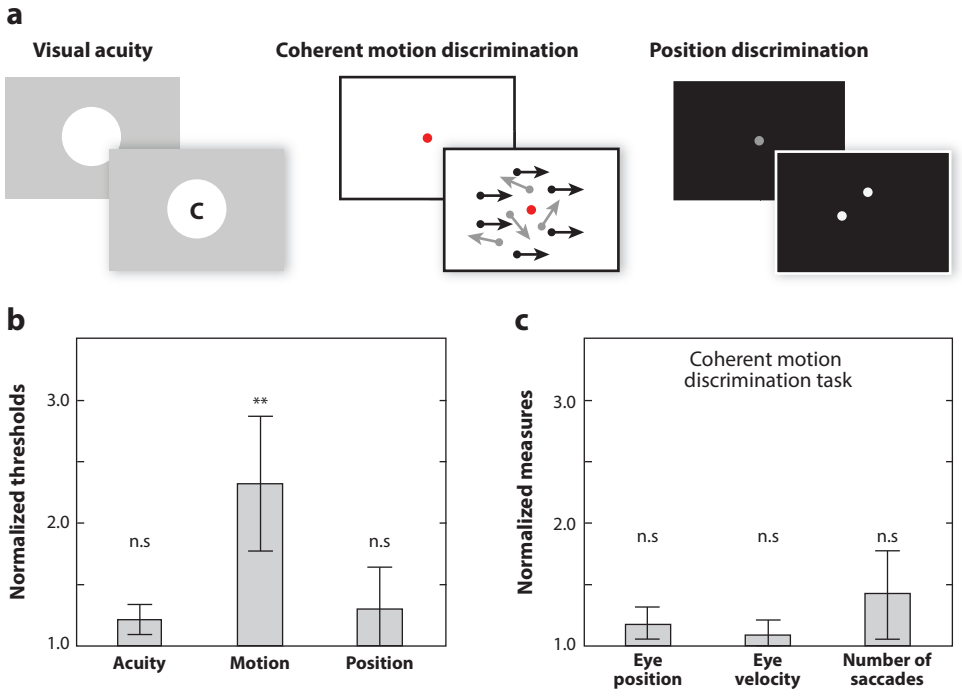

Figure 4

Visual tasks used to compare performance of healthy controls and patients with cerebellar pathology. (*a*, *left*) Visual acuity was assessed by asking subjects to discriminate the orientation of a Landolt C of varying size. (*Middle*) Motion perception thresholds were measured by determining the minimum percentage of coherently moving dots in random dot kinematograms, allowing reliable identification of the direction of global motion. (*Right*) Position discrimination was tested by asking subjects to decide which of two tiny dots stood higher. Eye movements were controlled by means of high-resolution video oculography. (*b*) Comparison of performance of patients and healthy controls ($n = 21$) tested on several visual tasks. Nine of 16 patients suffered from global cerebellar atrophy, whereas 7 had more circumscribed lesions of varying parts of the cerebellar cortex. In accordance with previous studies of patients with cerebellar pathology and monkeys with experimental lesions, this group of patients also exhibited a substantial motion perception deficit vis-à-vis normal motion-dependent visual functions. (*c*) The patient whose motion perception deficit is shown in panel *b* exhibited a fixation pattern based on measures of the mean number of saccades, mean eye drift, and mean position offset from the fixation point during vision of the random dot kinematogram that did not deviate from the fixation pattern of controls (H. Scherer, P. Thier & T. Haarmeier, unpublished data). Asterisks represent significant results. Abbreviation: n.s, not significant.

motion in the world. Copies of the motor commands responsible for the self-motion may serve as initial estimates of self-induced motion. However, the exact relationship between these efference copies and the self-induced motion signal is highly variable. For instance, the same movement may require motor commands of different strength; conversely, the same movement may cause different retinal input depending on the composition of the visual scene. Hence, continuous recalibration of the efference copy is needed. Functional MRI work that built on manipulating the relationship between an eye movement and the resulting percept of self-induced visual motion clearly indicated that the posterolateral cerebellum, a region that may overlap with parts of the HOR, plays a central role in this recalibration (Lindner et al. 2006). That is, we suggest that visual motion perception is impaired in patients with cerebellar pathology because of the lack of essential reference information that may be needed even during stationary fixation, for instance, owing

to microsaccades. We think that this interpretation of the role of the cerebellum in visual motion perception has implications for the more general question of whether the cerebellum contributes to cognition and why. We would argue that the cerebellum may be needed whenever the cognitive operation at stake requires time-critical information on the movement.

11. CONCLUSION

The OMV plays a key role in optimizing the kinematics of both types of fovea-serving eye movements, saccades, and SPEMs. However, it is not involved in visual motion perception. Rather the latter function is accommodated by relatively ill-defined posterior and lateral parts of the midline cerebellum. The OMV helps optimize saccades and SPEMs by deploying a SS signal that conveys information on key kinematic parameters such as eye movement velocity and duration. This population signal can be adjusted on a short timescale, a swiftness that is optimally suited to prevent a deterioration of eye movement precision due to motor fatigue, cognitive fatigue, or both. The necessary adjustments of the SS population signal are prompted by the CSs, which deploy information on acute and past performance errors and on expectations of future errors.

SUMMARY POINTS

1. The cerebellar cortex is a crystal-like structure composed of endless repetitions of canonical microcircuits, which offer the same computational principle to varying inputs.
2. Visually guided eye movements are accommodated essentially by three parts of the cerebellum: (*a*) the phylogenetically old flocculonodular lobe, which primarily subserves background image–stabilizing eye movements as well as smooth pursuit eye movements (SPEMs); (*b*) the hemispheric oculomotor region (HOR), a relatively unexplored part of the cerebellum, which probably contributes to visually guided eye movements and visual motion perception; and (*c*) the oculomotor vermis (OMV), phylogenetically recent like the HOR and a major substrate for goal-directed eye movements.
3. The simple spikes (SSs) fired by the Purkinje cells (PCs) in the OMV control movement kinematics.
4. The complex spikes (CSs) fired by the PCs in the OMV reflect information on current movement errors, past errors, and the expectation of future errors.
5. This information is used to update the SS code to avoid future movement errors.
6. The cerebellar cortex, adjoining the OMV, is involved in visual motion perception arguably by providing information on the visual consequences of self-motion relative to the world.

FUTURE ISSUES

Future work must address several burning questions about the role of the OMV.

1. What is the advantage of engaging the same microcircuit in the OMV to support two types of visually guided eye movements with different kinematic requirements, high speed saccades, and slow SPEMs?
2. What are the functional differences between the respective contributions of the OMV and the floccular complex to SPEMs and how do they interlock?

3. How do neurons in the caudal fastigial nuclei transform the eye movement control signals emitted by OMV PCs?
4. We may also hope that future work will succeed in more precisely delineating the parts of the cerebellar cortex relevant for visual motion perception and, moreover, that this work will critically assess the hypothesis that this region is essential for visual motion perception because it provides an adaptable eye-movement-related efference copy signal needed by the visual cortex to disentangle self-induced and externally induced retinal image slip.

DISCLOSURE STATEMENT

The authors are not aware of any affiliations, memberships, funding, or financial holdings that might be perceived as affecting the objectivity of this review.

ACKNOWLEDGMENTS

This work has been supported by the German Research Foundation (DFG) Research Unit FOR 1847-A3.

LITERATURE CITED

Akshoomoff NA, Courchesne E. 1992. A new role for the cerebellum in cognitive operations. *Behav. Neurosci.* 106:731–38

Akshoomoff NA, Courchesne E. 1994. ERP evidence for a shifting attention deficit in patients with damage to the cerebellum. *J. Cogn. Neurosci.* 6:388–99

Albus JS. 1971. A theory of cerebellar function. *Math. Biosci.* 10:25–61

Aschoff JC, Cohen B. 1971. Changes in saccadic eye movements produced by cerebellar cortical lesions. *Exp. Neurol.* 32:123–33

Bahill AT, Stark L. 1975. Overlapping saccades and glissades are produced by fatigue in the saccadic eye movement system. *Exp. Neurol.* 48:95–106

Barash S, Melikyan A, Sivakov A, Zhang M, Glickstein M, Thier P. 1999. Saccadic dysmetria and adaptation after lesions of the cerebellar cortex. *J. Neurosci.* 19:10931–39

Bostan AC, Dum RP, Strick PL. 2010. The basal ganglia communicate with the cerebellum. *PNAS* 107:8452–56

Bötzel K, Rottach K, Büttner U. 1993. Normal and pathological saccadic dysmetria. *Brain* 116:337–53

Brožek J. 1949. Quantitative criteria of oculomotor performance and fatigue. *J. Appl. Physiol.* 2:247–60

Büttner U, Büttner-Ennever J. 2006. Present concepts of oculomotor organization. *Prog. Brain Res.* 151:1–42

Catz N, Dicke PW, Thier P. 2005. Cerebellar complex spike firing is suitable to induce as well as to stabilize motor learning. *Curr. Biol.* 15:2179–89

Catz N, Dicke PW, Thier P. 2008. Cerebellar-dependent motor learning is based on pruning a Purkinje cell population response. *PNAS* 105:7309–14

Chen-Harris H, Joiner WM, Ethier V, Zee DS, Shadmehr R. 2008. Adaptive control of saccades via internal feedback. *J. Neurosci.* 28:2804–13

Dash S, Catz N, Dicke PW, Thier P. 2010. Specific vermal complex spike responses build up during the course of smooth-pursuit adaptation, paralleling the decrease of performance error. *Exp. Brain Res.* 205:41–55

Dash S, Thier P. 2013. Smooth pursuit adaptation (SPA) exhibits features useful to compensate changes in the properties of the smooth pursuit eye movement system due to usage. *Front. Syst. Neurosci.* 7:67

Dash S, Thier P. 2014. Cerebellum-dependent motor learning: lessons from adaptation of eye movements in primates. *Prog. Brain Res.* 210:121–55

Eccles JC, Llinás R, Sasaki K. 1966. The excitatory synaptic action of climbing fibres on the Purkinje cells of the cerebellum. *J. Physiol.* 182:268–96
Endres D, Foldiak P. 2005. Bayesian bin distribution inference and mutual information. *IEEE Trans. Inform. Theory* 51:3766–79
Fuchs AF, Binder MD. 1983. Fatigue resistance of human extraocular muscles. *J. Neurophysiol.* 49:28–34
Fujikado T, Noda H. 1987. Saccadic eye movements evoked by microstimulation of lobule VII of the cerebellar vermis of macaque monkeys. *J. Physiol.* 394:573–94
Fukushima K, Tanaka M, Suzuki Y, Fukushima J, Yoshida T. 1996. Adaptive changes in human smooth pursuit eye movement. *Neurosci. Res.* 25:391–98
Golla H, Thier P, Haarmeier T. 2005. Disturbed overt but normal covert shifts of attention in adult cerebellar patients. *Brain* 128:1525–35
Golla H, Tziridis K, Haarmeier T, Catz N, Barash S, Thier P. 2008. Reduced saccadic resilience and impaired saccadic adaptation due to cerebellar disease. *Eur. J. Neurosci.* 27:132–44
Händel B, Thier P, Haarmeier T. 2009. Visual motion perception deficits due to cerebellar lesions are paralleled by specific changes in cerebro-cortical activity. *J. Neurosci.* 29:15126–33
Helmuth LL, Ivry RB, Shimizu N. 1997. Preserved performance by cerebellar patients on tests of word generation, discrimination learning, and attention. *Learn. Mem.* 3:456–74
Herculano-Houzel S. 2009. The human brain in numbers: a linearly scaled-up primate brain. *Front. Hum. Neurosci.* 3:31
Herzfeld DJ, Kojima Y, Soetedjo R, Shadmehr R. 2015. Encoding of action by the Purkinje cells of the cerebellum. *Nature* 526:439–42
Herzfeld DJ, Kojima Y, Soetedjo R, Shadmehr R. 2018. Encoding of error and learning to correct that error by the Purkinje cells of the cerebellum. *Nat. Neurosci.* 21:736–43
Hillman DE. 1969. Light and electron microscopical study of the relationships between the cerebellum and the vestibular organ of the frog. *Exp. Brain Res.* 9:1–15
Hoshi E, Tremblay L, Féger J, Carras PL, Strick PL. 2005. The cerebellum communicates with the basal ganglia. *Nat. Neurosci.* 8:1491–93
Ignashchenkova A, Dash S, Dicke PW, Haarmeier T, Glickstein M, Thier P. 2009. Normal spatial attention but impaired saccades and visual motion perception after lesions of the monkey cerebellum. *J. Neurophysiol.* 102:3156–68
Ito M. 1972. Neural design of the cerebellar motor control system. *Brain Res.* 40:81–84
Ivry RB, Diener H. 1991. Impaired velocity perception in patients with lesions of the cerebellum. *J. Cogn. Neurosci.* 3:355–66
Jokisch D, Troje NF, Koch B, Schwarz M, Daum I. 2005. Differential involvement of the cerebellum in biological and coherent motion perception. *Eur. J. Neurosci.* 21:3439–46
Junker M, Endres D, Sun ZP, Dicke PW, Giese M, Thier P. 2018. Learning from the past: a reverberation of past errors in the cerebellar climbing fiber signal. *PLOS Biol.* 16:e2004344
Kahlon M, Lisberger SG. 1996. Coordinate system for learning in the smooth pursuit eye movements of monkeys. *J. Neurosci.* 16:7270–83
Kakizawa S, Kishimoto Y, Hashimoto K, Miyazaki T, Furutani K, et al. 2007. Junctophilin-mediated channel crosstalk essential for cerebellar synaptic plasticity. *EMBO J.* 26:1924–33
Kelly RM, Strick PL. 2003. Cerebellar loops with motor cortex and prefrontal cortex of a nonhuman primate. *J. Neurosci.* 23:8432–44
Kojima Y, Soetedjo R, Fuchs AF. 2010. Changes in simple spike activity of some Purkinje cells in the oculomotor vermis during saccade adaptation are appropriate to participate in motor learning. *J. Neurosci.* 30:3715–27
Krauzlis R, Miles F. 1998. Role of the oculomotor vermis in generating pursuit and saccades: effects of microstimulation. *J. Neurophysiol.* 80:2046–62
Lindner A, Haarmeier T, Erb M, Grodd W, Thier P. 2006. Cerebrocerebellar circuits for the perceptual cancellation of eye-movement-induced retinal image motion. *J. Cogn. Neurosci.* 18:1899–912
Lisberger SG, Fuchs AF. 1974. Response of flocculus Purkinje cells to adequate vestibular stimulation in the alert monkey: fixation versus compensatory eye movements. *Brain Res.* 69:347–53

Madigan JC, Carpenter MB. 1971. *Cerebellum of the Rhesus Monkey*. Baltimore, MD: University Park Press
Markanday A, Bellet J, Bellet ME, Hafed ZM, Thier P. 2019. Using deep neural networks to detect complex spikes of cerebellar Purkinje cells. bioRxiv 600536. **https://doi.org/10.1101/600536**
Markanday A, Messner J, Thier P. 2018. A loss of a velocity-duration trade-off impairs movement precision in patients with cerebellar degeneration. *Eur. J. Neurosci.* 48:1976–89
Marr D. 1969. A theory of cerebellar cortex. *J. Physiol.* 202:437–70
Mathews PJ, Lee KH, Peng Z, Houser CR, Otis TS. 2012. Effects of climbing fiber driven inhibition on Purkinje neuron spiking. *J. Neurosci.* 32:17988–97
McLaughlin SC. 1967. Parametric adjustment in saccadic eye movements. *Percept. Psychophys.* 2:359–62
Middleton FA, Strick PL. 2001. Cerebellar projections to the prefrontal cortex of the primate. *J. Neurosci.* 21:700–12
Monsivais P, Clark BA, Roth A, Häusser M. 2005. Determinants of action potential propagation in cerebellar Purkinje cell axons. *J. Neurosci.* 25:464–72
Napper RM, Harvey RJ. 1988. Number of parallel fiber synapses on an individual Purkinje cell in the cerebellum of the rat. *J. Comp. Neurol.* 274:168–77
Nawrot M, Rizzo M. 1995. Motion perception deficits from midline cerebellar lesions in human. *Vis. Res.* 35:723–31
Nawrot M, Rizzo M. 1998. Chronic motion perception deficits from midline cerebellar lesions in human. *Vis. Res.* 38:2219–24
Nixon PD, Passingham RE. 1999. The cerebellum and cognition: Cerebellar lesions do not impair spatial working memory or visual associative learning in monkeys. *Eur. J. Neurosci.* 11:4070–80
Noda H, Fujikado T. 1987a. Involvement of Purkinje cells in evoking saccadic eye movements by microstimulation of the posterior cerebellar vermis of monkeys. *J. Neurophysiol.* 57:1247–61
Noda H, Fujikado T. 1987b. Topography of the oculomotor area of the cerebellar vermis in macaques as determined by microstimulation. *J. Neurophysiol.* 58:359–78
Noda H, Mikami A. 1986. Discharges of neurons in the dorsal paraflocculus of monkeys during eye movements and visual stimulation. *J. Neurophysiol.* 56:1129–46
Noda H, Sugita S, Ikeda Y. 1990. Afferent and efferent connections of the oculomotor region of the fastigial nucleus in the macaque monkey. *J. Comp. Neurol.* 302:330–48
Noto CT, Watanabe S, Fuchs AF. 1999. Characteristics of simian adaptation fields produced by behavioral changes in saccade size and direction. *J. Neurophysiol.* 81:2798–813
Ohki M, Kitazawa H, Hiramatsu T, Kaga K, Kitamura T, et al. 2009. Role of primate cerebellar hemisphere in voluntary eye movement control revealed by lesion effects. *J. Neurophysiol.* 101:934–47
Ohmae S, Medina JF. 2015. Climbing fibers encode a temporal-difference prediction error during cerebellar learning in mice. *Nat. Neurosci.* 18:1798–803
Prsa M, Dash S, Catz N, Dicke PW, Thier P. 2009. Characteristics of responses of Golgi cells and mossy fibers to eye saccades and saccadic adaptation recorded from the posterior vermis of the cerebellum. *J. Neurosci.* 29:250–62
Prsa M, Dicke PW, Thier P. 2010. The absence of eye muscle fatigue indicates that the nervous system compensates for non-motor disturbances of oculomotor function. *J. Neurosci.* 30:15834–42
Prsa M, Thier P. 2011. The role of the cerebellum in saccadic adaptation as a window into neural mechanisms of motor learning. *Eur. J. Neurosci.* 33:2114–28
Ritchie L. 1976. Effects of cerebellar lesions on saccadic eye movements. *J. Neurophysiol.* 39:1246–56
Robinson DA. 1973. Models of the saccadic eye movement control system. *Kybernetik* 14:71–83
Ron S, Robinson DA. 1973. Eye movements evoked by cerebellar stimulation in the alert monkey. *J. Neurophysiol.* 36:1004–22
Sato H, Noda H. 1992. Saccadic dysmetria induced by transient functional decoration of the cerebellar vermis. *Exp. Brain Res.* 88:455–58
Schmahmann JD. 1991. An emerging concept: the cerebellar contribution to higher function. *Arch. Neurol.* 48:1178–87
Schmahmann JD. 2004. Disorders of the cerebellum: ataxia, dysmetria of thought, and the cerebellar cognitive affective syndrome. *J. Neuropsychiatry Clin. Neurosci.* 16:367–78

Schmahmann JD, Sherman JC. 1998. The cerebellar cognitive affective syndrome. *Brain* 121(Part 4):561–79
Schmidt D, Abel L, Dell'Osso L, Daroff R. 1979. Saccadic velocity characteristics: intrinsic variability and fatigue. *Aviat. Space Environ. Med.* 50:393–95
Schoch B, Gorissen B, Richter S, Ozimek A, Kaiser O, et al. 2004. Do children with focal cerebellar lesions show deficits in shifting attention? *J. Neurophysiol.* 92:1856–66
Scudder CA. 1988. A new local feedback model of the saccadic burst generator. *J. Neurophysiol.* 59:1455–75
Stone L, Lisberger S. 1990. Visual responses of Purkinje cells in the cerebellar flocculus during smooth-pursuit eye movements in monkeys. I. Simple spikes. *J. Neurophysiol.* 63:1241–61
Straube A, Robinson FR, Fuchs AF. 1997. Decrease in saccadic performance after many visually guided saccadic eye movements in monkeys. *Investig. Ophthalmol. Vis. Sci.* 38:2810–16
Strick PL, Dum RP, Fiez JA. 2009. Cerebellum and nonmotor function. *Annu. Rev. Neurosci.* 32:413–34
Sultan F, Mock M, Thier P. 2000. Functional architecture of the cerebellar system. *Neurol. Dis. Therapy* 50:1–52
Sun Z, Smilgin A, Junker M, Dicke PW, Thier P. 2017. The same oculomotor vermal Purkinje cells encode the different kinematics of saccades and of smooth pursuit eye movements. *Sci. Rep.* 7:40613
Suzuki DA, Keller EL. 1988. The role of the posterior vermis of monkey cerebellum in smooth-pursuit eye movement control. II. Target velocity-related Purkinje cell activity. *J. Neurophysiol.* 59:19–40
Takagi M, Zee DS, Tamargo RJ. 1998. Effects of lesions of the oculomotor vermis on eye movements in primate: saccades. *J. Neurophysiol.* 80:1911–31
Takagi M, Zee DS, Tamargo RJ. 2000. Effects of lesions of the oculomotor cerebellar vermis on eye movements in primate: smooth pursuit. *J. Neurophysiol.* 83:2047–62
Thach W. 1968. Discharge of Purkinje and cerebellar nuclear neurons during rapidly alternating arm movements in the monkey. *J. Neurophysiol.* 31:785–97
Thier P. 2011. The oculomotor cerebellum. In *The Oxford Handbook of Eye Movements*, ed. SP Liversedge, I Gilchrist, S Everling, pp. 173–93. New York: Oxford University Press
Thier P, Dicke PW, Haas R, Barash S. 2000. Encoding of movement time by populations of cerebellar Purkinje cells. *Nature* 405:72–76
Thier P, Haarmeier T, Treue S, Barash S. 1999. Absence of a common functional denominator of visual disturbances in cerebellar disease. *Brain* 122:2133–46
Thier P, Möck M. 2006. The oculomotor role of the pontine nuclei and the nucleus reticularis tegmenti pontis. *Prog. Brain Res.* 151:293–320
Townsend J, Courchesne E, Covington J, Westerfield M, Harris NS, et al. 1999. Spatial attention deficits in patients with acquired or developmental cerebellar abnormality. *J. Neurosci.* 19:5632–43
Townsend J, Harris NS, Courchesne E. 1996. Visual attention abnormalities in autism: delayed orienting to location. *J. Int. Neuropsychol. Soc.* 2:541–50
Vahedi K, Rivaud S, Amarenco P, Pierrot-Deseilligny C. 1995. Horizontal eye movement disorders after posterior vermis infarctions. *J. Neurol. Neurosurg. Psychiatry* 58:91–94
Xu-Wilson M, Chen-Harris H, Zee DS, Shadmehr R. 2009a. Cerebellar contributions to adaptive control of saccades in humans. *J. Neurosci.* 29:12930–39
Xu-Wilson M, Zee DS, Shadmehr R. 2009b. The intrinsic value of visual information affects saccade velocities. *Exp. Brain Res.* 196:475–81
Yamada J, Noda H. 1987. Afferent and efferent connections of the oculomotor cerebellar vermis in the macaque monkey. *J. Comp. Neurol.* 265:224–41
Zee D, Yamazaki A, Butler PH, Gücer G. 1981. Effects of ablation of flocculus and paraflocculus of eye movements in primate. *J. Neurophysiol.* 46:878–99

Annual Review of Vision Science

Volume 5, 2019

Contents

Errata

An online log of corrections to *Annual Review of Vision Science* articles may be found at http://www.annualreviews.org/errata/vision